Nonlinear Finite Elements: Modeling and Simulation of Earthquakes, Soils, Structures and their Interaction

Prof. Dr. Boris Jeremić; Борис Јеремић

University of California, Davis, USA

with significant contributions, as noted in Chapters, by:

Prof. Dr. Zhaohui Yang 杨朝晖 University of Alaska, USA	Dr. Zhao Cheng 程 昭 Itasca International Inc., USA	Dr. Guanzhou Jie 揭冠周 Wells Fargo Securities, USA
Dr. Nima Tafazzoli نیما تفضلی Tetra Tech EBA, CAN	Dr. Matthias Preisig GeoMod, CHE	Dr. Panagiota Tasiopoulou Παναγιώτα Τασιοπούλου Fugro, GRC
Dr. Federico Pisanò NGI, USA	Prof. Dr. José Abell University of the Andes, CHL	Mr. Kohei Watanabe 渡邊 航平 Shimizu Corporation, JPN
Dr. Yuan Feng 冯源 TuSimple, USA	Prof. Dr. Sumeet Kumar Sinha सुमित कुमार सिन्हा University of New Delhi, IND	Ms. Fatemah Behbehani فاطمة بهبهاني UC, San Diego, USA
Prof. Dr. Han Yang 杨涵 University of Tianjin, CHN	Dr. Hexiang Wang 王和祥 Berkshire Hathaway Inc., USA	Dr. Katarzyna Staszewska Gdańsk UT, POL

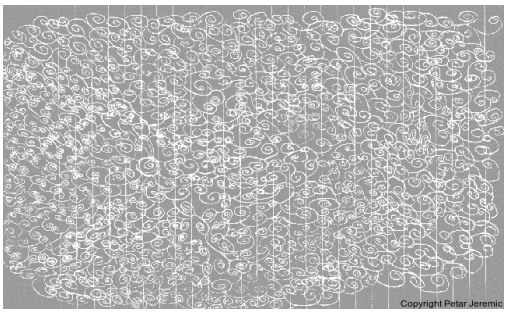

Version: 3Jul2025, 10:19

ISBN: 978-0-692-19875-9

Typeset in LaTeX

http://sokocalo.engr.ucdavis.edu/~jeremic/LectureNotes/

Motivation and Inspiration

The main motivation for development of the FEI system, comprised of these lecture notes and accompanying modeling tools, computational libraries and visualization tools, is to help research and teach modeling and simulation for civil engineering mechanics problems. Focus is on development and use of methods that reduce Kolmogorov complexity and modeling uncertainty. In other words, focus is on development and use of methods that predict and inform rather than fit. These lecture notes, in particular, are being developed to document research, teaching and practical problem solving work for Real-ESSI problems (Realistic modeling and simulation of Earthquakes, Soils, Structures and their Interaction). Almost all of the theories, formulations and algorithms described here can be directly analyzed using Real-ESSI Simulator system (http://real-essi.info/ ; http://real-essi.us/) on local computers or on Cloud Computers (Amazon Web Services, AWS, on Marketplace, search for ESSI). A number of theories and formulations, related to Real-ESSI problems, developed by us and others, as referenced, are collected within these Lecture Notes in order to have one location, one write-up, with all/most necessary material for the analysis of ESSI problems. These Lecture Notes are in perpetual development, and chapters and sections are being edited and added as you read this. In that sense, these Lecture Notes are not "polished" and there are some rough edges, however improvement work is underway.

Work on these lecture notes was inspired by a number of books and lecture notes that I have enjoyed over many years, (Bathe, 1982), (Bathe and Wilson, 1976), (Felippa, 1992b, 1989, 1993; Felippa and Park, 1995), (Willam, 1993), (Sture, 1993), (Lubliner, 1990), (Crisfield, 1991), (Chen and Han, 1988a), (Zienkiewicz and Taylor, 1991a,b), (Argyris and Mlejnek, 1991), (Malvern, 1969), (Saouma, 1992-2013), (Dunica and Kolundžija, 1986), (Kojić, 1997), (Hjelmstad, 1997), (Oberkampf et al., 2002). I particularly enjoyed book by Bathe (1982), the only one I had partial access to in the late '80s, with all the examples that could be worked out on paper. In '89 I managed to purchase a used book by Zienkiewicz (1977) for US$50, from my first salary as a young engineer in Energoprojekt Company, from a colleague. In the early '90s, I was lucky to get exposed to early, draft versions of books by Kojić (1993); Kojić (1997). Few years later, I enjoyed lectures and lecture notes by Felippa (1992b, 1989, 1993); Felippa and Park (1995), Willam (1993), and Sture (1993).

Current version of lecture notes, the one in front of you, aims to extend concepts described by my Teachers and Professors. Presented formulations and implementations are available within the Real-ESSI Simulator http://real-essi.info/, http://real-essi.us/. A number of available, provided models, some very simple, some more sophisticated, and some very sophisticated, can be analyzed and results visualized using Real-ESSI Simulator on local computers or on Cloud Computers (Amazon Web Services, AWS).

Dedication

This book is dedicated to friends, colleagues, supporters, promoters that I had a privilege to know and work with over last many years, and that are not with us anymore.
May they rest in peace!

Robert P. Kennedy, 1939-2018

"Response of a soil structure system is nonlinear, and I would really like to know what that response is!"
"There are engineers and then there are Engineers!"

Nebojša Orbović, Небојша Орбовић, 1962-2021

"As an engineer, I have to know, with good accuracy, what will happen to the structure during loading, and will use modeling and analysis to find out, hence verification and validation for modeling and analysis is really important"
"As an engineer, I have to know what are response sensitivities to modeling parameters."

Contributions

Useful contributions were also made by the following students, colleagues and collaborators (other than those listed on the front page): Mr. Babak Kamranimoghadam (بابک کامرانی), Mr. Chang-Gyun Jeong (정창균), Mr. Chao Luo (罗超), Mr. Max Sieber, Mr. Antonio Felipe Salazar, and Mr. Borko Miladinović (Борко Миладиновић).

Comments

Comments, corrections, edits &c. are much appreciated! Special thanks to (in chronological order): Miroslav Živković (Мирослав Живковић), Dmitry J. Nicolsky, Andrzej Niemunis, Robbie Jaeger, Yiorgos Perikleous (Γιώργος Περικλέους), Robert Roche, Viktor Vlaski, Edison Lam, Dr. Sukumar Baishya, Marco Andreini, Francisco "Paco" Beltran.

The best way to send a comment on these lecture notes is by email, however please read the following NOTE about sending an email to me. It would be great if you can place the following in the subject line of your email: `Draft CompMech Lecture Notes`. This will be much appreciated as it will help me filter your email and place it in Draft_CompMech_Lecture_Notes email-box that I regularly read.

Acknowledgement

Many developments described in these lecture notes, developed over many years, were made possible in collaborators with, and with financial support from the: US-DOE, US-NRC, CNSC/CCSN, US-NSF, CalTrans, CH-ENSI/IFSN, ATC/US-FEMA, UN-IAEA, US-ACE, and NASA. Their support and collaboration is much appreciated!

Software

Theoretical and computational developments described in these lecture notes are implemented in a program Real-ESSI Simulator (http://real-essi.info/; (http://real-essi.us/; http://sokocalo.engr.ucdavis.edu/~jeremic/Real_ESSI_Simulator/). The Real ESSI Simulator (Realistic Modeling and Simulation of Earthquakes, Soils, Structures and their Interaction), (pronunciation of ESSI is similar to easy, as in "as easy as pie") is a software, hardware and documentation system for select level of fidelity (high, low, intermediate), high performance, time domain, nonlinear/inelastic, deterministic or probabilistic, 3D, finite element modeling and simulation of

- statics and dynamics of soil,
- statics and dynamics of rock,
- statics and dynamics of structures,
- statics of soil-structure systems, and
- dynamics of earthquake-soil-structure system interaction.

The Real-ESSI Simulator systems is used for the analysis, design and assessment of static and dynamic behavior of infrastructure objects, including buildings, bridges, dams, nuclear energy installations, tunnels, etc. The Real-ESSI Simulator develops modeling and simulations that inform and predict.

The Real-ESSI Simulator program is available in source, in executable form and as debian package at http://real-essi.info/, http://real-essi.us/. The Real ESSI Simulator system is also available for use on Amazon Web Services Market Place, search for "Real ESSI" or "MS ESSI".

The name Real-ESSI, is explained in some detail in section 201.2.6 on page 710.

Distribution?

These Lecture Notes can be downloaded and distributed worldwide. If you use these Lecture Notes, please cite them as:

Boris Jeremić, Zhaohui Yang, Zhao Cheng, Guanzhou Jie, Nima Tafazzoli, Matthias Preisig, Panagiota Tasiopoulou, Federico Pisanò, José Abell, Kohei Watanabe, Yuan Feng, Sumeet Kumar Sinha, Fatemah Behbehani, Han Yang, and Hexiang Wang. Nonlinear Finite Elements: Modeling and Simulation of Earthquakes, Soils, Structures and their Interaction. University of California, Davis, CA, USA; 2021. ISBN: 978-0-692-19875-9

or

Jeremić et al. Nonlinear Finite Elements: Modeling and Simulation of Earthquakes, Soils, Structures and their Interaction. UCD, CA, USA, 2021. ISBN: 978-0-692-19875-9

Overview Table of Contents

Contents

Part 100

Theoretical and Computational Formulations

Chapter 101

Introduction

(1996-2003-2016-2017-2018-2019-2020-2021-)

101.1 Chapter Summary and Highlights

101.2 On Modeling

Modeling of mechanical behaviour of civil engineering problems is performed using models. It is important to note that everything we do for design or assessment is based on models. Models can range from very simple to very sophisticated.

Simple Model Example. For example, simple model for the strength of a beam, as developed by Leonardo da Vinci and noted by Timoshenko (1953), states: "In every article that is supported, but is free to bend, and is of uniform cross section and material, the part that is farthest from the support will bend the most." Leonardo da Vinci suggested a number of tests with variation in beam length and keeping the same cross section, and record what loads could these beams carry. He concluded that strength of beams supported on both ends, simple beams, varies inversely proportional to teh beam length and directly to the beam width.

This simple model for beam bending, as stated, is based directly on observations of experiments. These experiments represent the physics discovery experiments.

Sophisticated Model Example. The same simple beam problem can be analyzed using a sophisticated Bernoulli or Timoshenko beam finite elements, or even using 3D solid brick elements.

The importance of computer analysis for design and performance assessment of civil engineering systems has recently dramatically increased. With availability of fast, inexpensive computers, and availability of numerical analysis programs, computer analysis of civil engineering systems for design and for assessment of performance is commonly used. It is important to note that failure of civil engineering systems has high consequences. For safe and economical design and for assessment of performance (reliability, robustness and safety) of civil engineering systems, engineers have to perform proper analysis, usually a numerical, computer analysis.

Developers of computer analysis software, computational analysts/engineers and users of numerical analysis face a critical question: How should confidence in analysis results be critically assessed?

Verification and Validation (V&V) of computational analysis is the major process for assessing and quantifying this confidence. Verification is the assessment of the software correctness and numerical accuracy of the solution to a given computational model. Validation is the assessment of physical accuracy of a computational model based on comparisons between computation simulation and experimental data. For verification, the association or relationship of the simulation to the real world is not an issue while for

validation the relationship between computation and real world external data is the issue. Verification and validation are covered in much more detail in part 300 of this book, on pages after page 1436.

101.2.1 The Performance Challenge

Computational science challenges (Post, 2004):

- The Performance Challenge
- The Programming Challenge
- The Prediction Challenge

Parallel computing, development of portable Distributed Memory Parallel (DMP) applications, specifically Architecture Aware Plastic Domain Decomposition (AAPDD) Method (Feng et al., 2024) that addresses the challenge of multiple CPUs, multiple cores, multiple GPUs, multiple networks, etc.

The Programming Challenge.

Quality controlled, managed program development...

The Prediction Challenge

Epistemic, modeling uncertainties

Aliatory, parametric uncertainties

Development of numerical modeling tools for engineers to develop a hierarchy of models, to explore, try, different levels of modeling sophistication in order to understand, gain insight into the influence of epistemic/modeling uncertainty on analysis and to propagate aleatory/parametric uncertainty through models...

101.2.2 Analysis Governance

Analysis governance, sometimes also called simulations governance[1] (Szabó and Actis, 2011, 2012), is a very important components of numerical analysis in civil engineering.

Analysis governance is a process of increasing confidence in numerical analysis results. Analysis governance covers both

- Numerical analysis tools, the program that is used for analysis

[1] Analysis consists of modeling, the physics component, and simulation, the numerics component, hence analysis covers both modeling and simulation components (Analysis = Modeling + Simulation).

- Numerical analyst, expert engineer that is performing the analysis

The numerical analysis program has to be extensively verified and validated.

Numerical analyst, expert engineer has to have required level of expertise, knowledge, experience and, if possible, has to be certified to perform required analysis.

101.3 Specialization to Computational Mechanics

In this section we start from general mechanics and specialize our interest toward the field of computational mechanics (this is based on great lecture notes by Prof. Carlos Felippa (Felippa, 1993)):

101.3.1 Mechanics

- Theoretical
- Applied
- Computational
  - Nanomechanics
  - Micromechanics
  - Continuum Mechanics
    - Solids and Structures
    - Fluids
    - Multiphysics
  - Systems
- Experimental

101.3.2 Continuum Mechanics

- Statics
  - Time invariant
  - Transient (quasi-statics)
- Dynamics

101.3.3 Statics and Dynamics

- Linear
- Nonlinear
  - Elastic
  - Inelastic

101.3.4 Discretization Methods

- Finite Element Method (FEM)
  - FEM Formulation
    - Displacement
    - Equilibrium
    - Mixed
    - Hybrid
  - FEM Solution
    - Stiffness
    - Flexibility
    - Mixed
- Boundary Element Method
- Finite Difference Method
- Finite Volume Method
- Spectral Method
- Mesh-Free Method

101.3.5 The Solution Morass

A system of 1000 linear equations has one solution.

A system of 1000 cubic equations has $3^{1000} \approx 10^{477}$ solutions.

It is worth putting this number in prospective: number of atoms in the earth is about 10^{50}, and a number of atoms in the universe is about 10^{78} (Niemunis, 2015 –).

Solution: Continuation or Incremental analysis!

101.3.6 Smooth Nonlinearities

- Finite deflections
- Nonlinear elasticity
- Follower forces

101.3.7 Rough Nonlinearities

- Elasto-plasticity
- Contact/Interface/Joint
- Interface/joint Friction

101.4 Tour of Computational Mechanics

In this section we describe various examples of equilibrium path and set up basic terminology.

101.4.1 Equilibrium Path

101.4.2 Special Equilibrium Points

101.4.2.1 Critical Points

Limit Points

Bifurcation Points

101.4.2.2 Turning Points

101.4.2.3 Failure Points

101.4.3 Generalized Response

101.4.4 Sources of Nonlinearities

Tonti Diagrams

101.4.5 Simulation Process: Loading Stages, Increments and Iterations

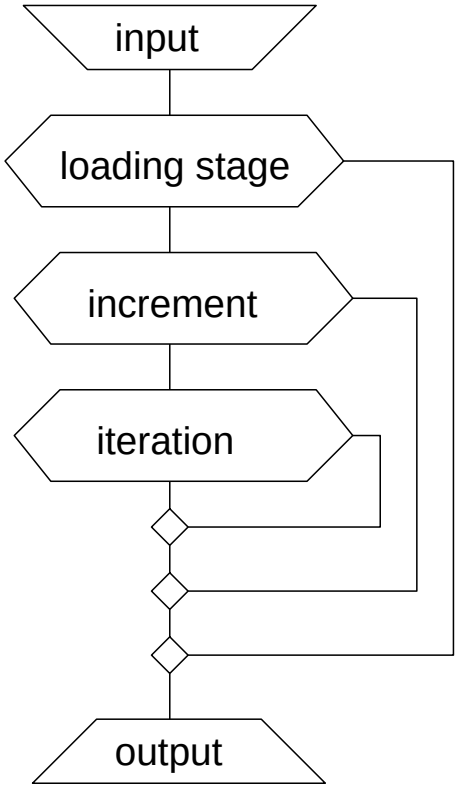

Figure 101.1: Nonlinear analysis loading stages, loading increments, equilibrium iterations.

Chapter 102

Finite Elements Formulation

(1989-1994-1999-2005-2010-2011-2012-2013-2015-2016-2017-2018-2019-2020-2021-)

(In collaboration with Dr. Zhao Cheng, Dr. Nima Tafazzoli, Prof. José Abell, Dr. Yuan Feng. Prof. Han Yang)

102.1 Chapter Summary and Highlights

This section uses basic principles of mechanics to derive finite element equations. We start with general setup, assuming large deformation in section 102.2, and then proceed to develop finite element formulation for small deformations in section 102.3 on page 104 . Further investigation of large deformation formulation is given in chapter 106 on page 482.

102.2 Formulation of the Continuum Mechanics Incremental Equations of Motion

This section follows Bathe (1982), Felippa (1989) and Felippa (1993).

Assume that a 3D solid is analyzed in a fixed Cartesian coordinate system, Figure (102.1). Also, assume that the solid can undergo large displacements and rotations, large strains, and nonlinear or inelastic constitutive response. The main aim is to evaluate the equilibrium of solid at discrete times $0, \Delta t, 2\Delta t, \dots$, where Δt is an increment in time. To do that, a continuation strategy is used. That is, assume that the solution for all the variables (generalized displacements, strain, stress, forces, etc.) is available, was solved for, for all time steps from 0 to time t. Solution for the next time step $t + \Delta t$ will be based on already obtained solution from the previous time step, at time t, (Felippa, 1993). This approach will be applied for each time step, repetitively until the solution for all time steps is obtained.

In following all parts of the solid, as they undergo displacements and rotations, from the original configuration to the final configuration, adopted is a Lagrangian (or material) formulation of the problem. This approach is contrasting Eulerian (or spatial) formulation , usually used in the analysis of fluid mechanics problems.

In the Lagrangian incremental analysis approach the equilibrium of the solid at time $t+\Delta t$ is expressed using the principle of virtual displacements. Using tensorial notation[1] this principle requires that:

$$\int_{^{t+\Delta t}V} {}^{t+\Delta t}\sigma_{ij}\ \delta\ {}_{t+\Delta t}\epsilon_{ij}\ {}^{t+\Delta t}dV = {}^{t+\Delta t}\mathcal{R} \tag{102.1}$$

where the ${}^{t+\Delta t}\sigma_{ij}$ are Cartesian components of the Cauchy stress tensor, see section 701.2.1 on page 2860, the ${}_{t+\Delta t}\epsilon_{ij}$ are the Cartesian components of an infinitesimal strain tensor, see section 701.2.2 on page 2863, and the δ means "variation in" i.e.:

[1] Einstein's summation rule is implied unless stated differently, all lower case indices ($i, j, p, q, m, n, o, r, s, t, \dots$) can have values of 1, 2, 3, and values for capital letter indices will be specified where need be.

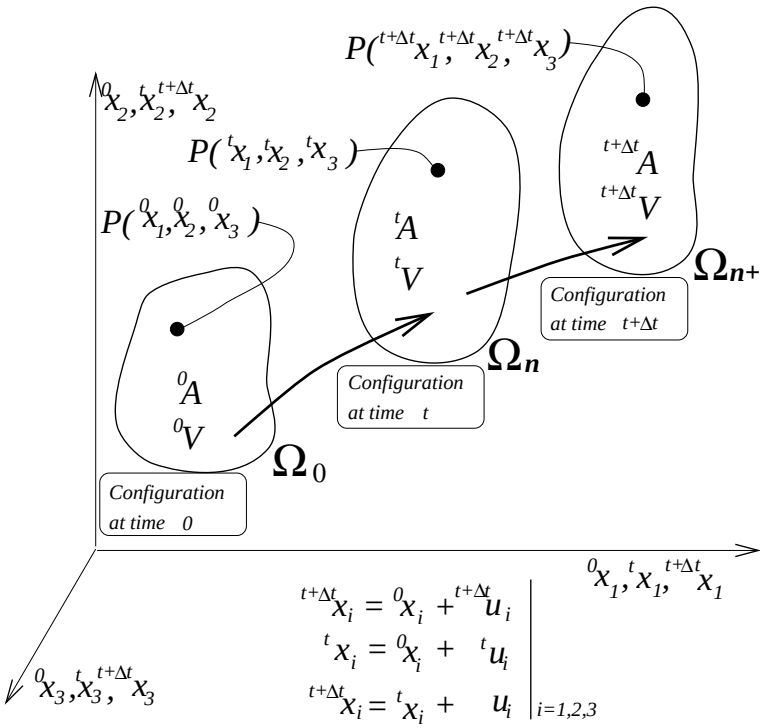

Figure 102.1: Motion of solid in a Cartesian coordinate system.

$$\delta\, {}_{t+\Delta t}\epsilon_{ij} = \delta \frac{1}{2}\left(\frac{\partial u_i}{\partial\, {}^{t+\Delta t}x_j} + \frac{\partial u_j}{\partial\, {}^{t+\Delta t}x_i}\right) = \frac{1}{2}\left(\frac{\partial \delta u_i}{\partial\, {}^{t+\Delta t}x_j} + \frac{\partial \delta u_j}{\partial\, {}^{t+\Delta t}x_i}\right) \tag{102.2}$$

It should be noted that Cauchy stresses are "body forces per unit area" in the configuration at time $t+\Delta t$, and the infinitesimal strain components are also referred to this as yet unknown configuration. The right hand side of equation (102.1), i.e. ${}^{t+\Delta t}\mathcal{R}$ is the virtual work performed when the solid is subjected to a virtual displacement at time $t+\Delta t$:

$${}^{t+\Delta t}\mathcal{R} = \int_{{}^{t+\Delta t}V} \left({}^{t+\Delta t}f_i^B - \rho \ddot{u}_i^{t+\Delta t}\right)\, \delta u_i^{t+\Delta t}\, {}^{t+\Delta t}dV + \int_{{}^{t+\Delta t}S} {}^{t+\Delta t}f_i^S\, \delta u_i^{t+\Delta t}\, {}^{t+\Delta t}dS$$

where ${}^{t+\Delta t}f_i^B$ and ${}^{t+\Delta t}f_i^S$ are the components of the externally applied body and surface force vectors, respectively, and $-\rho\ddot{u}_i^{t+\Delta t}$ is the inertial body force that is present if accelerations are present[2], δu_i is the ith component of the virtual displacement vector.

The main problem in applying equation (102.1) is that the configuration of the solid at a time $t+\Delta t$ is unknown. The continuous change in the configuration, deformation of the solid needs to be properly

[2] This is based on D'Alembert's principle (D'Alembert, 1758).

modeled. As an example, consider, for example, Cauchy stress at time $t + \Delta t$. This stress cannot be obtained by adding to the Cauchy stresses at time t, a stress increment that is due only to material deformation. The reason is that material might rotate, and stress state is a function of tractions (loads) and size and orientation of differentially small faces on which stress components act. For material only nonlinear analysis, the of large displacements, large rotations and large strain will be neglected. Large displacements, rotations and large strains will be addressed in more detail in Chapter 106 on page 482.

The continuous change in the configuration of the solid is dealt with by using appropriate stress and strain measures and constitutive relations. When solving the general problem[3] one possible approach is given in Simo (1988). The previous discussion was oriented toward small deformation, small-displacement analysis leading to the use of Cauchy stress tensor σ_{ij} and small strain tensor ϵ_{ij}.

In the following, covered briefly are other stress and strain measures particularly useful in large strain and large displacement analysis. More detailed description of large displacements, large rotations and large strains problems is addressed in Chapter 106 on page 482.

The solution is sought for equation 102.1, which expresses the equilibrium and compatibility requirements of the general solid considered in the configuration corresponding to time $t + \Delta t$. The nonlinear or inelastic behavior of material enters equation 102.1 through the stress-strain constitutive equations. In general, the solid can undergo large displacements, large rotations large strains, and since constitutive relations are nonlinear, the relation in equation 102.1 cannot be solved directly. However, an approximate solution can be obtained by referring all variables to a previously calculated known equilibrium configuration, and linearizing the resulting equations. Iterations can then improve this solution.

To develop the governing equations for the approximate solution obtained by linearization, recall that the solutions for time $0, \Delta t, 2\Delta t, \ldots, t$ have already been calculated and that the Piola–Kirchhoff stress tensor is energy conjugate to the Green–Lagrange strain tensor:

$$\int_{{}^0V} {}^t_0S_{ij}\ \delta {}^t_0\epsilon_{ij}\ {}^0dV = \int_{{}^0V} \left(\frac{{}^0\rho}{{}^t\rho}\ {}^0_t x_{i,m}\ {}^t\sigma_{mn}\ {}^0_t x_{j,n} \right)\ \left({}^t_0 x_{k,i}\ \delta {}^t_t\epsilon_{kl}\ {}^t_0\ x_{l,j} \right)\ {}^0dV = \int_{{}^0V} \frac{{}^0\rho}{{}^t\rho}\ {}^t\sigma_{mn}\ \delta {}^t_0\epsilon_{mn}\ {}^0dV \tag{102.3}$$

since

$${}^t_0x_{k,l}\ {}^0_t x_{l,m} = \delta_{km}$$

and

[3] That is, large displacements, large rotations, large deformations and material nonlinear and/or inelastic.

$$ {}_0\rho \, {}^0dV = {}^t\rho \, {}^tdV $$

one obtains

$$ \int_{{}^0V} {}^t_0S_{ij} \, \delta {}^t_0\epsilon_{ij} \, {}^0dV = \int_{{}^0V} {}^t\sigma_{mn} \, \delta {}^t_t\epsilon_{mn} \, {}^tdV \tag{102.4} $$

where 2nd Piola–Kirchhoff stress tensor is defined as:

$$ {}^t_0S_{ij} = \frac{{}^0\rho}{{}^t\rho} \, {}^0_t x_{i,m} \, {}^t\sigma_{mn} \, {}^0_t x_{j,n} \tag{102.5} $$

and ${}^0_t x_{j,n} = \frac{\partial {}^0x_i}{\partial {}^tx_m}$, and $\frac{{}^0\rho}{{}^t\rho}$ represents the ratio of the mass density at time 0 and time t, and the Green–Lagrange strain is defined as:

$$ {}^t_0\epsilon_{ij} = \frac{1}{2} \left({}^t_0u_{i,j} + {}^t_0u_{j,i} + {}^t_0u_{k,i} \, {}^t_0u_{k,j} \right) \tag{102.6} $$

By employing equation 102.4 stresses and strains are referenced to the known equilibrium configuration. The choice lies between two formulations, named (a)total Lagrangian and (b) updated Lagrangian formulations.

For the total Lagrangian formulations, all static and kinematic variables are referenced to the initial configuration at time 0. On the other hand, for the updated Lagrangian formulation, all static and kinematic variables are referenced to the previous step equilibrium configuration at time t. Both the total Lagrangian and updated Lagrangian formulations include all kinematic nonlinear effects due to large displacement, large rotations, and large strains. Whether the large strain behavior is modeled appropriately depends on the constitutive relations specified. The only advantage of using one over the other formulation lies in numerical efficiency.

Using equation 102.4 in the total Lagrangian formulation, considered is this equation:

$$ \int_{{}^0V} {}^{t+\Delta t}_0S_{ij} \, \delta {}^{t+\Delta t}_0\epsilon_{ij} \, {}^0dV = {}^{t+\Delta t}\mathcal{R} \tag{102.7} $$

while in the updated Lagrangian formulation considered is this equation:

$$ \int_{{}^tV} {}^{t+\Delta t}_tS_{ij} \, \delta {}^{t+\Delta t}_t\epsilon_{ij} \, {}^tdV = {}^{t+\Delta t}\mathcal{R} \tag{102.8} $$

where ${}^{t+\Delta t}\mathcal{R}$ is the external virtual work as defined in equation ??. Approximate solution to the equation 102.7 and equation 102.8 can be obtained by linearization. Comparison of the total Lagrangian and updated Lagrangian formulations reveal that they are quite similar, with the difference in the choice of different reference configurations for kinematic and static variables. If in the numerical solution the appropriate constitutive tensors are employed, identical results should be obtained.

102.3 Finite Element Discretization

Consider the equilibrium of a general three–dimensional solid such as in Figure (102.2) (Bathe, 1996). The external forces acting on a solid are surface tractions f_i^S and body forces f_i^B. Displacements are u_i and strain tensor[4] is ϵ_{ij} and the stress tensor corresponding to strain tensor is σ_{ij}.

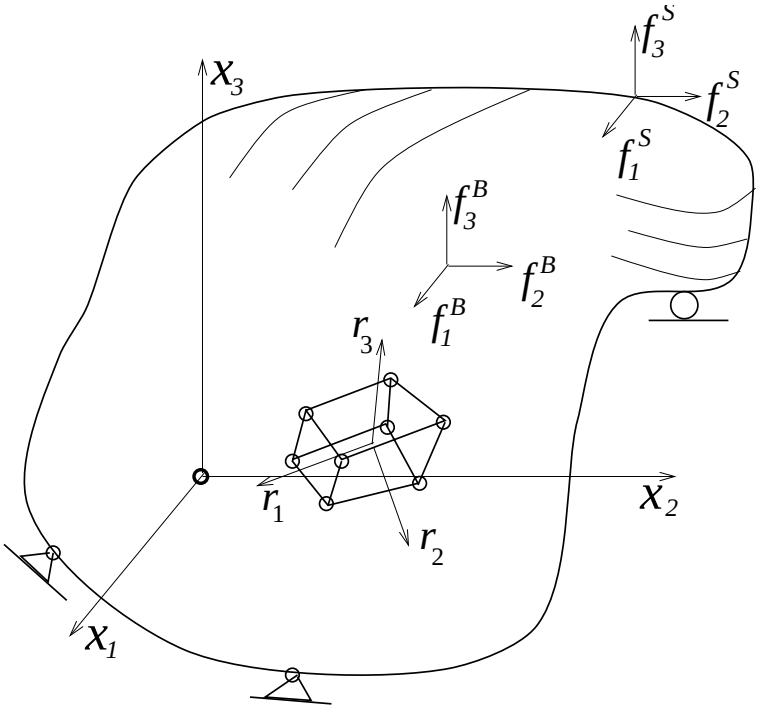

Figure 102.2: General three dimensional solid.

Dynamic equilibrium equation is given as

$$\sigma_{ij,j} = f_i - \rho \ddot{u}_i \tag{102.9}$$

where $\sigma_{ij,j}$ is a small deformation (Cauchy) stress tensor, f_i are external (body (f_i^B) and surface (f_i^S)) forces, ρ is material density and $\ddot{u}_i$ are accelerations. Inertial forces $\rho\ddot{u}_i$ follow from D'Alembert's principle

[4] small strain tensor as defined in equation: $\epsilon_{ij} = \frac{1}{2}\left(u_{i,j} + u_{j,i}\right)$.

(D'Alembert, 1758). The above equation can be premultiplied with virtual displacements δu_i and then integrated by parts to obtain the weak form, as further elaborated below.

For a given solid, loaded with external forces, with prescribed supports solution for displacements, strains and stresses are sought. The principle of virtual displacements (PVD) can be used to find a solution. Using PVD, equilibrium is achieved if the total internal virtual work is equal to the total external virtual work, for any compatible, small virtual displacements, that satisfy the essential boundary conditions.

Mathematically this is expressed using equation 102.10 for the solid at time $t + \Delta t$. Since the incremental approach is used, a time dimension is dropped so that all the equations are applied for the given increment[5], at time $t + \Delta t$. The equation is now, using tensorial notation[6]:

$$\int_V \sigma_{ij}\ \delta\epsilon_{ij}\ dV = \int_V \left(f_i^B - \rho\ddot{u}_i\right)\ \delta u_i\ dV + \int_S f_i^S\ \delta u_i\ dS \tag{102.10}$$

The internal work given on the left side of (102.10) is equal to the actual stresses σ_{ij} going through the virtual strains $\delta\epsilon_{ij}$ that corresponds to the imposed virtual displacements. The external work is on the right side of (102.10) and is equal to the actual surface forces f_i^S and body forces $f_i^B - \rho\ddot{u}_i$ going through the virtual displacements δu_i.

It is noted virtual strains used in equationi 102.10 correspond to the imposed virtual displacements that can be represented by any compatible set of displacements that satisfy the geometric boundary conditions. The equation 102.10 is an expression of equilibrium, and for different virtual displacements, correspondingly, different equations of equilibrium are obtained. Equation 102.10 also contains the compatibility and constitutive requirements. Displacements should be continuous and compatible and should satisfy the displacement boundary conditions, and the stresses should be evaluated from the strains using appropriate constitutive relations. Thus, the principle of virtual displacements contains all requirements that need to be fulfilled to analyze a problem in solid and structural mechanics. The principle of virtual displacements can be directly related to the principle that the total potential Π of the system must be stationary.

In the finite element analysis, approximation for the solid in Figure 102.2 is done by creating an assemblage of discrete finite elements with the elements connected at nodal points. The displacements measured in a local coordinate system r_1, r_2 and r_3 within each element are assumed to be a function of the displacements at the N finite element nodal points:

[5] $t + \Delta t$ will be dropped from now one in this chapter.

[6] Einstein's summation rule is implied unless stated differently, all lower case indices ($i, j, p, q, m, n, o, r, s, t, \dots$) can have values of 1, 2, 3, and values for capital letter indices will be specified where need be.

$$u_i \approx \hat{u}_a = H_I \bar{u}_{Ia} \tag{102.11}$$

where $I = 1, 2, 3, \ldots, n$ and n is number of nodes in a specific element, $a = 1, 2, 3$ represents a number of dimensions (can be 1 or 2 or 3). Real displacement field u_i is approximated with approximate displacement field $\hat{u}_a$, and H_I represent displacement interpolation functions, $\bar{u}_{Ia}$ is the tensor of global approximate generalized displacement components at all element nodes. The term generalized displacements mean that both translations, rotations, or any other nodal unknown are modeled independently. Here specifically, only translational degrees of freedom are considered. The strain tensor is defined as:

$$\epsilon_{ab} = \frac{1}{2}\left(u_{a,b} + u_{b,a}\right) \tag{102.12}$$

and by using equation 102.11, approximate strain tensor can be defined as:

$$\begin{aligned} \epsilon_{ab} \approx \hat{e}_{ab} &= \frac{1}{2}\left(\hat{u}_{a,b} + \hat{u}_{b,a}\right) = \\ &= \frac{1}{2}\left((H_I\ \bar{u}_{Ia})_{,b} + (H_I\ \bar{u}_{Ib})_{,a}\right) = \\ &= \frac{1}{2}\left(\left(H_{I,b}\ \bar{u}_{Ia}\right) + \left(H_{I,a}\ \bar{u}_{Ib}\right)\right) \end{aligned} \tag{102.13}$$

The most general stress-strain relationship[7] for an isotropic material is:

$$\hat{\sigma}_{ab} = E_{abcd}\left(\hat{e}_{cd} - \epsilon^0_{cd}\right) + \sigma^0_{ab} \tag{102.14}$$

where $\hat{\sigma}_{ab}$ is the approximate Cauchy stress tensor, E_{abcd} is the constitutive tensor[8], $\hat{e}_{cd}$ is the infinitesimal approximate strain tensor, ϵ^0_{cd} is the infinitesimal initial strain tensor and σ^0_{ab} is the initial Cauchy stress tensor.

Using the assumption of the displacements within each finite element, as expressed in equation 102.11, equilibrium equations that correspond to nodal point displacements of the assemblage of finite elements can be derived. Equation 102.10 can be rewritten as a sum[9] of integrations over the volume and areas of all finite elements:

$$\bigcup_m \int_{V^m} \hat{\sigma}_{ab}\ \delta\hat{e}_{ab}\ dV^m = \bigcup_m \int_{V^m} \left(f^B_a - \rho\ddot{u}_a\right)\ \delta\hat{u}_a\ dV^m + \bigcup_m \int_{S^m} f^S_a\ \delta\hat{u}^S_a\ dS^m$$

[7] in terms of exact stress and strain fields, but it holds for approximate fields as well.

[8] This tensor can be elastic or elastoplastic constitutive tensor.

[9] Or, more correctly as a union $\bigcup_m$ since we are integrating over the union of elements.

where $m = 1, 2, 3, \ldots, k$ and k is the number of elements. It is important to note that the integrations in (??) are performed over the element volumes and surfaces, and that for convenience different element coordinate systems may be used in the calculations. If we substitute equations 102.11, 102.12, 102.13 and 102.14 in ??, it follows:

$$\bigcup_m \int_{V^m} \left(E_{abcd} \left(\hat{e}_{cd} - \epsilon^0_{cd} \right) + \sigma^0_{ab} \right) \delta \left(\frac{1}{2} \left(H_{I,b}\, \bar{u}_{Ia} + H_{I,a}\, \bar{u}_{Ib} \right) \right) dV^m = \bigcup_m \int_{V^m} f^B_a\, \delta \left(H_I \bar{u}_{Ia} \right) dV^m - \bigcup_m \int_{V^m} H_J\, \ddot{\bar{u}}_{Ja}\, \rho\, \delta \left(H_I \bar{u}_{Ia} \right) dV^m + \bigcup_m \int_{S^m} f^S_a\, \delta \left(H_I \bar{u}_{Ia} \right) dS^m \tag{102.15}$$

or:

$$\bigcup_m \int_{V^m} \left(E_{abcd} \left(\left(\frac{1}{2} \left(H_{J,d}\, \bar{u}_{Jc} + H_{J,c}\, \bar{u}_{Jd} \right) \right) - \epsilon^0_{cd} \right) + \sigma^0_{ab} \right) \delta \left(\frac{1}{2} \left(H_{I,b}\, \bar{u}_{Ia} + H_{I,a}\, \bar{u}_{Ib} \right) \right) dV^m = = \bigcup_m \int_{V^m} f^B_a\, \delta \left(H_I \bar{u}_{Ia} \right) dV^m - \bigcup_m \int_{V^m} H_J\, \ddot{\bar{u}}_{Ja}\, \rho\, \delta \left(H_I \bar{u}_{Ia} \right) dV^m + \bigcup_m \int_{S^m} f^S_a\, \delta \left(H_I \bar{u}_{Ia} \right) dS^m \tag{102.16}$$

We can observe that δ in the previous equations represents a virtual quantity, but the rules for δ are quite similar to regular differentiation so that δ can enter the brackets and "virtualize" the nodal displacement[10]. It thus follows:

$$\bigcup_m \int_{V^m} \left(E_{abcd} \left(\left(\frac{1}{2} \left(H_{J,d}\, \bar{u}_{Jc} + H_{J,c}\, \bar{u}_{Jd} \right) \right) - \epsilon^0_{cd} \right) + \sigma^0_{ab} \right) \left(\frac{1}{2} \left(H_{I,b}\, \delta\bar{u}_{Ia} + H_{I,a}\, \delta\bar{u}_{Ib} \right) \right) dV^m = = \bigcup_m \int_{V^m} f^B_a\, \left(H_I \delta\bar{u}_{Ia} \right) dV^m - \bigcup_m \int_{V^m} H_J\, \ddot{\bar{u}}_{Ja}\, \rho\, \left(H_I \delta\bar{u}_{Ia} \right) dV^m + \bigcup_m \int_{S^m} f^S_a\, \left(H_I \delta\bar{u}_{Ia} \right) dS^m \tag{102.17}$$

Let us now work out some algebra on the left-hand side of the equation (102.17):

$$\bigcup_m \int_{V^m} \left(E_{abcd} \left(\frac{\left(H_{J,d}\, \bar{u}_{Jc} + H_{J,c}\, \bar{u}_{Jd} \right)}{2} \right) - E_{abcd} \epsilon^0_{cd} + \sigma^0_{ab} \right) \left(\frac{\left(H_{I,b}\, \delta\bar{u}_{Ia} + H_{I,a}\, \delta\bar{u}_{Ib} \right)}{2} \right) dV^m = = \bigcup_m \int_{V^m} f^B_a\, \left(H_I \delta\bar{u}_{Ia} \right) dV^m - \bigcup_m \int_{V^m} H_J\, \ddot{\bar{u}}_{Ja}\, \rho\, H_I \delta\bar{u}_{Ia}\, dV^m + \bigcup_m \int_{S^m} f^S_a\, \left(H_I \delta\bar{u}_{Ia} \right) dS^m \tag{102.18}$$

and further:

[10] since they are driving variables that define the overall displacement field through interpolation functions

$$\begin{aligned}
\bigcup_m \int_{V^m} \left(\left(\frac{1}{2} \left(H_{J,d}\ \bar{u}_{Jc} + H_{J,c}\ \bar{u}_{Jd} \right) \right)\ E_{abcd}\ \left(\frac{1}{2} \left(H_{I,b}\ \delta\bar{u}_{Ia} + H_{I,a}\ \delta\bar{u}_{Ib} \right) \right) \right)\ dV^m + \\
+ \bigcup_m \int_{V^m} \left(-E_{abcd}\ \epsilon^0_{cd}\ \left(\frac{1}{2} \left(H_{I,b}\ \delta\bar{u}_{Ia} + H_{I,a}\ \delta\bar{u}_{Ib} \right) \right) \right)\ dV^m + \\
+ \bigcup_m \int_{V^m} \left(\sigma^0_{ab} \right)\ \left(\frac{1}{2} \left(H_{I,b}\ \delta\bar{u}_{Ia} + H_{I,a}\ \delta\bar{u}_{Ib} \right) \right)\ dV^m = \\
\bigcup_m \int_{V^m} f^B_a\ \left(H_I \delta\bar{u}_{Ia} \right)\ dV^m \\
- \bigcup_m \int_{V^m} H_J\ \ddot{\bar{u}}_{Ja}\ \rho\ H_I \delta\bar{u}_{Ia}\ dV^m \\
+ \bigcup_m \int_{S^m} f^S_a\ \left(H_I \delta\bar{u}_{Ia} \right)\ dS^m
\end{aligned} \tag{102.19}$$

Several things should be observed in the equation (102.19). Namely, the first three lines in the equation can be simplified if one takes into account symmetries of E_{ijkl} and σ_{ij}. In the case of the elastic stiffness tensor E_{ijkl} major and both minor symmetries exist. In the case of the elastoplastic stiffness tensor, such symmetries exist if a flow rule is associated. If the flow rule is non–associated, only minor symmetries exist while major symmetry is destroyed[11]. As a matter of fact, both minor symmetries in E_{ijkl} are the only symmetries needed, and the first line of (102.19) can be rewritten as:

$$\begin{aligned}
& \bigcup_m \int_{V^m} \left(\left(\frac{1}{2} \left(H_{J,d}\ \bar{u}_{Jc} + H_{J,c}\ \bar{u}_{jd} \right) \right)\ E_{abcd}\ \left(\frac{1}{2} \left(H_{I,b}\ \delta\bar{u}_{Ia} + H_{I,a}\ \delta\bar{u}_{Ib} \right) \right) \right)\ dV^m = \\
= & \bigcup_m \int_{V^m} \left(H_{J,d}\ \bar{u}_{Jc} \right)\ E_{abcd}\ \left(H_{I,b}\ \delta\bar{u}_{Ia} \right)\ dV^m = \\
= & \bigcup_m \int_{V^m} \left(H_{I,b}\ \delta\bar{u}_{Ia} \right)\ E_{abcd}\ \left(H_{J,d}\ \bar{u}_{Jc} \right)\ dV^m
\end{aligned} \tag{102.20}$$

Similar simplifications are possible in the second and third line of the equation (102.19). Namely, in the second line both minor symmetries of E_{ijkl} can be used so that:

[11] for more on stiffness tensor symmetries, see sections (104.6.1, 104.3 and 104.4)

$$\begin{aligned}
&\bigcup_m \int_{V^m} \left(-E_{abcd}\ \epsilon^0_{cd}\ \left(\frac{1}{2} \left(H_{I,b}\ \delta\bar{u}_{Ia} + H_{I,a}\ \delta\bar{u}_{Ib} \right) \right) \right)\ dV^m = \\
= &\bigcup_m \int_{V^m} \left(-E_{abcd}\ \epsilon^0_{cd}\ \left(H_{I,b}\ \delta\bar{u}_{Ia} \right) \right)\ dV^m
\end{aligned} \tag{102.21}$$

and the third line can be simplified due to the symmetry in Cauchy stress tensor σ_{ij} as:

$$\begin{aligned}
&\bigcup_m \int_{V^m} \left(\sigma^0_{ab} \right)\ \left(\frac{1}{2} \left(H_{I,b}\ \delta\bar{u}_{Ia} + H_{I,a}\ \delta\bar{u}_{Ib} \right) \right)\ dV^m = \\
= &\bigcup_m \int_{V^m} \left(\sigma^0_{ab} \right)\ \left(H_{I,b}\ \delta\bar{u}_{Ia} \right)\ dV^m
\end{aligned} \tag{102.22}$$

After these simplifications, equation (102.19) looks like this:

$$\begin{aligned}
&\bigcup_m \int_{V^m} \left(H_{I,b}\ \delta\bar{u}_{Ia} \right)\ E_{abcd}\ \left(H_{J,d}\ \bar{u}_{Jc} \right)\ dV^m + \\
+ &\bigcup_m \int_{V^m} \left(-E_{abcd}\ \epsilon^0_{cd}\ \left(H_{I,b}\ \delta\bar{u}_{Ia} \right) \right)\ dV^m + \bigcup_m \int_{V^m} \left(\sigma^0_{ab} \right)\ \left(H_{I,b}\ \delta\bar{u}_{Ia} \right)\ dV^m = \\
= &\bigcup_m \int_{V^m} f^B_a\ \left(H_I \delta\bar{u}_{Ia} \right)\ dV^m - \bigcup_m \int_{V^m} H_J\ \ddot{\bar{u}}_{Ja}\ \rho\ H_I \delta\bar{u}_{Ia}\ dV^m + \bigcup_m \int_{S^m} f^S_a\ \left(H_I \delta\bar{u}_{Ia} \right)\ dS^m
\end{aligned} \tag{102.23}$$

or if unknown nodal accelerations[12] $\ddot{\bar{u}}_{Jc}$ and displacements $\bar{u}_{Jc}$ are left on the left hand side and all known quantities are moved to the right hand side:

$$\begin{aligned}
&\bigcup_m \int_{V^m} H_J\ \delta_{ac}\ \ddot{\bar{u}}_{Jc}\ \rho\ H_I \delta\bar{u}_{Ia}\ dV^m + \bigcup_m \int_{V^m} \left(H_{I,b}\ \delta\bar{u}_{Ia} \right)\ E_{abcd}\ \left(H_{J,d}\ \bar{u}_{Jc} \right)\ dV^m = \\
= &\bigcup_m \int_{V^m} f^B_a\ \left(H_I \delta\bar{u}_{Ia} \right)\ dV^m + \bigcup_m \int_{S^m} f^S_a\ \left(H_I \delta\bar{u}_{Ia} \right)\ dS^m + \\
+ &\bigcup_m \int_{V^m} \left(E_{abcd}\ \epsilon^0_{cd}\ \left(H_{I,b}\ \delta\bar{u}_{Ia} \right) \right)\ dV^m - \bigcup_m \int_{V^m} \left(\sigma^0_{ab} \right)\ \left(H_{I,b}\ \delta\bar{u}_{Ia} \right)\ dV^m
\end{aligned} \tag{102.24}$$

To obtain the equation for the unknown nodal generalized displacements from equation 102.24, invoke the virtual displacement theorem. This theorem states that virtual displacements are any, non

[12] It is noted that $\ddot{\bar{u}}_{Jc} = \delta_{ac}\ddot{\bar{u}}_{Ja}$ relationship was used here, where δ_{ac} is the Kronecker delta.

zero, kinematically admissible displacements. In that case, we can factor out nodal virtual displacements $\delta\bar{u}_{Ia}$ so that equation 102.24 becomes:

$$\begin{aligned}
&\left[\bigcup_m \int_{V^m} H_J\ \delta_{ac}\ \ddot{\bar{u}}_{Jc}\ \rho\ H_I\ dV^m + \bigcup_m \int_{V^m} \left(H_{I,b}\right)\ E_{abcd}\ \left(H_{J,d}\ \bar{u}_{Jc}\right)\ dV^m\right]\ \delta\bar{u}_{Ia} = \\
= &\bigcup_m \left[\int_{V^m} f_a^B\ H_I\ dV^m\right] \delta\bar{u}_{Ia} + \bigcup_m \left[\int_{S^m} f_a^S\ H_I\ dS^m\right] \delta\bar{u}_{Ia} + \\
+ &\bigcup_m \left[\int_{V^m} \left(E_{abcd}\ \epsilon^0_{cd}\ H_{I,b}\right)\ dV^m\right] \delta\bar{u}_{Ia} - \bigcup_m \left[\int_{V^m} \left(\sigma^0_{ab}\right)\ H_{I,b}\ dV^m\right] \delta\bar{u}_{Ia}
\end{aligned} \tag{102.25}$$

and now just cancel $\delta\bar{u}_{Ia}$ on both sides:

$$\begin{aligned}
&\bigcup_m \int_{V^m} H_J\ \ \delta_{ac}\ \rho\ H_I\ \ddot{\bar{u}}_{Jc} dV^m + \\
&\bigcup_m \int_{V^m} \left(H_{I,b}\right)\ E_{abcd}\ \left(H_{J,d}\ \bar{u}_{Jc}\right)\ dV^m = \\
= &\bigcup_m \int_{V^m} f_a^B\ H_I\ dV^m + \bigcup_m \int_{S^m} f_a^S\ H_I\ dS^m + \\
+ &\bigcup_m \int_{V^m} \left(E_{abcd}\ \epsilon^0_{cd}\ H_{I,b}\right)\ dV^m - \bigcup_m \int_{V^m} \left(\sigma^0_{ab}\right)\ H_{I,b}\ dV^m
\end{aligned} \tag{102.26}$$

One should also observe that in the first line of equation (102.26) generalized nodal accelerations $\ddot{\bar{u}}_{Jc}$ and generalized nodal displacements $\bar{u}_{Jc}$ are unknowns that are not subjected to integration so they can be factored out of the integral:

$$\begin{aligned}
&\bigcup_m \int_{V^m} H_J\ \delta_{ac}\ \rho\ H_I\ dV^m\ \ddot{\bar{u}}_{Jc} \\
+ &\bigcup_m \int_{V^m} H_{I,b}\ E_{abcd}\ H_{J,d}\ dV^m\ \bar{u}_{Jc} \\
= &\bigcup_m \int_{V^m} f_a^B\ H_I\ dV^m + \bigcup_m \int_{S^m} f_a^S\ H_I\ dS^m + \\
+ &\bigcup_m \int_{V^m} \left(E_{abcd}\ \epsilon^0_{cd}\ H_{I,b}\right)\ dV^m - \bigcup_m \int_{V^m} \left(\sigma^0_{ab}\right)\ H_{I,b}\ dV^m
\end{aligned} \tag{102.27}$$

We can now define several tensors from equation (102.27):

$$ {}^{(m)}M_{IacJ} = \int_{V^m} H_J \; \delta_{ac} \; \rho \; H_I \; dV^m \tag{102.28} $$

$$ {}^{(m)}K_{IacJ} = \int_{V^m} H_{I,b} \; E_{abcd} \; H_{J,d} \; dV^m \tag{102.29} $$

$$ {}^{(m)}F^{B}_{Ia} = \int_{V^m} f^{B}_{a} \; H_I \; dV^m \tag{102.30} $$

$$ {}^{(m)}F^{S}_{Ia} = \int_{S^m} f^{S}_{a} \; H_I \; dS^m \tag{102.31} $$

$$ {}^{(m)}F^{\epsilon^0_{mn}}_{Ia} = \int_{V^m} E_{abcd} \; \epsilon^0_{cd} \; H_{I,b} \; dV^m \tag{102.32} $$

$$ {}^{(m)}F^{\sigma^0_{mn}}_{Ia} = \int_{V^m} \sigma^0_{ab} \; H_{I,b} \; dV^m \tag{102.33} $$

where ${}^{(m)}M_{IacJ}$ is the element mass tensor, ${}^{(m)}K_{IacJ}$ is the element stiffness tensor, ${}^{(m)}F^{B}_{Ia}$ is the tensor of element body forces, ${}^{(m)}F^{S}_{Ia}$ is the tensor of element surface forces, ${}^{(m)}F^{\epsilon^0_{mn}}_{Ia}$ is the tensor of element initial strain effects, ${}^{(m)}F^{\sigma^0_{mn}}_{Ia}$ is the tensor of element initial stress effects. Now equation (102.27) becomes:

$$ \bigcup_{(m)} {}^{(m)}M_{IacJ} \; \ddot{\bar{u}}_{Jc} + \bigcup_{(m)} {}^{(m)}K_{IacJ} \; \bar{u}_{Jc} = \bigcup_{m} {}^{(m)}F^{B}_{Ia} + \bigcup_{m} {}^{(m)}F^{S}_{Ia} + \bigcup_{m} {}^{(m)}F^{\epsilon^0_{mn}}_{Ia} - \bigcup_{m} {}^{(m)}F^{\sigma^0_{mn}}_{Ia} \tag{102.34} $$

By summing[13] all the relevant tensors, a well known equation is obtained:

$$ \begin{aligned} M_{AacB} \; \ddot{\bar{u}}_{Bc} + K_{AacB} \; \bar{u}_{Bc} &= F_{Aa} \\ A, B &= 1, 2, \ldots, \# \text{ of nodes} \\ a, c &= 1, \ldots, \# \text{ of dimensions (1, 2 or 3)} \end{aligned} \tag{102.35} $$

where:

[13] Summation of the element volume integrals expresses the direct addition of the element tensors to obtain global, system tensors. This method of direct addition is usually referred to as the direct stiffness method.

$$M_{AacB} = \bigcup_{m}{}^{(m)}M_{IacJ} \quad ; \quad K_{AacB} = \bigcup_{m}{}^{(m)}K_{IacJ} \tag{102.36}$$

are the system mass and stiffness tensors, respectively, $\ddot{\bar{u}}_{Bc}$ is the tensor of unknown nodal accelerations, and $\bar{u}_{Bc}$ is the tensor of unknown generalized nodal displacements, while the load tensor is given as:

$$F_{Aa} = \bigcup_{m}{}^{(m)}F^{B}_{Ia} + \bigcup_{m}{}^{(m)}F^{S}_{Ia} + \bigcup_{m}{}^{(m)}F^{\epsilon^0_{mn}}_{Ia} - \bigcup_{m}{}^{(m)}F^{\sigma^0_{mn}}_{Ia} \tag{102.37}$$

After assembling the system of equations in (102.36), it is relatively easy to solve for the unknown displacements $\bar{u}_{Lc}$ either for static or fully dynamic case. It is also very important to note that in all previous equations, omissions of inertial force term (all terms with ρ) will yield static equilibrium equations. Description of solutions procedures for static linear and nonlinear problems are described in some detail in chapter 107. In addition to that, solution procedures for dynamic, linear and nonlinear problems are described in some detail in chapter 108.

A note on the final form of the tensors used is in order. In order to use readily available system of equation solvers equation (102.36) will be rewritten in the following form:

$$M_{PQ}\,\ddot{\bar{u}}_{P} + K_{PQ}\,\bar{u}_{P} = F_{Q} \quad P,Q = 1,2,\ldots,(\#ofDOFs)N \tag{102.38}$$

where M_{PQ} is system mass matrix, K_{PQ} is system stiffness matrix and F_Q is the loading vector. Matrix form of equation 102.36, presented as equation 102.38 is obtained flattening the system mass tensor M_{AacB}, system stiffness tensor K_{AacB}, unknown acceleration tensor $\ddot{\bar{u}}_{Bc}$, unknown displacement tensor $\bar{u}_{Bc}$ and the system loading tensor F_{Aa}. Flattening from the fourth order mass/stiffness tensors to two-dimensional mass/stiffness matrix is done by simply performing appropriate (re–) numbering of nodal DOFs in each dimension. A similar approach is used for unknown accelerations/displacements and loadings.

102.3.1 Static Analysis: Internal and External Loads.

Internal and external loading tensors is defined as:

$$(f_{Ia})_{int} = \bigcup_{(m)} {}^{(m)}K_{IacJ}\ \bar{u}_{Jc} = \bigcup_{m} \int_{V^m} \sigma_{ab}\ H_{I,b}\ dV^m \tag{102.39}$$

$$(f_{Ia})_{ext} = \bigcup_{m} {}^{(m)}F^{B}_{Ia} + \bigcup_{m} {}^{(m)}F^{S}_{Ia} + \bigcup_{m} {}^{(m)}F^{\epsilon^0_{mn}}_{Ia} - \bigcup_{m} {}^{(m)}F^{\sigma^0_{mn}}_{Ia} \tag{102.40}$$

where $(f_{Ia})_{int}$ is the internal force tensor and $(f_{Ia})_{ext}$ is the external force tensor. Equilibrium is obtained when residual:

$$r_{Ia}(\bar{u}_{Jc}, \lambda) = (f_{Ia}\,(\bar{u}_{Jc}))_{int} - \lambda\,(f_{Ia})_{ext} \tag{102.41}$$

is equal to zero, $\mathbf{r}(\mathbf{u}, \lambda) = 0$. The same equation in flattened form yields:

$$\mathbf{r}(\mathbf{u}, \lambda) = \mathbf{f}_{int}(\mathbf{u}) - \lambda \mathbf{f}_{ext} = 0 \tag{102.42}$$

102.4 Isoparametric Solid Finite Elements

102.4.1 8 Node Brick

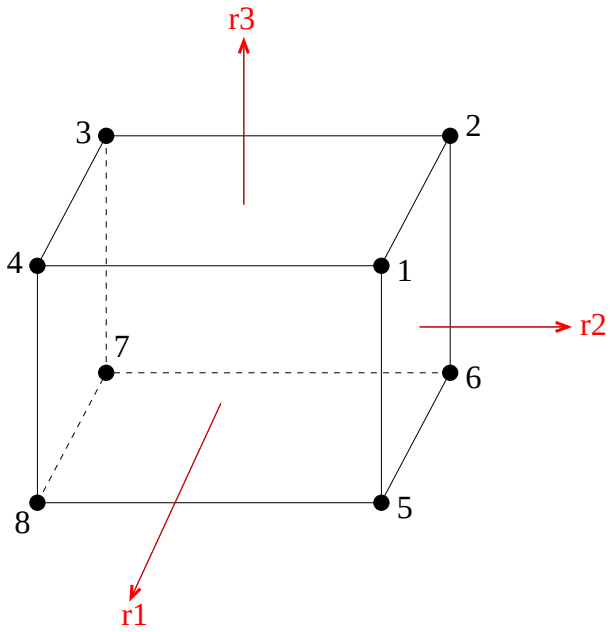

Figure 102.3: 8 node brick element

Table 102.1: Values of r_1, r_2, and r_3 at each of the eight nodes

Node	r_1	r_2	r_3
1	+1	+1	+1
2	-1	+1	+1
3	-1	-1	+1
4	+1	-1	+1
5	+1	+1	-1
6	-1	+1	-1
7	-1	-1	-1
8	+1	-1	-1

Shape function of the nodes which i indicates the node number:

$$N_i^{(e)} = \frac{1}{8}(1 + r_1(r_1)_i)(1 + r_2(r_2)_i)(1 + r_3(r_3)_i) \tag{102.43}$$

102.4.2 Collapsed 8 Node Brick

It is sometimes required to mesh finite element models using collapsed brick elements. Collapsed brick elements are finite elements that do not feature all 8 nodes, rather some nodes are merged. This is done to help generate meshes for complicated geometries where it is impossible to rely on solid bricks with eight (8) nodes only. For example, SASSI2000 (System for Analysis of Soil-Structure Interaction) program (Ostadan, 2007) uses such elements. For example, solid elements with 7, 6, and 5 nodes are used extensively and are created by collapsing/combining nodes of 8 node brick into solid elements with 7, 6 or 5 nodes. There are three types of collapsed SASSI 8 node brick element, as shown in Figure 102.4.

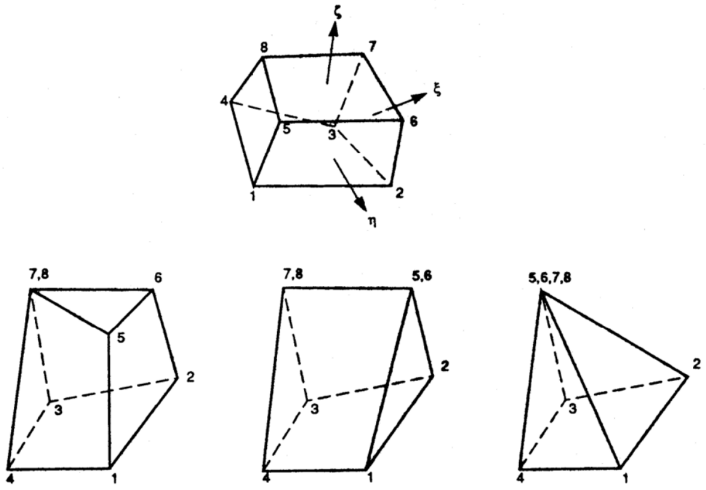

Figure 102.4: Three types of collapsed brick elements in SASSI (Ostadan, 2007).

Verification tests for collapsed brick finite elements are provided in verification section ?? on page 1547.

102.4.3 20 Node Brick

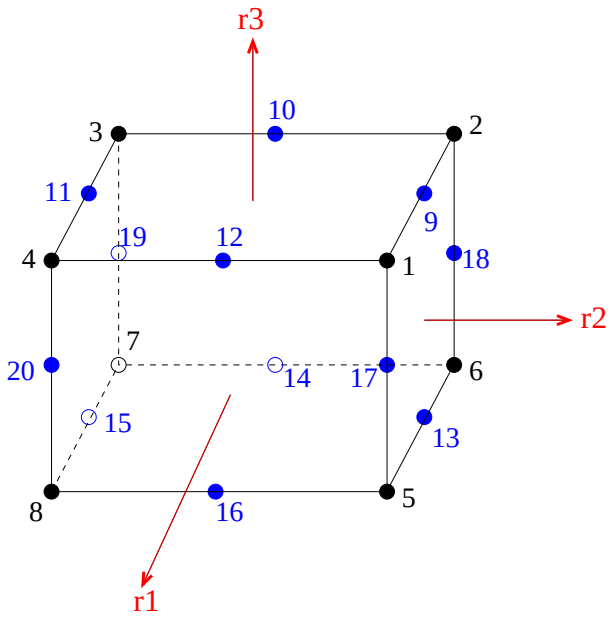

Figure 102.5: 20 node brick element

Table 102.2: Values of r_1, r_2, and r_3 at each of the 9^{th} to 20^{th} nodes

Node	r_1	r_2	r_3
9	0	+1	+1
10	-1	0	+1
11	0	-1	+1
12	+1	0	+1
13	0	+1	-1
14	-1	0	-1
15	0	-1	-1
16	+1	0	-1
17	+1	+1	0
18	-1	+1	0
19	-1	-1	0
20	+1	-1	0

Shape function of the 8 corner nodes (1 to 8) which i indicates the node number:

$$N_i^{(e)} = \frac{1}{8}(1 + r_1(r_1)_i)(1 + r_2(r_2)_i)(1 + r_3(r_3)_i)(r_1(r_1)_i + r_2(r_2)_i + r_3(r_3)_i - 2) \tag{102.44}$$

Shape function of the node numbers 9, 11, 13, and 15 which i indicates the node number:

$$N_i^{(e)} = \frac{1}{4}(1 - r_1^2)(1 + r_2(r_2)_i)(1 + r_3(r_3)_i) \tag{102.45}$$

Shape function of the node numbers 10, 12, 14, and 16 which i indicates the node number:

$$N_i^{(e)} = \frac{1}{4}(1 - r_2^2)(1 + r_1(r_1)_i)(1 + r_3(r_3)_i) \tag{102.46}$$

Shape function of the node numbers 17, 18, 19, and 20 which i indicates the node number:

$$N_i^{(e)} = \frac{1}{4}(1 - r_3^2)(1 + r_1(r_1)_i)(1 + r_2(r_2)_i) \tag{102.47}$$

102.4.4 27 Node Brick

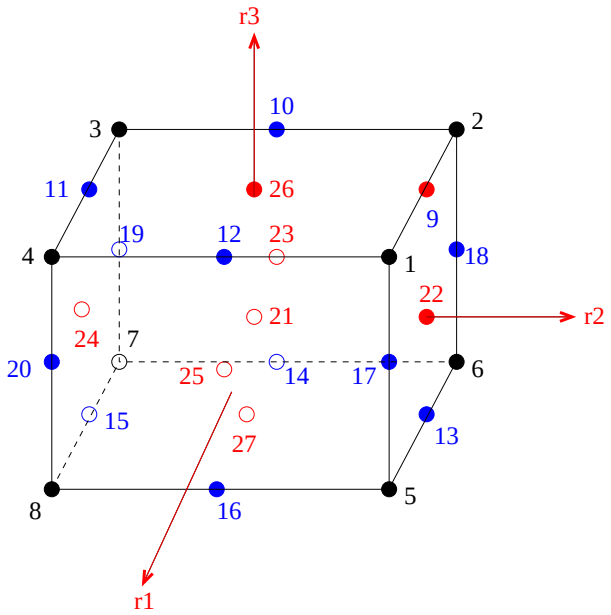

Figure 102.6: 27 node brick element

Table 102.3: Values of r_1, r_2, and r_3 at each of the 21^{th} to 27^{th} nodes

Node	r_1	r_2	r_3
21	0	0	0
22	0	+1	0
23	-1	0	0
24	0	-1	0
25	+1	0	0
26	0	0	+1
27	0	0	-1

Shape function of the 8 corner nodes (1 to 8) which i indicates the node number:

$$N_i^{(e)} = \frac{1}{8}(1 + r_1(r_1)_i)(1 + r_2(r_2)_i)(1 + r_3(r_3)_i)(r_1(r_1)_i)(r_2(r_2)_i)(r_3(r_3)_i) \tag{102.48}$$

Shape function of the node numbers 9, 11, 13, and 15 which i indicates the node number:

$$N_i^{(e)} = \frac{1}{4}(1 - r_1^2)(1 + r_2(r_2)_i)(1 + r_3(r_3)_i)(r_2(r_2)_i)(r_3(r_3)_i) \tag{102.49}$$

Shape function of the node numbers 10, 12, 14, and 16 which i indicates the node number:

$$N_i^{(e)} = \frac{1}{4}(1 + r_1(r_1)_i)(1 - r_2^2)(1 + r_3(r_3)_i)(r_1(r_1)_i)(r_3(r_3)_i) \tag{102.50}$$

Shape function of the node numbers 17, 18, 19, and 20 which i indicates the node number:

$$N_i^{(e)} = \frac{1}{4}(1 + r_1(r_1)_i)(1 + r_2(r_2)_i)(1 - r_3^2)(r_1(r_1)_i)(r_2(r_2)_i) \tag{102.51}$$

Shape function of the node number 21:

$$N_{21}^{(e)} = (1 - r_1^2)(1 - r_2^2)(1 - r_3^2) \tag{102.52}$$

Shape function of the node numbers 22 and 24 which i indicates the node number:

$$N_i^{(e)} = \frac{1}{2}(1 - r_1^2)(1 + r_2(r_2)_i)(1 - r_3^2)(r_2(r_2)_i) \tag{102.53}$$

Shape function of the node numbers 23 and 25 which i indicates the node number:

$$N_i^{(e)} = \frac{1}{2}(1 + r_1(r_1)_i)(1 - r_2^2)(1 - r_3^2)(r_1(r_1)_i) \tag{102.54}$$

Shape function of the node numbers 26 and 27 which i indicates the node number:

$$N_i^{(e)} = \frac{1}{2}(1 - r_1^2)(1 - r_2^2)(1 + r_3(r_3)_i)(r_3(r_3)_i) \tag{102.55}$$

102.4.5 Isoparametric 8 – 20 Node Finite Element

The basic procedure in the isoparametric[14] finite element formulation is to express the element coordinates and element displacements in the form of interpolations using the local three dimensional[15] coordinate system of the element. Considering the general 3D element, the coordinate interpolations, using indicial notation[16] are:

[14] name isoparametric comes from the fact that both displacements and coordinates are defined in terms of nodal values. Superparametric and subparametric finite elements exists also.

[15] in the case of element presented here, that is isoparametric 8 – 20 node finite element.

[16] Einstein's summation rule is implied unless stated differently, all lower case indices ($i, j, p, q, m, n, o, r, s, t, \dots$) can have values of 1, 2, 3, and values for capital letter indices will be specified where need be.

$$x_i = H_A(r_k)\ \bar{x}_{Ai} \tag{102.56}$$

where $A = 1, 2, \ldots, n$ and n is the total number of nodes associated with that specific element, $\bar{x}_{Ai}$ is the i-th coordinate of node A, $i = 1, 2, 3$, $k = 1, 2, 3$ and H_A are the interpolation functions defined in local coordinate system of the element, with variables r_1, r_2 and r_3 varying from –1 to +1.

The interpolation functions H_A for the isoparametric 8–20 node are the so called serendipity interpolation functions mainly because they were derived by inspection. For the finite element with nodes numbered as in Figure (102.7) they are given[17] in the following set of formulae:

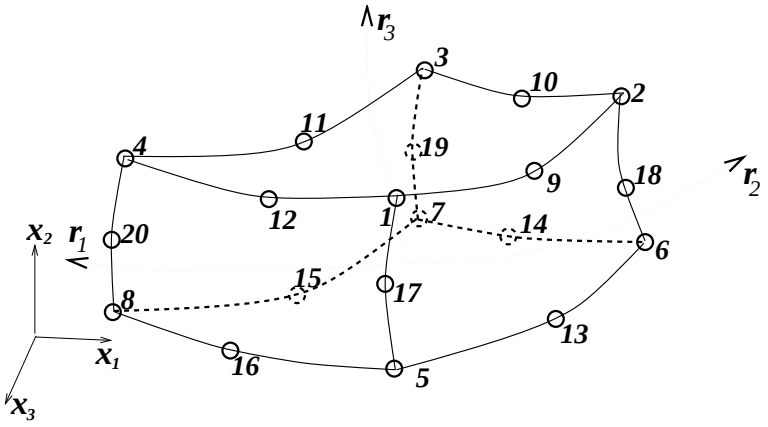

Figure 102.7: Isoparametric 8–20 node brick element in global and local coordinate systems

$$H_{20} = \frac{isp(20)\ (1+r_1)\ (1-r_2)\ \left(1-r_3^2\right)}{4} \qquad H_{19} = \frac{isp(19)\ (1-r_1)\ (1-r_2)\ \left(1-r_3^2\right)}{4}$$

$$H_{18} = \frac{isp(18)\ (1-r_1)\ (1+r_2)\ \left(1-r_3^2\right)}{4} \qquad H_{17} = \frac{isp(17)\ (1+r_1)\ (1+r_2)\ \left(1-r_3^2\right)}{4}$$

$$H_{16} = \frac{isp(16)\ (1+r_1)\ \left(1-r_2^2\right)\ (1-r_3)}{4} \qquad H_{15} = \frac{isp(15)\ \left(1-r_1^2\right)\ (1-r_2)\ (1-r_3)}{4}$$

$$H_{14} = \frac{isp(14)\ (1-r_1)\ \left(1-r_2^2\right)\ (1-r_3)}{4} \qquad H_{13} = \frac{isp(13)\ \left(1-r_1^2\right)\ (1+r_2)\ (1-r_3)}{4}$$

$$H_{12} = \frac{isp(12)\ (1+r_1)\ \left(1-r_2^2\right)\ (1+r_3)}{4} \qquad H_{11} = \frac{isp(11)\ \left(1-r_1^2\right)\ (1-r_2)\ (1+r_3)}{4}$$

$$H_{10} = \frac{isp(10)\ (1-r_1)\ \left(1-r_2^2\right)\ (1+r_3)}{4} \qquad H_9 = \frac{isp(9)\ \left(1-r_1^2\right)\ (1+r_2)\ (1+r_3)}{4}$$

[17] for more details see Bathe (1982).

$$
\begin{aligned}
H_8 &= \frac{(1+r_1)\,(1-r_2)\,(1-r_3)}{8} + \frac{-H_{15}-H_{16}-H_{20}}{2} \\
H_7 &= \frac{(1-r_1)\,(1-r_2)\,(1-r_3)}{8} + \frac{-H_{14}-H_{15}-H_{19}}{2} \\
H_6 &= \frac{(1-r_1)\,(1+r_2)\,(1-r_3)}{8} + \frac{-H_{13}-H_{14}-H_{18}}{2} \\
H_5 &= \frac{(1+r_1)\,(1+r_2)\,(1-r_3)}{8} + \frac{-H_{13}-H_{16}-H_{17}}{2} \\
H_4 &= \frac{(1+r_1)\,(1-r_2)\,(1+r_3)}{8} + \frac{-H_{11}-H_{12}-H_{20}}{2} \\
H_3 &= \frac{(1-r_1)\,(1-r_2)\,(1+r_3)}{8} + \frac{-H_{10}-H_{11}-H_{19}}{2} \\
H_2 &= \frac{(1-r_1)\,(1+r_2)\,(1+r_3)}{8} + \frac{-H_{10}-H_{18}-H_9}{2} \\
H_1 &= \frac{(1+r_1)\,(1+r_2)\,(1+r_3)}{8} + \frac{-H_{12}-H_{17}-H_9}{2}
\end{aligned}
$$

where r_1, r_2 and r_3 are the axes of natural, local, curvilinear coordinate system and $isp\,(nod\_num)$ is boolean function that returns +1 if node number (nod_num) is present and 0 if node number (nod_num) is not present.

To be able to evaluate various important element tensors[18], to calculate the strain–displacement transformation tensor[19] is needed. The element strains are obtained in terms of derivatives of element displacements with respect to the local coordinate system. Because the element displacements are defined in the local coordinate system, there is a need to relate global x_1, x_2 and x_3 derivatives to the r_1, r_2 and r_3 derivatives. In order to obtain derivatives with respect to global coordinate system, i.e. $\frac{\partial}{\partial x_a}$, use chain rule for differentiation in the following form:

$$
\frac{\partial}{\partial x_k} = \frac{\partial r_a}{\partial x_k}\frac{\partial}{\partial r_a} = J^{-1}_{ak}\,\frac{\partial}{\partial r_a} \tag{102.57}
$$

while the inverse relation is:

$$
\frac{\partial}{\partial r_k} = \frac{\partial x_a}{\partial r_k}\frac{\partial}{\partial x_a} = J_{ak}\,\frac{\partial}{\partial x_a} \tag{102.58}
$$

where J_{ak} is the Jacobian operator relating local coordinate derivatives to the global coordinate derivatives:

[18] i.e. ${}^{(m)}K_{IacJ}$, ${}^{(m)}F^{B}_{Ia}$, ${}^{(m)}F^{S}_{Ia}$, ${}^{(m)}F^{\epsilon^0_{mn}}_{Ia}$, ${}^{(m)}F^{\sigma^0_{mn}}_{Ia}$, that are defined in chapter (102.3).

[19] from the equation $\hat{\epsilon}_{ab} = \frac{1}{2}\left(\left(H_{I,b}\,\bar{u}_{Ia}\right) + \left(H_{I,a}\,\bar{u}_{Ib}\right)\right)$

$$J_{ak} = \frac{\partial x_a}{\partial r_k} = \begin{bmatrix} \frac{\partial x_1}{\partial r_1} & \frac{\partial x_2}{\partial r_1} & \frac{\partial x_3}{\partial r_1} \\ \frac{\partial x_1}{\partial r_2} & \frac{\partial x_2}{\partial r_2} & \frac{\partial x_3}{\partial r_2} \\ \frac{\partial x_1}{\partial r_3} & \frac{\partial x_2}{\partial r_3} & \frac{\partial x_3}{\partial r_3} \end{bmatrix} \tag{102.59}$$

The existence of equation (102.57) requires that the inverse of J_{ak} exists and that inverse exists provided that there is a one–to–one[20] correspondence between the local and the global coordinates of element.

It should be pointed out that except for the very simple cases, volume and surface element tensor[21] integrals are evaluated by means of numerical integration[22] Numerical integration rules is quite a broad subject and will not be covered here[23].

102.4.6 Isoparametric 8 - 27 Node Finite Element

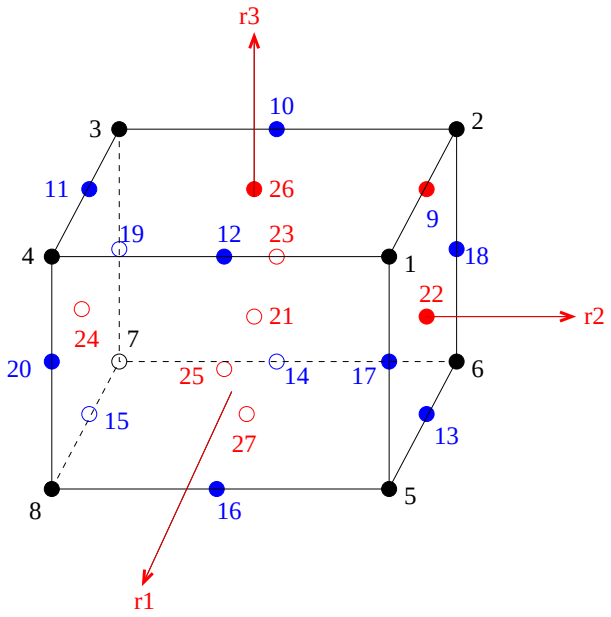

Figure 102.8: 8-27 variable node brick element

[20] unique.

[21] as defined in chapter (102.3) by equations (102.29), (102.30), (102.31), (102.32) and (102.33).

[22] Gauss–Legendre, Newton–Coates, Lobatto are among the most used integration rules.

[23] nice explanation with examples is given in Bathe (1982).

$$
\begin{aligned}
H_1 &= \frac{(1+r_1)(1+r_2)(1+r_3)}{8} - \frac{H_9+H_{12}+H_{17}}{2} - \frac{H_{22}+H_{25}+H_{26}}{4} - \frac{H_{21}}{8}\\
H_2 &= \frac{(1-r_1)(1+r_2)(1+r_3)}{8} - \frac{H_9+H_{10}+H_{18}}{2} - \frac{H_{22}+H_{23}+H_{26}}{4} - \frac{H_{21}}{8}\\
H_3 &= \frac{(1-r_1)(1-r_2)(1+r_3)}{8} - \frac{H_{10}+H_{11}+H_{19}}{2} - \frac{H_{23}+H_{24}+H_{26}}{4} - \frac{H_{21}}{8}\\
H_4 &= \frac{(1+r_1)(1-r_2)(1+r_3)}{8} - \frac{H_{11}+H_{12}+H_{20}}{2} - \frac{H_{24}+H_{25}+H_{26}}{4} - \frac{H_{21}}{8}\\
H_5 &= \frac{(1+r_1)(1+r_2)(1-r_3)}{8} - \frac{H_{13}+H_{16}+H_{17}}{2} - \frac{H_{22}+H_{25}+H_{27}}{4} - \frac{H_{21}}{8}\\
H_6 &= \frac{(1-r_1)(1+r_2)(1-r_3)}{8} - \frac{H_{13}+H_{14}+H_{18}}{2} - \frac{H_{22}+H_{23}+H_{27}}{4} - \frac{H_{21}}{8}\\
H_7 &= \frac{(1-r_1)(1-r_2)(1-r_3)}{8} - \frac{H_{14}+H_{15}+H_{19}}{2} - \frac{H_{23}+H_{24}+H_{27}}{4} - \frac{H_{21}}{8}\\
H_8 &= \frac{(1+r_1)(1-r_2)(1-r_3)}{8} - \frac{H_{15}+H_{16}+H_{20}}{2} - \frac{H_{24}+H_{25}+H_{27}}{4} - \frac{H_{21}}{8}
\end{aligned}
$$

$$
\begin{aligned}
H_9 &= \frac{1}{4}(1-r_1^2)(1+r_2)(1+r_3) - \frac{H_{22}+H_{26}}{2} - \frac{H_{21}}{4}\\
H_{10} &= \frac{1}{4}(1-r_2^2)(1-r_1)(1+r_3) - \frac{H_{23}+H_{26}}{2} - \frac{H_{21}}{4}\\
H_{11} &= \frac{1}{4}(1-r_1^2)(1-r_2)(1+r_3) - \frac{H_{24}+H_{26}}{2} - \frac{H_{21}}{4}\\
H_{12} &= \frac{1}{4}(1-r_2^2)(1+r_1)(1+r_3) - \frac{H_{25}+H_{26}}{2} - \frac{H_{21}}{4}\\
H_{13} &= \frac{1}{4}(1-r_1^2)(1+r_2)(1-r_3) - \frac{H_{22}+H_{27}}{2} - \frac{H_{21}}{4}\\
H_{14} &= \frac{1}{4}(1-r_2^2)(1-r_1)(1-r_3) - \frac{H_{23}+H_{27}}{2} - \frac{H_{21}}{4}\\
H_{15} &= \frac{1}{4}(1-r_1^2)(1-r_2)(1-r_3) - \frac{H_{24}+H_{27}}{2} - \frac{H_{21}}{4}\\
H_{16} &= \frac{1}{4}(1-r_2^2)(1+r_1)(1-r_3) - \frac{H_{25}+H_{27}}{2} - \frac{H_{21}}{4}
\end{aligned}
$$

$$
\begin{aligned}
H_{17} &= \frac{1}{4}(1-r_3^2)(1+r_1)(1+r_2) - \frac{H_{22}+H_{25}}{2} - \frac{H_{21}}{4}\\
H_{18} &= \frac{1}{4}(1-r_3^2)(1-r_1)(1+r_2) - \frac{H_{22}+H_{23}}{2} - \frac{H_{21}}{4}\\
H_{19} &= \frac{1}{4}(1-r_3^2)(1-r_1)(1-r_2) - \frac{H_{23}+H_{24}}{2} - \frac{H_{21}}{4}\\
H_{20} &= \frac{1}{4}(1-r_3^2)(1+r_1)(1-r_2) - \frac{H_{24}+H_{25}}{2} - \frac{H_{21}}{4}
\end{aligned}
$$

$$
H_{21} = (1-r_1^2)(1-r_2^2)(1-r_3^2)
$$

$$H_{22} = \frac{1}{2}(1-r_1^2)(1+r_2)(1-r_3^2)r_2$$
$$H_{23} = -\frac{1}{2}(1-r_1)(1-r_2^2)(1-r_3^2)r_1$$
$$H_{24} = -\frac{1}{2}(1-r_1^2)(1-r_2)(1-r_3^2)r_2$$
$$H_{25} = \frac{1}{2}(1+r_1)(1-r_2^2)(1-r_3^2)r_1$$
$$H_{26} = \frac{1}{2}(1-r_1^2)(1-r_2^2)(1+r_3)r_3$$
$$H_{27} = -\frac{1}{2}(1-r_1^2)(1-r_2^2)(1-r_3)r_3$$

102.4.7 Surface Loads for Solid Bricks

To apply surface load on brick elements, equivalent nodal forces have to be applied instead of the surface load. The equivalent force of the i-th node F_i is given by the following equation with shape function H_i and load distribution function f .

$$F_i = \int_S f H_i ds \tag{102.60}$$

Assuming that the load distribution is uniform

$$F_i = f \int_S H_i ds \tag{102.61}$$

Furthermore, when the magnitude of the load per unit area is 1, and the size of the element is $1 \times 1 \times 1$, equivalent nodal forces are given as shown in Figure 102.9 for 8 node brick element, 20 brick element, and 27 nodes brick element.

Figure 102.9 shows cases of normal loads on vertical upper surface (with nodes: 1, 2, 3, 4 for 8 node brick; 1, 2, 3, 4, 9, 10, 11, and 12 for 20 node brick; and 1, 2, 3, 4, 9, 10, 11, 12 and 26 for the 27 node brick).

Nodal loads from uniform surface loads for 27 node brick are obtained as:

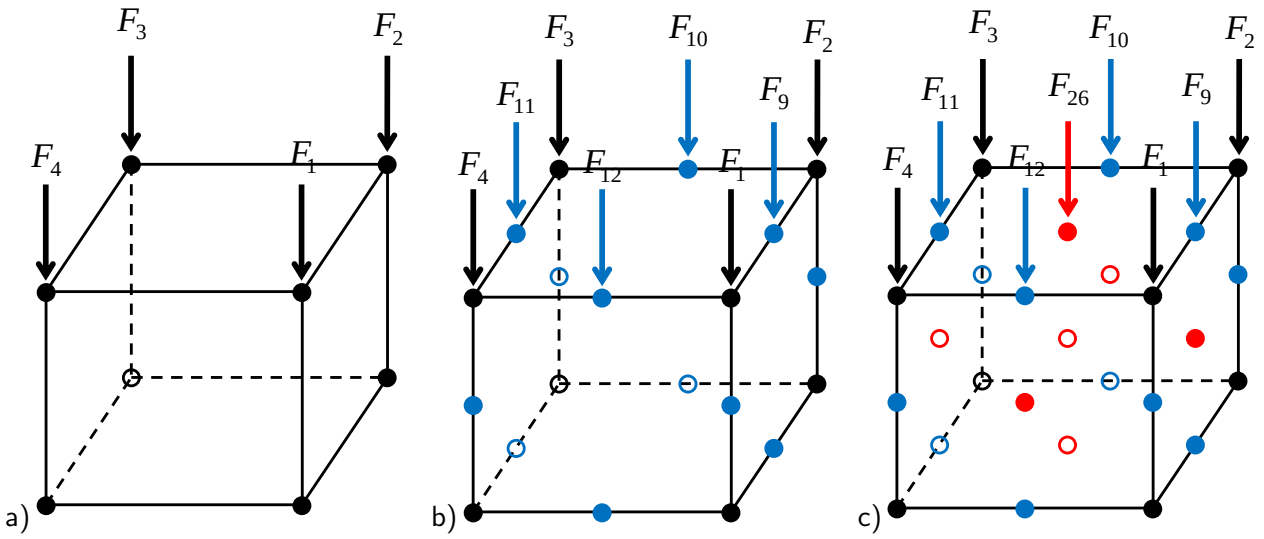

Figure 102.9: Nodal loads for brick elements: (a) $F_1 = F_2 = F_3 = F_4 = +1/4$; (b) $F_1 = F_2 = F_3 = F_4 = -\frac{1}{12}$, $F_9 = F_{10} = F_{11} = F_{12} == +\frac{1}{3}$; (c) $F_1 = F_2 = F_3 = F_4 = +\frac{1}{36}$, $F_9 = F_{10} = F_{11} = F_{12} == +\frac{1}{9}, F_{36} = \frac{4}{9}$.

- for nodes 1, 2, 3, and 4, $N_i^{(e)} = \frac{1}{8}(1 + r_1(r_1)_i)(1 + r_2(r_2)_i)(1 + r_3(r_3)_i)(r_1(r_1)_i)(r_2(r_2)_i)(r_3(r_3)_i)$

$$\begin{aligned}\int_{-1}^{+1} H_i dS &= \\ &= \frac{1}{8}(1 + r_3(r_3)_i)(r_3(r_3)_i)\int_{-1}^{+1}\int_{-1}^{+1}(1 + r_1(r_1)_i)(1 + r_2(r_2)_i)(r_1(r_1)_i)(r_2(r_2)_i)(r_2(r_2)_i)dr_1dr_2 \\ &= \frac{1}{8}(1 + r_3(r_3)_i)(r_3(r_3)_i)((r_1)_i)^2((r_2)_i)^2(\frac{2}{3})^2 \\ &= \frac{1}{18}(1 + r_3(r_3)_i)(r_3(r_3)_i)((r_1)_i)^2((r_2)_i)^2 \end{aligned} \tag{102.62}$$

- for nodes 9, 10, 11 and 12, $N_i^{(e)} = \frac{1}{4}(1 - r_1^2)(1 + r_2(r_2)_i)(1 + r_3(r_3)_i)(r_2(r_2)_i)(r_3(r_3)_i)$

$$\begin{aligned}\int_{-1}^{+1} H_i dS &= \\ &= \frac{1}{4}(1 + r_3(r_3)_i)(r_3(r_3)_i)\int_{-1}^{+1}(1 - r_1^2)(1 + r_2(r_2)_i)(r_2(r_2)_i)dr_1dr_2 \\ &= \frac{1}{8}(1 + r_3(r_3)_i)(r_3(r_3)_i)((r_2)_i)^2(\frac{4}{3})(\frac{2}{3}) \\ &= \frac{2}{9}(1 + r_3(r_3)_i)(r_3(r_3)_i)((r_2)_i)^2 \end{aligned} \tag{102.63}$$

- for nodes 26 $N_i^{(e)} = \frac{1}{2}(1-r_1^2)(1-r_2^2)(1+r_3(r_3)_i)(r_3(r_3)_i)$

$$\begin{aligned}\int_{-1}^{+1} H_i dS &= \\ &= \frac{1}{4}(1+r_3(r_3)_i)(r_3(r_3)_i)\int_{-1}^{+1}\int_{-1}^{+1}(1-r_1^2)(1-r_2^2)dr_1dr_2 \\ &= \frac{1}{8}(1+r_3(r_3)_i)(r_3(r_3)_i)(\frac{4}{3})(\frac{4}{3}) \\ &= \frac{8}{9}(1+r_3(r_3)_i)(r_3(r_3)_i) \end{aligned} \quad (102.64)$$

102.5 Numerical Integration for Solid Brick Elements

Gauss integration rule, see Bathe (1996), section 5.5.3. While using the regular Newton-Coates integration formula, one uses $(n+1)$ equally spaced points to integrate exactly polynomial of order n. On the other hand, while using the Gauss integration formula, one uses n unequally spaced points to integrate exactly polynomial of order $(2n-1)$.

102.6 Two Node, 3D Truss Finite Element

Bathe and Wilson (1976); Bathe (1982)

102.7 3D Beam-Column Finite Element, 12 Degrees of Freedom

Bathe and Wilson (1976); Bathe (1982); Przemieniecki (1985)

Stiffness Matrix: Equation 102.65

Mass Matrix: Equation 102.66

$$
[K] = \begin{bmatrix}
\frac{EA}{L} & 0 & 0 & 0 & 0 & 0 & -\frac{EA}{L} & 0 & 0 & 0 & 0 & 0 \\
0 & \frac{12EI_z}{L^3} & 0 & 0 & 0 & \frac{6EI_z}{L^2} & 0 & -\frac{12EI_z}{L^3} & 0 & 0 & 0 & \frac{6EI_z}{L^2} \\
0 & 0 & \frac{12EI_y}{L^3} & 0 & -\frac{6EI_y}{L^2} & 0 & 0 & 0 & -\frac{12EI_y}{L^3} & 0 & -\frac{6EI_y}{L^2} & 0 \\
0 & 0 & 0 & \frac{GJ_x}{L} & 0 & 0 & 0 & 0 & 0 & -\frac{GJ_x}{L} & 0 & 0 \\
0 & 0 & -\frac{6EI_y}{L^2} & 0 & \frac{4EI_y}{L} & 0 & 0 & 0 & \frac{6EI_y}{L^2} & 0 & \frac{2EI_y}{L} & 0 \\
0 & \frac{6EI_z}{L^2} & 0 & 0 & 0 & \frac{4EI_z}{L} & 0 & -\frac{6EI_z}{L^2} & 0 & 0 & 0 & \frac{2EI_z}{L} \\
-\frac{EA}{L} & 0 & 0 & 0 & 0 & 0 & \frac{EA}{L} & 0 & 0 & 0 & 0 & 0 \\
0 & -\frac{12EI_z}{L^3} & 0 & 0 & 0 & -\frac{6EI_z}{L^2} & 0 & \frac{12EI_z}{L^3} & 0 & 0 & 0 & -\frac{6EI_z}{L^2} \\
0 & 0 & -\frac{12EI_y}{L^3} & 0 & \frac{6EI_y}{L^2} & 0 & 0 & 0 & \frac{12EI_y}{L^3} & 0 & \frac{6EI_y}{L^2} & 0 \\
0 & 0 & 0 & -\frac{GJ_x}{L} & 0 & 0 & 0 & 0 & 0 & \frac{GJ_x}{L} & 0 & 0 \\
0 & 0 & -\frac{6EI_y}{L^2} & 0 & \frac{2EI_y}{L} & 0 & 0 & 0 & \frac{6EI_y}{L^2} & 0 & \frac{4EI_y}{L} & 0 \\
0 & \frac{6EI_z}{L^2} & 0 & 0 & 0 & \frac{2EI_z}{L} & 0 & -\frac{6EI_z}{L^2} & 0 & 0 & 0 & \frac{4EI_z}{L}
\end{bmatrix} \tag{102.65}
$$

$$
[M] = \rho AL \begin{bmatrix}
\frac{1}{3} & 0 & 0 & 0 & 0 & 0 & \frac{1}{6} & 0 & 0 & 0 & 0 & 0 \\
0 & \frac{13}{35}+\frac{6I_z}{5Al^2} & 0 & 0 & 0 & \frac{11l}{210}+\frac{I_z}{10Al} & 0 & \frac{9}{70}-\frac{6I_z}{5Al^2} & 0 & 0 & 0 & -\frac{13l}{420}+\frac{I_z}{10Al} \\
0 & 0 & \frac{13}{35}+\frac{6I_y}{5Al^2} & 0 & -\frac{11l}{210}-\frac{I_y}{10Al} & 0 & 0 & 0 & \frac{9}{70}-\frac{6I_y}{5Al^2} & 0 & \frac{13l}{420}-\frac{I_y}{10Al} & 0 \\
0 & 0 & 0 & \frac{J_x}{3A} & 0 & 0 & 0 & 0 & 0 & \frac{J_x}{6A} & 0 & 0 \\
0 & 0 & -\frac{11l}{210}-\frac{I_y}{10Al} & 0 & \frac{l^2}{105}+\frac{2I_y}{15A} & 0 & 0 & 0 & -\frac{13l}{420}+\frac{I_y}{10Al} & 0 & -\frac{l^2}{140}-\frac{I_y}{30A} & 0 \\
0 & \frac{11l}{210}+\frac{I_z}{10Al} & 0 & 0 & 0 & \frac{l^2}{105}+\frac{2I_z}{15A} & 0 & \frac{13l}{420}-\frac{I_z}{10Al} & 0 & 0 & 0 & -\frac{l^2}{140}-\frac{I_z}{30A} \\
\frac{1}{6} & 0 & 0 & 0 & 0 & 0 & \frac{1}{3} & 0 & 0 & 0 & 0 & 0 \\
0 & \frac{9}{70}-\frac{6I_z}{5Al^2} & 0 & 0 & 0 & \frac{13l}{420}-\frac{I_z}{10Al} & 0 & \frac{13}{35}+\frac{6I_z}{5Al^2} & 0 & 0 & 0 & -\frac{11l}{210}-\frac{I_z}{10Al} \\
0 & 0 & \frac{9}{70}-\frac{6I_y}{5Al^2} & 0 & -\frac{13l}{420}+\frac{I_y}{10Al} & 0 & 0 & 0 & \frac{13}{35}+\frac{6I_y}{5Al^2} & 0 & \frac{11l}{210}+\frac{I_y}{10Al} & 0 \\
0 & 0 & 0 & \frac{J_x}{6A} & 0 & 0 & 0 & 0 & 0 & \frac{J_x}{3A} & 0 & 0 \\
0 & 0 & \frac{13l}{420}-\frac{I_y}{10Al} & 0 & -\frac{l^2}{140}-\frac{I_y}{30A} & 0 & 0 & 0 & \frac{11l}{210}+\frac{I_y}{10Al} & 0 & \frac{l^2}{105}+\frac{2I_y}{15A} & 0 \\
0 & -\frac{13l}{420}+\frac{I_z}{10Al} & 0 & 0 & 0 & -\frac{l^2}{140}-\frac{I_z}{30A} & 0 & -\frac{11l}{210}-\frac{I_z}{10Al} & 0 & 0 & 0 & \frac{l^2}{105}+\frac{2I_z}{15A}
\end{bmatrix} \tag{102.66}
$$

102.8 3D Beam-Column Finite Element, 9 Degrees of Freedom

Przemieniecki (1985)

Condensation Formulation: Equations 102.67 to 102.73

Rearranged 12dof Stiffness Matrix: Equation 102.74

K_{rr} part of stiffness matrix: Equation 102.75

K_{rc} part of stiffness matrix: Equation 102.76

K_{cr} part of stiffness matrix: Equation 102.77

K_{cc} part of stiffness matrix: Equation 102.78

Stiffness Matrix: Equation 102.79

T Matrix: Equation 102.80

Rearranged Mass Matrix: Equation 102.81

Mass Matrix: Equation 102.82

$$\begin{bmatrix} k_{rr} & k_{rc} \\ k_{cr} & k_{cc} \end{bmatrix} \begin{Bmatrix} d_r \\ d_c \end{Bmatrix} = \begin{Bmatrix} r_r \\ r_c \end{Bmatrix} \tag{102.67}$$

$$\left(\left[k_{rr} \right] - \left[K_{rc} \right] \left[K_{cc} \right]^{-1} \left[K_{cr} \right] \right) \left\{ d_r \right\} = \left\{ r_r \right\} - \left[K_{rc} \right] \left[K_{cc} \right]^{-1} \left\{ r_c \right\} \tag{102.68}$$

$$[k_{condensed}] = \left[k_{rr} \right] - \left[K_{rc} \right] \left[K_{cc} \right]^{-1} \left[K_{cr} \right] \tag{102.69}$$

$$r_{condensed} = \left\{ r_r \right\} - \left[K_{rc} \right] \left[K_{cc} \right]^{-1} \left\{ r_c \right\} \tag{102.70}$$

$$[T] = \begin{bmatrix} I \\ - \left[K_{cc} \right]^{-1} \left[K_{cr} \right] \end{bmatrix} \tag{102.71}$$

$$[K_{condensed}] = [T]^T [K][T] \tag{102.72}$$

$K_{condensed}$ should give the same results using either method.

$$[M_{condensed}] = [T]^T [M][T] \tag{102.73}$$

$$
[K_{rearranged}] = \left[\begin{array}{cccccccccccc}
\frac{EA}{L} & 0 & 0 & -\frac{EA}{L} & 0 & 0 & 0 & 0 & 0 & 0 & 0 & 0 \\
0 & \frac{12EI_z}{L^3} & 0 & 0 & -\frac{12EI_z}{L^3} & 0 & 0 & 0 & 0 & 0 & 0 & \frac{6EI_z}{L^2} \\
0 & 0 & \frac{12EI_y}{L^3} & 0 & 0 & -\frac{12EI_y}{L^3} & 0 & -\frac{6EI_y}{L^2} & 0 & 0 & 0 & 0 \\
-\frac{EA}{L} & 0 & 0 & \frac{EA}{L} & 0 & 0 & 0 & 0 & 0 & 0 & 0 & 0 \\
0 & -\frac{12EI_z}{L^3} & 0 & 0 & \frac{12EI_z}{L^3} & 0 & 0 & 0 & -\frac{6EI_z}{L^2} & 0 & 0 & -\frac{6EI_z}{L^2} \\
0 & 0 & -\frac{12EI_y}{L^3} & 0 & 0 & \frac{12EI_y}{L^3} & 0 & \frac{6EI_y}{L^2} & 0 & 0 & \frac{6EI_y}{L^2} & 0 \\
0 & 0 & 0 & 0 & 0 & 0 & \frac{GJ_x}{L} & 0 & 0 & -\frac{GJ_x}{L} & 0 & 0 \\
0 & 0 & -\frac{6EI_y}{L^2} & 0 & 0 & \frac{6EI_y}{L^2} & 0 & \frac{4EI_y}{L} & 0 & 0 & \frac{2EI_y}{L} & 0 \\
0 & \frac{6EI_z}{L^2} & 0 & 0 & -\frac{6EI_z}{L^2} & 0 & 0 & 0 & \frac{4EI_z}{L} & 0 & 0 & \frac{2EI_z}{L} \\
0 & 0 & 0 & 0 & 0 & 0 & -\frac{GJ_x}{L} & 0 & 0 & \frac{GJ_x}{L} & 0 & 0 \\
0 & 0 & \frac{6EI_y}{L^2} & 0 & 0 & -\frac{6EI_y}{L^2} & 0 & \frac{2EI_y}{L} & 0 & 0 & \frac{4EI_y}{L} & 0 \\
0 & \frac{6EI_z}{L^2} & 0 & 0 & -\frac{6EI_z}{L^2} & 0 & 0 & 0 & \frac{2EI_z}{L} & 0 & 0 & \frac{4EI_z}{L}
\end{array}\right] \tag{102.74}
$$

$$[K_{rr}] = \begin{bmatrix} \frac{EA}{L} & 0 & 0 & -\frac{EA}{L} & 0 & 0 & 0 & 0 & 0 \\ 0 & \frac{12EI_z}{L^3} & 0 & 0 & -\frac{12EI_z}{L^3} & 0 & 0 & 0 & \frac{6EI_z}{L^2} \\ 0 & 0 & \frac{12EI_y}{L^3} & 0 & 0 & -\frac{12EI_y}{L^3} & 0 & -\frac{6EI_y}{L^2} & 0 \\ -\frac{EA}{L} & 0 & 0 & \frac{EA}{L} & 0 & 0 & 0 & 0 & 0 \\ 0 & -\frac{12EI_z}{L^3} & 0 & 0 & \frac{12EI_z}{L^3} & 0 & 0 & 0 & -\frac{6EI_z}{L^2} \\ 0 & 0 & -\frac{12EI_y}{L^3} & 0 & 0 & \frac{12EI_y}{L^3} & 0 & \frac{6EI_y}{L^2} & 0 \\ 0 & 0 & 0 & 0 & 0 & 0 & \frac{GJ_x}{L} & 0 & 0 \\ 0 & 0 & -\frac{6EI_y}{L^2} & 0 & 0 & \frac{6EI_y}{L^2} & 0 & \frac{4EI_y}{L} & 0 \\ 0 & \frac{6EI_z}{L^2} & 0 & 0 & -\frac{6EI_z}{L^2} & 0 & 0 & 0 & \frac{4EI_z}{L} \end{bmatrix} \tag{102.75}$$

$$[K_{rc}] = \begin{bmatrix} 0 & 0 & 0 \\ 0 & 0 & \frac{6EI_z}{L^2} \\ 0 & -\frac{6EI_y}{L^2} & 0 \\ 0 & 0 & 0 \\ 0 & 0 & -\frac{6EI_z}{L^2} \\ 0 & \frac{6EI_y}{L^2} & 0 \\ -\frac{GJ_x}{L} & 0 & 0 \\ 0 & \frac{2EI_y}{L} & 0 \\ 0 & 0 & \frac{2EI_z}{L} \end{bmatrix} \tag{102.76}$$

$$[K_{cr}] = \begin{bmatrix} 0 & 0 & 0 & 0 & 0 & 0 & -\frac{GJ_x}{L} & 0 & 0 \\ 0 & 0 & -\frac{6EI_y}{L^2} & 0 & 0 & \frac{6EI_y}{L^2} & 0 & \frac{2EI_y}{L} & 0 \\ 0 & \frac{6EI_z}{L^2} & 0 & 0 & -\frac{6EI_z}{L^2} & 0 & 0 & 0 & \frac{2EI_z}{L} \end{bmatrix} \tag{102.77}$$

$$[K_{cc}] = \begin{bmatrix} \frac{GJ_x}{L} & 0 & 0 \\ 0 & \frac{4EI_y}{L} & 0 \\ 0 & 0 & \frac{4EI_z}{L} \end{bmatrix} \tag{102.78}$$

$$[K_{condensed}] = \begin{bmatrix} \frac{EA}{L} & 0 & 0 & -\frac{EA}{L} & 0 & 0 & 0 & 0 & 0 \\ 0 & \frac{3EI_z}{L^3} & 0 & 0 & -\frac{3EI_z}{L^3} & 0 & 0 & 0 & \frac{3EI_z}{L^2} \\ 0 & 0 & \frac{3EIy}{L^3} & 0 & 0 & -\frac{3EI_y}{L^3} & 0 & -\frac{3EIy}{L^2} & 0 \\ -\frac{EA}{L} & 0 & 0 & \frac{EA}{L} & 0 & 0 & 0 & 0 & 0 \\ 0 & -\frac{3EI_z}{L^3} & 0 & 0 & \frac{3EI_z}{L^3} & 0 & 0 & 0 & -\frac{3EI_z}{L^2} \\ 0 & 0 & -\frac{3EI_y}{L^3} & 0 & 0 & \frac{3EI_y}{L^3} & 0 & \frac{3EI_y}{L^2} & 0 \\ 0 & 0 & 0 & 0 & 0 & 0 & 0 & 0 & 0 \\ 0 & 0 & -\frac{3EI_y}{L^2} & 0 & 0 & \frac{3EI_y}{L^2} & 0 & \frac{3EI_y}{L} & 0 \\ 0 & \frac{3EI_z}{L^2} & 0 & 0 & -\frac{3EI_z}{L^2} & 0 & 0 & 0 & \frac{3EI_z}{L} \end{bmatrix} \tag{102.79}$$

$$[T] = \begin{bmatrix} 1 & 0 & 0 & 0 & 0 & 0 & 0 & 0 & 0 \\ 0 & 1 & 0 & 0 & 0 & 0 & 0 & 0 & 0 \\ 0 & 0 & 1 & 0 & 0 & 0 & 0 & 0 & 0 \\ 0 & 0 & 0 & 1 & 0 & 0 & 0 & 0 & 0 \\ 0 & 0 & 0 & 0 & 1 & 0 & 0 & 0 & 0 \\ 0 & 0 & 0 & 0 & 0 & 1 & 0 & 0 & 0 \\ 0 & 0 & 0 & 0 & 0 & 0 & 1 & 0 & 0 \\ 0 & 0 & 0 & 0 & 0 & 0 & 0 & 1 & 0 \\ 0 & 0 & 0 & 0 & 0 & 0 & 0 & 0 & 1 \\ 0 & 0 & 0 & 0 & 0 & 0 & 1 & 0 & 0 \\ 0 & 0 & \frac{3}{2L} & 0 & 0 & -\frac{3}{2L} & 0 & -\frac{1}{2} & 0 \\ 0 & -\frac{3}{2L} & 0 & 0 & \frac{3}{2L} & 0 & 0 & 0 & -\frac{1}{2} \end{bmatrix} \tag{102.80}$$

$$
[M_{rearranged}] = \rho AL
\left[\begin{array}{cccccccccccc}
\frac{1}{3} & 0 & 0 & \frac{1}{6} & 0 & 0 & 0 & 0 & 0 & 0 & 0 & 0 \\
0 & \frac{13}{35}+\frac{6I_z}{5Al^2} & 0 & 0 & \frac{9}{70}-\frac{6I_z}{5Al^2} & 0 & 0 & 0 & -\frac{13l}{420}+\frac{I_z}{10Al} & 0 & 0 & \frac{11l}{210}+\frac{I_z}{10Al} \\
0 & 0 & \frac{13}{35}+\frac{6I_y}{5Al^2} & 0 & 0 & \frac{9}{70}-\frac{6I_y}{5Al^2} & 0 & \frac{13l}{420}-\frac{I_y}{10Al} & 0 & 0 & -\frac{11l}{210}-\frac{I_y}{10Al} & 0 \\
\frac{1}{6} & 0 & 0 & \frac{1}{3} & 0 & 0 & 0 & 0 & 0 & 0 & 0 & 0 \\
0 & \frac{9}{70}-\frac{6I_z}{5Al^2} & 0 & 0 & \frac{13}{35}+\frac{6I_z}{5Al^2} & 0 & 0 & 0 & -\frac{11l}{210}-\frac{I_z}{10Al} & 0 & 0 & \frac{13l}{420}-\frac{I_z}{10Al} \\
0 & 0 & \frac{9}{70}-\frac{6I_y}{5Al^2} & 0 & 0 & \frac{13}{35}+\frac{6I_y}{5Al^2} & 0 & \frac{11l}{210}+\frac{I_y}{10Al} & 0 & 0 & -\frac{13l}{420}+\frac{I_y}{10Al} & 0 \\
0 & 0 & 0 & 0 & 0 & 0 & \frac{I_x}{3A} & 0 & 0 & \frac{I_x}{6A} & 0 & 0 \\
0 & 0 & \frac{13l}{420}-\frac{I_y}{10Al} & 0 & 0 & \frac{11l}{210}+\frac{I_y}{10Al} & 0 & \frac{l^2}{105}+\frac{2I_y}{15A} & 0 & 0 & \frac{l^2}{140}-\frac{I_y}{30A} & 0 \\
0 & -\frac{13l}{420}+\frac{I_z}{10Al} & 0 & 0 & -\frac{11l}{210}-\frac{I_z}{10Al} & 0 & 0 & 0 & \frac{l^2}{105}+\frac{2I_z}{15A} & 0 & 0 & -\frac{l^2}{140}-\frac{I_z}{30A} \\
0 & 0 & 0 & 0 & 0 & 0 & \frac{I_x}{6A} & 0 & 0 & \frac{I_x}{3A} & 0 & 0 \\
0 & 0 & -\frac{11l}{210}-\frac{I_y}{10Al} & 0 & 0 & -\frac{13l}{420}+\frac{I_y}{10Al} & 0 & -\frac{l^2}{140}-\frac{I_y}{30A} & 0 & 0 & \frac{l^2}{105}+\frac{2I_y}{15A} & 0 \\
0 & \frac{11l}{210}+\frac{I_z}{10Al} & 0 & 0 & \frac{13l}{420}-\frac{I_z}{10Al} & 0 & 0 & 0 & -\frac{l^2}{140}-\frac{I_z}{30A} & 0 & 0 & \frac{l^2}{105}+\frac{2I_z}{15A}
\end{array}\right] \tag{102.81}
$$

$$
[M_{condensed}] = \rho AL
\begin{bmatrix}
\frac{1}{3} & 0 & 0 & 0 & \frac{1}{6} & 0 & 0 & 0 & 0 & 0 & 0 & 0 \\
0 & \frac{33}{140} + \frac{6I_z}{5AL^2} & 0 & 0 & 0 & \frac{39}{280} - \frac{6I_z}{5AL^2} & 0 & 0 & 0 & -\frac{11L}{280} + \frac{I_z}{5AL} & 0 & 0 \\
0 & 0 & \frac{33}{140} + \frac{6I_y}{5AL^2} & 0 & 0 & 0 & \frac{39}{280} - \frac{6I_y}{5AL^2} & 0 & \frac{11L}{280} - \frac{I_y}{5AL} & 0 & 0 & 0 \\
\frac{1}{6} & 0 & 0 & \frac{1}{3} & 0 & 0 & 0 & 0 & 0 & 0 & 0 & 0 \\
0 & \frac{39}{280} - \frac{6I_z}{5AL^2} & 0 & 0 & \frac{17}{35} + \frac{6I_z}{5AL^2} & 0 & 0 & 0 & 0 & -\frac{3L}{35} - \frac{I_z}{5AL} & 0 & 0 \\
0 & 0 & \frac{39}{280} - \frac{6I_y}{5AL^2} & 0 & 0 & \frac{17}{35} + \frac{6I_y}{5AL^2} & 0 & \frac{3L}{35} + \frac{I_y}{5AL} & 0 & 0 & 0 & 0 \\
0 & 0 & 0 & 0 & 0 & 0 & \frac{I_x}{A} & 0 & 0 & 0 & 0 & 0 \\
0 & 0 & \frac{11L}{280} - \frac{I_y}{5AL} & 0 & 0 & \frac{3L}{35} + \frac{I_y}{5AL} & 0 & \frac{2L^2}{105} + \frac{I_y}{5A} & 0 & 0 & 0 & 0 \\
0 & -\frac{11L}{280} + \frac{I_z}{5AL} & 0 & 0 & -\frac{3L}{35} - \frac{I_z}{5AL} & 0 & 0 & 0 & 0 & 0 & 0 & \frac{2L^2}{105} + \frac{I_z}{5A}
\end{bmatrix}
\tag{102.82}
$$

102.9 Shear Beam Finite Element

102.10 Quadrilateral Shell Finite Element with 6DOFs per Node

Based on works by Bergan and Felippa (1985); Alvin et al. (1992); Felippa and Militello (1992); Felippa and Alexander (1992); Militello and Felippa (1991). The stiffness matrix for this element is obtained by averaging two quad shells made up of two ANDES triangular shells (with an alternating orientation of diagonals, Stošić (1984-2022))

102.11 Seismic Isolator and Dissipator Finite Elements

Base isolation system are used to change dynamic characteristics of seismic motions that excite structure and also to dissipate seismic energy before it excites structure. Therefore there are two main types of devices:

- Base Isolators (Kelly, 1991a,b; Toopchi-Nezhad et al., 2008; Huang et al., 2010; Vassiliou et al., 2013) are usually made of low damping (energy dissipation) elastomers and are primarily meant to change (reduce) frequencies of input motions. They are not designed nor modeled as energy dissipators.
- Base Dissipators Kelly and Hodder (1982); Fadi and Constantinou (2010); Kumar et al. (2014) are developed to dissipate seismic energy before it excites the structure. There two main types of such dissipators:
  - Elastomers made of high dissipation rubber, and
  - Frictional pendulum dissipators

Both isolators and dissipators are usually developed to work in two horizontal dimensions, while motions in vertical direction are not isolated or dissipated. This can create potential problems and need to be carefully modeled.

Modeling of base isolation and dissipation system is done using two-node finite elements of relatively short length.

102.11.1 Base Isolation Systems

Base isolation systems are modeled using linear or nonlinear elastic elements. Stiffness is provided from either tests on a full-sized base isolators, or from material characterization of rubber (and steel plates if used in a sandwich isolator construction). Depending on rubber used, a number of models can be used to develop stiffness of the device Ogden (1984); Simo and Miehe (1992); Simo and Pister (1984).

Particularly important is to properly account for vertical stiffness as vertical motions can be amplified depending on characteristics of seismic motions, structure and stiffness of the isolators Hijikata et al. (2012); Araki et al. (2009). It is also important to note that assumption of small deformation is used in most cases. In other words, the stability of the isolator, for example, overturning or rolling is not modeled. It is assumed that elastic stiffness will not suddenly change if the isolator becomes unstable (rolls or overturns).

102.11.2 Base Dissipator Systems

Base dissipator systems are modeled using inelastic (nonlinear) two node elements. There are three basic types of dissipator models used:

- High damping rubber dissipators
- Rubber dissipators with lead core
- Frictional pendulum (double or triple) dissipators

Each one is calibrated using tests done on a full dissipator. It is important to be able to take into account the influence of (an increase in) temperature on resulting behavior. Energy dissipation results in heating of devices, and an increase in temperature influences material properties of dissipators.

102.11.3 Two Node, 3D, Rubber Isolator Finite Element

Kelly (1991a,b)

Behavior of rubber (Ogden, 1984; Simo and Miehe, 1992; Simo and Pister, 1984)

102.11.4 Two Node, 3D, Frictional Pendulum Finite Element

102.12 Fully Coupled, Porous Solid – Pore Fluid Finite Elements

102.12.1 u-p-U Formulation

102.12.1.1 Background

This section follows developments by Zienkiewicz and Shiomi (1984).

The relationship between effective stress, total stress and pore pressure is given as:

$$\sigma''_{ij} = \sigma_{ij} - \alpha\delta_{ij}p \tag{102.83}$$

where σ''_{ij} is effective stress tensor, σ_{ij} is total stress tensor, δ_{ij} is Kronecker delta. $\delta_{ij} = 1$, when i=j, and $\delta_{ij} = 0$, when $i \neq j$. It is assumed that tensile components of effective and total stress are positive, and the pore fluid pressure p is also positive in tension, hence for compressions (usual case) pore fluid pressure is negative ($p < 0$) (Zienkiewicz et al., 1999a). For isotropic materials, $\alpha = 1 - K_T/K_S$. K_T is the total bulk modulus of the solid matrix, K_S is the bulk modulus of the solid particle. For most of the soil mechanics problems, as the bulk modulus K_S of the solid particles is much larger than that of the whole material, $\alpha \approx 1$ can be assumed. Equation (102.83) becomes

$$\sigma''_{ij} = \sigma_{ij} - \delta_{ij}p \tag{102.84}$$

In the next sections, a detailed derivation of formulation and numerical implementation for a fully coupled (pore fluid and porous soil) solid mechanics problem is given. Derivations are based in part on earlier work by Zienkiewicz et al. (1999a).

102.12.1.2 Governing Equations of Porous Media

The following notation is used:

- σ_{ij}, the total Cauchy stress in the mixture,
- u_i, the displacement of the solid skeleton,
- w_i, the displacement of the fluid phase relative to the skeleton of solid,
- p, the pore water pressure,
- $\varepsilon_{ij} = \frac{1}{2}(u_{i,j} + u_{j,i})$, the strain increment of the solid phase,
- $\omega_{ij} = \frac{1}{2}(u_{i,j} - u_{j,i})$, the rotation increment of the solid phase,
- ρ, ρ_s, ρ_f, the densities of the mixture, solid phase and water respectively,
- n the porosity,
- $\theta = -\dot{w}_{i,i}$, the rate of change of volume of water per unit total volume of mixture.

The Equilibrium Equation of the Mixture. The overall equilibrium or momentum balance equation for the soil-fluid mixture is written as

$$\sigma_{ij,j} - \rho\ddot{u}_i - \rho_f[\ddot{w}_i + \underline{\dot{w}_j\dot{w}_{i,j}}] + \rho b_i = 0 \tag{102.85}$$

here $\ddot{u}_i$ is the acceleration of the solid part, b_i is the body force per unit mass, $\ddot{w}_i + \underline{\dot{w}_j\dot{w}_{i,j}}$ is the fluid acceleration relative to the solid part, $\ddot{w}_i$ is local acceleration, $\underline{\dot{w}_j\dot{w}_{i,j}}$ is convective acceleration.

The underlined terms in the above equation represent the fluid acceleration relative to the solid and convective terms of this acceleration. Generally, this acceleration is so small that it is frequently omitted. For static problems, equation 102.85 only consists of the first and last terms.

For fully saturated porous media (no air inside), from definition

$$\begin{aligned}
\rho &= \frac{M_t}{V_t} \\
&= \frac{M_s + M_f}{V_t} \\
&= \frac{V_s\rho_s + V_f\rho_f}{V_t} \\
&= \frac{V_f}{V_t}\rho_f + \frac{V_t - V_f}{V_t}\rho_s \\
&= n\rho_f + (1-n)\rho_s \\
\rho &= n\rho_f + (1-n)\rho_s
\end{aligned} \tag{102.86}$$

where M_t, M_s and M_f are the mass of total, solid part and fluid part respectively. V_t, V_s and V_f are the volume of total, solid part and fluid part respectively.

The Equilibrium Equation of the Fluid. For the pore fluid, the equation of momentum balance is written as

$$-p_{,i} - R_i - \rho_f\ddot{u}_i - \rho_f[\ddot{w}_i + \underline{\dot{w}_j\dot{w}_{i,j}}]/n + \rho_f b_i = 0 \tag{102.87}$$

where R is the viscous drag forces. It is noted that the underlined terms in equation 102.87 represent the convective fluid acceleration again and are generally small. Also note that the permeability $\mathbf{k}$ is used with dimensions of $[length]^3[time]/[mass]$, which is different from the usual soil mechanics convention, where the permeability has the dimension of velocity, i.e., $[length]/[time]$. Their values are related by $k = K/\rho_f g$, where g is the gravitational acceleration at which the permeability is measured. Assuming the Darcy seepage law: $n\dot{w} = Ki$, here i is the head gradient. Seepage force is then $R = \rho_f g i$. R can be written as

$$R_i = k_{ij}^{-1}\dot{w}_j \qquad \text{or} \qquad R_i = k^{-1}\dot{w}_i \tag{102.88}$$

where k_{ij} or k are Darcy permeability coefficients for anisotropic and isotropic conditions respectively.

Flow Conservation Equation. The final equation is supplied by the mass conservation of the fluid flow

$$\dot{w}_{i,i} + \alpha\dot{\varepsilon}_{ii} + \frac{\dot{p}}{Q} + \underline{n\frac{\dot{\rho}_f}{\rho_f}} + \dot{s}_0 = 0 \tag{102.89}$$

The first term of equation(102.89) is the flow divergence of a unit volume of mixture. The second term is the volume change of the mixture. In the third term, Q is relative to the compressibility of the solid

and fluid. The underlined terms represent change of density and rate of volume expansion of the solid in case of thermal changes. They are generally negligible.

$$\frac{1}{Q} \equiv \frac{n}{K_f} + \frac{\alpha - n}{K_s} \cong \frac{n}{K_f} + \frac{1-n}{K_s} \tag{102.90}$$

where K_s and K_f are the bulk moduli of the solid and fluid phases respectively. Note that the bulk modulus of the solid phase K_s is the actual bulk modulus of the solid particle.

Obtained are the total mixture equilibrium equation (102.85), fluid equilibrium equation (102.87) and the flow conservation equation (102.89) for saturated soil. By omitting the convective acceleration (the underline terms in (102.85) and (102.87)), density variation and the volume expansion due to the thermal change (the underline terms in (102.89)), the equations of coupled system can be further simplified, as summarized below

$$\sigma_{ij,j} - \rho \ddot{u}_i - \rho_f \ddot{w}_i + \rho b_i = 0 \tag{102.91}$$

$$-p_{,i} - R_i - \rho_f \ddot{u}_i - \frac{\rho_f \ddot{w}_i}{n} + \rho_f b_i = 0 \tag{102.92}$$

$$\dot{w}_{i,i} + \alpha \dot{\varepsilon}_{ii} + \frac{\dot{p}}{Q} = 0 \tag{102.93}$$

Bulk Modulus of Fluid (see Verruijt (2012) page 97... compressibility of water and with air bubbles)...

102.12.1.3 Modified Governing Equations.

Solid Part Equilibrium Equation. A new variable U_i is introduced in place of the relative pseudo-displacement w_i

$$U_i = u_i + U_i^R = u_i + \frac{w_i}{n} \tag{102.94}$$

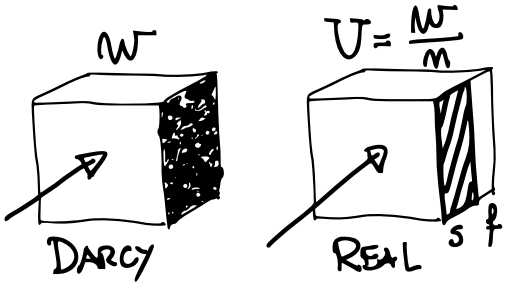

Figure 102.10: Fluid mechanics of Darcy's flow (w_i) versus real flow ($U_i = w_i/n$).

Change of variables is finalized by insertion of equation 102.94 into equations 102.91 and 102.92, and then by subtraction of term ([$n \times$ *equation* 102.92]) from equation 102.91, which leads to the equation of skeleton equilibrium

$$\sigma_{ij,j} - \rho\ddot{u}_i + \rho b_i + np_{,i} + nR_i + n\rho_f\ddot{u}_i - n\rho_f b_i = 0 \tag{102.95}$$

By substituting $\rho = (1-n)\rho_s + n\rho_f$

$$\begin{aligned}\sigma_{ij,j} - (1-n)\rho_s\ddot{u}_i - n\rho_f\dot{u}_i + (1-n)\rho_s b_i + n\rho_f b_i + np_{,i} + nR_i + n\rho_f\ddot{u}_i - n\rho_f b_i = 0\\ \sigma_{ij,j} + np_{,i} + (1-n)\rho_s b_i - (1-n)\rho_s\ddot{u}_i + nR_i = 0\end{aligned} \tag{102.96}$$

By using the definition of effective stress, equation 102.83, equation 102.95 becomes

$$\sigma''_{ij,j} - (\alpha - n)p_{,i} + (1-n)\rho_s b_i - (1-n)\rho_s\ddot{u}_i + nR_i = 0 \tag{102.97}$$

Fluid Part Equilibrium Equation. The fluid part equilibrium equation can be obtained simply by [$n \times$ (102.92]],i.e.

$$\begin{aligned}-np_{,i} - nR_i - n\rho_f\ddot{u}_i - \rho_f\ddot{w}_i + n\rho_f b_i = 0\\ -np_{,i} - nR_i - n\rho_f(\ddot{u}_i + \frac{\ddot{w}_i}{n}) + n\rho_f b_i = 0\end{aligned} \tag{102.98}$$

From equation (102.94),

$$\ddot{U}_i = \ddot{u}_i + \frac{\ddot{w}_i}{n} \tag{102.99}$$

so that equation (102.98) becomes:

$$-np_{,i} + n\rho_f b_i - n\rho_f\ddot{U}_i - nR_i = 0 \tag{102.100}$$

Mixture Balance of Mass. By differentiating equation (102.94) in time and space

$$\dot{w}_{i,i} = n\dot{U}_{i,i} - n\dot{u}_{i,i} \tag{102.101}$$

Notice that $\dot{\varepsilon}_{ii} = \dot{u}_{i,i}$, so that equation (102.101) becomes

$$\dot{w}_{i,i} = n\dot{U}_{i,i} - n\dot{\varepsilon}_{ii} \tag{102.102}$$

By substituting (102.102) to (102.93)

$$n\dot{U}_{i,i} - n\dot{\varepsilon}_{ii} + \alpha\dot{\varepsilon}_{ii} + \frac{\dot{p}}{Q} = 0 \tag{102.103}$$

or:

$$-n\dot{U}_{i,i} = (\alpha - n)\dot{\varepsilon}_{ii} + \frac{1}{Q}\dot{p} \tag{102.104}$$

Developed is a set of modified governing equations (102.97), (102.100) and (102.104). They are summarized below

$$\overset{''}{\sigma}_{ij,j} - (\alpha - n)p_{,i} + (1-n)\rho_s b_i - (1-n)\rho_s \ddot{u}_i + nR_i = 0 \tag{102.105}$$

$$-np_{,i} + n\rho_f b_i - n\rho_f \ddot{U}_i - nR_i = 0 \tag{102.106}$$

$$-n\dot{U}_{i,i} = (\alpha - n)\dot{\varepsilon}_{ii} + \frac{1}{Q}\dot{p} \tag{102.107}$$

From the modified equation set (102.105), (102.106) and (102.107), it is noted that only $\ddot{u}_i$ occurs in the first equation, and only $\ddot{U}_i$ in the second, thus leading to a convenient diagonal form in discretization.

Obtained is a a complete equation system given by (102.105), (102.106) and (102.107). With the basic definitions introduced earlier, there are three essential unknowns:

1. three solid displacement u_i
2. pore pressure p
3. three fluid displacement U_i

The boundary conditions imposed on these variables will complete the problem. These boundary conditions are:

- For the momentum balance part,
  - on boundary Γ_t, traction $t_i(t)$(or $\sigma_{ij}n_j$), where n_i is the i-th component of the normal to the boundary.
  - On boundary Γ_u, the displacement u_i is given.
- For the fluid part, again the boundary is divided into two parts:
  - On Γ_p, the pressure p is specified,
  - on Γ_w, the normal outflow $\dot{w}_n$ is specified. For impermeable boundary a zero value for the outflow should be specified.

The boundary conditions can be summarized below

$$\begin{aligned} \Gamma &= \Gamma_t \cup \Gamma_u \\ t_i &= \sigma_{ij} n_j = \bar{t}_i \qquad \text{on} \qquad \Gamma = \Gamma_t \\ u_i &= \bar{u}_i \qquad \text{on} \qquad \Gamma = \Gamma_u \end{aligned} \tag{102.108}$$

and

$$\begin{aligned} \Gamma &= \Gamma_p \cup \Gamma_w \\ p &= \bar{p} \qquad \text{on} \qquad \Gamma = \Gamma_p \\ n^T w &= w_n \qquad \text{on} \qquad \Gamma = \Gamma_w \end{aligned} \tag{102.109}$$

102.12.1.4 Numerical Solution of the u-p-U Governing Equations

The solutions to the problems governed by the modified governing equation set (102.105), (102.106) and (102.107) can be found by solving partial differential equations, which can be written as

$$A\ddot{\Phi} + B\dot{\Phi} + L(\Phi) = 0 \tag{102.110}$$

where A, B are constant matrices, and L is an operator involving spatial differentials. The dot notation represents the time differentiation. Vector of dependent variables, Φ represents the displacement u or the pore fluid pressure p.

The finite element solution of a problem proceeds as follows.

1. Discretize or approximate the unknown functions Φ by a finite set of parameters $\overline{\Phi}_k$ and shape function H_k. They are specified in space dimensions. Thus

$$\Phi \cong \Phi^h = \sum_{k=1}^{n} H_k \overline{\Phi}_k \tag{102.111}$$

2. Insert the value of the approximating function $\hat{\Phi}$ into the differential equations to obtain a residual, then a set of weighted residual equations can be written in the form

$$\int^{\Omega} W_j^T (A\ddot{\Phi}^h + B\dot{\Phi}^h + L(\Phi^h)) d\Omega = 0 \tag{102.112}$$

In the finite element method, the weighting functions W_j are usually identical to the shape functions.

The solid displacement u_i, the pore pressure p, and the absolute fluid displacement U_i can be approximated using shape functions and nodal values.

$$\begin{aligned} u_i &= H^u_K \overline{u}_{Ki} \\ p &= H^p_K \overline{p}_K \\ U_i &= H^U_K \overline{U}_{Ki} \end{aligned} \tag{102.113}$$

where H^u_K, H^p_K, and H^U_K are shape functions for solid displacement, pore pressure and fluid displacement, respectively, $\overline{u}_{Ki}$,$\overline{p}_K$,$\overline{U}_{Ki}$ are nodal values of solid displacement, pore pressure and fluid displacement, respectively.

Numerical Solution of solid part equilibrium equation. To obtain the numerical solution of the first equation, premultiply equation 102.105 by H^u_K and integrate over the domain.

First term of (102.105) becomes

$$\begin{aligned} \int_\Omega H^u_K \sigma''_{ij,j} d\Omega &= \int_{\Gamma_t} H^u_K n_j \sigma''_{ij} d\Gamma - \int_\Omega H^u_{K,j} \sigma''_{ij} d\Omega \\ &= \int_{\Gamma_t} H^u_K (\overline{t}_i + n_i \alpha p) d\Gamma - \int_\Omega H^u_{K,j} \sigma''_{ij} d\Omega \\ &= (f^u_1)_{Ki} - \int_\Omega H^u_{K,j} D_{ijml} \varepsilon_{ml} d\Omega \\ &= (f^u_1)_{Ki} - [\int_\Omega H^u_{K,j} D_{ijml} H^u_{P,l} d\Omega] \overline{u}_{Pm} \\ &= (f^u_1)_{Ki} - K^{EP}_{KimP} \overline{u}_{Pm} \\ &= (f^u_1)_{Ki} - K^{EP}_{KijL} \overline{u}_{Lj} \\ &= \boldsymbol{(f^u_1) - K^{EP} \overline{u}} \end{aligned} \tag{102.114}$$

where K^{EP} is the stiffness matrix of the solid part,n_i is the direction of the normal on the boundary.

Second term of (102.105) becomes

$$\begin{aligned} -\int_\Omega H^u_K (\alpha - n) p_{,i} d\Omega &= -\int_{\Gamma_p} H^u_K (\alpha - n) n_i p d\Gamma + \int_\Omega H^u_{K,i} (\alpha - n) p d\Omega \\ &= -\int_{\Gamma_p} H^u_K (\alpha - n) n_i p d\Gamma + [\int_\Omega H^u_{K,i} (\alpha - n) H^p_M d\Omega] \overline{p}_M \\ &= -(f^u_4)_{Ki} + (G_1)_{KiM} \overline{p}_M \\ &= \boldsymbol{-f^u_4 + (G_1)\overline{p}} \end{aligned} \tag{102.115}$$

Third term of (102.105) (solid body force) is then

$$\int_\Omega H^u_K(1-n)\rho_s b_i d\Omega = (f^u_5)_{Ki} \tag{102.116}$$

Fourth term of (102.105) can be written as

$$\begin{aligned} -\int_\Omega H^u_K(1-n)\rho_s\delta_{ij}\ddot{u}_j d\Omega &= -[\int_\Omega H^u_K(1-n)\rho_s\delta_{ij}H^u_L d\Omega]\ddot{\overline{u}}_{Lj} \\ &= -(M_s)_{KijL}\ddot{\overline{u}}_{Lj} \\ &= \boldsymbol{-M_s\ddot{\overline{u}}} \end{aligned} \tag{102.117}$$

where M_s is the mass matrix of solid part. By substituting equations (102.88) and (102.94), last term of (102.105) (Damping Matrix) becomes

$$\begin{aligned} \int_\Omega H^u_K n R_i d\Omega &= \int_\Omega H^u_K n k^{-1}_{ij}\dot{w}_j d\Omega \\ &= \int_\Omega H^u_K n^2 k^{-1}_{ij}\dot{U}_j d\Omega - \int_\Omega H^u_K n^2 k^{-1}_{ij}\dot{u}_j d\Omega \\ &= [\int_\Omega H^u_K n^2 k^{-1}_{ij}H^U_L d\Omega]\dot{\overline{U}}_{Lj} - [\int_\Omega H^u_K n^2 k^{-1}_{ij}H^U_L d\Omega]\dot{\overline{u}}_{Lj} \\ &= (C_2)_{KijL}\dot{\overline{U}}_{Lj} - (C_1)_{KijL}\dot{\overline{u}}_{Lj} \\ &= \boldsymbol{C_2\dot{\overline{U}} - C_1\dot{\overline{u}}} \end{aligned} \tag{102.118}$$

Equation (102.105) becomes

$$\boldsymbol{-K^{EP}\overline{u} + f^u_1 - f^u_4 + G_1\overline{p} + f^u_5 + M_s\ddot{\overline{u}} + C_2\dot{\overline{U}} - C_1\dot{\overline{u}} = 0} \tag{102.119}$$

or

$$\boldsymbol{K^{EP}\overline{u} - G_1\overline{p} - C_2\dot{\overline{U}} + C_1\dot{\overline{u}} + M_s\ddot{\overline{u}} = \overline{f}_s} \tag{102.120}$$

where

$$\overline{f}_s = f^u_1 - f^u_4 + f^u_5 \tag{102.121}$$

and in index form

$$K^{EP}_{KijL} - (G_1)_{KiL}\overline{p}_L + (C_2)_{KijL}\dot{\overline{U}}_{Lj} - (C_1)_{KijL}\dot{\overline{u}}_{Lj} + (M_s)_{KijL}\ddot{\overline{u}}_{Ki} = (\overline{f}_s)_{Ki} \tag{102.122}$$

where

$$\begin{aligned}
\boldsymbol{K^{EP}} = (K^{EP})_{KimP} &= \int_\Omega H^u_{K,j} D_{ijml} H^u_{P,l} d\Omega \\
\boldsymbol{G_1} = (G_1)_{KiM} &= \int_\Omega H^u_{K,i} (\alpha - n) H^p_M d\Omega \\
\boldsymbol{C_2} = (C_2)_{KijL} &= \int_\Omega H^u_K n^2 k^{-1}_{ij} H^U_L d\Omega \\
\boldsymbol{C_1} = (C_1)_{KijL} &= \int_\Omega H^u_K n^2 k^{-1}_{ij} H^u_L d\Omega \\
\boldsymbol{M_s} = (M_s)_{KijL} &= \int_\Omega H^u_K (1-n) \rho_s \delta_{ij} H^u_L d\Omega \\
\overline{\boldsymbol{f}} = (\overline{f}_s)_{Ki} &= (f^u_1)_{Ki} - (f^u_4)_{Ki} + (f^u_5)_{Ki}
\end{aligned} \tag{102.123}$$

Numerical Solution of fluid part equilibrium equation. From equations (102.88) and (102.94),

$$R_i = n k^{-1}_{ij} (\dot{U}_j - \dot{u}_j) \tag{102.124}$$

By substituting (102.124) into equation (102.106),

$$-n p_{,i} + n \rho_f b_i - n \rho_f \ddot{U}_i - n^2 k^{-1}_{ij} (\dot{U}_j - \dot{u}_j) = 0 \tag{102.125}$$

By premultiplying (102.125) by H^U_K and integrating over the domain, first term of (102.125) becomes

$$\begin{aligned}
-\int_\Omega n H^U_K p_{,i} d\Omega &= -\int_{\Gamma_p} n H^U_K n_i p d\Gamma + \int_\Omega n H^U_{K,i} p d\Omega \\
&= -(f_1)_{Ki} + [\int_\Omega n H^U_{K,i} H^p_M d\Omega] \overline{p}_M \\
&= -(f_1)_{Ki} + (G_2)_{KiM} \overline{p}_M \\
&= \boldsymbol{-(f_1)_{Ki} + (G_2)\overline{p}}
\end{aligned} \tag{102.126}$$

Second term of (102.125) is then

$$\int_\Omega H^U_K \rho_f b_i d\Omega = (f_2)_{Ki} \tag{102.127}$$

Third term of (102.125) (Lumped mass matrix obtained by multiplying δ_{ij}) becomes

$$\begin{aligned}
-\int_\Omega H^U_K n \rho_f \delta_{ij} \ddot{U}_j d\Omega &= -[\int_\Omega H^U_K n \rho_f \delta_{ij} H^U_L d\Omega] \ddot{\overline{U}}_{Lj} \\
&= -(M_f)_{KijL} \ddot{\overline{U}}_{Lj} \\
&= \boldsymbol{-M_f \ddot{\overline{U}}}
\end{aligned} \tag{102.128}$$

Forth term of (102.125) becomes

$$
\begin{aligned}
-\int_\Omega H^U_K n^2 k^{-1}_{ij} \dot{U}_j d\Omega + \int_\Omega H^U_K n^2 k^{-1}_{ij} \dot{u}_j d\Omega &= -[\int_\Omega H^U_K n^2 k^{-1}_{ij} H^U_L d\Omega]\dot{\overline{U}}_{Lj} \qquad (102.129)\\
+[\int_\Omega H^U_K n^2 k^{-1}_{ij} H^u_L d\Omega]\dot{\overline{u}}_{Lj} & \\
&= -(C_3)_{KijL}\dot{\overline{U}}_{Lj} + (C_2)^T_{LjiK}\dot{\overline{u}}_{Lj}\\
&= \boldsymbol{C_3}\dot{\overline{\boldsymbol{U}}} + \boldsymbol{C_2^T}\dot{\overline{\boldsymbol{u}}} \qquad (102.130)
\end{aligned}
$$

Equation (102.125) becomes

$$\boldsymbol{-f_1 + G_2\overline{p} + f_2 - M_f\ddot{\overline{U}} - C_3\dot{\overline{U}} + C_2^T\dot{\overline{u}} = 0} \qquad (102.131)$$

or

$$\boldsymbol{-G_2\overline{p} - C_2^T\dot{\overline{u}} + C_3\dot{\overline{U}} + M_f\ddot{\overline{U}} = \overline{f}_f} \qquad (102.132)$$

where

$$\overline{f}_f = f_2 - f_1 \qquad (102.133)$$

and in index form

$$-(G_2)_{KiM}\overline{p}_M - (C_2)^T_{LjiK}\dot{\overline{u}}_{Lj} + (C_3)_{KijL}\dot{\overline{U}}_{Lj} + (M_f)_{KijL}\ddot{U}_{Lj} = (f_f)_{Ki} \qquad (102.134)$$

where

$$
\begin{aligned}
\boldsymbol{(f_f)_{Ki}} &= (f_1)_{Ki} - (f_2)_{Ki}\\
\boldsymbol{G_2} &= (G_2)_{KiN} = \int_\Omega n H^U_{K,i} H^p_M d\Omega\\
\boldsymbol{C_2^T} &= (C_2^T)_{KijL} = \int_\Omega H^U_K n^2 k^{-1}_{ij} H^u_L d\Omega\\
\boldsymbol{C_3} &= (C_3)_{KijL} = \int_\Omega H^U_K n^2 k^{-1}_{ij} H^U_L d\Omega\\
\boldsymbol{M_f} &= (M_f)_{KijL} = \int_\Omega H^U_K n \rho_f \delta_{ij} H^U_L d\Omega \qquad (102.135)
\end{aligned}
$$

Numerical Solution of flow conservation equation. By integrating (102.107) in time and noticing that $\varepsilon_{ii} = u_{i,i}$,

$$-nU_{i,i} = (\alpha - n)\varepsilon_{ii} + \frac{1}{Q}p \qquad (102.136)$$

By multiplying (102.136) by H^p_M and integrating over domain, first term of (102.136) becomes

$$-[\int_\Omega H^p_M n H^U_{L,j} d\Omega]\overline{U}_{Lj} = -(G_2)_{MLj}\overline{U}_{Li} = -\boldsymbol{G_2^T}\overline{\boldsymbol{U}} \qquad (102.137)$$

Second term of (102.136) is

$$\begin{aligned}\int_\Omega H^p_M(\alpha-n)u_{i,i}d\Omega &= [\int_\Omega H^p_M(\alpha-n)H^u_{L,j}d\Omega]\overline{u}_{Lj}\\ &= (G_1)_{LjM}\overline{u}_{Lj}\\ &= \boldsymbol{G_1^T\overline{u}}\end{aligned} \tag{102.138}$$

Third term of (102.136) becomes

$$[\int_\Omega H^p_N\frac{1}{Q}H^p_M d\Omega]p_N = P_{NM}p_M = \boldsymbol{P\overline{p}} \tag{102.139}$$

The equation (102.136) becomes

$$\boldsymbol{G_2^T\overline{U} + G_1^T\overline{u} + P\overline{p} = 0} \tag{102.140}$$

in index form

$$(G_2)_{LiK}\overline{U}_{Li} + (G_1)_{LiK}\overline{u}_{Li} + P_{KL}\overline{p}_L = 0 \tag{102.141}$$

102.12.1.5 Matrix form of the governing equations.

The numerical forms of governing equations (102.120),(102.132) and (102.140) can be written together in the matrix form as

$$\begin{bmatrix} M_s & 0 & 0\\ 0 & 0 & 0\\ 0 & 0 & M_f\end{bmatrix}\begin{bmatrix}\ddot{\overline{u}}\\ \ddot{\overline{p}}\\ \ddot{\overline{U}}\end{bmatrix} + \begin{bmatrix} C_1 & 0 & -C_2\\ 0 & 0 & 0\\ -C_2^T & 0 & C_3\end{bmatrix}\begin{bmatrix}\dot{\overline{u}}\\ \dot{\overline{p}}\\ \dot{\overline{U}}\end{bmatrix} + \begin{bmatrix} K^{EP} & -G_1 & 0\\ -G_1^T & -P & -G_2^T\\ 0 & -G_2 & 0\end{bmatrix}\begin{bmatrix}\overline{u}\\ \overline{p}\\ \overline{U}\end{bmatrix} = \begin{bmatrix}\overline{f}_s\\ 0\\ \overline{f}_f\end{bmatrix} \tag{102.142}$$

or in index form

$$\begin{bmatrix} (M_s)_{KijL} & 0 & 0\\ 0 & 0 & 0\\ 0 & 0 & (M_f)_{KijL}\end{bmatrix}\begin{bmatrix}\ddot{\overline{u}}_{Lj}\\ \ddot{\overline{p}}_N\\ \ddot{\overline{U}}_{Lj}\end{bmatrix} + \begin{bmatrix} (C_1)_{KijL} & 0 & -(C_2)_{KijL}\\ 0 & 0 & 0\\ -(C_2)_{LjiK} & 0 & (C_3)_{KijL}\end{bmatrix}\begin{bmatrix}\dot{\overline{u}}_{Lj}\\ \dot{\overline{p}}_N\\ \dot{\overline{U}}_{Lj}\end{bmatrix} + \begin{bmatrix} (K^{EP})_{KijL} & -(G_1)_{KiM} & 0\\ -(G_1)_{LjM} & -P_{MN} & -(G_2)_{LjM}\\ 0 & -(G_2)_{KiL} & 0\end{bmatrix}\begin{bmatrix}\overline{u}_{Lj}\\ \overline{p}_M\\ \overline{U}_{Lj}\end{bmatrix} = \begin{bmatrix}\overline{f}^{solid}_{Ki}\\ 0\\ \overline{f}^{fluid}_{Ki}\end{bmatrix} \tag{102.143}$$

where

$$
\begin{aligned}
\boldsymbol{M_s} &= (M_s)_{KijL} = \int_\Omega H^u_K (1-n)\rho_s \delta_{ij} H^u_L d\Omega \\
\boldsymbol{M_f} &= (M_f)_{KijL} = \int_\Omega H^U_K n\rho_f \delta_{ij} H^U_L d\Omega \\
\boldsymbol{C_1} &= (C_1)_{KijL} = \int_\Omega H^u_K n^2 k^{-1}_{ij} H^u_L d\Omega \\
\boldsymbol{C_2} &= (C_2)_{KijL} = \int_\Omega H^u_K n^2 k^{-1}_{ij} H^U_L d\Omega \\
\boldsymbol{C_3} &= (C_3)_{KijL} = \int_\Omega H^U_K n^2 k^{-1}_{ij} H^U_L d\Omega \\
\boldsymbol{K^{EP}} &= (K^{EP})_{KijL} = \int_\Omega H^u_{K,m} D_{imjn} H^u_{L,n} d\Omega \\
\boldsymbol{G_1} &= (G_1)_{KiM} = \int_\Omega H^u_{K,i} (\alpha - n) H^p_M d\Omega \\
\boldsymbol{G_2} &= (G_2)_{KiM} = \int_\Omega n H^U_{K,i} H^p_M d\Omega \\
\boldsymbol{P} &= P_{NM} = \int_\Omega H^p_N \frac{1}{Q} H^p_M d\Omega
\end{aligned}
\tag{102.144}
$$

$$
\begin{aligned}
\bar{f}^{solid}_{Ki} &= (f^u_1)_{Ki} - (f^u_4)_{Ki} + (f^u_5)_{Ki} \\
\bar{f}^{fluid}_{Ki} &= -(f^U_1)_{Ki} + (f^U_2)_{Ki} \\
(f^u_1)_{Ki} &= \int_{\Gamma_t} H^u_K n_j \sigma''_{ij} d\Gamma \\
(f^u_4)_{Ki} &= \int_{\Gamma_p} H^u_K (\alpha - n) n_i p d\Gamma \\
(f^u_5)_{Ki} &= \int_\Omega H^u_K (1-n)\rho_s b_i d\Omega \\
(f^U_1)_{Ki} &= \int_{\Gamma_p} n H^U_K n_i p d\Gamma \\
(f^U_2)_{Ki} &= \int_\Omega n H^U_K \rho_f b_i d\Omega
\end{aligned}
\tag{102.145}
$$

Functions N^u,N^p,N^U are shape functions for unknown field of skeleton dispalacements, pore fluid pressures and fluid displacements, respectively, while ρ, ρ_s, ρ_f are the density of the total, solid and fluid phases, respectively, n is the porosity, and by its definition $\rho = (1-n)\rho_s + n\rho_f$, the symbol n_i is the direction of the normal on the boundary, u_i is the displacement of the solid part, p is pore fluid pressure and U_i is the absolute displacement of the fluid part. Equation (102.142) represents the general form $(u-p-U)$ for coupled system which can be written in a familiar form as

$$
\boldsymbol{M\ddot{x} + C\dot{x} + Kx = f} \tag{102.146}
$$

where x represents the generalized unknown variable. The solution of this equation for each time step will render an unknown field for given initial and boundary conditions.

102.12.1.6 Choice of shape functions

Isoparametric elements are used in previous sections, where the coordinates are interpolated using the same shape functions as for the unknown. This mapping allows using elements of more arbitrary shape than simple forms such as rectangles and triangles. But in static or dynamic undrained analysis the permeability (and compressibility) matrices are zero, i.e.($Q \to \infty$,and $P \to 0$),resulting in a zero-matrix diagonal term in the equation(102.143).

The matrix to be solved is the same as that in the solutions of problems of incompressible elasticity or fluid mechanics. Actually, a wide choice of shape functions is available if the limiting(undrained) condition is never imposed. Due to the presence of first derivatives in space in all the equations, it is necessary to use "C_o-continuous" interpolation functions and the suitable element forms are shown in Fig.102.11.

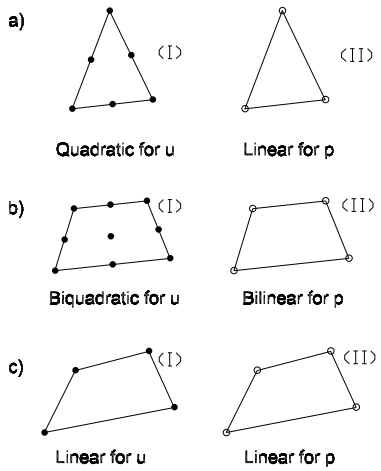

Figure 102.11: Shape functions used for coupled analysis, displacement u and pore pressure p formulation

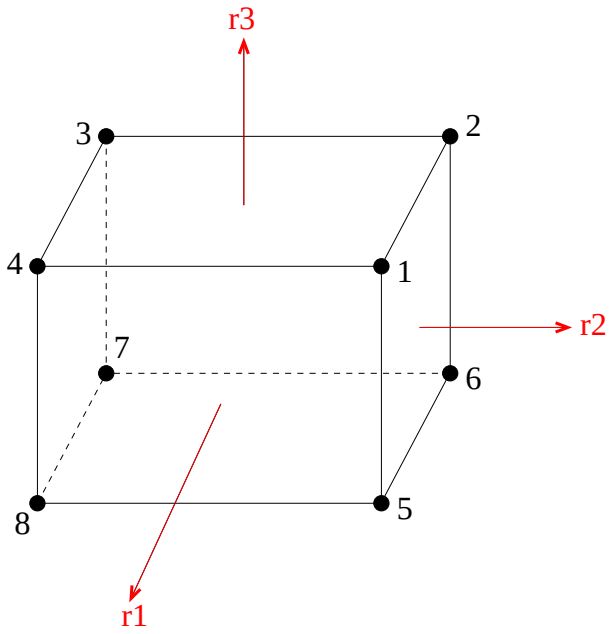

Figure 102.12: 8 node u-p-U brick element. Note that all seven DOFs (three porous solid displacements u_i, pore fluid pressure p and pore fluid displacements U_i are defined at each node.

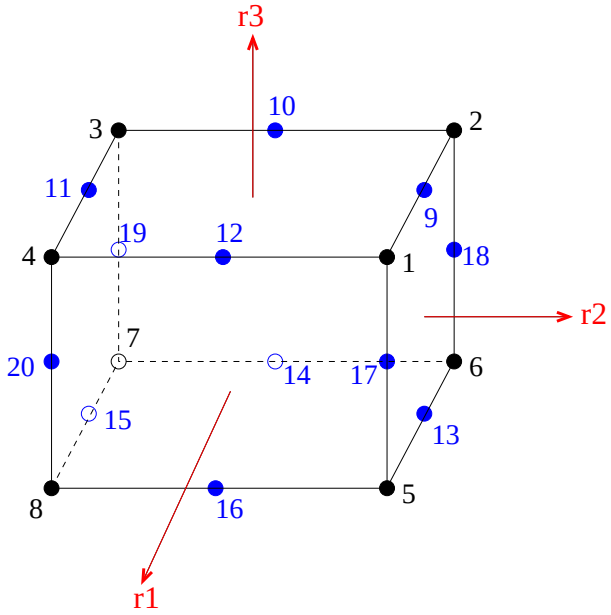

Figure 102.13: 20 node brick element. Note that all seven DOFs (three porous solid displacements u_i, pore fluid pressure p and pore fluid displacements U_i are defined at each node.

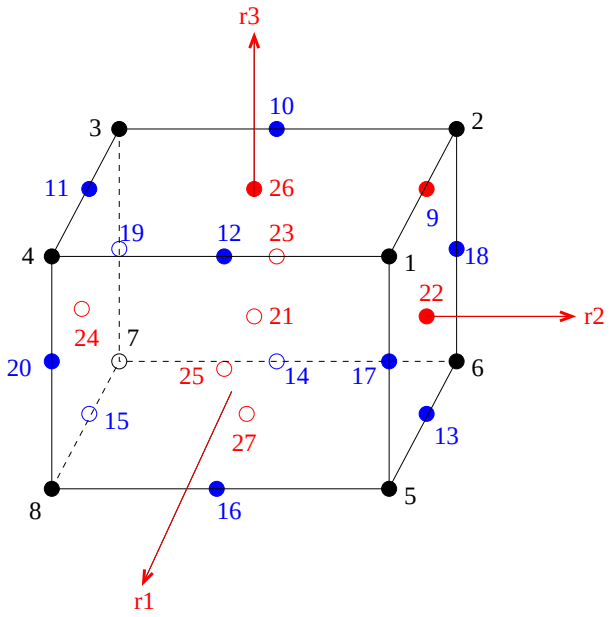

Figure 102.14: 27 node brick element. Note that all seven DOFs (three porous solid displacements u_i, pore fluid pressure p and pore fluid displacements U_i are defined at each node.

102.12.1.7 8 Node $u-p-U$ Brick

102.12.1.8 20 Node $u-p-U$ Brick

102.12.1.9 27 Node $u-p-U$ Brick

102.12.2 u-p-U Formulation for Partially Saturated, Unsaturated Material

Coming SOON, by end of Winter 2020

102.12.3 u-p Formulation

102.12.3.1 Governing Equations of Porous Media

The formulation given here is based on Zienkiewicz et al. (1999b).

The first governing equation of porous media is total momentum balance equation:

$$\sigma_{ij,j} - \rho\ddot{u}_i + \rho b_i = 0 \tag{102.147}$$

where $\sigma_{ij} = \sigma''_{ij} - \alpha p\delta_{ij}$ and $\rho = (1-n)\rho_s + n\rho_f$.

The second governing equation is the fluid mass balance equation:

$$\left(k_{ij}(-p_{,j} + \rho_f b_j)\right)_{,i} + \alpha\dot{u}_{i,i} + \frac{\dot{p}}{Q_{sf}} = 0 \tag{102.148}$$

where

$$k_{ij} = \frac{k'_{ij}}{g\rho_f} = \frac{k'_{ij}}{\gamma_f} \tag{102.149}$$

and k'_{ij} is the permeability in Darcy's law with the same unit as velocity.

$$Q_{sf} = \frac{K_s K_f}{K_s + K_f} \tag{102.150}$$

is the total compression modulus, K_s and K_f are solid and fluid compression modulus, respectively.

The boundary conditions are

$$\sigma_{ij} n_j = \bar{t}_i \quad \text{on} \quad \Gamma = \Gamma_t \tag{102.151}$$

$$u_i = \bar{u}_i \quad \text{on} \quad \Gamma = \Gamma_u \tag{102.152}$$

$$n_i w_i = n_i k_{ij}(-p_{,j} + \rho_f b_j) = \bar{w} = -\bar{q} \quad \text{on} \quad \Gamma = \Gamma_w \tag{102.153}$$

$$p = \bar{p} \quad \text{on} \quad \Gamma = \Gamma_p \tag{102.154}$$

where $\bar{w}$ is the outflow and $\bar{q}$ is the influx.

102.12.3.2 Numerical Solutions of the Governing Equations

The solid displacement u_i and the pore pressure p can be approximated using shape functions and nodal values:

$$u_i = N^u_K \bar{u}_{Ki} \tag{102.155}$$

$$p = N^p_L \bar{p}_L \tag{102.156}$$

Similar approximations are applied to $\dot{u}_i$, $\ddot{u}_i$, $\dot{p}$ and $\ddot{p}$.

Numerical solution of the total momentum balance The numerical solution of the total momentum balance is

$$\int_\Omega N^u_K \left(\sigma_{ij,j} - \rho\ddot{u}_i + \rho b_i\right) \mathrm{d}\Omega = 0 \tag{102.157}$$

First-term of (102.157) becomes

$$\begin{aligned}
\int_\Omega N^u_K \sigma_{ij,j} \mathrm{d}\Omega &= \int_{\Gamma_t} N^u_K \sigma_{ij,j} n_j \mathrm{d}\Omega - \int_\Omega N^u_{K,j} \sigma_{ij} \mathrm{d}\Omega \\
&= \int_{\Gamma_t} N^u_K \bar{t}_i \mathrm{d}\Omega - \int_\Omega N^u_{K,j} (\sigma''_{ij} - \alpha p \delta_{ij}) \mathrm{d}\Omega \\
&= (f^u_1)_{Ki} - \int_\Omega N^u_{K,j} \sigma''_{ij} \mathrm{d}\Omega + \int_\Omega N^u_{K,i} \alpha p \mathrm{d}\Omega \\
&= (f^u_1)_{Ki} - \int_\Omega N^u_{K,j} D_{ijml} \varepsilon_{ml} \mathrm{d}\Omega + [\int_\Omega \alpha N^u_{K,i} N^p_N \mathrm{d}\Omega] \bar{p}_N \\
&= (f^u_1)_{Ki} - [\int_\Omega N^u_{K,j} D_{ijml} N^u_{P,m} \mathrm{d}\Omega] \bar{u}_{Pm} + [\int_\Omega \alpha N^u_{K,i} N^p_N \mathrm{d}\Omega] \bar{p}_N \\
&= (f^u_1)_{Ki} - (K^{ep}_{KimP}) \bar{u}_{Pm} + (Q_{KiN}) \bar{p}_N \\
&= \boldsymbol{f^u_1 - (K^{ep}) \bar{u} + Q \bar{p}}
\end{aligned} \tag{102.158}$$

Second term of (102.157) becomes

$$\begin{aligned}
-\int_\Omega N^u_K \rho \ddot{u}_i \mathrm{d}\Omega &= -\int_\Omega N^u_K \rho N^u_L \mathrm{d}\Omega \ddot{u}_{Li} \\
&= -[\int_\Omega N^u_K \rho N^u_L \mathrm{d}\Omega] \ddot{\bar{u}}_{Li} \\
&= -[\delta_{ij} \int_\Omega N^u_K \rho N^u_L \mathrm{d}\Omega] \ddot{\bar{u}}_{Lj} \\
&= -(M_{KijL}) \ddot{\bar{u}}_{Lj} \\
&= \boldsymbol{-M \ddot{\bar{u}}}
\end{aligned} \tag{102.159}$$

The third term of (102.157) becomes

$$\begin{aligned}
\int_\Omega N^u_K \rho b_i \mathrm{d}\Omega &= (f^u_2)_{Ki} \\
&= \boldsymbol{f^u_2}
\end{aligned} \tag{102.160}$$

The equation (102.157) thus becomes

$$(M_{KijL}) \ddot{\bar{u}}_{Lj} - (Q_{KiN}) \bar{p}_N + (K^{ep}_{KijL}) \bar{u}_{Lj} = (f^u_1)_{Ki} + (f^u_2)_{Ki} = (f^u)_{Ki} \tag{102.161}$$

or

$$\boldsymbol{M \ddot{\bar{u}} - Q \bar{p} + (K^{ep}) \bar{u} = f^u_1 + f^u_2 = f^u} \tag{102.162}$$

Numerical solution of the fluid mass balance The numerical solution of the fluid mass balance is

$$\int_\Omega N^p_M \left(k_{ij} (-p_{,j} + \rho_f b_j)_{,j} + \alpha \dot{u}_{i,i} + \frac{\dot{p}}{Q_{sf}} \right) \mathrm{d}\Omega = 0 \tag{102.163}$$

First term of (102.163) becomes

$$\int_\Omega N_M^p \left(k_{ij}(-p_{,j}+\rho_f b_j)\right)_{,i} \mathrm{d}\Omega \tag{102.164}$$

$$\begin{aligned}
&= \int_{\gamma_w} N_M^p w_i n_i \mathrm{d}\Omega - \int_\Omega N_{M,i}^p k_{ij}(-p_{,j}+\rho_f b_j)\mathrm{d}\Omega \\
&= \int_{\gamma_w} N_M^p \bar{w}\mathrm{d}\Omega + \int_\Omega N_{M,i}^p k_{ij} p_{,j}\mathrm{d}\Omega - \int_\Omega N_{M,i}^p k_{ij}\rho_f b_j \mathrm{d}\Omega \\
&= (f_1^p)_M + \int_\Omega N_{M,i}^p k_{ij} p_{,j}\mathrm{d}\Omega - \int_\Omega N_{M,i}^p k_{ij}\rho_f b_j \mathrm{d}\Omega \\
&= (f_1^p)_M + [\int_\Omega N_{M,i}^p k_{ij} N_{N,j}^p \mathrm{d}\Omega]\bar{p}_N - (f_2^p)_M \\
&= (f_1^p)_M + (H_{MN})\bar{p}_N - (f_2^p)_M \\
&= \boldsymbol{f_1^p + H\bar{p} - f_2^p}
\end{aligned} \tag{102.165}$$

Second term of (102.163) becomes

$$\begin{aligned}
\int_\Omega N_M^p \alpha \dot{u}_{i,i}\mathrm{d}\Omega &= [\int_\Omega N_M^p \alpha N_{L,j}^u \mathrm{d}\Omega]\dot{\bar{u}}_{Lj} \\
&= (Q_{LjM})\dot{\bar{u}}_{Lj} \\
&= \boldsymbol{Q^T \dot{\bar{u}}}
\end{aligned} \tag{102.166}$$

The third term of (102.163) becomes

$$\begin{aligned}
\int_\Omega N_M^p \frac{\dot{p}}{Q_{sf}}\mathrm{d}\Omega &= [\int_\Omega N_M^p \frac{1}{Q_{sf}} N_N^p \mathrm{d}\Omega]\dot{\bar{p}}_N \\
&= (S_{MN})\dot{\bar{p}}_N \\
&= \boldsymbol{S\dot{\bar{p}}}
\end{aligned} \tag{102.167}$$

The equation (102.163) thus becomes

$$(H_{MN})\bar{p}_N + (Q_{LjM})\dot{\bar{u}}_{Lj} + (S_{MN})\dot{\bar{p}}_N = -(f_1^p)_M + (f_2^p)_M = (f^p)_M \tag{102.168}$$

or

$$\boldsymbol{H\bar{p} + Q^T\dot{\bar{u}} + S\dot{\bar{p}} = -f_1^p + f_2^p = f^p} \tag{102.169}$$

Matrix form of the governing equations Combine equation (102.161) and (102.168), to obtain

$$\begin{aligned}
&\begin{bmatrix} M_{KiLj} & 0 \\ 0 & 0 \end{bmatrix}\begin{bmatrix} \ddot{u}_{Lj} \\ \ddot{p}_N \end{bmatrix} + \begin{bmatrix} 0 & 0 \\ Q_{LjM} & S_{MN} \end{bmatrix}\begin{bmatrix} \dot{u}_{Lj} \\ \dot{p}_N \end{bmatrix} \\
&\quad + \begin{bmatrix} (K^{ep})_{KiLj} & -Q_{KiN} \\ 0 & H_{MN} \end{bmatrix}\begin{bmatrix} u_{Lj} \\ p_N \end{bmatrix} = \begin{bmatrix} f_{Ki}^u \\ f_M^p \end{bmatrix}
\end{aligned} \tag{102.170}$$

or, by combining equations (102.162) and (102.169), obtain

$$\begin{bmatrix} \boldsymbol{M} & \boldsymbol{0} \\ \boldsymbol{0} & \boldsymbol{0} \end{bmatrix} \begin{bmatrix} \ddot{\boldsymbol{u}} \\ \ddot{\boldsymbol{p}} \end{bmatrix} + \begin{bmatrix} \boldsymbol{0} & \boldsymbol{0} \\ \boldsymbol{Q^T} & \boldsymbol{S} \end{bmatrix} \begin{bmatrix} \dot{\boldsymbol{u}} \\ \dot{\boldsymbol{p}} \end{bmatrix} + \begin{bmatrix} \boldsymbol{K^{ep}} & \boldsymbol{Q} \\ \boldsymbol{0} & \boldsymbol{H} \end{bmatrix} \begin{bmatrix} \boldsymbol{u} \\ \boldsymbol{p} \end{bmatrix} = \begin{bmatrix} \boldsymbol{f^u} \\ \boldsymbol{f^p} \end{bmatrix} \tag{102.171}$$

where

$$\boldsymbol{f^u} \leftrightarrow f^u_{Ki} = (f^u_1)_{Ki} + (f^u_2)_{Ki} \tag{102.172}$$

$$\boldsymbol{f^p} \leftrightarrow f^p_M = -(f^p_1)_M + (f^p_2)_M \tag{102.173}$$

and

$$\boldsymbol{f^u_1} \leftrightarrow (f^u_1)_{Ki} = \int_{\Gamma_t} N^u_K \bar{t}_i \mathrm{d}\Gamma \tag{102.174}$$

$$\boldsymbol{f^u_2} \leftrightarrow (f^u_2)_{Ki} = \int_{\Omega} N^u_K \rho b_i \mathrm{d}\Omega \tag{102.175}$$

$$\boldsymbol{f^p_1} \leftrightarrow (f^p_1)_M = \int_{\Gamma_w} N^p_M \bar{w} \mathrm{d}\Gamma \tag{102.176}$$

$$\boldsymbol{f^p_2} \leftrightarrow (f^p_2)_M = \int_{\Omega} N^p_{M,i} k_{ij} \rho_f b_j \mathrm{d}\Omega \tag{102.177}$$

$$\boldsymbol{M} \leftrightarrow M_{KiLj} = \delta_{ij} \int_{\Omega} N^u_K \rho N^u_L \mathrm{d}\Omega \tag{102.178}$$

$$\boldsymbol{Q} \leftrightarrow Q_{KiN} = \int_{\Omega} \alpha N^u_{K,i} N^p_N \mathrm{d}\Omega \tag{102.179}$$

$$\boldsymbol{S} \leftrightarrow S_{MN} = \int_{\Omega} N^p_M \frac{1}{Q_{sf}} N^p_N \mathrm{d}\Omega \tag{102.180}$$

$$\boldsymbol{H} \leftrightarrow H_{MN} = \int_{\Omega} N^p_{M,i} k_{ij} N^p_{N,j} \mathrm{d}\Omega \tag{102.181}$$

102.12.3.3 8 Node $u-p$ Brick

102.13 Material and Geometric Non–Linear Finite Element Formulation

102.13.1 Introduction

Presented here is a detailed formulation of material and geometric non–linear static finite element system of equations. The configuration of choice is material or Lagrangian. Eulerian and mixed Eulerian-Lagrangian configuration will be mentioned as need be.

102.13.2 Equilibrium Equations

The local form of equilibrium equations in material format (Lagrangian) for static case can be written as:

$$P_{iJ,J} - \rho_0 b_i = 0 \tag{102.182}$$

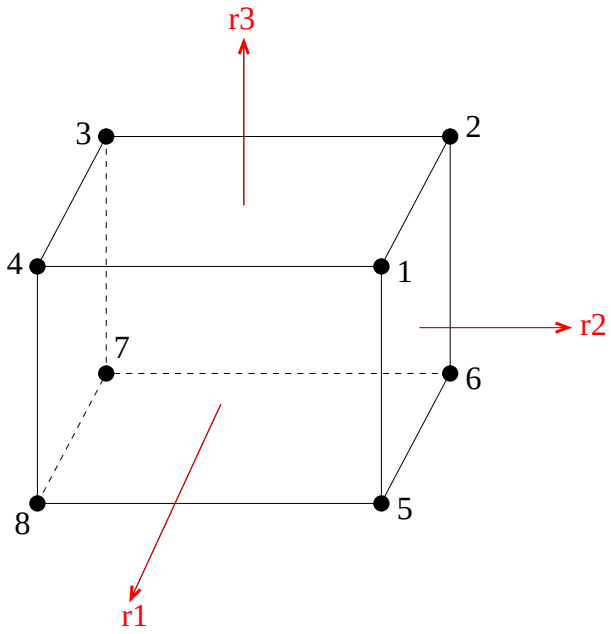

Figure 102.15: 8 node $u-p$ brick element. Note that all four DOFs (three porous solid displacements u_i and a pore fluid pressure p are defined at each node.

where $P_{iJ} = S_{IJ}(F_{iI})^t$ and S_{IJ} are first and second Piola–Kirchhoff stress tensors, respectively and b_I are body forces.

Weak form of equilibrium equations is obtained by premultiplying 102.182 with virtual displacements δu_i and integrating by parts on the initial configuration B_0 (initial volume V_0):

$$\int_{V_0} \delta u_{i,j} P_{ij} dV = \int_{V_0} \rho_0 \delta u_i b_i dV - \int_{S_0} \delta u_i \bar{t}_i dS \tag{102.183}$$

It proves beneficial to rewrite Lagrangian format of weak form of equilibrium equilibrium by using symmetric second Piola–Kirchhoff stress tensor S_{ij}:

$$\begin{aligned}
\int_{V_0} \delta u_{i,j} F_{jl} S_{il} dV &= \\
\int_{V_0} \frac{1}{2} \left(\delta u_{i,j} F_{jl} + F_{lj} \delta u_{j,i} + \right) S_{il} dV &= \\
\int_{V_0} \frac{1}{2} \left(\delta u_{i,j} \left(\delta_{jl} + u_{j,l} \right) + \left(\delta_{lj} + u_{l,j} \right) \delta u_{j,i} \right) S_{il} dV &= \\
\int_{V_0} \frac{1}{2} \left(\delta u_{i,l} + \delta ui, j u_{j,l} \right) + \left(\delta u_{l,i} + u_{l,j} \delta u_{j,i} \right) S_{il} dV &= \\
\int_{V_0} \frac{1}{2} \left(\left(\delta u_{i,l} + \delta u_{l,i} \right) + \left(\delta u_{i,j} u_{j,l} + u_{l,j} \delta u_{j,i} \right) \right) S_{il} dV &=
\end{aligned} \tag{102.184}$$

where symmetry of S_{il} was used, definition for deformation gradient $F_{ki} = \delta_{ki} + u_{k,i}$. In addition, conveniently defined was differential operator $\hat{E}_{il}(\delta u_i, u_i)$ as

$$\hat{E}_{il}(\delta u_i, u_i) = \frac{1}{2}\left(\delta u_{l,i} + \delta u_{i,l}\right) + \frac{1}{2}\left(u_{l,j}\delta u_{j,i} + \delta u_{i,j}u_{j,l}\right) \tag{102.185}$$

102.13.3 Formulation of Non–Linear Finite Element Equations

Consider the motion of a general solid in a fixed, non-moving Cartesian coordinate system, as shown in Figure (102.16), and assume that the solid can experience large displacements, large strains, and nonlinear constitutive response. The aim is to evaluate the equilibrium positions of the complete solid at discrete time points $0, \Delta t, 2\Delta t, \ldots$, where Δt is an increment in time. To develop the solution strategy, assume that the solutions for the static and kinematic variables for all time steps from 0 to time t inclusive, have been obtained. The solution process for the next required equilibrium position corresponding to time $t + \Delta t$ is typical and would be applied repetitively until a complete solution path has been found. Hence, in the analysis one follows all particles of the solid in their motion, from the original to the final configuration of the solid. In so doing, a Lagrangian (or material) formulation of the problem was adopted.

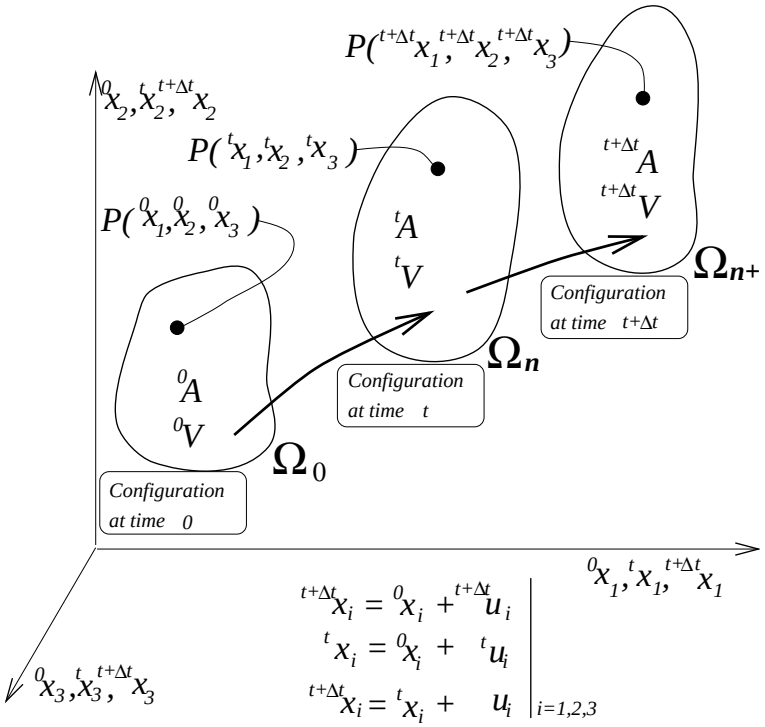

Figure 102.16: Motion of a solid in non-moving Cartesian coordinate system.

Weak format of the equilibrium equations can be obtained by premultiplying 102.182 with virtual

displacements δu_i and integrating by parts. We obtain the virtual work equations in the Lagrangian format:

$$\int_{V_0} \delta u_{i,j} P_{ij} dV = \int_{V_0} \rho_0 \delta u_i b_i dV - \int_{S_0} \delta u_i \bar{t}_i dV \tag{102.186}$$

Virtual work equations can also be written in terms of second Piola–Kirchhoff stress tensor S_{IJ} as:

$$\int_{V_0} \delta u_{i,j} F_{jl} S_{il} dV = \int_{V_0} \rho_0 \delta u_i b_i dV + \int_{S_0} \delta u_i \bar{t}_i dV \tag{102.187}$$

which after some algebraic manipulations, and after observing that $S_{IJ} = S_{JI}$ yields (SEE ABOVE!) By introducing a differential operator $\hat{E}(u_1, u_2)$ as:

$$\hat{E}_{il}({}^1u_i, {}^2u_i) = \frac{1}{2} \left({}^1u_{i,l} + {}^1u_{l,i} \right) + \frac{1}{2} \left({}^1u_{l,j} \, {}^2u_{j,i} + {}^2u_{i,j} \, {}^1u_{j,l} \right) \tag{102.188}$$

virtual work equation 102.185 can be written as:

$$\int_{V_0} \hat{E}_{il}(\delta u_i, u_i) S_{il} dV = \int_{V_0} \rho_0 \delta u_i b_i dV + \int_{S_0} \delta u_i \bar{t}_i dV \tag{102.189}$$

or as:

$$W(\delta u_i, u_i^{(k)})^{int} + W^{ext}(\delta u_i) = 0 \tag{102.190}$$

with:

$$\begin{aligned} W^{int}(\delta u_i, {}^{n+1}_0 u_i^{(k)}) &= \int_{\Omega_c} \hat{E}_{ij}(\delta u_i, {}^{n+1}_0 u_i^{(k)}) \, {}^{n+1}_0 S_{ij}^{(k)} \, dV \\ &= \int_{\Omega_c} \left(\left(\delta u_{j,i} + \delta u_{i,j} \right) + \left(u_{j,r} \delta u_{r,i} + \delta u_{i,r} u_{r,j} \right) \right) \, S_{ij}^{(k)} \, dV \end{aligned} \tag{102.191}$$

$$W^{ext}(\delta u_i) = - \int_{\Omega_c} \rho_0 \, \delta u_i \, {}^{n+1}_0 b_i \, dV - \int_{\partial \Omega_c} \delta u_i \, {}^{n+1}_0 t_i \, dS \tag{102.192}$$

102.13.4 Computational Domain in Incremental Analysis

This chapter elaborates on the choice of Total Lagrangian (TL) formulations as a computational domain. In addition, a Newton-type procedure is chosen for satisfying equilibrium, i.e., virtual work for a given computational domain. Given the displacement field $u_i^{(k)}(X_j)$, in iteration k, the iterative change δu_i

$$u_i^{(k+1)} = u_i^{(k)} + \Delta u_i \tag{102.193}$$

is obtained from the linearized virtual work expression

$$W(\delta u_i, u_i^{(k+1)}) \simeq W(\delta u_i, u_i^{(k)}) + \Delta W(\delta u_i, \Delta u_i; u_i^{(k)}) \tag{102.194}$$

Here, $W(\delta u_i, u_i^{(k)})$ is the virtual work expression

$$W(\delta u_i, u_i^{(k)}) = W(\delta u_i, u_i^{(k)})^{int} + W^{ext}(\delta u_i) \tag{102.195}$$

with

$$W^{int}(\delta u_i, {}^{n+1}_{0}u_i^{(k)}) = \int_{\Omega_c} \hat{E}_{ij}(\delta u_i, {}^{n+1}_{0}u_i^{(k)})\ {}^{n+1}_{0}S_{ij}^{(k)}\ dV \tag{102.196}$$

$$W^{ext}(\delta u_i) = -\int_{\Omega_c} \rho_0\ \delta u_i\ {}^{n+1}_{0}b_i\ dV - \int_{\partial\Omega_c} \delta u_i\ {}^{n+1}_{0}t_i\ dS \tag{102.197}$$

and the $\Delta W(\delta u_i, \Delta u_i; u_i^{(k)})$ is the linearization of virtual work

$$\begin{aligned}\Delta W(\delta u_i, \Delta u_i; u_i^{(k)}) &= \lim_{\epsilon\to 0} \frac{\partial W(\delta u_i, u_i + \epsilon \Delta u_i)}{\partial \epsilon} \\ &= \int_{\Omega_c} \hat{E}_{ij}(\delta u_i, u_i)\ dS_{ij}\ dV + \int_{\Omega_c} \Delta\hat{E}_{ij}(\delta u_i, u_i)\ S_{ij} dV \\ &= \int_{\Omega_c} \hat{E}_{ij}(\delta u_i, u_i)\ \mathcal{L}_{ijkl}\ \hat{E}_{kl}(\Delta u_i, u_i)\ dV + \int_{\Omega_c} \Delta\hat{E}_{ij}(\delta u_i, u_i)\ S_{ij}\ dV\end{aligned} \tag{102.198}$$

Here it was used that $dS_{ij} = 1/2\ \mathcal{L}_{ijkl} dC_{kl} = \mathcal{L}_{ijkl}\hat{E}_{kl}(\Delta u_i, u_i)$.

In order to obtain expressions for stiffness matrix, work is done on equation 102.198 in some more details. To this end, equation 102.198 can be rewritten by expanding definitions for $\hat{E}$ as

$$\begin{aligned}&\Delta W(\delta u_i, \Delta u_i; u_i^{(k)}) = \\ &\frac{1}{4}\int_{\Omega_c} \left(\left(\delta u_{j,i} + \delta u_{i,j}\right) + \left(u_{j,r}\delta u_{r,i} + \delta u_{i,r}u_{r,j}\right)\right)\ \mathcal{L}_{ijkl}\ \left(\left(\Delta u_{k,l} + \Delta u_{l,k}\right) + \left(u_{k,s}\Delta u_{s,l} + \Delta u_{l,s}u_{s,k}\right)\right)\ dV + \\ &+ \int_{\Omega_c} \frac{1}{2}\left(\Delta u_{j,l}\delta u_{l,i} + \delta u_{i,l}\Delta u_{l,j}\right) S_{ij}\ dV\end{aligned} \tag{102.199}$$

Or, by conveniently splitting the above equation

$$\begin{aligned}&\Delta^1 W(\delta u_i, \Delta u_i; u_i^{(k)}) = \\ &\frac{1}{4}\int_{\Omega_c} \left(\left(\delta u_{j,i} + \delta u_{i,j}\right) + \left(u_{j,r}\delta u_{r,i} + \delta u_{i,r}u_{r,j}\right)\right)\ \mathcal{L}_{ijkl}\ \left(\left(\Delta u_{k,l} + \Delta u_{l,k}\right) + \left(u_{k,s}\Delta u_{s,l} + \Delta u_{l,s}u_{s,k}\right)\right)\ dV\end{aligned} \tag{102.200}$$

$$\Delta^2 W(\delta u_i, \Delta u_i; u_i^{(k)}) = \int_{\Omega_c} \frac{1}{2}\left(\Delta u_{j,l}\delta u_{l,i} + \delta u_{i,l}\Delta u_{l,j}\right) S_{ij}\ dV \tag{102.201}$$

By further working on equation 102.200

$$\begin{aligned}\Delta^1 W(\delta u_i, \Delta u_i; u_i^{(k)}) = &\int_{\Omega_c} \left(\frac{1}{2}\left(\delta u_{j,i} + \delta u_{i,j}\right)\right)\ \mathcal{L}_{ijkl}\ \left(\frac{1}{2}\left(\Delta u_{k,l} + \Delta u_{l,k}\right)\right)\ dV \\ &+ \int_{\Omega_c} \left(\frac{1}{2}\left(\delta u_{j,i} + \delta u_{i,j}\right)\right)\ \mathcal{L}_{ijkl}\ \left(\frac{1}{2}\left(u_{k,s}\Delta u_{s,l} + \Delta u_{l,s}u_{s,k}\right)\right) dV \\ &+ \int_{\Omega_c} \frac{1}{2}\left(u_{j,r}\delta u_{r,i} + \delta u_{i,r}u_{r,j}\right)\mathcal{L}_{ijkl}\ \frac{1}{2}\left(u_{k,s}\Delta u_{s,l} + \Delta u_{l,s}u_{s,k}\right) dV \\ &+ \int_{\Omega_c} \frac{1}{2}\left(u_{j,r}\delta u_{r,i} + \delta u_{i,r}u_{r,j}\right)\mathcal{L}_{ijkl}\ \left(\frac{1}{2}\left(\Delta u_{k,l} + \Delta u_{l,k}\right)\right)\ dV\end{aligned} \tag{102.202}$$

It should be noted that the Algorithmic Tangent Stiffness (ATS) tensor $\mathcal{L}_{ijkl}$ poses both minor symmetries ($\mathcal{L}_{ijkl} = \mathcal{L}_{jikl} = \mathcal{L}_{ijlk}$). However, Major symmetry cannot be guaranteed. Non–associated flow rules in elastoplasticity lead to the loss of major symmetry ($\mathcal{L}_{ijkl} \neq \mathcal{L}_{klij}$). Moreover, it can be shown (i.e., Jeremić and Sture (1997)) that there is algorithmic induced symmetry loss even for associated flow rules.

With the minor symmetry of $\mathcal{L}_{ijkl}$ one can write (102.202) as:

$$\begin{aligned}\Delta^1 W(\delta u_i, \Delta u_i; u_i^{(k)}) = & \int_{\Omega_c} \delta u_{i,j}\ \mathcal{L}_{ijkl}\ \Delta u_{l,k} dV \\ + & \int_{\Omega_c} \delta u_{i,j}\ \mathcal{L}_{ijkl}\ u_{k,s} \Delta u_{l,s} dV \\ + & \int_{\Omega_c} \delta u_{i,r} u_{r,j}\ \mathcal{L}_{ijkl}\ u_{k,s} \Delta u_{l,s} dV \\ + & \int_{\Omega_c} \delta u_{i,r} u_{r,j}\ \mathcal{L}_{ijkl}\ \Delta u_{l,k} dV \end{aligned} \tag{102.203}$$

Similarly, by observing symmetry of second Piola–Kirchhoff stress tensor S_{ij}

$$\Delta^2 W(\delta u_i, \Delta u_i; u_i^{(k)}) = \int_{\Omega_c} \delta u_{i,l} \Delta u_{l,j}\ S_{ij} dV \tag{102.204}$$

Weak form of equilibrium expressions (i.e. (102.192) and (102.192)) for internal (W^{int}) and external (W^{ext}) virtual work, with the above mentioned symmetry of S_{ij} can be written as

$$W^{int}(\delta u_i, {}^{n+1}_{0}u_i^{(k)}) = \int_{\Omega_c} \delta u_{i,j}\ S_{ij} dV + \int_{\Omega_c} \delta u_{i,r} u_{r,j}\ S_{ij} dV \tag{102.205}$$

$$W^{ext}(\delta u_i) \quad = \quad - \int_{\Omega_c} \rho_0\ \delta u_i b_i\ dV - \int_{\partial\Omega_c} \delta u_i\ t_i\ dS \tag{102.206}$$

Standard finite element discretization of displacement field yields:

$$u_i \approx \hat{u}_i = H_I \bar{u}_{Ii} \tag{102.207}$$

where $\hat{u}_i$ is the approximation to exact, analytic (if it exists) displacement field u_i, H_I are standard FEM shape functions and $\bar{u}_{Ii}$ are nodal displacements. With this approximation

$$\begin{aligned}\Delta^1 W(\delta u_i, \Delta u_i; u_i^{(k)}) = & \int_{\Omega_c} \left(H_{I,j} \delta \bar{u}_{Ii}\right)\ \mathcal{L}_{ijkl}\ \left(H_{Q,k} \Delta \bar{u}_{Ql}\right) dV \\ + & \int_{\Omega_c} \left(H_{I,j} \delta \bar{u}_{Ii}\right)\ \mathcal{L}_{ijkl}\ \left(H_{J,k} \bar{u}_{Js}\right) \left(H_{Q,s} \Delta \bar{u}_{Ql}\right) dV \\ + & \int_{\Omega_c} \left(H_{I,r} \delta \bar{u}_{Ii}\right) \left(H_{J,j} \bar{u}_{Jr}\right) \mathcal{L}_{ijkl}\ \left(H_{J,k} \bar{u}_{Js}\right) \left(H_{Q,s} \Delta \bar{u}_{Ql}\right) dV \\ + & \int_{\Omega_c} \left(H_{I,r} \delta \bar{u}_{Ii}\right) \left(H_{J,j} \bar{u}_{Jr}\right) \mathcal{L}_{ijkl}\ \left(H_{Q,k} \Delta \bar{u}_{Ql}\right) dV \end{aligned} \tag{102.208}$$

$$\Delta^2 W(\delta u_i, \Delta u_i; u_i^{(k)}) = \int_{\Omega_c} \left(H_{I,l}\delta\bar{u}_{Ii}\right)\left(H_{Q,j}\Delta\bar{u}_{Ql}\right) S_{ij} dV \tag{102.209}$$

$$W^{int}(\delta u_i, {}^{n+1}_{0}u_i^{(k)}) = \int_{\Omega_c} \left(H_{I,j}\delta\bar{u}_{Ii}\right)\ S_{ij} dV + \int_{\Omega_c} \left(H_{I,r}\delta\bar{u}_{Ii}\right)\ \left(H_{J,j}\bar{u}_{Jr}\right)\ S_{ij} dV \tag{102.210}$$

$$W^{ext}(\delta u_i) \ = \ -\int_{\Omega_c} \rho_0\ (H_I\delta\bar{u}_{Ii})\ b_i\ dV - \int_{\partial\Omega_c} (H_I\delta\bar{u}_{Ii})\ t_i\ dS \tag{102.211}$$

Upon noting that virtual nodal displacements δu_{Ii} are any non–zero, continuous displacements, and since they occur in all expressions for linearized virtual work (from Equations (102.194), (102.195), (102.196), (102.197) and (102.198)) they can be factored out so that (while remembering that $\Delta W^1 + \Delta W^2 + W^{ext} + W^{int} = 0$):

$$\begin{aligned}
&\int_{\Omega_c} \left(H_{I,j}\right)\ \mathcal{L}_{ijkl}\ \left(H_{Q,k}\Delta\bar{u}_{Ql}\right) dV \\
+\ &\int_{\Omega_c} \left(H_{I,j}\right)\ \mathcal{L}_{ijkl}\ \left(H_{J,k}\bar{u}_{Js}\right)\left(H_{Q,s}\Delta\bar{u}_{Ql}\right) dV \\
+\ &\int_{\Omega_c} \left(H_{I,r}\right)\left(H_{J,j}\bar{u}_{Jr}\right)\mathcal{L}_{ijkl}\ \left(H_{J,k}\bar{u}_{Js}\right)\left(H_{Q,s}\Delta\bar{u}_{Ql}\right) dV \\
+\ &\int_{\Omega_c} \left(H_{I,r}\right)\left(H_{J,j}\bar{u}_{Jr}\right)\mathcal{L}_{ijkl}\ \left(H_{Q,k}\Delta\bar{u}_{Ql}\right) dV \\
+\ &\int_{\Omega_c} \left(H_{I,l}\right)\left(H_{Q,j}\Delta\bar{u}_{Ql}\right) S_{ij} dV \\
+\ &\int_{\Omega_c} \left(H_{I,j}\right)\ S_{ij} dV + \int_{\Omega_c} \left(H_{I,r}\right)\ \left(H_{J,j}\bar{u}_{Jr}\right)\ S_{ij} dV \\
=\ &\int_{\Omega_c} \rho_0\ (H_I)\ b_i\ dV + \int_{\partial\Omega_c} (H_I)\ t_i\ dS
\end{aligned} \tag{102.212}$$

By rearranging previous equations, one can write:

$$\begin{aligned}
&\left(\int_{\Omega_c} H_{I,j}\mathcal{L}_{ijkl}H_{Q,k} dV + \int_{\Omega_c} H_{I,j}\mathcal{L}_{ijkl}H_{J,k}\bar{u}_{Js}H_{Q,s} dV + \int_{\Omega_c} H_{I,r}H_{J,j}\bar{u}_{Jr}\mathcal{L}_{ijkl}H_{J,k}\bar{u}_{Js}H_{Q,s} dV\right. \\
+\ &\left.\int_{\Omega_c} H_{I,r}H_{J,j}\bar{u}_{Jr}\mathcal{L}_{ijkl}H_{Q,k} dV + \int_{\Omega_c} H_{I,l}H_{Q,j}S_{ij} dV\right)\Delta\bar{u}_{Ql} \\
+\ &\int_{\Omega_c} \left(H_{I,j}\right)\ S_{ij} dV + \int_{\Omega_c} \left(H_{I,r}\right)\ \left(H_{J,j}\bar{u}_{Jr}\right)\ S_{ij} dV \\
=\ &\int_{\Omega_c} \rho_0\ (H_I)\ b_i\ dV + \int_{\partial\Omega_c} (H_I)\ t_i\ dS
\end{aligned} \tag{102.213}$$

The vectors of external and internal forces are

$$\mathbf{f}_{int} \ = \ \frac{\partial(W^{int}(\delta u_i, {}^{n+1}_{0}u_i^{(k)}))}{\partial(\delta u_i)} \tag{102.214}$$

$$\mathbf{f}_{ext} \ = \ \frac{\partial(W^{ext}(\delta u_i))}{\partial(\delta u_i)} \tag{102.215}$$

The Algorithmic Tangent Stiffness (ATS) tensor $\mathcal{L}^{ATS}_{ijkl}$ is defined as a linearization of second Piola–Kirchhoff stress tensor S_{ij} with respect to the right deformation tensor C_{kl}

$$dS_{ij} = \frac{1}{2}\,\mathcal{L}_{ijkl}\,dC_{kl} \quad \text{with} \quad dC_{kl} = 2\,\hat{E}_{kl}(du_i, u_i) \tag{102.216}$$

Then, the global algorithmic tangent stiffness matrix (tensor) is given as

$$\mathbf{K}_t = \frac{\partial(\Delta W(\delta u_i, \Delta u_i; u_i^{(k)}))}{\partial(\delta u_i)} \tag{102.217}$$

The iterative change in displacement vector Δu_i is obtained by setting a linearized virtual work to zero

$$W(\delta u_i, u_i^{(k+1)}) = 0 \quad \Rightarrow \quad W(\delta u_i, u_i^{(k)}) = -\Delta W(\delta u_i, \Delta u_i; u_i^{(k)}) \tag{102.218}$$

102.13.4.1 Total Lagrangian Format

The undeformed configuration Ω_0 is chosen as the computational domain ($\Omega_c = \Omega_0$). The iterative displacement Δu_i is obtained from the equation

$$W(\delta u_i, {}^{n+1}u_i^{(k)}) = -\Delta W(\delta u_i, \Delta u_i; {}^{n+1}u_i^{(k)}) \tag{102.219}$$

where

$$\begin{aligned} W(\delta u_i, {}^{n+1}u_i^{(k)}) \;=\; & \int_{\Omega_c} \hat{E}_{ij}(\delta u_i, {}^{n+1}u_i^{(k)})\; {}^{n+1}S_{ij}^{(k)}\; dV \\ & - \int_{\Omega_c} \rho_0\; \delta u_i\; {}^{n+1}b_i\; dV - \int_{\partial\Omega_c} \delta u_i\; {}^{n+1}t_i\; dS \end{aligned} \tag{102.220}$$

and

$$\begin{aligned} \Delta W(\delta u_i, \Delta u_i; {}^{n+1}u_i^{(k)}) \;=\; & \int_{\Omega_c} \hat{E}_{ij}(\delta u_i, {}^{n+1}u_i^{(k)})\; {}^{n+1}\mathcal{L}_{ijkl}^{(k)}\; \hat{E}_{kl}(\Delta u_i, {}^{n+1}u_i^{(k)})\; dV \\ & + \int_{\Omega_c} d\hat{E}_{ij}(\delta u_i, \Delta u_i)\; {}^{n+1}S_{ij}^{(k)}\; dV \end{aligned} \tag{102.221}$$

In the case of hyperelastic–plastic response, second Piola–Kirchhoff stress ${}^{n+1}S_{ij}^{(k)}$ is obtained by integrating the constitutive law, described in Chapter 106.4. It should be noted that by integrating in the intermediate configuration, obtained is Mandel stress ${}^{n+1}\bar{T}_{ij}$ and subsequently[24] the second Piola–Kirchhoff stress $\bar{S}_{kj}$. The ATS tensor $\bar{\mathcal{L}}_{ijkl}$ is then obtained based on $\bar{S}_{kj}$. In order to obtain second Piola–Kirchhoff stress S_{kj} and ATS tensor in initial configuration, a pull-back from the intermediate configuration to the initial configuration is performed

$${}^{n+1}S_{ij} = {}^{n+1}F^p_{ip}\; {}^{n+1}F^p_{jq}\; {}^{n+1}\bar{S}_{pq} \tag{102.222}$$

$${}^{n+1}\mathcal{L}_{ijkl} = {}^{n+1}F^p_{im}\; {}^{n+1}F^p_{jn}\; {}^{n+1}F^p_{kr}\; {}^{n+1}F^p_{ls}\; {}^{n+1}\bar{\mathcal{L}}_{mnrs} \tag{102.223}$$

[24] $\bar{S}_{kj} = \left(\bar{C}_{ik}\right)^{-1} \bar{T}_{ij}$

102.13.5 Finite Element Formulations

Presented here is a slightly different approach to developing large deformation FEM in total Lagrangian form. Lower case indices are used for variables in current configuration, while the capital case indices are used for the reference configuration.

102.13.5.1 Strong Form

The static, strong form of momentum balance in the current configuration is

$$\frac{\partial \sigma_{ij}}{\partial x_j} + \rho b_i = 0 \tag{102.224}$$

where σ_{ij} is the Cauchy stress, *rho* is the material density, b_i is the material body force.

Used here was the so-called Total Lagrangian formulation that is based on the reference configuration. The strong form of momentum balance can be expressed in the reference configuration

$$\frac{\partial P_{iJ}}{\partial X_J} + \rho_0 b_i = 0 \tag{102.225}$$

where P_{iJ} is the first Pialo-Kirchhoff stress, ρ_0 is the material Lagrangian density and $\rho_0 = J\rho$.

102.13.5.2 Weak Form

The corresponding weak form of Equation 102.225 can be expressed as

$$\int_{\Omega_0} \delta u_i \left(\frac{\partial P_{iJ}}{\partial X_J} + \rho_0 b_i \right) dV = 0 \tag{102.226}$$

where δu_i is some arbitrary virtual displacement, Ω_0 is the concerned domain of the reference configuration. Using the partial integration rule, the above equation can be alternatively expressed as

$$\int_{\Omega_0} \frac{\partial}{\partial X_J} (P_{iJ} \delta u_i)\, dV - \int_{\Omega_0} P_{iJ} \frac{\partial \delta u_i}{\partial X_J} dV + \int_{\Omega_0} \rho_0 b_i \delta u_i dV = 0 \tag{102.227}$$

The first term of Equation 102.227 can be rewritten in terms of the surface traction

$$\int_{\Omega_0} \frac{\partial}{\partial X_J} (P_{iJ} \delta u_i)\, dV = \int_{\partial\Omega_0} \delta u_i P_{iJ} H_J dA = \int_{\partial\Omega_0} t_i \delta u_i dA \tag{102.228}$$

with the traction $t_i = P_{iJ} H_J$, where H_J the unit surface normal vector in the reference configuration, and $\partial\Omega_0$ is the boundary of the reference domain Ω_0.

The second term of Equation 102.227 can be rewritten as

$$\int_{\Omega_0} P_{iJ} \frac{\partial \delta u_i}{\partial X_J} dV = \int_{\Omega_0} P_{iJ} \delta F_{iJ} dV = \int_{\Omega_0} S_{IJ} \delta E_{IJ} dV \tag{102.229}$$

where S_{IJ} is the second Pialo-Kirchhoff stress and E_{IJ} is the Lagrangian-Green strain. $\delta F_{iJ} = \partial \delta u_i / \partial X_J$ is used.

The overall weak form in the reference configuration is now

$$\int_{\Omega_0} S_{IJ} \delta E_{IJ} dV = \int_{\partial \Omega_0} t_i \delta u_i dA + \int_{\Omega_0} \rho_0 b_i \delta u_i dV \tag{102.230}$$

102.13.5.3 Linearized Form

To utilize the iterative algorithm for incremental strategy, needed is the linearized form the governing equation 102.230.

The first term linearization of Equation 102.230 is

$$\begin{aligned} \Delta \int_{\Omega_0} S_{IJ} \delta E_{IJ} &= \int_{\Omega_0} [\Delta S_{IJ} \delta E_{IJ} + S_{IJ} \delta(\Delta E_{IJ})] \, dV \\ &= \int_{\Omega_0} [\mathcal{L}_{IJKL} \Delta E_{KL} \delta E_{IJ} + S_{IJ} \delta(\Delta E_{IJ})] \, dV \end{aligned} \tag{102.231}$$

where $\mathcal{L}_{IJKL}$ is the Lagrangian stiffness linked the second Pialo-Kirchhoff stress S_{IJ} and the Lagrangian-Green strain E_{KL} by the relation

$$S_{IJ} = \mathcal{L}_{IJKL} E_{KL} \tag{102.232}$$

The linearization of E_{KL} is

$$\Delta E_{KL} = Sym \left(F_K \frac{\partial \Delta u_b}{\partial X_L} \right) \tag{102.233}$$

where Sym is the operator of tensor symmetry, defined as $Sym(A_{ij}) := (1/2)(A_{ij} + A_{ji})$. Similarly,

$$\delta E_{IJ} = Sym \left(F_{aI} \frac{\partial \delta u_a}{\partial X_J} \right) \tag{102.234}$$

and

$$\delta(\Delta E_{IJ}) = Sym \left(\frac{\partial \delta u_c}{\partial X_I} \frac{\partial \Delta u_c}{\partial X_J} \right) \tag{102.235}$$

Note that S_{IJ} is a symmetric tensor, and L_{IJKL} is a tensor with major and minor symmetries, Equation 102.231 can be expressed as

$$\begin{aligned} \Delta \int_{\Omega_0} S_{IJ} \delta E_{IJ} &= \int_{\Omega_0} \left[\mathcal{L}_{IJKL} \left(F_{bK} \frac{\partial \Delta u_b}{\partial X_L} \right) \left(F_{aI} \frac{\partial \delta u_a}{\partial X_J} \right) + S_{IJ} \left(\frac{\partial \delta u_c}{\partial X_I} \frac{\partial \Delta u_c}{\partial X_J} \right) \right] dV \\ &= \int_{\Omega_0} \left[\frac{\partial \delta u_a}{\partial X_J} \left(F_{aI} F_{bK} \mathcal{L}_{IJKL} + \delta_{ab} S_{JL} \right) \frac{\partial \Delta u_b}{\partial X_L} \right] dV \end{aligned} \tag{102.236}$$

The overall linearization form is thus

$$\int_{\Omega_0} \left[\frac{\partial \delta u_a}{\partial X_J} \left(F_{aI} F_{bK} \mathcal{L}_{IJKL} + \delta_{ab} S_{JL} \right) \frac{\partial \Delta u_b}{\partial X_L} \right] dV = \int_{\partial \Omega_0} \Delta t_i \delta u_i dA + \int_{\Omega_0} \rho_0 \Delta b_i \delta u_i dV \tag{102.237}$$

102.13.5.4 Finite Element Form

In finite element form, the displacements u_i are interpolated from the element nodal displacements $\bar{u}_{Ai}$:

$$u_i = H_A \bar{u}_{Ai} \tag{102.238}$$

where H_A is the element shape function of the node A, $\bar{u}_{Ai}$ is the node A displacements, and

$$\frac{\partial \delta u_a}{\partial X_J} = \frac{\partial H_A}{\partial X_J} \delta \bar{u}_{Aa}, \quad \frac{\partial \Delta u_b}{\partial X_L} = \frac{\partial H_B}{\partial X_L} \Delta \bar{u}_{Bb} \tag{102.239}$$

Equation 102.237 can be expressed as

$$\left(K_{AaBb} \, \Delta \bar{u}_{Bb} \, - \Delta f^{ex}_{Aa} \right) \delta \bar{u}_{Aa} = 0 \tag{102.240}$$

where

$$K_{AaBb} = \int_{\Omega_0} \frac{\partial H_A}{\partial X_J} \left(F_{aI} F_{bK} \mathcal{L}_{IJKL} + \delta_{ab} S_{JL} \right) \frac{\partial H_B}{\partial X_L} dV \tag{102.241}$$

$$\Delta f^{ex}_{Aa} = \int_{\partial \Omega_0} H_A \Delta t_i dA + \int_{\Omega_0} \rho_0 H_A \Delta b_i dV \tag{102.242}$$

Due to the arbitrariness of the virtual nodal displacements, the expression in the parentheses should be zero in Equation 102.240, which gives the incremental finite element form:

$$K_{AaBb} \, \Delta \bar{u}_{Bb} \, = \Delta f^{ex}_{Aa} \tag{102.243}$$

102.14 Cosserat Continuum Finite Element Formulation

102.14.1 Introduction

The classical theory of elasticity describes well the behavior of metals, like steel and aluminum. But when the micro-structure of the material becomes significant, like soil and sand, the classical elasticity lacks the ability to represent the granular media properties. In 1909, Cosserat Cosserat (1909) brothers published their prominent work on the Cosserat continua to remove the shortcomings of the classical elasticity. Compared to the classical continua, Cosserat continua has the additional couple stress to reflect the free rotations on the particles.

102.14.1.1 3D Finite Element Formulation for Cosserat Continua

Pothier Pothier and Rencis (1994) proposed the three-dimensional finite element formulation for micro-polar elasticity with both classical strain and the micro-polar strain components. Riahi Dehkordi (2008) developed the finite element Cosserat formulation with the application in layered structures. This article

contributes the three-dimensional finite element formulation with the micro-polar strain, which simplifies further development in the elastoplasticity algorithm. In addition, the formulation for the isoparametric brick element is provided.

102.14.1.2 Cosserat Elastoplastic Algorithm

Vardoulakis et al. Vardoulakis (1989); Papamichos et al. (1990) developed the 2D Cosserat plasticity to predict the thickness of shear bands in granular materials. De Borst de Borst (1993, 1991) applied the 2D Cosserat elastoplasticity to analyze the strain localization. Li Li and Bing Chen (2005) applied the 2D pressure-dependent Cosserat elastoplasticity to simulate the strain localization. Grammenoudis Grammenoudis and Tsakmakis (2005) implemented the micro-polar plasticity in the finite deformation framework. This article developed the implicit algorithms for 3D Cosserat plasticity. Rotational kinematic hardening is introduced to the Cosserat elastoplasticity.

102.14.2 Cosserat Elasticity

The Cosserat (micro-polar) elasticity has 6 parameters Pothier and Rencis (1994) , including λ, μ, χ, π_1, π_2, π_3.

The units of λ, μ, and χ are $Newton/(meter^2)$. The units of π_1, π_2, and π_3 are $Newton$.

102.14.2.1 Stress

The stress is the same to the classical elastic stress Riahi and Curran (2009); Dehkordi (2008),

$$\sigma = \begin{pmatrix} \sigma_{11} & \sigma_{12} & \sigma_{13} \\ \sigma_{21} & \sigma_{22} & \sigma_{23} \\ \sigma_{31} & \sigma_{32} & \sigma_{33} \end{pmatrix} \tag{102.244}$$

where the unit of σ is force per unit area $(Newton/meter^2)$.

102.14.2.2 Couple Stress

The couple-stress is the couple stress of the classical elastic stress.

$$\boldsymbol{t} = \begin{pmatrix} t_{11} & t_{12} & t_{13} \\ t_{21} & t_{22} & t_{23} \\ t_{31} & t_{32} & t_{33} \end{pmatrix} \tag{102.245}$$

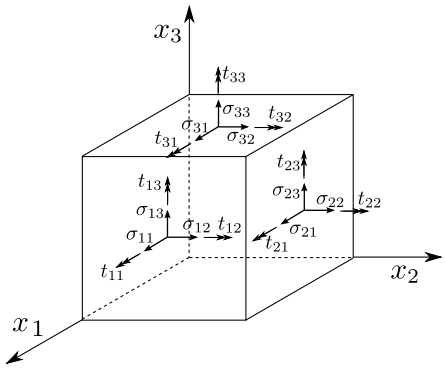

Figure 102.17: Illustration of Stress and Couple Stress

where the unit of $\boldsymbol{t}$ is torque per unit area ($Newton/meter$).

In the classical elasticity, the stress is symmetric: $\sigma_{12} = \sigma_{21}$. This is no longer true in the Cosserat materials. Namely, $\sigma_{12} \neq \sigma_{21}$ due to the couple stress.

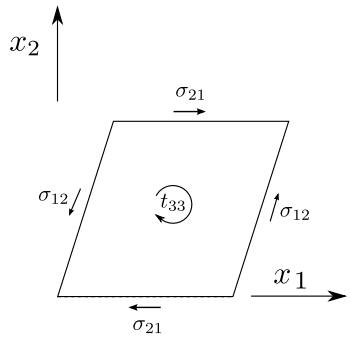

Figure 102.18: Illustration of Asymmetric Stress due to Couple Stress

102.14.2.3 Generalized Stress

In the calculation, for the purpose of simplification, the generalized stress are defined by :

$$\begin{aligned} \boldsymbol{\sigma} &= [\sigma \vdots t] \\ \boldsymbol{\sigma} &= [\sigma_{11}\ \sigma_{12}\ \sigma_{13}\ \sigma_{21}\ \sigma_{22}\ \sigma_{23}\ \sigma_{31}\ \sigma_{32}\ \sigma_{33} \vdots t_{11}\ t_{12}\ t_{13}\ t_{21}\ t_{22}\ t_{23}\ t_{31}\ t_{32}\ t_{33}] \end{aligned} \tag{102.246}$$

Namely, the generalized stress $\boldsymbol{\sigma}$ (18×1) is a horizontal combination of σ and t.

102.14.2.4 Cosserat Strain

$$\boldsymbol{\epsilon} = u_{j,i} - e_{ijk}\phi_k = \begin{pmatrix} u_{1,1} & u_{2,1} - \phi_3 & u_{3,1} + \phi_2 \\ u_{1,2} + \phi_3 & u_{2,2} & u_{3,2} - \phi_1 \\ u_{1,3} - \phi_2 & u_{2,3} + \phi_1 & u_{3,3} \end{pmatrix} \tag{102.247}$$

where e_{ijk} is the permutation symbol.

where u and ϕ are the displacement and micro-rotation respectively.

Note that generally $\epsilon_{12} \neq \epsilon_{21}$ even when $\boldsymbol{\phi} = 0$.

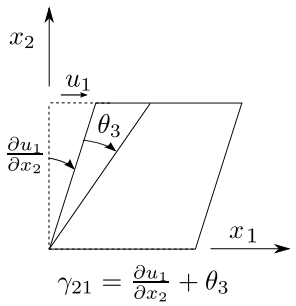

Figure 102.19: Illustration of Asymmetric Strain due to Rotations

102.14.2.5 Curvature

$$\boldsymbol{\omega} = \phi_{i,j} = \begin{pmatrix} \phi_{1,1} & \phi_{1,2} & \phi_{1,3} \\ \phi_{2,1} & \phi_{2,2} & \phi_{2,3} \\ \phi_{3,1} & \phi_{3,2} & \phi_{3,3} \end{pmatrix} \tag{102.248}$$

where ϕ is called the micro-rotation and ω is called the Cosserat rotation gradient (curvature).

102.14.2.6 Generalized Strain

In the calculation, for the purpose of simplification, the Generalized Strain are defined by :

$$\begin{aligned} \xi &= [\epsilon \vdots \omega] \\ \xi &= [\epsilon_{11}\ \epsilon_{12}\ \epsilon_{13}\ \epsilon_{21}\ \epsilon_{22}\ \epsilon_{23}\ \epsilon_{31}\ \epsilon_{32}\ \epsilon_{33} \vdots \omega_{11}\ \omega_{12}\ \omega_{13}\ \omega_{21}\ \omega_{22}\ \omega_{23}\ \omega_{31}\ \omega_{32}\ \omega_{33}] \end{aligned} \tag{102.249}$$

The generalized strain ξ (18×1) is a horizontal combination of ϵ and κ.

102.14.2.7 Constitutive Equations

Force Tangent: The relationship between the stress and strain Pothier and Rencis (1994) is

$$\sigma_{ij} = \lambda\epsilon_{kk}\delta_{ij} + \mu\epsilon_{ij} + (\mu + \chi)\epsilon_{ji} \tag{102.250}$$

Therefore, the tangent between stress and strain is

$$E_{ijkl} = \lambda\delta_{ij}\delta_{kl} + \mu\delta_{ik}\delta_{jl} + (\mu + \chi)\delta_{jk}\delta_{il} \tag{102.251}$$

Curvature Tangent: The relationship between the couple-stress and curvature is

$$t_{ij} = \pi_1\omega_{kk}\delta_{ij} + \pi_2\omega_{ij} + \pi_3\omega_{ji} \tag{102.252}$$

Therefore, the tangent between couple-stress and curvature is

$$C_{ijkl} = \pi_1\delta_{ij}\delta_{kl} + \pi_2\delta_{ik}\delta_{jl} + \pi_3\delta_{jk}\delta_{il} \tag{102.253}$$

102.14.2.8 Relation to the classical elasticity tangent

When $\chi = \pi_1 = \pi_2 = \pi_3 = 0$, the curvature tangent is zero, and the force tangent is the same to the classical elasticity tangent.

Full tangent matrix for one Cosserat point:

$$\mathcal{D}^{full}_{18\times18} = \begin{pmatrix} D^{force}_{9\times9} & [0]_{9\times9} \\ [0]_{9\times9} & D^{curvature}_{9\times9} \end{pmatrix}_{18\times18} \tag{102.254}$$

102.14.2.9 Flatten the tensor of force tangent and curvature tangent

Corresponding to the defined generalized stress and generalized strain, flatten the $3\times3\times3\times3$ tensor C_{ijkl} to 9×9 matrix D.

$$D_{9\times9} = \begin{pmatrix} C_{1111} & C_{1112} & C_{1113} & C_{1121} & C_{1122} & C_{1123} & C_{1131} & C_{1132} & C_{1133} \\ C_{1211} & C_{1212} & C_{1213} & C_{1221} & C_{1222} & C_{1223} & C_{1231} & C_{1232} & C_{1233} \\ C_{1311} & C_{1312} & C_{1313} & C_{1321} & C_{1322} & C_{1323} & C_{1331} & C_{1332} & C_{1333} \\ C_{2111} & C_{2112} & C_{2113} & C_{2121} & C_{2122} & C_{2123} & C_{2131} & C_{2132} & C_{2133} \\ C_{2211} & C_{2212} & C_{2213} & C_{2221} & C_{2222} & C_{2223} & C_{2231} & C_{2232} & C_{2233} \\ C_{2311} & C_{2312} & C_{2313} & C_{2321} & C_{2322} & C_{2323} & C_{2331} & C_{2332} & C_{2333} \\ C_{3111} & C_{3112} & C_{3113} & C_{3121} & C_{3122} & C_{3123} & C_{3131} & C_{3132} & C_{3133} \\ C_{3211} & C_{3212} & C_{3213} & C_{3221} & C_{3222} & C_{3223} & C_{3231} & C_{3232} & C_{3233} \\ C_{3311} & C_{3312} & C_{3313} & C_{3321} & C_{3322} & C_{3323} & C_{3331} & C_{3332} & C_{3333} \end{pmatrix}_{9\times9} \tag{102.255}$$

102.14.3 3D Finite Element Formulation

102.14.3.1 Force Equilibrium

$\sigma_{ji,j} + b_i = \rho \ddot{u}_i$ in dynamic problems.

$$\begin{aligned} \frac{\partial \sigma_{xx}}{\partial x} + \frac{\partial \sigma_{yx}}{\partial y} + \frac{\partial \sigma_{zx}}{\partial z} + b_x &= \rho \ddot{u}_x \\ \frac{\partial \sigma_{xy}}{\partial x} + \frac{\partial \sigma_{yy}}{\partial y} + \frac{\partial \sigma_{zy}}{\partial z} + b_y &= \rho \ddot{u}_y \\ \frac{\partial \sigma_{xz}}{\partial x} + \frac{\partial \sigma_{yz}}{\partial y} + \frac{\partial \sigma_{zz}}{\partial z} + b_z &= \rho \ddot{u}_z \end{aligned} \tag{102.256}$$

where b_i is the body force, and $\ddot{u}_i$ is the acceleration of the point.

102.14.4 Momentum Equilibrium

$t_{ji,j} + e_{ijk}\sigma_{jk} + M_i = J\ddot{\theta}_i$ in dynamic problems.

$$\begin{aligned} \frac{\partial t_{xx}}{\partial x} + \frac{\partial t_{yx}}{\partial y} + \frac{\partial t_{zx}}{\partial z} + \sigma_{xy} - \sigma_{yx} + M_x &= J_x \theta_x \\ \frac{\partial t_{xy}}{\partial x} + \frac{\partial t_{yy}}{\partial y} + \frac{\partial t_{zy}}{\partial z} + \sigma_{zx} - \sigma_{xz} + M_y &= J_y \theta_y \\ \frac{\partial t_{xz}}{\partial x} + \frac{\partial t_{yz}}{\partial y} + \frac{\partial t_{zz}}{\partial z} + \sigma_{yz} - \sigma_{zy} + M_z &= J_z \theta_z \end{aligned} \tag{102.257}$$

where M_i is the body rotation force per unit area ($Newton/meter^2$).

102.14.4.1 Illustration in 2D

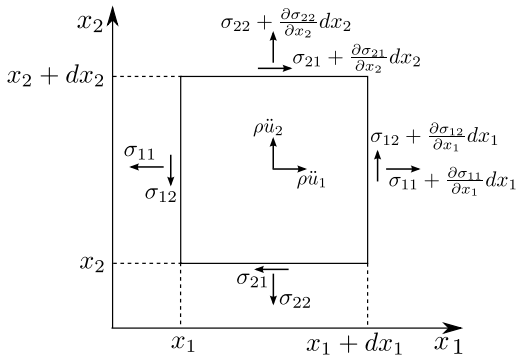

Figure 102.20: Illustration of Force Equilibrium in Cosserat Continua

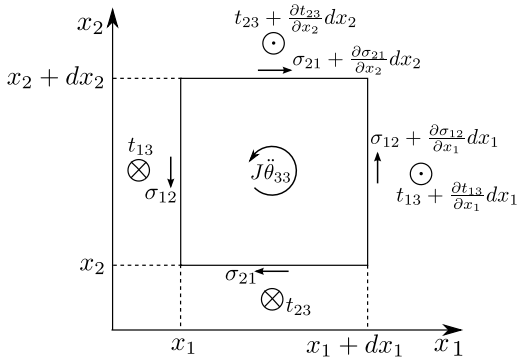

Figure 102.21: Illustration of Moment Equilibrium in Cosserat Continua

102.14.4.2 Strain-Displacement Relationship

Define the DOFs and the generalized strain. For the 8-node brick element. Each node has 6 DOFs.

The vector of nodal DOFs is defined by :

$$\mathcal{U} = [\boldsymbol{u} \quad \boldsymbol{\phi}]^T = [u_x \; u_y \; u_z \; \phi_x \; \phi_y \; \phi_z]^T_{1\times 6} \tag{102.258}$$

The vector of generalized strain ξ (18×1) is a horizontal combination of ϵ and κ.

$$\xi = [\epsilon_{11} \; \epsilon_{12} \; \epsilon_{13} \; \epsilon_{21} \; \epsilon_{22} \; \epsilon_{23} \; \epsilon_{31} \; \epsilon_{32} \; \epsilon_{33} \vdots \omega_{11} \; \omega_{12} \; \omega_{13} \; \omega_{21} \; \omega_{22} \; \omega_{23} \; \omega_{31} \; \omega_{32} \; \omega_{33}] \tag{102.259}$$

Strain-displacement for one node. Therefore,

$$\xi_{18\times 1} = \mathcal{B}_{18\times 6}\mathcal{U}_{6\times 1} \tag{102.260}$$

So the dimension of matrix $\mathcal{B}$ (strain-displacement matrix) for 1 node is 18×6.

According to the definition of force strain (Eq 102.247) and curvature (Eq 102.248), express the matrix $\mathcal{B}$ for 1 node Riahi and Curran (2009); Padovan (1978) by

$$\mathcal{B}_N = \begin{pmatrix} \mathcal{B}_{Na} & \mathcal{B}_{Nb} \\ [0]_{9\times 3} & \mathcal{B}_{Nc} \end{pmatrix}_{18\times 6} \tag{102.261}$$

where

$$\mathcal{B}_{Na} = \begin{pmatrix} H_{N,x} & 0 & 0 \\ 0 & H_{N,x} & 0 \\ 0 & 0 & H_{N,x} \\ H_{N,y} & 0 & 0 \\ 0 & H_{N,y} & 0 \\ 0 & 0 & H_{N,y} \\ H_{N,z} & 0 & 0 \\ 0 & H_{N,z} & 0 \\ 0 & 0 & H_{N,z} \end{pmatrix}_{9\times 3}, \quad \mathcal{B}_{Nb} = \begin{pmatrix} 0 & 0 & 0 \\ 0 & 0 & -H_N \\ 0 & +H_N & 0 \\ 0 & 0 & +H_N \\ 0 & 0 & 0 \\ -H_N & 0 & 0 \\ 0 & -H_N & 0 \\ +H_N & 0 & 0 \\ 0 & 0 & 0 \end{pmatrix}_{9\times 3}, \tag{102.262}$$

$$\mathcal{B}_{Nc} = \begin{pmatrix} -H_{N,x} & 0 & 0 \\ -H_{N,y} & 0 & 0 \\ -H_{N,z} & 0 & 0 \\ 0 & -H_{N,x} & 0 \\ 0 & -H_{N,y} & 0 \\ 0 & -H_{N,z} & 0 \\ 0 & 0 & -H_{N,x} \\ 0 & 0 & -H_{N,y} \\ 0 & 0 & -H_{N,z} \end{pmatrix}_{9\times 3} \tag{102.263}$$

where H is the shape function. N is the node number, which can be 1, 2, ..., 8.

Strain-displacement for 8 node brick. So the dimension of matrix $\mathcal{B}$ (strain-displacement matrix) for 8 node brick is 18×48.

$$\mathscr{B} = [\ \mathcal{B}_1\ \ \mathcal{B}_2\ \ \mathcal{B}_3\ \ \mathcal{B}_4\ \ \mathcal{B}_5\ \ \mathcal{B}_6\ \ \mathcal{B}_7\ \ \mathcal{B}_8\ ]_{18\times 48} \tag{102.264}$$

Express the 8 node displacement by

$$\mathscr{U} = [\ \mathcal{U}_1\ \ \mathcal{U}_2\ \ \mathcal{U}_3\ \ \mathcal{U}_4\ \ \mathcal{U}_5\ \ \mathcal{U}_6\ \ \mathcal{U}_7\ \ \mathcal{U}_8\ ]^T_{48\times 1} \tag{102.265}$$

Note that matrix $\mathscr{B}$ is a field function obtained by the interpolation of the displacements at 8 nodes.

For a specified Gauss point, the Gauss coordinates should be substituted to calculate the corresponding generalized strain.

So the generalized strain at a specific Gauss coordinates is

$$\mathscr{E}|_{x_i,y_i,z_i} = \mathscr{B}|_{x_i,y_i,z_i}\mathscr{U} \tag{102.266}$$

102.14.4.3 Isoparametric 8 Node Brick

For the purpose of completeness, the shape function Bathe (1996) for the isoparametric 8 node brick is given by

$$H_i = \frac{1}{8}(1+\xi_i\xi)(1+\eta_i\eta)(1+\zeta_i\zeta) \tag{102.267}$$

where the values of ξ_i, η_i, ζ_i for eight nodes are listed.

Node	ξ_i	η_i	ζ_i
1	+1	+1	+1
2	-1	+1	+1
3	-1	-1	+1
4	+1	-1	+1
5	+1	-1	+1
6	-1	+1	-1
7	-1	-1	-1
8	+1	-1	-1

In addition, the shape function is used for both the displacement interpolation in Eq (102.268) and coordinate transformation formula in Eq (102.269) from the global coordinate to the natural coordinate system.

$$\begin{aligned} u_x &= \sum_{i=1}^{8} H_i(\xi,\eta,\zeta)u_x^i \qquad u_y = \sum_{i=1}^{8} H_i(\xi,\eta,\zeta)u_y^i \qquad u_z = \sum_{i=1}^{8} H_i(\xi,\eta,\zeta)u_z^i \\ \phi_x &= \sum_{i=1}^{8} H_i(\xi,\eta,\zeta)\phi_x^i \qquad \phi_y = \sum_{i=1}^{8} H_i(\xi,\eta,\zeta)\phi_y^i \qquad \phi_z = \sum_{i=1}^{8} H_i(\xi,\eta,\zeta)\phi_z^i \end{aligned} \tag{102.268}$$

The coordinate transformation formula from the global coordinate to the natural coordinate system is

$$x = \sum_{i=1}^{8} H_i(\xi,\eta,\zeta)x_i \qquad y = \sum_{i=1}^{8} H_i(\xi,\eta,\zeta)y_i \qquad z = \sum_{i=1}^{8} H_i(\xi,\eta,\zeta)z_i \tag{102.269}$$

where the x_i, y_i, z_i are the nodal coordinates. Therefore, with the help of Eq (102.269), the global coordinate (x,y,z) become a function of (ξ,η,ζ), which is the natural coordinate in the isoparametric element.

To construct the strain-displacement matrix, the derivative with respect to the global coordinate (x,y,z) is required. Jacobian transformation is used to calculate the derivatives in Eq (102.262, 102.263).

$$\begin{pmatrix} \frac{\partial H_i}{\partial x} \\ \\ \frac{\partial H_i}{\partial y} \\ \\ \frac{\partial H_i}{\partial z} \end{pmatrix} = \boldsymbol{J}^{-1} \begin{pmatrix} \frac{\partial H_i}{\partial \xi} \\ \\ \frac{\partial H_i}{\partial \eta} \\ \\ \frac{\partial H_i}{\partial \zeta} \end{pmatrix} \tag{102.270}$$

where

$$\boldsymbol{J} = \begin{pmatrix} \frac{\partial x}{\partial \xi} & \frac{\partial y}{\partial \xi} & \frac{\partial z}{\partial \xi} \\ \frac{\partial x}{\partial \eta} & \frac{\partial y}{\partial \eta} & \frac{\partial z}{\partial \eta} \\ \frac{\partial x}{\partial \zeta} & \frac{\partial y}{\partial \zeta} & \frac{\partial z}{\partial \zeta} \end{pmatrix} = \begin{pmatrix} \sum_{i=1}^{8} \frac{\partial H_i}{\partial \xi} x_i & \sum_{i=1}^{8} \frac{\partial H_i}{\partial \xi} y_i & \sum_{i=1}^{8} \frac{\partial H_i}{\partial \xi} z_i \\ \\ \sum_{i=1}^{8} \frac{\partial H_i}{\partial \eta} x_i & \sum_{i=1}^{8} \frac{\partial H_i}{\partial \eta} y_i & \sum_{i=1}^{8} \frac{\partial H_i}{\partial \eta} z_i \\ \\ \sum_{i=1}^{8} \frac{\partial H_i}{\partial \zeta} x_i & \sum_{i=1}^{8} \frac{\partial H_i}{\partial \zeta} y_i & \sum_{i=1}^{8} \frac{\partial H_i}{\partial \zeta} z_i \end{pmatrix} \tag{102.271}$$

Note that $\mathcal{B}_{Nb}$ in Eq (102.262) has the original shape functions. Jacobian transformation is not required on $\mathcal{B}_{Nb}$ because the interpolated rotation is used directly to construct the strain in Eq (102.247) .

Chapter 103

Micromechanical Origins of Elasto-Plasticity

(1994-2002-2010-2019-2021-)

103.1 Chapter Summary and Highlights

This chapter is based in large part on lecture notes by Prof. Stein Sture (Sture, 1993).

103.2 Friction

103.2.1 Early Works

- Leonardo da Vinci, (1452-1519), worked and wrote about friction in 1493... (https://en.wikipedia.org/wiki/Leonardo_da_Vinci)
- Guillaume Amontons (1663-1705), Law of friction, rediscovered in 1699 (since da Vinci's notes were lost), (https://en.wikipedia.org/wiki/Guillaume_Amontons)
- Charles-Augistine de Coulomb (1736-1806), verified laws of friction in 1791 (https://en.wikipedia.org/wiki/Charles-Augustin_de_Coulomb)

Surface with asperities
grain assemblies, loose and dense
Saw-Teeth model analog
Frictional response of solids, friction angle for the polished mineral and dilatancy angle
Particle shapes
Particle rotations
types of packaging of particles

103.3 Particle Contact Mechanics

103.3.1 Particle Contact Mechanics, Axial Behavior

- Hertz contact theory, elastic (1885)
- Cattaneo and Midnlin theories, 1938 elastic and plastic contact

Two equal particles in normal contact
equations for a, Δ, σ_N, σ_N^{max}
Two unequal particles in normal contact
average normal stress and average normal strain
tangent stiffness, function of $\sqrt[3]{\sigma_{avg}}$

Bulk modulus for loose and dense packaging

Mindlin and Deresiewicz (1953)

Hashin (1983)

Rowe (1962)

Cosserat (1909)

103.3.2 Particle Contact Mechanics, Shear Behavior

Shear Behavior

closed form solution for no-slip behavior

equilibrium, integral of τ

slip ring

SLIP ring

There is NO elastic behavior of particles in contact if there is ANY small amount of shear!

Example values for typical contact stress parameters

typical stiffness parameters for sands

103.4 Dilatancy

Chapter 104

Small Deformation Elasto-Plasticity

(1991-1994-2002-2006-2010-2016-2017-2018-2019-2020-2021-)

(In collaboration with Prof. Zhaohui Yang, Dr. Zhao Cheng, Dr. Nima Tafazzoli, Dr. Federico Pisanò, and Prof. Han Yang)

104.1 Chapter Summary and Highlights

104.2 Elasto–plasticity

104.2.1 Constitutive Relations for Infinitesimal Plasticity

A wide range of elasto–plastic materials can be characterized by means of a set of incremental constitutive relations of the general form:

$$d\epsilon_{ij} = d\epsilon^e_{ij} + d\epsilon^p_{ij} \tag{104.1}$$

$$d\sigma_{ij} = E_{ijkl} d\epsilon^e_{kl} \tag{104.2}$$

$$d\epsilon^p_{ij} = d\lambda \, \frac{\partial Q}{\partial \sigma_{ij}} = d\lambda \, m_{ij}(\sigma_{ij}, q_*) \tag{104.3}$$

$$dq_* = d\lambda \, h_*(\tau_{ij}, q_*) \tag{104.4}$$

where, following standard notation ϵ_{ij}, ϵ^e_{ij} and ϵ^p_{ij} denotes the total, elastic and plastic strain tensor, (and $d\epsilon_{ij}$ is an increment of a strain tensor ϵ_{ij}), σ_{ij} is the Cauchy stress tensor, and q_* signifies some suitable set of internal variables[1]. The asterisk in the place of indices in q_* replaces n indices[2]. Equation (104.1) expresses the commonly assumed additive decomposition of the infinitesimal strain tensor into elastic and plastic parts. Equation (104.2) represents the generalized Hooke's law[3] which linearly relates stresses and elastic strains through a stiffness modulus tensor E_{ijkl}. Equation (104.3) expresses a generally associated or non-associated flow rule for the plastic strain and (104.4) describes a suitable set of hardening laws, which govern the evolution of the plastic variables. In these equations, m_{ij} is the plastic flow direction, h_* the plastic moduli and $d\lambda$ is a plastic parameter to be determined with the aid of the loading—unloading criterion, which can be expressed in terms of the Karush–Kuhn–Tucker condition (Karush, 1939; Kuhn and Tucker, 1951) as:

$$F(\sigma_{ij}, q_*) \leq 0 \tag{104.5}$$

[1] In the simplest models of plasticity the internal variables are taken as either plastic strain components ϵ^p_{ij} or the hardening variables κ defined, for example as a function of inelastic (plastic) work, i.e. $\kappa = f\left(W^p\right)$. See Lubliner (1990) page 115.

[2] for example $_{ij}$ if the variable is ϵ^p_{ij}, or nothing if the variable is a scalar value, i.e. κ .

[3] also Eq. 104.157

$$d\lambda \geq 0 \tag{104.6}$$

$$F\, d\lambda = 0 \tag{104.7}$$

In the previous equations $F(\sigma_{ij}, q_*)$ denotes the yield function of the material and (104.5) characterizes the corresponding elastic domain, which is presumably convex. Along any process of loading, conditions (104.5), (104.6) and (104.7) must hold simultaneously. For $F < 0$, equation (104.7) yields $d\lambda = 0$, i.e. elastic behavior, while plastic flow is characterized by $d\lambda > 0$, which with (104.7) is possible only if the yield criterion is satisfied, i.e. $F = 0$. From the latter constraint, in the process of plastic loading the plastic consistency conditions[4] is obtained in the form:

$$dF = \frac{\partial F}{\partial \sigma_{ij}} d\sigma_{ij} + \frac{\partial F}{\partial q_*} dq_* = n_{ij} d\sigma_{ij} + \xi_* dq_* = 0 \tag{104.8}$$

where :

$$n_{ij} = \frac{\partial F}{\partial \sigma_{ij}} \tag{104.9}$$

$$\xi_* = \frac{\partial F}{\partial q_*} \tag{104.10}$$

Equation (104.8) has the effect of confining the stress trajectory to the yield surface[5]. It is worthwhile noting that n_{ij} and ξ_* are normals to the yield surface in stress space and the plastic variable space respectively.

An interesting alternative way of representing non–associated flow rules can be found in Runesson (1987). A fictitious plastic strain derived from associated flow rule, e^p_{ij} is introduced. This fictitious plastic strain is assumed to be related to the real plastic strain ϵ^p_{ij}, which is derived from a non–associated flow rule[6] through the linear transformation:

$$e^p_{ij} = A_{ijkl} \epsilon^p_{kl} \tag{104.11}$$

Linear transformation tensor A_{ijkl} may be state dependent in general case, and it reduces to the symmetric part of the fourth order identity tensor[7] for the case of associated plasticity.

[4] first order accuracy condition.

[5] Since it is only linear expansion stress trajectory is confined to the tangential plane only.

[6] as in equation 104.3.

[7] $A_{ijkl} \equiv I^{sym}_{ijkl} \equiv \frac{1}{2}\left(\delta_{ik}\delta_{jl} + \delta_{il}\delta_{jk}\right)$.

It is often of interest to model deviatoric strains by an associated flow rule while the volumetric part is non–associated. For this case, A_{ijkl} can be formulated as:

$$A_{ijkl} = \left(\beta \frac{1}{3} \left(\delta_{ij}\delta_{kl} \right) + \frac{1}{2} \left(\delta_{ik}\delta_{jl} + \delta_{il}\delta_{jk} \right) \right) \tag{104.12}$$

$$A^{-1}_{ijkl} = \left(-\frac{\beta}{1+\beta} \frac{1}{3} \left(\delta_{ij}\delta_{kl} \right) + \frac{1}{2} \left(\delta_{ik}\delta_{jl} + \delta_{il}\delta_{jk} \right) \right) \tag{104.13}$$

and it is obvious that the non–associated flow rule is obtained with $\beta \neq 0$ and the associated flow rule with $\beta = 0$. It is useful to choose $\beta \geq 0$ and retain nice, positive definite properties of adjusted constitutive tensors later.

Let the $\| \cdot \|$ norm, be the complementary energy norm[8]:

$$\|\sigma_{ij}\|^2 = \sigma_{ij} D_{ijkl} \sigma_{kl} \tag{104.14}$$

where D_{ijkl} is the elastic compliance tensor ($D_{ijkl} = E^{-1}_{ijkl}$), and let us introduce the adjusted complementary energy norm as:

$${}^{A}\|\sigma_{ij}\|^2 = \sigma_{ij} \left(A_{ijkl} D_{klmn} \right) \sigma_{mn} = \sigma_{ij} \left({}^{A}D_{ijmn} \right) \sigma_{mn} \tag{104.15}$$

where ${}^{A}D_{ijmn}$ is the elastic compliance tensor transformed with respect to the non–associativity involved. It is clear that when $A_{ijkl} \equiv I^{sym}_{ijkl} \Longrightarrow {}^{A}\|\sigma_{ij}\|^2 \equiv \|\sigma_{ij}\|^2$

104.2.2 On Integration Algorithms

In the section Constitutive Relations for Infinitesimal Plasticity we have summarized constitutive equations that are capable of representing a wide variety of elasto–plastic materials. The problem in Computational Elasto–plasticity is to devise accurate and efficient algorithms for the integration of such constitutive relations. In the context of finite element analysis using isoparametric elements, the integration of constitutive equations is carried out at Gauss points. In each step the deformation increments are given or known, and the unknowns to be found are updated stresses and plastic variables. According to Ortiz and Popov (1985) an acceptable algorithm should satisfy:

- consistency with the constitutive relations to be integrated or first order accuracy,
- Numerical stability,

[8] This norm will be reintroduced later on!

- incremental plastic consistency

A non—required but desirable feature to be added to the above list is:

- higher[9] order accuracy

First two conditions are needed for attaining convergence for the numerical solution as the step or increment becomes vanishingly small. The third condition is the algorithmic counterpart of the plastic consistency condition and requires that the state of stress computed from the algorithm be contained within the elastic domain.

104.2.3 Midpoint Rule Algorithm

A class of algorithms for integrating constitutive equations with potential to satisfy the above mentioned conditions are the Generalized Midpoint rule algorithms. They are given in the following form:

$$d({}^{n+1}\sigma_{ij}) = E_{ijkl}\left(d({}^{n+1}\epsilon_{kl}) - d({}^{n+1}\epsilon^{p}_{kl})\right) \tag{104.16}$$

$$d({}^{n+1}\epsilon^{p}_{ij}) = d({}^{n}\epsilon^{p}_{ij}) + d\lambda\ {}^{n+\alpha}m_{ij} \tag{104.17}$$

$$d({}^{n+1}q_{*}) = d({}^{n}q_{*}) + d\lambda\ {}^{n+\alpha}h_{*} \tag{104.18}$$

$$F_{n+1} = 0 \tag{104.19}$$

where:

$${}^{n+\alpha}m_{ij} = m_{ij}\left((1-\alpha)\ {}^{n}\sigma_{ij} + \alpha\ \left({}^{n+1}\sigma_{ij}\right), (1-\alpha)\ {}^{n}q_{*} + \alpha\ \left({}^{n+1}q_{*}\right)\right) \tag{104.20}$$

$${}^{n+\alpha}h_{*} = h_{*}\left((1-\alpha)\ {}^{n}\sigma_{ij} + \alpha\ \left({}^{n+1}\sigma_{ij}\right), (1-\alpha)\ {}^{n}q_{*} + \alpha\ \left({}^{n+1}q_{*}\right)\right) \tag{104.21}$$

It is quite clear that the case $\alpha = 0$ corresponds to the Forward Euler approach[10], the case $\alpha = 1$ corresponds to the Backward Euler approach[11], and the case $\alpha = 1/2$ to the Crank – Nicholson scheme. Equations (104.16), (104.17), (104.18), (104.19), (104.20) and (104.21) are the nonlinear algebraic

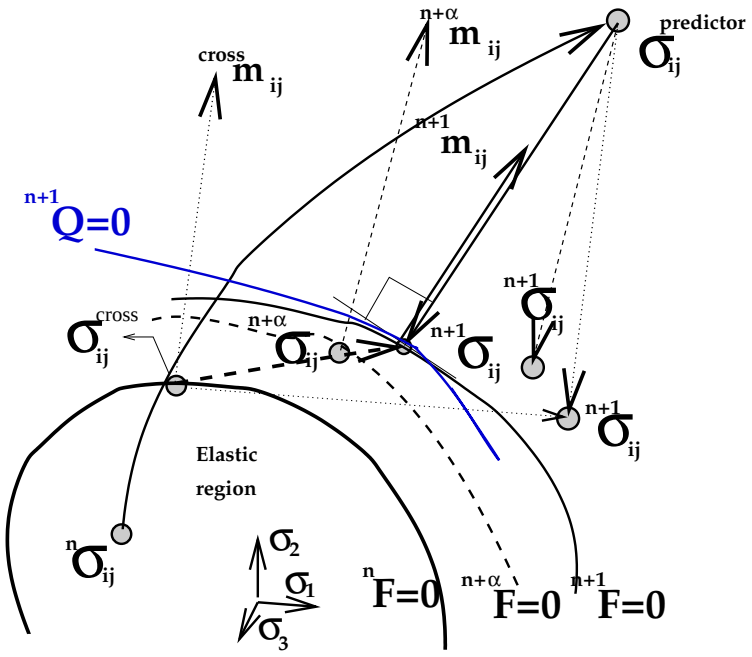

Figure 104.1: integration algorithms in elasto–plasticity

equations to be solved for the unknowns $d(^{n+1}\sigma_{ij})$, $d(^{n+1}\epsilon^p_{ij})$, $d(^{n+1}q_*)$ and $d\lambda$. From the Figure (104.1)[12] it can be seen that the Generalized Midpoint rule may be regarded as a returning mapping algorithm in which the elastic predictor $^{pred}\sigma_{ij}$ is projected on the updated yield surface along the flow direction evaluated at the midpoint $\left(^{n+\alpha}\sigma_{ij}, ^{n+\alpha}q_*\right)$.

104.2.3.1 Accuracy Analysis

Bearing in mind the context of the displacement based finite element analysis the integration of constitutive equations is performed for the given strain increment. The updated strains $^{n+1}\epsilon_{ij} = \epsilon_{ij}(t_n + \Delta t)$ may be viewed as the known function of the step size Δt. The remaining updated variables $^{n+1}\sigma_{ij}$, $^{n+1}\epsilon^p_{ij}$, $^{n+1}q_*$, as well as the incremental plastic parameter λ become functions of Δt implicitly defined through equations (104.16), (104.17), (104.18) and (104.19). It should be clear from (104.16), (104.17), (104.18) and (104.19) that as $\Delta t \to 0$ than $^{n+1}\epsilon_{ij} \to {}^{n}\epsilon_{ij}$, and thus the limiting values of $^{n+1}\sigma_{ij}$, $^{n+1}\epsilon^p_{ij}$, $^{n+1}q_*$ and λ are obtained:

[9] at least second order accuracy.

[10] explicit scheme.

[11] implicit scheme.

[12] it should be pointed out that the vectors, as drawn on this figure, are pointing in the right direction only if we assume that $E_{ijkl} \equiv I_{ijkl}$. For any general elasticity tensor E_{ijkl} all vectors are defined in the E_{ijkl} metric, so the term "normal", as we are used to it, does not apply here.

$$\begin{aligned}
\lim_{\Delta t\to 0}\left({}^{n+1}\sigma_{ij}\right) &= {}^{n}\sigma_{ij}\\
\lim_{\Delta t\to 0}\left({}^{n+1}\epsilon^{p}_{ij}\right) &= {}^{n}\epsilon^{p}_{ij}\\
\lim_{\Delta t\to 0}\left({}^{n+1}q_{*}\right) &= {}^{n}q_{*}\\
\lim_{\Delta t\to 0}\lambda &= 0
\end{aligned} \tag{104.22}$$

It can also be argued that, by virtue of the implicit function theorem ((Abraham et al., 1988) Chapter 2.5), ${}^{n+1}\sigma_{ij}$, ${}^{n+1}\epsilon^{p}_{ij}$, ${}^{n+1}q_{*}$ and λ are differentiable functions of Δt, if the functions ${}^{n+\alpha}m_{ij}$, ${}^{n+\alpha}h_{*}$ and F are sufficiently smooth. Sufficient smoothness will be assumed as needed.

First Order Accuracy. First order accuracy[13] of the algorithm, defined by the equations (104.16), (104.17), (104.18) and (104.19) with the constitutive equations given by (104.1), (104.2), (104.3) and (104.4) necessitates that the numerically integrated variables ${}^{n+1}\sigma_{ij}$, ${}^{n+1}\epsilon^{p}_{ij}$ and ${}^{n+1}q_{*}$ agree with their exact values $\sigma_{ij}(t+\Delta t)$, $\epsilon^{p}_{ij}(t+\Delta t)$ and $q_{*}(t+\Delta t)$ to within second order terms in the Taylor's expansion around the initial state ${}^{n}\sigma_{ij}=\sigma_{ij}(t)$, ${}^{n}\epsilon^{p}_{ij}=\epsilon^{p}_{ij}(t)$ and ${}^{n}q_{*}=q_{*}(t)$ in Δt. First order accuracy can be written in the following form:

$$\lim_{\Delta t\to 0}\frac{d\left({}^{n+1}\sigma_{ij}\right)}{d(\Delta t)}=\frac{d\left({}^{n}\sigma_{ij}\right)}{d(\Delta t)}=E_{ijkl}\left(\frac{d\left({}^{n}\epsilon_{ij}\right)}{d(\Delta t)}-\frac{d\left({}^{n}\epsilon^{p}_{ij}\right)}{d(\Delta t)}\right) \tag{104.23}$$

$$\lim_{\Delta t\to 0}\frac{d\left({}^{n+1}\epsilon^{p}_{ij}\right)}{d(\Delta t)}=\frac{d\left({}^{n}\epsilon^{p}_{ij}\right)}{d(\Delta t)}=\frac{d({}^{n}\lambda)}{d(\Delta t)}{}^{n}m_{ij} \tag{104.24}$$

$$\lim_{\Delta t\to 0}\frac{d\left({}^{n+1}q_{*}\right)}{d(\Delta t)}=\frac{d({}^{n}q_{*})}{d(\Delta t)}=\frac{d({}^{n}\lambda)}{d(\Delta t)}{}^{n}h_{*} \tag{104.25}$$

$$\lim_{\Delta t\to 0}\frac{d(\lambda)}{d(\Delta t)}=\frac{d({}^{n}\lambda)}{d(\Delta t)} \tag{104.26}$$

and the plastic parameter $d({}^{n}\lambda)/d(\Delta t)$ is determined with the aid of the plastic consistency condition at t:

[13] first order consistency.

$$\frac{d\ ({}^{n}F)}{d\,(\Delta t)} = \frac{\partial\,({}^{n}F)}{\partial \sigma_{ij}}\frac{d\sigma_{ij}}{d\,(\Delta t)} + \frac{\partial\,({}^{n}F)}{\partial q_*}\frac{dq_*}{d\,(\Delta t)} = {}^{n}n_{ij}\frac{d\sigma_{ij}}{d\,(\Delta t)} + {}^{n}\xi_*\frac{dq_*}{d\,(\Delta t)} = 0 \tag{104.27}$$

It is now rather straightforward to check whether the Generalized Midpoint rule satisfies the consistency conditions as given by (104.23), (104.24), (104.25) and (104.26). We can proceed further on by differentiating (104.16), (104.17), (104.18) and (104.19) with respect to Δt[14]:

$$\frac{d\left({}^{n+1}\sigma_{ij}\right)}{d\,(\Delta t)} = E_{ijkl}\left(\frac{d\left({}^{n+1}\epsilon_{kl}\right)}{d\,(\Delta t)} - \frac{d\left({}^{n+1}\epsilon^{p}_{kl}\right)}{d\,(\Delta t)}\right) \tag{104.28}$$

$$\begin{aligned}\frac{d\left({}^{n+1}\epsilon^{p}_{ij}\right)}{d\,(\Delta t)} &= \frac{d\lambda}{d\,(\Delta t)}\left({}^{n+\alpha}m_{ij}\right) + \lambda\,\frac{d\left({}^{n+\alpha}m_{ij}\right)}{d\,(\Delta t)} = \\ \frac{d\lambda}{d\,(\Delta t)}\left({}^{n+\alpha}m_{ij}\right) &+ \lambda\alpha\left(\left.\frac{\partial m_{ij}}{\partial \sigma_{ij}}\right|_{n+1}\frac{d\left({}^{n+1}\sigma_{ij}\right)}{d\,(\Delta t)} + \left.\frac{\partial m_{ij}}{\partial q_*}\right|_{n+1}\frac{d\left({}^{n+1}q_*\right)}{d\,(\Delta t)}\right)\end{aligned} \tag{104.29}$$

$$\begin{aligned}\frac{d\left({}^{n+1}q^{p}_{*}\right)}{d\,(\Delta t)} &= \frac{d\lambda}{d\,(\Delta t)}\left({}^{n+\alpha}h_*\right) + \lambda\frac{d\left({}^{n+\alpha}h_*\right)}{d\,(\Delta t)} = \\ \frac{d\lambda}{d\,(\Delta t)}\left({}^{n+\alpha}h_*\right) &+ \lambda\alpha\left(\left.\frac{\partial h_*}{\partial \sigma_{ij}}\right|_{n+1}\frac{d\left({}^{n+1}\sigma_{ij}\right)}{d\,(\Delta t)} + \left.\frac{\partial h_*}{\partial q_*}\right|_{n+1}\frac{d\left({}^{n+1}q_*\right)}{d\,(\Delta t)}\right)\end{aligned} \tag{104.30}$$

$$\frac{d\ \left({}^{n+1}F\right)}{d\,(\Delta t)} = \frac{\partial\left({}^{n+1}F\right)}{\partial\left({}^{n+1}\sigma_{ij}\right)}\frac{d\left({}^{n+1}\sigma_{ij}\right)}{d\,(\Delta t)} + \frac{\partial\left({}^{n+1}F\right)}{\partial\left({}^{n+1}q_*\right)}\frac{d\left({}^{n+1}{}^{n+1}q_*\right)}{d\,(\Delta t)} = 0 \tag{104.31}$$

where ${}^{n+\alpha}m_{ij}$ and ${}^{n+\alpha}h_*$ are defined by the equations (104.20) and (104.21).

By taking Δt to the limit value, $\Delta t \to 0$, in the (104.28), (104.29), (104.30) and (104.31) and using the relations from (104.22) one finds:

[14] bearing in mind that values at t are constants and that only variables at $t + \Delta t$ are changing with respect to Δt.

$$\lim_{\Delta t\to 0}\frac{d\left({}^{n+1}\sigma_{ij}\right)}{d\left(\Delta t\right)}=E_{ijkl}\left(\frac{d\left({}^{n}\epsilon_{kl}\right)}{d\left(\Delta t\right)}-\frac{d\left({}^{n+1}\epsilon^{p}_{kl}\right)_{\Delta t=0}}{d\left(\Delta t\right)}\right) \tag{104.32}$$

$$\lim_{\Delta t\to 0}\frac{d\left({}^{n+1}\epsilon^{p}_{ij}\right)}{d\left(\Delta t\right)}=\frac{d\lambda}{d\left(\Delta t\right)}\left({}^{n}m_{ij}\right) \tag{104.33}$$

$$\lim_{\Delta t\to 0}\frac{d\left({}^{n+1}q_{*}\right)}{d\left(\Delta t\right)}=\frac{d\lambda}{d\left(\Delta t\right)}\left({}^{n}h_{*}\right) \tag{104.34}$$

$$\lim_{\Delta t\to 0}\frac{d\left({}^{n+1}F\right)}{d\left(\Delta t\right)}=\frac{\partial\left({}^{n}F\right)}{\partial\sigma_{ij}}\left(\lim_{\Delta t\to 0}\frac{d\left({}^{n+1}\sigma_{ij}\right)}{d\left(\Delta t\right)}\right)+\frac{\partial\left({}^{n}F\right)}{\partial q_{*}}\left(\lim_{\Delta t\to 0}\frac{d\left({}^{n+1}q_{*}\right)}{d\left(\Delta t\right)}\right)=0 \tag{104.35}$$

In the previous equations it is quite clear that since $\Delta t = 0$, then equations (104.22) hold and since the variables ${}^{n}\sigma_{ij}$, ${}^{n}\epsilon^{p}_{ij}$ and ${}^{n}q_{*}$ are constant with respect to the change in Δt, the result follows readily, i.e. the Midpoint rule satisfies first order accuracy.

Second Order Accuracy To investigate second order accuracy of the algorithm given by (104.16), (104.17), (104.18) and (104.19) together with the constitutive equations given by (104.1), (104.2), (104.3) and (104.4) we shall proceed in the following manner. Second order accuracy actually means that the numerically integrated variables ${}^{n+1}\sigma_{ij}$, ${}^{n+1}\epsilon^{p}_{ij}$ and ${}^{n+1}q_{*}$ agree with their "exact" values $\sigma_{ij}(t+\Delta t)$, $\epsilon^{p}_{ij}(t+\Delta t)$ and $q_{*}(t+\Delta t)$ to within third order terms in the Taylor's expansion around the initial state ${}^{n}\sigma_{ij}=\sigma_{ij}(t)$, ${}^{n}\epsilon^{p}_{ij}=\epsilon^{p}_{ij}(t)$ and ${}^{n}q_{*}=q_{*}(t)$ in Δt. This verbal statement can be written in the following mathematical form:

$$\lim_{\Delta t\to 0}\frac{d^2\left({}^{n+1}\sigma_{ij}\right)}{d\left(\Delta t\right)^2}=$$
$$E_{ijkl}\left(\lim_{\Delta t\to 0}\frac{d^2\left({}^{n+1}\epsilon_{kl}\right)}{d\left(\Delta t\right)^2}-\lim_{\Delta t\to 0}\frac{d^2\left({}^{n}\epsilon^p_{kl}\right)}{d\left(\Delta t\right)^2}\right)=E_{ijkl}\left(\frac{d^2\left({}^{n}\epsilon_{kl}\right)}{d\left(\Delta t\right)^2}-\frac{d^2\left({}^{n}\epsilon^p_{kl}\right)}{d\left(\Delta t\right)^2}\right) \tag{104.36}$$

$$\lim_{\Delta t\to 0}\frac{d^2\left({}^{n+1}\epsilon^p_{ij}\right)}{d\left(\Delta t\right)^2}=$$
$$\frac{d^2\lambda}{d\left(\Delta t\right)^2}\lim_{\Delta t\to 0}\left({}^{n+1}m_{ij}\right)+\lim_{\Delta t\to 0}\frac{d\left({}^{n+1}\lambda\right)}{d\left(\Delta t\right)}\frac{d\left({}^{n+\alpha}m_{ij}\right)}{d\left(\Delta t\right)}=$$
$$\frac{d^2\lambda}{d\left(\Delta t\right)^2}\left({}^{n}m_{ij}\right)+\frac{d\left({}^{n}\lambda\right)}{d\left(\Delta t\right)}\frac{d\left({}^{n+\alpha}m_{ij}\right)}{d\left(\Delta t\right)}=$$
$$\frac{d^2\lambda}{d\left(\Delta t\right)^2}\left({}^{n}m_{ij}\right)+\frac{d\left({}^{n}\lambda\right)}{d\left(\Delta t\right)}\left(\frac{\partial m_{ij}}{\partial\sigma_{ij}\,|_n}\frac{d\left({}^{n}\sigma_{ij}\right)}{d\left(\Delta t\right)}+\frac{\partial m_{ij}}{\partial q_*\,|_n}\frac{d\left({}^{n}q_*\right)}{d\left(\Delta t\right)}\right) \tag{104.37}$$

$$\lim_{\Delta t\to 0}\frac{d^2\left({}^{n+1}q^p_*\right)}{d\left(\Delta t\right)^2}=$$
$$\frac{d^2\lambda}{d\left(\Delta t\right)^2}\lim_{\Delta t\to 0}\left({}^{n+1}h_*\right)+\lim_{\Delta t\to 0}\frac{d\left({}^{n+1}\lambda\right)}{d\Delta t}\frac{d\left({}^{n+1}h_*\right)}{d\left(\Delta t\right)}=$$
$$\frac{d^2\lambda}{d\left(\Delta t\right)^2}\left({}^{n}h_*\right)+\frac{d\left({}^{n+1}\lambda\right)}{d\Delta t}\frac{d\left({}^{n}h_*\right)}{d\left(\Delta t\right)}=$$
$$\frac{d^2\lambda}{d\left(\Delta t\right)^2}\left({}^{n}h_*\right)+\frac{d\left({}^{n+1}\lambda\right)}{d\Delta t}\left(\frac{\partial h_*}{\partial\sigma_{ij}\,|_n}\frac{d\left({}^{n}\sigma_{ij}\right)}{d\left(\Delta t\right)}+\frac{\partial h_*}{\partial q_*\,|_n}\frac{d\left({}^{n}q_*\right)}{d\left(\Delta t\right)}\right) \tag{104.38}$$

$$\lim_{\Delta t\to 0}\frac{d^2\left(\lambda\right)}{d\left(\Delta t\right)^2}=\frac{d^2\left({}^{n}\lambda\right)}{d\left(\Delta t\right)^2} \tag{104.39}$$

and the plastic parameter $d^2\left({}^{n}\lambda\right)/d\left(\Delta t\right)^2$ is determined with the aid of the second order oscillatory satisfaction of the plastic consistency condition:

$$\frac{d^2\ \left({}^{n}F\right)}{d\left(\Delta t\right)^2}=\left.\frac{dn_{ij}}{d\Delta t}\right|_n\frac{d\sigma_{ij}}{d\left(\Delta t\right)}+{}^{n}n_{ij}\left.\frac{d^2\left(\sigma_{ij}\right)}{d\left(\Delta t\right)^2}\right|_n+\left.\frac{d\left(\xi_*\right)}{d\Delta t}\right|_n\frac{d^n q_*}{d\left(\Delta t\right)}+{}^{n}\xi_*\frac{d^2\left({}^{n}q_*\right)}{d\left(\Delta t\right)^2}=0 \tag{104.40}$$

Now we can proceed by taking the second derivative of the equations (104.16), (104.17), (104.18) and (104.19) or use the already derived first derivatives from equations (104.28), (104.29), (104.30) and (104.31), and then differentiate them again so that we get:

$$\frac{d^2\left({}^{n+1}\sigma_{ij}\right)}{d\left(\Delta t\right)^2} = E_{ijkl}\left(\frac{d^2\left({}^{n+1}\epsilon_{kl}\right)}{d\left(\Delta t\right)^2} - \frac{d^2\left({}^{n+1}\epsilon^p_{kl}\right)}{d\left(\Delta t\right)^2}\right) \tag{104.41}$$

$$\begin{aligned}\frac{d^2\left({}^{n+1}\epsilon^p_{ij}\right)}{d\left(\Delta t\right)^2} = \\ \frac{d^2\lambda}{d\left(\Delta t\right)^2}\left({}^{n+\alpha}m_{ij}\right) + \\ 2\frac{d\lambda}{d\left(\Delta t\right)}\alpha\left(\left.\frac{\partial m_{ij}}{\partial\sigma_{ij}}\right|_{n+1}\frac{d\left({}^{n+1}\sigma_{ij}\right)}{d\left(\Delta t\right)} + \left.\frac{\partial m_{ij}}{\partial q_*}\right|_{n+1}\frac{d\left({}^{n+1}q_*\right)}{d\left(\Delta t\right)}\right) + \\ \lambda\alpha\frac{d}{d\left(\Delta t\right)}\left(\left.\frac{\partial m_{ij}}{\partial\sigma_{ij}}\right|_{n+1}\frac{d\left({}^{n+1}\sigma_{ij}\right)}{d\left(\Delta t\right)} + \left.\frac{\partial m_{ij}}{\partial q_*}\right|_{n+1}\frac{d\left({}^{n+1}q_*\right)}{d\left(\Delta t\right)}\right)\end{aligned} \tag{104.42}$$

$$\begin{aligned}\frac{d^2\left({}^{n+1}q^p_*\right)}{d\left(\Delta t\right)^2} = \\ \frac{d^2\lambda}{d\left(\Delta t\right)^2}\left({}^{n+\alpha}h_*\right) + \\ 2\frac{d\lambda}{d\left(\Delta t\right)}\alpha\left(\left.\frac{\partial h_*}{\partial\sigma_{ij}}\right|_{n+1}\frac{d\left({}^{n+1}\sigma_{ij}\right)}{d\left(\Delta t\right)} + \left.\frac{\partial h_*}{\partial q_*}\right|_{n+1}\frac{d\left({}^{n+1}q_*\right)}{d\left(\Delta t\right)}\right) + \\ \lambda\alpha\frac{d}{d\left(\Delta t\right)}\left(\left.\frac{\partial h_*}{\partial\sigma_{ij}}\right|_{n+1}\frac{d\left({}^{n+1}\sigma_{ij}\right)}{d\left(\Delta t\right)} + \left.\frac{\partial h_*}{\partial q_*}\right|_{n+1}\frac{d\left({}^{n+1}q_*\right)}{d\left(\Delta t\right)}\right)\end{aligned} \tag{104.43}$$

$$\begin{aligned}\frac{d^2\left({}^{n+1}F\right)}{d\left(\Delta t\right)^2} = \\ \frac{d\left({}^{n+1}n_{ij}\right)}{d\sigma_{ij}}\frac{d\left({}^{n+1}\sigma_{ij}\right)}{d\left(\Delta t\right)} + {}^{n+1}n_{ij}\frac{d^2\left({}^{n+1}\sigma_{ij}\right)}{d\left(\Delta t\right)^2} + \\ + \frac{d\left({}^{n+1}\xi_*\right)}{d\sigma_{ij}}\frac{d\left({}^{n+1}q_*\right)}{d\left(\Delta t\right)} + {}^{n+1}\xi\frac{d^2\left({}^{n+1}q_*\right)}{d\left(\Delta t\right)^2} = 0\end{aligned} \tag{104.44}$$

If we drive Δt to the limit, namely by taking $\lim_{\Delta t\to 0}$ and keeping in mind equations (104.22) and the assumed consistency of the algorithm[15] as given by the equations (104.23), (104.24), (104.25) and (104.26) one finds:

[15] actually the first order accuracy that is already proven.

$$\lim_{\Delta t\to 0}\frac{d^2\left({}^{n+1}\sigma_{ij}\right)}{d\left(\Delta t\right)^2}=E_{ijkl}\left(\frac{d^2\left({}^{n}\epsilon_{kl}\right)}{d\left(\Delta t\right)^2}-\lim_{\Delta t\to 0}\frac{d^2\left({}^{n+1}\epsilon^p_{kl}\right)}{d\left(\Delta t\right)^2}\right) \tag{104.45}$$

$$\lim_{\Delta t\to 0}\frac{d^2\left({}^{n+1}\epsilon^p_{ij}\right)}{d\left(\Delta t\right)^2}=$$
$$\lim_{\Delta t\to 0}\frac{d^2\left({}^{n+1}\lambda\right)}{d\left(\Delta t\right)^2}\left({}^{n+\alpha}m_{ij}\right)+2\frac{d\left({}^{n}\lambda\right)}{d\left(\Delta t\right)}\alpha\left(\left.\frac{\partial m_{ij}}{\partial\sigma_{ij}}\right|_n\frac{d\left({}^{n}\sigma_{ij}\right)}{d\left(\Delta t\right)}+\left.\frac{\partial m_{ij}}{\partial q_*}\right|_n\frac{d\left({}^{n}q_*\right)}{d\left(\Delta t\right)}\right) \tag{104.46}$$

$$\lim_{\Delta t\to 0}\frac{d^2\left({}^{n+1}q^p_*\right)}{d\left(\Delta t\right)^2}=$$
$$\lim_{\Delta t\to 0}\frac{d^2\left({}^{n+1}\lambda\right)}{d\left(\Delta t\right)^2}\left({}^{n+\alpha}h_*\right)+2\frac{d\left({}^{n}\lambda\right)}{d\left(\Delta t\right)}\alpha\left(\left.\frac{\partial h_*}{\partial\sigma_{ij}}\right|_n\frac{d\left({}^{n}\sigma_{ij}\right)}{d\left(\Delta t\right)}+\left.\frac{\partial h_*}{\partial q_*}\right|_n\frac{d\left({}^{n}q_*\right)}{d\left(\Delta t\right)}\right) \tag{104.47}$$

$$\lim_{\Delta t\to 0}\frac{d^2\left({}^{n+1}F\right)}{d\left(\Delta t\right)^2}=$$
$$\frac{d\left({}^{n}n_{ij}\right)}{d\sigma_{ij}}\frac{d\left({}^{n}\sigma_{ij}\right)}{d\left(\Delta t\right)}+{}^{n}n_{ij}\lim_{\Delta t\to 0}\frac{d^2\left({}^{n+1}\sigma_{ij}\right)}{d\left(\Delta t\right)^2}+$$
$$+\frac{d\left({}^{n}\xi_*\right)}{d\sigma_{ij}}\frac{d\left({}^{n}q_*\right)}{d\left(\Delta t\right)}+{}^{n}\xi\lim_{\Delta t\to 0}\frac{d^2\left({}^{n+1}q_*\right)}{d\left(\Delta t\right)^2}=0 \tag{104.48}$$

By comparing equations (104.45), (104.46), (104.47) and (104.48) with the second order accuracy condition stated in equations (104.36), (104.37), (104.38) and (104.39) it is quite clear that the second order accuracy is obtained iff[16] $\alpha = 1/2$!

The conclusion is that the Midpoint–rule algorithm is consistent[17] for all $\alpha \in [0,1]$ and it is second order accurate for $\alpha = 1/2$. However, one should not forget that these results are obtained for the limiting case $\Delta t \to 0$, i.e. the strain increments are small and tend to zero.

[16] if and only if ($\Longleftrightarrow$).

[17] first order accurate.

104.2.3.2 Numerical Stability Analysis

Numerical stability of an algorithm plays a central role in approximation theory for initial value problems. In fact, it can be stated that consistency and stability are necessary and sufficient conditions for convergence of an algorithm as the time step tends to zero. In the approach presented by Ortiz and Popov (1985) a new methodology is proposed by which the stability properties of an integration algorithm for elasto–plastic constitutive relations can be established. Our attention is confined to perfect plasticity and a smooth yield surface.

The purpose of the following stability analysis is to determine under what conditions a finite perturbation in the initial stresses is diluted by the algorithm. In other words:

$$d\left({}^{n+1}\sigma_{ij}^{(2)}, {}^{n+1}\sigma_{ij}^{(1)}\right) \leq d\left({}^{n}\sigma_{ij}^{(2)}, {}^{n}\sigma_{ij}^{(1)}\right) \tag{104.49}$$

where $d(\cdot,\cdot)$ is some suitable distance on the yield surface and ${}^{n+1}\sigma_{ij}^{(1)}$ and ${}^{n+1}\sigma_{ij}^{(2)}$ are two sets of updated stresses corresponding to arbitrary initial stress values ${}^{n}\sigma_{ij}^{(1)}$ and ${}^{n}\sigma_{ij}^{(2)}$, respectively, and all of the previous stress values are assumed to lie on the yield surface. Stability in the sense of equation (104.49) is referred to as large scale stability. It is shown in Helgason (1978)[18] that for nonlinear initial value problems defined on Banach manifolds, consistency and large scale stability with respect to a complete metric are sufficient for convergence.

The task of directly establishing estimates of the type expressed in (104.49) is rather difficult, and so despite the conceptual appeal of large scale stability, simplified solutions are sought. It should be recognized that attention can be restricted to infinitesimal perturbation in the initial conditions of the type ${}^{n}\sigma_{ij} \rightarrow {}^{n}\sigma_{ij} + d\left({}^{n}\sigma_{ij}\right)$. This simplification is founded on the fact that the dilution or attenuation, by the algorithm of infinitesimal perturbations:

$$\|d\ {}^{n+1}\sigma_{ij}\| \leq \|d\ {}^{n}\sigma_{ij}\| \tag{104.50}$$

with respect to some suitable norm $\|\cdot\|$, of small scale stability, implies large scale stability in the sense of equation (104.49).

Let the $\|\cdot\|$ norm, be the energy norm:

$$\|\sigma_{ij}\|^2 = \sigma_{ij} D_{ijkl} \sigma_{kl} \tag{104.51}$$

[18] the first Chapter of Helgason's book.

where D_{ijkl} is the elastic compliance tensor ($D_{ijkl} = E^{-1}_{ijkl}$), and let the distance $d(\cdot,\cdot)$ on the yield surface be defined as

$$d\left(\sigma^{(1)}_{ij}, \sigma^{(2)}_{ij}\right) = \inf_{\gamma} \int_{\gamma} \|\sigma^{'}_{ij}(s)\| ds \tag{104.52}$$

where the infinum is taken over all possible stress paths γ on the yield surface that are joining two stress states, namely $\sigma^{(1)}_{ij}$ and $\sigma^{(2)}_{ij}$. It can be found in Helgason (1978) that for a smooth yield surface, equation (104.52) defines the geodesic distance which endows the yield surface with a complete metric structure.

Suppose that we have any two initial states of stress ${}^{n}\sigma^{(1)}_{ij}$ and ${}^{n}\sigma^{(2)}_{ij}$ and let ${}^{n+1}\sigma^{(1)}_{ij}$ and ${}^{n+1}\sigma^{(2)}_{ij}$ be the corresponding updated values, respectively, and all the previous stress states are assumed to lie on the yield surface. Then, according to Helgason (1978), there exists a unique geodesic curve that joins ${}^{n}\sigma^{(1)}_{ij}$ and ${}^{n}\sigma^{(2)}_{ij}$ for which the infinum in equation (104.52) is attained. If γ_n is such a curve, then by definition:

$$d\left({}^{n}\sigma^{(1)}_{ij}, {}^{n}\sigma^{(2)}_{ij}\right) = \int_{\gamma_n} \|\sigma^{'}_{ij}(s)\| ds \tag{104.53}$$

Let the new curve γ_{n+1} be the transform of curve γ_n by the algorithm. By definition γ_{n+1} lies on the yield surface and joins two stress states ${}^{n+1}\sigma^{(1)}_{ij}$ and ${}^{n+1}\sigma^{(2)}_{ij}$. By the definition given in (104.52), it follows that:

$$d\left({}^{n+1}\sigma^{(1)}_{ij}, {}^{n+1}\sigma^{(2)}_{ij}\right) = \int_{\gamma_{n+1}} \|\sigma^{'}_{ij}(s)\| ds \tag{104.54}$$

Under the assumption of small scale stability of the algorithm one can write:

$$\|\sigma^{'}_{ij}(s_{n+1})\| ds = \|d\sigma_{ij}(s_{n+1})\| \leq \|d\sigma_{ij}(s_n)\| = \|\sigma^{'}_{ij}(s_n)\| ds \tag{104.55}$$

for every pair of corresponding points s_n and s_{n+1} on γ_n and γ_{n+1} respectively, so it follows:

$$\int_{\gamma_{n+1}} \|\sigma^{'}_{ij}(s_{n+1})\| ds \leq \int_{\gamma_n} \|\sigma^{'}_{ij}(s_n)\| ds \tag{104.56}$$

By combining equations (104.54), (104.55) and (104.56) it is concluded that:

$$d\left({}^{n+1}\sigma^{(1)}_{ij}, {}^{n+1}\sigma^{(2)}_{ij}\right) \leq d\left({}^{n}\sigma^{(1)}_{ij}, {}^{n}\sigma^{(2)}_{ij}\right) \tag{104.57}$$

which proves large scale stability. The main conclusion of the above argument may be stated as follows: small scale stability in the energy norm is equivalent to large scale stability in the associated geodesic distance.

The previous result is of practical importance, since it shows that the stability analysis for the integration algorithm in elasto–plasticity can be carried out by the assessment of small scale stability. The small scale stability analysis of the Generalized Midpoint rule is necessary to determine how the algorithm propagates infinitesimal perturbations in the initial conditions. By differentiating equations (104.16), (104.17), (104.18) and (104.19)and considering that we are dealing with perfectly plastic case here so that $\left({}^{n+1}q_*\right) = ({}^{n}q_*) =$ constants, it follows:

$$d\left({}^{n+1}\sigma_{ij}\right) = -E_{ijkl}\; d\left({}^{n+1}\epsilon^p_{kl}\right) \tag{104.58}$$

$$d\left({}^{n}\sigma_{ij}\right) = -E_{ijkl}\; d\left({}^{n}\epsilon^p_{kl}\right) \tag{104.59}$$

$$d\left({}^{n+1}\epsilon^p_{ij}\right) - d\left({}^{n}\epsilon^p_{ij}\right) = d\,\lambda\;\left({}^{n+\alpha}m_{ij}\right) + \lambda\, d\left({}^{n+\alpha}m_{ij}\right) \tag{104.60}$$

$$d\;\left({}^{n+1}F\right) = \left.\frac{\partial F}{\partial \sigma_{ij}}\right|_{n+1} d\left({}^{n+1}\sigma_{ij}\right) = {}^{n+1}n_{ij}\; d\left({}^{n+1}\sigma_{ij}\right) = 0 \tag{104.61}$$

Let us now examine the shape of $d\left({}^{n+\alpha}m_{ij}\right)$ having in mind the original definition[19] given in equation (104.20):

$${}^{n+\alpha}m_{ij} = m_{ij}\left((1-\alpha)\;{}^{n}\sigma_{ij} + \alpha\;\left({}^{n+1}\sigma_{ij}\right), (1-\alpha)\;{}^{n}q_* + \alpha\;\left({}^{n+1}q_*\right)\right)$$

and the differential of the previous equation is:

$$d\left({}^{n+\alpha}m_{ij}\right) = (1-\alpha)\left.\frac{\partial m_{ij}}{\partial \sigma_{kl}}\right|_{n+\alpha} d\left({}^{n}\sigma_{kl}\right) + \alpha\;\left.\frac{\partial m_{ij}}{\partial \sigma_{kl}}\right|_{n+\alpha} d\left({}^{n+1}\sigma_{kl}\right)$$

To ease writing let us introduce the following fourth order tensor:

[19] the remark about restraining analysis to perfectly plastic case still holds, so that $\left({}^{n+1}q_*\right)$ and $({}^{n}q_*)$ are constant.

$$M_{ijkl} = \frac{\partial m_{ij}}{\partial \sigma_{kl}}$$

The equation (104.60) now reads:

$$d\left({}^{n+1}\epsilon^{p}_{ij}\right) - d\left({}^{n}\epsilon^{p}_{ij}\right) = d\lambda\ \left({}^{n+\alpha}m_{ij}\right) + \lambda\left((1-\alpha)\left({}^{n+\alpha}M_{ijkl}\right)\ d\left({}^{n}\sigma_{kl}\right) + \alpha\ \left({}^{n+\alpha}M_{ijkl}\right)\ d\left({}^{n+1}\sigma_{kl}\right)\right) \tag{104.62}$$

By using equations (104.58) and (104.59) and knowing that $E^{-1}_{ijkl} = D_{ijkl}$ one can write:

$$d\left({}^{n+1}\epsilon^{p}_{ij}\right) = -D_{ijkl}\ d\left({}^{n+1}\sigma_{kl}\right)$$

$$d\left({}^{n}\epsilon^{p}_{ij}\right) = -D_{ijkl}\ d\left({}^{n}\sigma_{kl}\right)$$

so that the equation (104.62) now reads:

$$-D_{ijkl}\ d\left({}^{n+1}\sigma_{kl}\right) + D_{ijkl}\ d\left({}^{n}\sigma_{kl}\right) = d\lambda\ \left({}^{n+\alpha}m_{ij}\right) + \lambda\left((1-\alpha)\left({}^{n+\alpha}M_{ijkl}\right)\ d\left({}^{n}\sigma_{kl}\right) + \alpha\ \left({}^{n+\alpha}M_{ijkl}\right)\ d\left({}^{n+1}\sigma_{kl}\right)\right)$$

Now we are proceeding by solving the previous equation for $d\left({}^{n+1}\sigma_{kl}\right)$:

$$\left(D_{ijkl} + \lambda\ \alpha\left({}^{n+\alpha}M_{ijkl}\right)\right)\ d\left({}^{n+1}\sigma_{kl}\right) = \left(D_{ijkl} - \lambda\ (1-\alpha)\left({}^{n+\alpha}M_{ijkl}\right)\right) d\left({}^{n}\sigma_{kl}\right) - d\lambda\ \left({}^{n+\alpha}m_{ij}\right)$$

and by denoting :

$$\Psi_{ijkl} = D_{ijkl} - \lambda\ (1-\alpha)\left({}^{n+\alpha}M_{ijkl}\right)$$

$$\Gamma_{ijkl} = D_{ijkl} + \lambda\ \alpha\left({}^{n+\alpha}M_{ijkl}\right)$$

it follows:

$$d\left({}^{n+1}\sigma_{kl}\right) = \Gamma^{-1}_{ijkl}\left(\Psi_{ijkl}\; d\left({}^{n}\sigma_{kl}\right) - d\lambda\;\left({}^{n+\alpha}m_{ij}\right)\right) \tag{104.63}$$

Then by inserting the solution for $d\left({}^{n+1}\sigma_{kl}\right)$ in the consistency condition (104.61):

$$d\;\left({}^{n+1}F\right) = {}^{n+1}n_{kl}\; d\left({}^{n+1}\sigma_{kl}\right) = 0$$

one gets:

$$d\;\left({}^{n+1}F\right) =$$
$${}^{n+1}n_{kl}\;\Gamma^{-1}_{ijkl}\left(\Psi_{ijkl}\; d\left({}^{n}\sigma_{kl}\right) - d\lambda\;\left({}^{n+\alpha}m_{ij}\right)\right) = 0 \tag{104.64}$$

then if we solve for $d\lambda$:

$$d\lambda\;{}^{n+\alpha}m_{ij}\,{}^{n+1}n_{kl}\;\Gamma^{-1}_{ijkl} = {}^{n+1}n_{kl}\;\Gamma^{-1}_{ijkl}\Psi_{ijkl}\; d\left({}^{n}\sigma_{kl}\right) \tag{104.65}$$

or[20]:

$$d\lambda = \frac{{}^{n+1}n_{rs}\;\Gamma^{-1}_{pqrs}\Psi_{pqrs}\; d\left({}^{n}\sigma_{rs}\right)}{\left({}^{n+\alpha}m_{pq}\right)\left({}^{n+1}n_{rs}\right)\Gamma^{-1}_{pqrs}} \tag{104.66}$$

then by using the solution for $d\left({}^{n+1}\sigma_{kl}\right)$ from (104.63) and the solution for $d\lambda$ from (104.66) one can find:

$$d\left({}^{n+1}\sigma_{kl}\right) = \Gamma^{-1}_{ijkl}\Psi_{ijkl}\; d\left({}^{n}\sigma_{kl}\right) - \Gamma^{-1}_{pqrs}\;\Psi_{pqrs}\frac{{}^{n+1}n_{rs}\;\Gamma^{-1}_{ijkl}\;\left({}^{n+\alpha}m_{ij}\right)}{{}^{n+\alpha}m_{pq}\,{}^{n+1}n_{rs}\;\Gamma^{-1}_{pqrs}} d\left({}^{n}\sigma_{rs}\right) \tag{104.67}$$

$$d\left({}^{n+1}\sigma_{kl}\right) = \Gamma^{-1}_{ijkl}\Psi_{ijkl}\left(\delta_{ks}\delta_{rl} - \frac{{}^{n+1}n_{rs}\;\Gamma^{-1}_{ijkl}\;\left({}^{n+\alpha}m_{ij}\right)}{{}^{n+\alpha}m_{pq}\,{}^{n+1}n_{rs}\;\Gamma^{-1}_{pqrs}}\right) d\left({}^{n}\sigma_{rs}\right) \tag{104.68}$$

to ease the writing we can define the following notation:

[20] where the change in dummy indices is possible because $d\lambda$ is scalar.

$$\Phi_{klrs} = \delta_{ks}\delta_{rl} - \frac{{}^{n+1}n_{rs}\ \Gamma^{-1}_{ijkl}\ \left({}^{n+\alpha}m_{ij}\right)}{{}^{n+\alpha}m_{pq}\ {}^{n+1}n_{rs}\ \Gamma^{-1}_{pqrs}} \tag{104.69}$$

so that the equation (104.68) now reads:

$$d\left({}^{n+1}\sigma_{kl}\right) = \Gamma^{-1}_{ijkl}\Psi_{ijkl}\ \Phi_{klrs}\ d\left({}^{n}\sigma_{rs}\right) \tag{104.70}$$

In order to derive the estimate of the type (104.50) from (104.70) we shall proceed in the following way. The norm of a tensor is defined as:

$$\|A_{ijkl}\| = \sup_{\sigma} \frac{\|A_{ijkl}\sigma_{kl}\|}{\|\sigma_{kl}\|} \tag{104.71}$$

If we take the norm of (104.70), while recalling the inequalities:

$$\|A_{ijkl}\sigma_{kl}\| \leq \|A_{ijkl}\|\ \|\sigma_{kl}\| \quad ; \quad \|A_{ijkl}B_{ijkl}\| \leq \|A_{ijkl}\|\ \|B_{ijkl}\| \tag{104.72}$$

it follows:

$$\|d\left({}^{n+1}\sigma_{kl}\right)\| = \|\Gamma^{-1}_{ijkl}\Psi_{ijkl}\ \Phi_{klrs}\ d\left({}^{n}\sigma_{rs}\right)\| \tag{104.73}$$

then by using equations (104.72), we are able to write:

$$\|d\left({}^{n+1}\sigma_{kl}\right)\| \leq \|\Gamma^{-1}_{ijkl}\ \Psi_{ijkl}\|\ \|\Phi_{klrs}\|\ \|d\left({}^{n}\sigma_{rs}\right)\| \tag{104.74}$$

Considering the norm of $\|\Phi_{klrs}\|$ it should be noted that Φ_{klrs} defines a projection along the direction of $\Gamma^{-1}_{ijkl}\ {}^{n+\alpha}m_{ij}$ onto the hyperplane that is orthogonal to ${}^{n+1}n_{rs}$, so that the following properties hold:

$$(\Phi_{klrs})\left(\Gamma^{-1}_{ijkl}\ {}^{n+\alpha}m_{ij}\right) = \emptyset \tag{104.75}$$

$$(\Phi_{klrs})\,(\sigma_{rs}) = \sigma_{rs} \tag{104.76}$$

for every σ_{rs} that is orthogonal to ${}^{n+1}n_{rs}$. From these properties and the definition in equation (104.71) it follows that:

$$\|\Phi_{klrs}\| \equiv 1 \tag{104.77}$$

In what follows it is assumed that the fourth order tensor field

$$M_{ijkl} = \partial m_{ij}/\partial \sigma_{kl}$$

is symmetric and positive definite everywhere on the yield surface. The assumption is valid, if the flow direction m_{ij} is derived from the convex potential function, which is a rather common feature among yield criteria. It is now clear that :

$$\|\Gamma^{-1}_{ijkl}\ \Psi_{ijkl}\| = \left| \frac{{}^{max}\gamma_{ij}\ \Psi_{ijkl}\ {}^{max}\gamma_{kl}}{{}^{max}\gamma_{ij}\ \Gamma_{ijkl}\ {}^{max}\gamma_{kl}} \right| \tag{104.78}$$

where ${}^{max}\gamma_{ij}$ is the eigentensor corresponding to the maximum eigenvalue of the eigenproblem:

$$\left(\Psi_{ijkl} - \mu\ \Gamma_{ijkl}\right) \gamma_{kl} = 0 \tag{104.79}$$

which is normalized to satisfy:

$$\|{}^{max}\gamma_{ij}\|\|{}^{max}\gamma_{ij}\| = {}^{max}\gamma_{ij}\ D_{ijkl}\ {}^{max}\gamma_{kl} = 1 \tag{104.80}$$

If we denote:

$${}^{n+\alpha}\beta = {}^{max}\gamma_{ij}\ {}^{n+\alpha}M_{ijkl}\ {}^{max}\gamma_{kl} \tag{104.81}$$

as the maximum eigenvalue of the fourth order tensor ${}^{n+\alpha}M_{ijkl}$ and that value is a positive real number[21], then from equations (104.78), (104.80), (104.81) and from the definition[22] of Ψ_{ijkl} and Γ_{ijkl}, it follows:

$$\|\Gamma^{-1}_{ijkl}\ \Psi_{ijkl}\| = \left| \frac{1 - (1-\alpha)\ \lambda\ \left({}^{n+\alpha}\beta\right)}{1 + \alpha\ \lambda\ \left({}^{n+\alpha}\beta\right)} \right| \tag{104.82}$$

which, when inserted in the equation (104.74) yields:

[21] because ${}^{n+\alpha}M_{ijkl}$ is derived from a convex potential function.

[22] $\Psi_{ijkl} = D_{ijkl} - \lambda\ (1-\alpha)\left({}^{n+\alpha}M_{ijkl}\right)$ and $\Gamma_{ijkl} = D_{ijkl} + \lambda\ \alpha\left({}^{n+\alpha}M_{ijkl}\right)$

$$\| d\left({}^{n+1}\sigma_{kl}\right) \| \leq \left| \frac{1-(1-\alpha)\ \lambda\ \left({}^{n+\alpha}\beta\right)}{1+\alpha\ \lambda\ \left({}^{n+\alpha}\beta\right)} \right| \ \| d\left({}^{n}\sigma_{rs}\right) \| \tag{104.83}$$

Since it is said that ${}^{n+\alpha}\beta$ is a positive real number it follows that:

$$\left| \frac{1-(1-\alpha)\ \lambda\ \left({}^{n+\alpha}\beta\right)}{1+\alpha\ \lambda\ \left({}^{n+\alpha}\beta\right)} \right| \leq \left| \frac{1-\alpha}{\alpha} \right| \frac{{}^{n+\alpha}\beta}{{}^{n+\alpha}\beta} = \left| \frac{1-\alpha}{\alpha} \right| \tag{104.84}$$

and $\alpha \in [0,1]$. The new form of equation (104.83) is now:

$$\| d\left({}^{n+1}\sigma_{kl}\right) \| \leq \left| \frac{1-\alpha}{\alpha} \right| \ \| d\left({}^{n}\sigma_{rs}\right) \| \tag{104.85}$$

which in conjunction with the requirement for unconditional stability[23] yields:

$$\left| \frac{1-\alpha}{\alpha} \right| \leq 1 \tag{104.86}$$

and so it is necessary that:

$$\alpha \geq {}^{min}\alpha = \frac{1}{2} \tag{104.87}$$

The conclusion is that the Generalized Midpoint rule is unconditionally stable for $\alpha \geq 1/2$. In the case when $\alpha < 1/2$ the Generalized Midpoint rule is only conditionally stable. To obtain a stability condition for $\alpha \leq 1/2$ one has to go back to equation (104.83), and we conclude that:

$$\left| \frac{1-(1-\alpha)\ \lambda\ \left({}^{n+\alpha}\beta\right)}{1+\alpha\ \lambda\ \left({}^{n+\alpha}\beta\right)} \right| \leq 1 \quad \Rightarrow \quad \lambda \leq \frac{2}{{}^{max}\beta\ (1-2\alpha)} \quad \text{for} \quad \alpha \leq \frac{1}{2} \tag{104.88}$$

and when $\alpha = 1/2$, then ${}^{critical}\lambda \to \infty$, and thus the unconditional stability is recovered.

[23] that is $\| d\ {}^{n+1}\sigma_{ij} \| \leq \| d\ {}^{n}\sigma_{ij} \|$

104.2.4 Crossing the Yield Surface

Midpoint rule algorithms in computational elasto–plasticity require[24] the evaluation of the intersection[25] stress. Despite the appeal of the closed form solution, as found in Bićanić (1989), and numerical iterative procedures as found in Marques (1984) and Nayak and Zienkiewicz (1972), for some yield criteria[26] the solution is not that simple to find. Special problems arises, even with the numerical iterative methods in the area of a apex. The apex area problems are connected to the derivatives of yield a function.

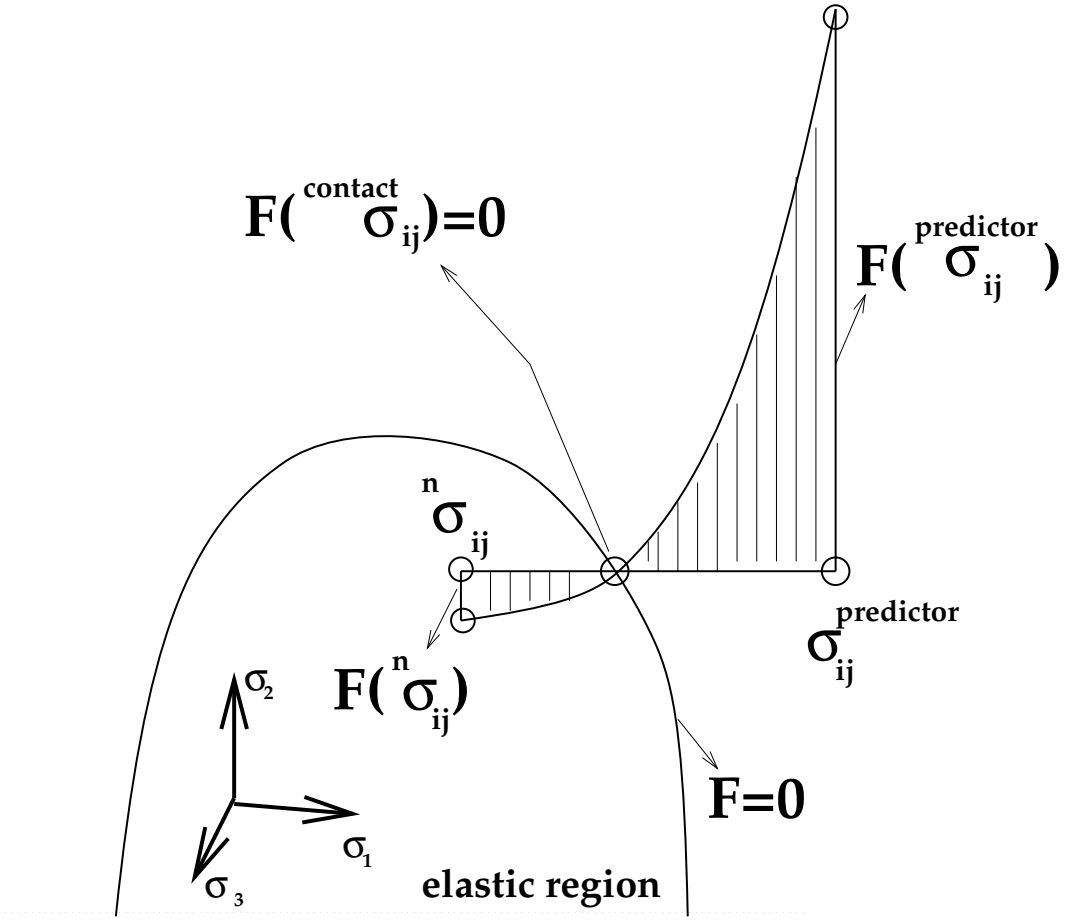

Figure 104.2: The pictorial representation of the intersection point problem in computational elasto–plasticity: which must be resolved for the Forward and Midpoint schemes

Having in mind the before mentioned problems, a different numerical scheme, that does not need derivatives, was sought for solving this problem. One possible solution was found in Press et al. (1988b)

[24] except for the fully implicit Backward Euler algorithm.

[25] contact, penetration point, i.e the point along the stress path where $F = 0$ or the point where stress state crosses from the elastic to the plastic region.

[26] namely for the MRS-Lade elasto–plastic model.

in the form of an excellent algorithm that combines root bracketing, bisection, and inverse quadratic interpolation to converge from a neighborhood of a zero crossing. The algorithm was developed in the 1960s by van Wijngaarden, Dekker and others at the Mathematical Center in Amsterdam. The algorithm was later improved by Brent, and so it is better known as Brent's method. The method is guaranteed to converge, so long as the function[27] can be evaluated within the initial interval known to contain a root. While the other iterative methods that do not require derivatives[28] assume approximately linear behavior between two prior estimates, inverse quadratic interpolation uses three prior points to fit an inverse quadratic function[29], whose value at $y = 0$ is taken as the next estimate of the root x. Lagrange's classical formula for interpolating the polynomial of degree $N-1$ through N points $y_1 = f(x_1)$, $y_2 = f(x_2)$, $\ldots y_3 = f(x_3)$ is given by:

$$\begin{aligned} P(x) = & \frac{(x-x_2)(x-x_3)\cdots(x-x_N)}{(x_1-x_2)(x_1-x_3)\cdots(x_1-x_N)}\, y_1 + \\ & + \frac{(x-x_1)(x-x_3)\cdots(x-x_N)}{(x_2-x_1)(x_2-x_3)\cdots(x_2-x_N)}\, y_2 + \cdots \\ \cdots & + \frac{(x-x_1)(x-x_2)\cdots(x-x_N)}{(x_N-x_1)(x_N-x_3)\cdots(x_N-x_{N-1})}\, y_N \end{aligned} \tag{104.89}$$

If the three point pairs are $[a, f(a)], [b, f(b)], [c, f(c)]$, then the interpolating formula (104.89) yields:

$$\begin{aligned} x = & \frac{(y-f(a))(y-f(b))}{(f(c)-f(a))(f(c)-f(b))}\, c + \\ & + \frac{(y-f(b))(y-f(c))}{(f(a)-f(b))(f(a)-f(c))}\, a + \\ & + \frac{(y-f(c))(y-f(a))}{(f(b)-f(a))(f(b)-f(a))}\, b \end{aligned} \tag{104.90}$$

By setting $y = 0$, we obtain a result for the next root estimate, which can be written as:

$$x = b + \frac{\frac{f(b)}{f(a)}\left(\frac{f(a)}{f(c)}\left(\frac{f(b)}{f(c)} - \frac{f(a)}{f(c)}\right)(c-b) - \left(1 - \frac{f(b)}{f(c)}\right)(b-a)\right)}{\left(\frac{f(a)}{f(c)} - 1\right)\left(\frac{f(b)}{f(c)} - 1\right)\left(\frac{f(b)}{f(a)} - 1\right)} \tag{104.91}$$

In practice b is the current best estimate of the root and the term:

[27] in our case yield function $F(\sigma_{ij})$.

[28] false position and secant method.

[29] x as a quadratic function of y.

$$\frac{\frac{f(b)}{f(a)}\left(\frac{f(a)}{f(c)}\left(\frac{f(b)}{f(c)}-\frac{f(a)}{f(c)}\right)(c-b)-\left(1-\frac{f(b)}{f(c)}\right)(b-a)\right)}{\left(\frac{f(a)}{f(c)}-1\right)\left(\frac{f(b)}{f(c)}-1\right)\left(\frac{f(b)}{f(a)}-1\right)}$$

is a correction. Quadratic methods[30] work well only when the function behaves smoothly. However, they run serious risk of giving bad estimates of the next root or causing floating point overflows, if divided by a small number

$$\left(\frac{f(a)}{f(c)}-1\right)\left(\frac{f(b)}{f(c)}-1\right)\left(\frac{f(b)}{f(a)}-1\right)\approx 0$$

Brent's method prevents against this problem by maintaining brackets on the root and checking where the interpolation would land before carrying out the division. When the correction of type (104.92) would not land within bounds, or when the bounds are not collapsing rapidly enough, the algorithm takes a bisection step. Thus, Brent's method combines the sureness of bisection with the speed of a higher order method when appropriate.

104.2.5 Singularities in the Yield Surface

104.2.5.1 Corner Problem

Some yield criteria are defined with more that one yield surface[31]. We will restrict our attention to a two–surface yield criterion[32]. Koiter has shown in Koiter (1960) and Koiter (1953) that in the case when two yield surfaces are active, the plastic strain rate from equation (104.3) can be derived as follows:

$$d\epsilon_{ij}^{p} = d\lambda_{cone}\,{}^{cone}m_{ij}\left(\sigma_{ij},q_{*}\right)+d\lambda_{cap}\,{}^{cap}m_{ij}\left(\sigma_{ij},q_{*}\right) \tag{104.92}$$

where ${}^{cone}m_{ij}\left(\sigma_{ij},q_{*}\right)$ and ${}^{cap}m_{ij}\left(\sigma_{ij},q_{*}\right)$ are normals to the potential functions at a corner, which belongs to the yield functions that are active, i.e. F_{cone} and F_{cap}. We now observe that we have two non–negative plastic multipliers $d\lambda_{cone}$ and $d\lambda_{cap}$ instead of one. We must require that at the end of the loading step[33], neither of the two yield functions is violated. These multipliers $d\lambda_{cone}$ and $d\lambda_{cap}$ can be determined from the conditions:

[30] Newton's method for example.

[31] for example MRS-Lade yield criterion has two surfaces.

[32] having in mind MRS-Lade cone-cap yield criterion.

[33] after stress correction, i.e. return to the yield surface(s).

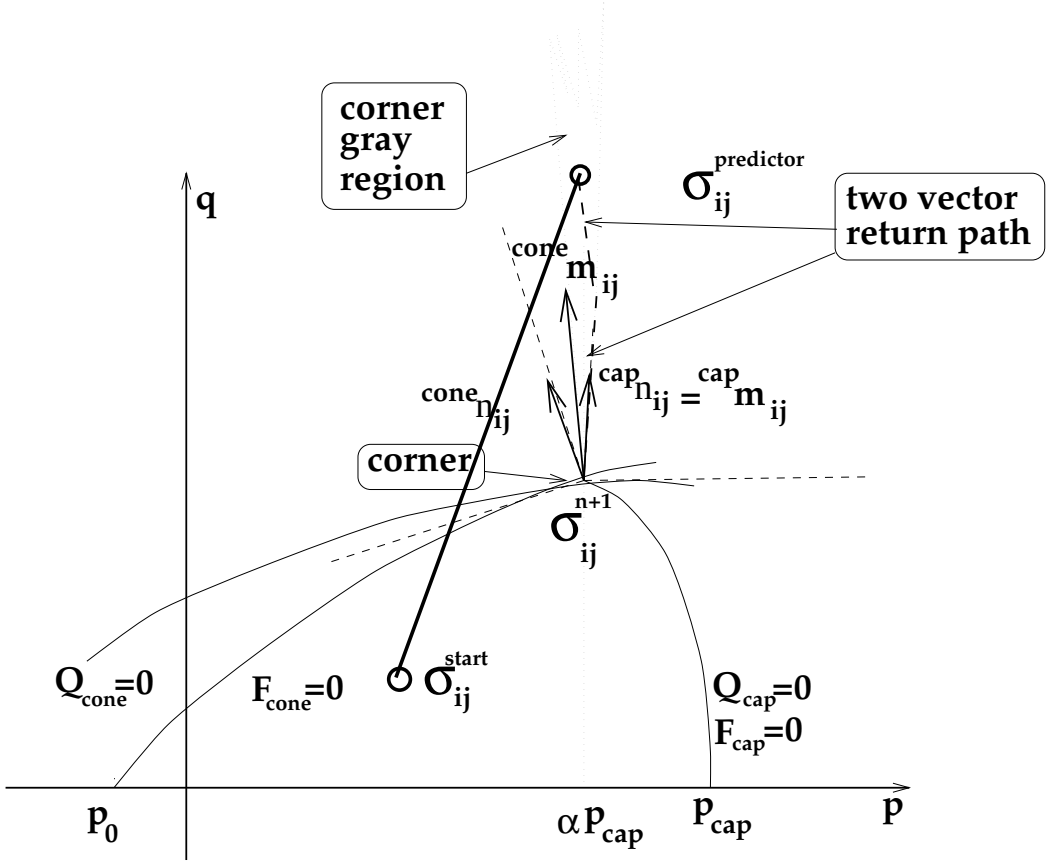

Figure 104.3: Pictorial representation of the corner point problem in computational elasto–plasticity: Yield surfaces with singular points

$$F_{cone}\left({}^{n+1}\sigma_{ij}, {}^{n+1}q_{*}\right) = 0 \tag{104.93}$$

$$F_{cap}\left({}^{n+1}\sigma_{ij}, {}^{n+1}q_{*}\right) = 0 \tag{104.94}$$

noting that by virtue of equation (104.92) we have at the corner singular point:

$${}^{n+1}\sigma_{ij} = {}^{pred}\sigma_{ij} - d\lambda_{cone}\, E_{ijkl}\, {}^{cone}m_{kl} - d\lambda_{cap}\, E_{ijkl}\, {}^{cap}m_{kl} \tag{104.95}$$

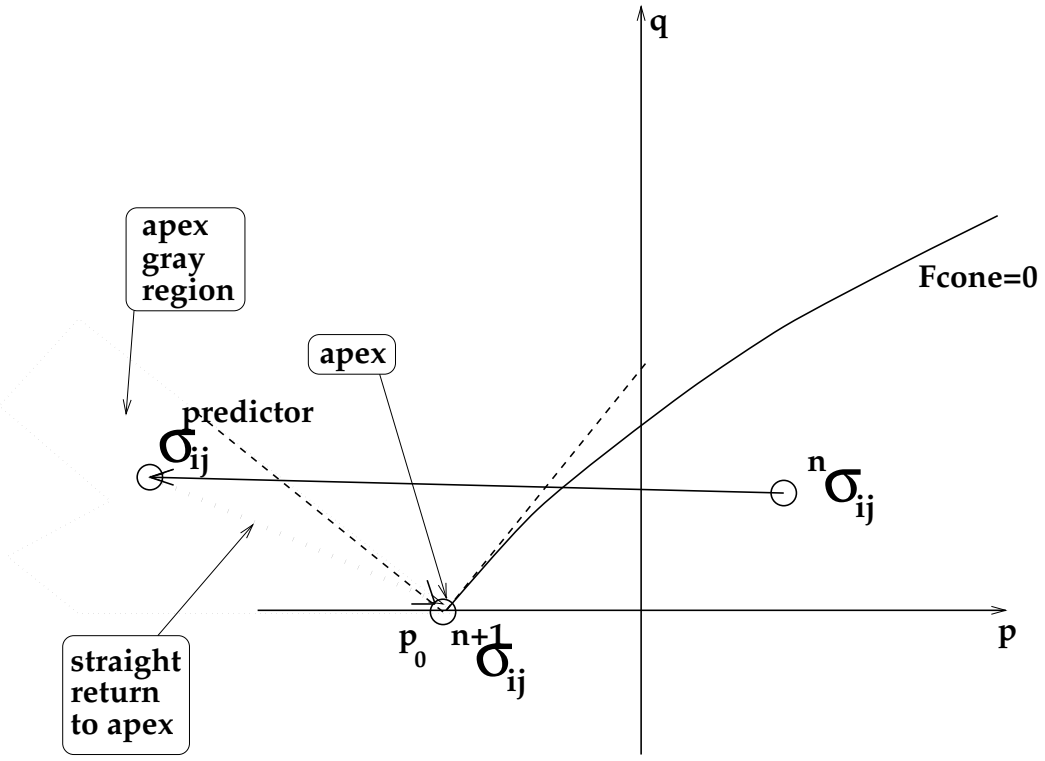

Figure 104.4: The pictorial representation of the apex point problem in computational elasto–plasticity: Yield surfaces with singular points

104.2.5.2 Apex Problem

The apex problem, as depicted in Figure (104.4) is solved in an empirical fashion. Rather than facing the complexity of solving a complex differential geometry problem[34] the stress point that is situated in the gray apex region is immediately returned to the apex point.

In the case when the hardening rule for the cone portion has developed to the stage that it affects the size of that cone portion of the yield criterion and not the position of intersection with the hydrostatic axis, then all stress returns from any part of apex gray region will be to the apex point itself. This strategy was used by Crisfield (1987). Nevertheless, the problem of integrating the rate equations in the apex gray region is readily solvable for the piecewise flat yield criteria[35] by using Koiter's conditions as found in Koiter (1960) and Koiter (1953). The apex problem for yield criteria that are smooth and differentiable everywhere except at the apex point, is solvable by means of differential geometry. Further

[34] using Koiter's work described in Koiter (1960) and Koiter (1953) and the fact that the sum $d\epsilon^p_{ij} = \sum_k d\lambda_k \left(\partial F_k/\partial\sigma_{ij}\right)$ can be transformed into the integral equation $d\epsilon^p_{ij} = \int d\lambda \left(\partial F/\partial\sigma_{ij}\right)\big|_{aroundapex}$ where the integration should be carried out infinitesimally close to, but in the vicinity of the apex point.

[35] Mohr - Coulomb for example.

work is needed for solving the problem, when the yield surface is not piecewise flat in the apex vicinity.

104.2.5.3 Influence Regions in Meridian Plane

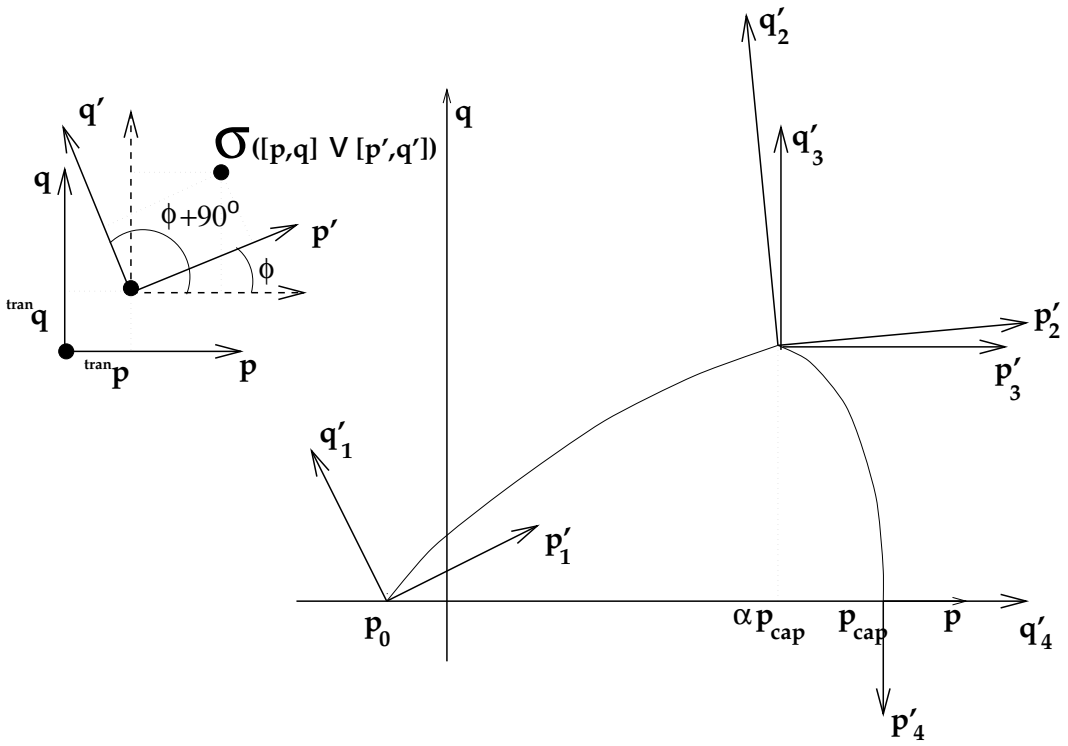

Figure 104.5: Influence regions in the meridian plane for the cone/cap surface of the MRS-Lade material model.

In order to define which surface is active and which is not for the current state of stress, a simple two dimensional analysis will be conducted. The fortunate fact for the MRS-Lade material model is that such an analysis can be conducted in the $p-q$ meridian plane, only, i.e. the value for θ can be "frozen". The concept is to calculate the stress invariants p, q and θ for the current state of stress[36], calculate the position of the apex and corner points in $p-q$ space for given the θ, calculate the two dimensional gradients at these points, perform linear transformation of the current stress state[37] to the new coordinate systems, and then check for the values of p'_i, $i = 1,2,3,4$, where p'_i is the transformed p_i axis.

The angle ψ is defined as the angle between the p axis and the tangent to the potential function.

The gradients to the cone portion of the potential surface are defined as:

[36] by using equations (104.138) and (104.139) as defined in section (104.4.4).

[37] now in p, q and θ space.

$$\frac{\partial Q_{cone}}{\partial p} = -n\,\eta_{cone}$$

$$\frac{\partial Q_{cone}}{\partial q} = g(\theta)\left(1+\frac{q}{q_a}\right)^{m} + \frac{g(\theta)\,m\,q\left(1+\frac{q}{q_a}\right)^{-1+m}}{q_a}$$

The gradients of the cap portion of the yield/potential surface is defined as:

$$\frac{\partial Q_{cap}}{\partial p} = \frac{2\,(p-p_m)}{p_r^2}$$

$$\frac{\partial Q_{cap}}{\partial q} = \frac{2\,g(\theta)^2\,q\left(1+\frac{q}{q_a}\right)^{2\,m}}{{f_r}^2} + \frac{2\,g(\theta)^2\,m\,q^2\left(1+\frac{q}{q_a}\right)^{-1+2\,m}}{{f_r}^2\,q_a}$$

The vector of gradients in $p-q$ space is defined as:

$$\begin{bmatrix} \frac{\partial Q}{\partial p} \\ \frac{\partial Q}{\partial q} \end{bmatrix} \tag{104.96}$$

and the angle ϕ is calculated as:

$$\phi = \arctan\left(\frac{\left(\frac{\partial Q}{\partial p}\right)}{\left(\frac{\partial Q}{\partial q}\right)}\right) - 90^{\circ} \tag{104.97}$$

Care must be exercised with regard to which potential function is to be used in angle calculations. It should be mentioned that for the cap portion, the angle at the corner is $\phi = 0^{\circ}$, while at the tip of the cap, the angle is $\phi = -90^{\circ}$. If a new definition, as found in Ferrer (1992), is used for the cone potential function, where n is variable and $n \to 0$ as $p \to \alpha p_{cap}$, then the corner gray region is empty.

The linear transformation[38] between coordinate systems $p'-q'$ and $p-q$ is defined as:

$$\begin{bmatrix} p' \\ q' \end{bmatrix} = \begin{bmatrix} \cos\phi & \sin\phi \\ -\sin\phi & \cos\phi \end{bmatrix} \begin{bmatrix} p - {}^{tran}p \\ q - {}^{tran}q \end{bmatrix} \tag{104.98}$$

and by using that linear transformation, one can check the region where our current stress state, in p, q and θ space, belongs. Figure (104.5) depicts the transformation scheme and the new coordinate systems at three important points[39].

[38] translation and rotation.

[39] at the apex point, corner point and the cap tip point.

104.3 A Forward Euler (Explicit) Algorithm

The explicit algorithm (Forward Euler) is based on using the starting point (the state stress σ_{ij}^n and internal variable space q_*^n on the yield surface) for finding all the relevant derivatives and variables.

The Explicit algorithm can be derived by starting from a first order Taylor expansion about starting point (σ_{ij}^n, q_*^n):

$$\begin{aligned} F^{new} &= F^{old} + \left.\frac{\partial F}{\partial \sigma_{mn}}\right|_n d\left({}^n\sigma_{mn}\right) + \left.\frac{\partial F}{\partial q_*}\right|_n dq_* = \\ &= {}^n n_{mn}\, d\sigma_{mn} + \xi_* h_* d\lambda = 0 \end{aligned} \tag{104.99}$$

From the differential form of equation (104.16) it follows:

$$d\left({}^{fE}\sigma_{mn}\right) = E_{mnpq}\left(d\left(\epsilon_{pq}\right) - d\left(\epsilon_{pq}^p\right)\right) =$$

$$= E_{mnpq} d\left(\epsilon_{pq}\right) - E_{mnpq}\, d\left(\epsilon_{pq}^p\right) = E_{mnpq} d\left(\epsilon_{pq}\right) - E_{mnpq}\, d\lambda\left({}^{cross}m_{pq}\right)$$

so that equation (104.99) becomes:

$${}^n n_{mn}\, E_{mnpq}\, d\epsilon_{pq} - {}^n n_{mn}\, E_{mnpq}\, d\lambda\, {}^n m_{pq} + \xi_* h_* d\lambda = 0$$

and it follows, after solving for $d\lambda$

$$d\lambda = \frac{{}^n n_{mn}\, E_{mnpq}\, d\epsilon_{pq}}{{}^{cros}n_{ab}\, E_{abcd}\, {}^{cros}m_{cd} - \xi_* h_*}$$

With this solution for $d\lambda$ one can obtain the increments in stress tensor and internal variables as

$$d\sigma_{mn} = E_{mnpq}\, d\epsilon_{pq} - E_{mnpq}\, \frac{{}^n n_{rs}\, E_{rstu}\, d\epsilon_{tu}}{{}^n n_{ab}\, E_{abcd}\, {}^n m_{cd} - \xi_A h_A}\, {}^n m_{pq} \tag{104.100}$$

$$dq_A = \left(\frac{{}^n n_{mn}\, E_{mnpq}\, d\epsilon_{pq}}{{}^{cros}n_{ab}\, E_{abcd}\, {}^{cros}m_{cd} - \xi_B h_B}\right) h_A \tag{104.101}$$

where ${}^n()$ denotes the starting elastic–plastic point for that increment. It should be noted that the explicit algorithm performs only one step of the computation and does not check on the equilibrium of the obtained solutions. This usually results in the slow drift of the stress–internal variable point from the yield surface for monotonic loading. It also results in spurious plastic deformations during elastic unloading for cyclic loading–unloading.

104.3.1 Continuum Tangent Stiffness Tensor.

The continuum tangent stiffness tensor $({}^{cont}E_{pqmn}^{ep})$ is obtained from the explicit (forward Euler) integration procedure (Jeremić and Sture, 1997):

$${}^{cont}E_{pqmn}^{ep} = E_{pqmn} - \frac{E_{pqkl}\, {}^n m_{kl}\, {}^n n_{ij} E_{ijmn}}{{}^n n_{ot} E_{otrs}\, {}^n m_{rs} - {}^n\xi_A\, h_A} \tag{104.102}$$

It is important to note that continuum tangent stiffness $({}^{cont}E_{pqmn}^{ep})$ posses minor symmetries $({}^{cont}E_{pqmn}^{ep} =$

${}^{cont}E^{ep}_{qpmn} = {}^{cont}E^{ep}_{pqnm}$), while major symmetry (${}^{cont}E^{ep}_{pqmn} = {}^{cont}E^{ep}_{mnpq}$), is only retained for associated elastic–plastic materials, when $n_{ij} \equiv m_{ij}$.

104.4 A Backward Euler (Implicit) Algorithm

In previous sections, the general theory of elasto–plasticity was presented. The accuracy and stability for the general Midpoint rule algorithm has been shown. In this chapter, the focus is on the Backward Euler algorithm, which is derived from the general Midpoint algorithm by setting $\alpha = 1$. The advantage of the Backward Euler scheme over other midpoint schemes is that the solution is sought by using the normal[40] at the final stress state. By implicitly assuming that such a stress state exists, the Backward Euler scheme is guaranteed to provide a solution, despite the size of the strain step[41]. However, it was shown in section (104.2.3.1) that the Backward Euler algorithm is only accurate to the first order.

The full implicit Backward Euler algorithm is based on the equation:

$$ {}^{n+1}\sigma_{ij} = {}^{pred}\sigma_{ij} - \Delta\lambda \; E_{ijkl} \; {}^{n+1}m_{kl} \tag{104.103} $$

where ${}^{pred}\sigma_{ij} = E_{ijkl} \; \epsilon_{kl}$ is the elastic trial stress state, Q is the plastic potential function and ${}^{n+1}m_{kl} = \left.\frac{\partial Q}{\partial \sigma_{kl}}\right|_{n+1}$ is the gradient to the plastic potential function in the stress space at the final stress position, and

$$ {}^{pred}\sigma_{ij} = {}^{n}\sigma_{ij} + E_{ijkl} \; {}^{pred}\Delta\epsilon_{kl} \tag{104.104} $$

is the elastic predicted (trial) stress state.

An initial estimate for the stress ${}^{n+1}\sigma_{ij}$ can be obtained using various other methods. This estimate generally does not satisfy the yield condition, so some kind of iterative scheme is necessary to return the stress to the yield surface.

104.4.1 Single Vector Return Algorithm.

If the predictor stress ${}^{pred}\sigma_{ij}$ is not in a corner or apex gray regions, a single vector return to the yield surface is possible. In order to derive such a scheme for a single vector return algorithm, a tensor of residuals r_{ij} will be defined as [42] :

$$ r_{ij} = \sigma_{ij} - \left({}^{pred}\sigma_{ij} - \Delta\lambda \; E_{ijkl} \; m_{kl} \right) \tag{104.105} $$

[40] $m_{ij} = \partial Q / \partial \sigma_{ij}$

[41] large strain step increments were tested, the scheme converged to the solution even for deviatoric strain steps of 20% in magnitude.

[42] By default at increment $n+1$, and ${}^{n+1}()$ is omitted for simplicity.

This tensor represents the difference between the current stress state σ_{ij} and the Backward Euler stress state ${}^{pred}\sigma_{ij} - \Delta\lambda\, E_{ijkl}\, m_{kl}$.

The trial stress state ${}^{pred}\sigma_{ij}$ is kept fixed during the iteration process. The first order Taylor series expansion can be applied to Equation 104.105 to obtain the new residual ${}^{new}r_{ij}$ from the old one ${}^{old}r_{ij}$

$$ {}^{new}r_{ij} = {}^{old}r_{ij} + \mathrm{d}\sigma_{ij} + \mathrm{d}(\Delta\lambda)\, E_{ijkl}\, m_{kl} + \Delta\lambda\, E_{ijkl} \left(\frac{\partial m_{kl}}{\partial \sigma_{mn}} \mathrm{d}\sigma_{mn} + \frac{\partial m_{kl}}{\partial q_A} \mathrm{d}q_A \right) \tag{104.106} $$

where $\mathrm{d}\sigma_{ij}$ is the change in σ_{ij}, $\mathrm{d}(\Delta\lambda)$ is the change in $\Delta\lambda$, and $\frac{\partial m_{kl}}{\partial \sigma_{mn}} \mathrm{d}\sigma_{mn} + \frac{\partial m_{kl}}{\partial q_A} \mathrm{d}q_A$ is the change in m_{kl}. The goal is let ${}^{new}r_{ij} = \emptyset$, so one can write

$$ \emptyset = {}^{old}r_{ij} + \mathrm{d}\sigma_{ij} + \mathrm{d}(\Delta\lambda)\, E_{ijkl}\, m_{kl} + \Delta\lambda\, E_{ijkl} \left(\frac{\partial m_{kl}}{\partial \sigma_{mn}} \mathrm{d}\sigma_{mn} + \frac{\partial m_{kl}}{\partial q_A} \mathrm{d}q_A \right) \tag{104.107} $$

Similarly,

$$ q_A = {}^{n}q_A + \Delta\lambda\, h_A \tag{104.108} $$

r_A will be defined as:

$$ r_A = q_A - \left({}^{n}q_A + \Delta\lambda\, h_A \right) \tag{104.109} $$

and ${}^{n}q_A$ is kept fixed during iteration, that

$$ \emptyset = {}^{old}r_A + \mathrm{d}q_A - \mathrm{d}(\Delta\lambda)\, h_A - \Delta\lambda \left(\frac{\partial h_A}{\partial \sigma_{ij}} \mathrm{d}\sigma_{ij} + \frac{\partial h_A}{\partial q_B} \mathrm{d}q_B \right) \tag{104.110} $$

From equation 104.107 and 104.110, one obtains

$$ \begin{bmatrix} I^s_{ijmn} + \Delta\lambda E_{ijkl} \frac{\partial m_{kl}}{\partial \sigma_{mn}} & \Delta\lambda E_{ijkl} \frac{\partial m_{kl}}{\partial q_A} \\ -\Delta\lambda \frac{\partial h_A}{\partial \sigma_{ij}} & \delta_{AB} - \Delta\lambda \frac{\partial h_A}{\partial q_B} \end{bmatrix} \begin{Bmatrix} \mathrm{d}\sigma_{mn} \\ \mathrm{d}q_B \end{Bmatrix} + \mathrm{d}(\Delta\lambda) \begin{Bmatrix} E_{ijkl} m_{kl} \\ -h_A \end{Bmatrix} + \begin{Bmatrix} {}^{old}r_{ij} \\ {}^{old}r_A \end{Bmatrix} = \emptyset \tag{104.111} $$

Since $f(\sigma_{ij}, q_A) = 0$, one obtains

$$ \emptyset = {}^{old}f + n_{mn}\mathrm{d}\sigma_{mn} + \xi_B \mathrm{d}q_B \tag{104.112} $$

From equations 104.111 and 104.112,

$$ \mathrm{d}(\Delta\lambda) = \frac{ {}^{old}f - \begin{Bmatrix} n_{mn} & \xi_B \end{Bmatrix} \begin{bmatrix} I^s_{ijmn} + \Delta\lambda E_{ijkl} \frac{\partial m_{kl}}{\partial \sigma_{mn}} & \Delta\lambda E_{ijkl} \frac{\partial m_{kl}}{\partial q_A} \\ -\Delta\lambda \frac{\partial h_A}{\partial \sigma_{ij}} & \delta_{AB} - \Delta\lambda \frac{\partial h_A}{\partial q_B} \end{bmatrix}^{-1} \begin{Bmatrix} {}^{old}r_{ij} \\ {}^{old}r_A \end{Bmatrix} }{ \begin{Bmatrix} n_{mn} & \xi_B \end{Bmatrix} \begin{bmatrix} I^s_{ijmn} + \Delta\lambda E_{ijkl} \frac{\partial m_{kl}}{\partial \sigma_{mn}} & \Delta\lambda E_{ijkl} \frac{\partial m_{kl}}{\partial q_A} \\ -\Delta\lambda \frac{\partial h_A}{\partial \sigma_{ij}} & \delta_{AB} - \Delta\lambda \frac{\partial h_A}{\partial q_B} \end{bmatrix}^{-1} \begin{Bmatrix} E_{ijkl} m_{kl} \\ -h_A \end{Bmatrix} } \tag{104.113} $$

The iteration of $\Delta\lambda$ is then

$$\Delta\lambda^{k+1} = \Delta\lambda^k + \mathrm{d}(\Delta\lambda)^k \tag{104.114}$$

The iterative procedure is continued until the yield criterion $f = 0$, $\|r_{ij}\| = \emptyset$, and $\|r_A\| = \emptyset$ are satisfied within some tolerances at the final stress state [43].

In Equation 104.113, the generalized matrix $\mathbb{C}$, which is defined by

$$\mathbb{C} = \begin{bmatrix} I^s_{ijmn} + \Delta\lambda E_{ijkl}\frac{\partial m_{kl}}{\partial \sigma_{mn}} & \Delta\lambda E_{ijkl}\frac{\partial m_{kl}}{\partial q_A} \\ -\Delta\lambda\frac{\partial h_A}{\partial \sigma_{ij}} & \delta_{AB} - \Delta\lambda\frac{\partial h_A}{\partial q_B} \end{bmatrix}^{-1} \tag{104.115}$$

plays an important role in the implicit algorithm. It should be mentioned here that the above definition is a simplified expression for very general model with various isotropic and kinematic hardening. Specifically, if there is no hardening,

$$\mathbb{C} = \left[I^s_{ijmn} + \Delta\lambda E_{ijkl}\frac{\partial m_{kl}}{\partial \sigma_{mn}} \right]^{-1} \tag{104.116}$$

If there is only one isotropic internal variable q,

$$\mathbb{C} = \begin{bmatrix} I^s_{ijmn} + \Delta\lambda E_{ijkl}\frac{\partial m_{kl}}{\partial \sigma_{mn}} & \Delta\lambda E_{ijkl}\frac{\partial m_{kl}}{\partial q} \\ -\Delta\lambda\frac{\partial h}{\partial \sigma_{ij}} & 1 - \Delta\lambda\frac{\partial h}{\partial q} \end{bmatrix}^{-1} \tag{104.117}$$

For only one kinematic internal variable α_{ij},

$$\mathbb{C} = \begin{bmatrix} I^s_{ijmn} + \Delta\lambda E_{ijkl}\frac{\partial m_{kl}}{\partial \sigma_{mn}} & \Delta\lambda E_{ijkl}\frac{\partial m_{kl}}{\partial \alpha_{mn}} \\ -\Delta\lambda\frac{\partial h_{mn}}{\partial \sigma_{ij}} & I^s_{ijmn} - \Delta\lambda\frac{\partial h_{mn}}{\partial \alpha_{ij}} \end{bmatrix}^{-1} \tag{104.118}$$

For one isotropic variable q and one kinematic variable α_{ij},

$$\mathbb{C} = \begin{bmatrix} I^s_{ijmn} + \Delta\lambda E_{ijkl}\frac{\partial m_{kl}}{\partial \sigma_{mn}} & \Delta\lambda E_{ijkl}\frac{\partial m_{kl}}{\partial q} & \Delta\lambda E_{ijkl}\frac{\partial m_{kl}}{\partial \alpha_{mn}} \\ -\Delta\lambda\frac{\partial h}{\partial \sigma_{ij}} & 1 - \Delta\lambda\frac{\partial h}{\partial q} & -\Delta\lambda\frac{\partial h}{\partial \alpha_{ij}} \\ -\Delta\lambda\frac{\partial h_{mn}}{\partial \sigma_{ij}} & -\Delta\lambda\frac{\partial h_{mn}}{\partial q} & I^s_{ijmn} - \Delta\lambda\frac{\partial h_{mn}}{\partial \alpha_{ij}} \end{bmatrix}^{-1} \tag{104.119}$$

or for two kinematic variables z_{ij} and α_{ij},

$$\mathbb{C} = \begin{bmatrix} I^s_{ijmn} + \Delta\lambda E_{ijkl}\frac{\partial m_{kl}}{\partial \sigma_{mn}} & \Delta\lambda E_{ijkl}\frac{\partial m_{kl}}{\partial z_{mn}} & \Delta\lambda E_{ijkl}\frac{\partial m_{kl}}{\partial \alpha_{mn}} \\ -\Delta\lambda\frac{\partial h^z}{\partial \sigma_{ij}} & I^s_{ijmn} - \Delta\lambda\frac{\partial h^z}{\partial z_{mn}} & -\Delta\lambda\frac{\partial h^z}{\partial \alpha_{ij}} \\ -\Delta\lambda\frac{\partial h^\alpha_{mn}}{\partial \sigma_{ij}} & -\Delta\lambda\frac{\partial h^\alpha_{mn}}{\partial z_{mn}} & I^s_{ijmn} - \Delta\lambda\frac{\partial h^\alpha_{mn}}{\partial \alpha_{ij}} \end{bmatrix}^{-1} \tag{104.120}$$

If we define

$$\mathbf{n} = \begin{Bmatrix} n_{mn} \\ \xi_B \end{Bmatrix} \tag{104.121}$$

[43] $\|\|$ is some normal of the tensor

$$\mathbf{m} = \left\{ \begin{array}{c} E_{ijkl} m_{kl} \\ -h_A \end{array} \right\} \tag{104.122}$$

$$^{old}\mathbf{r} = \left\{ \begin{array}{c} ^{old}\sigma_{ij} \\ ^{old}r_A \end{array} \right\} \tag{104.123}$$

Equation 104.114 can be simplified as

$$\mathrm{d}(\Delta\lambda) = \frac{^{old}f - \mathbf{n}^T \, \mathbb{C} \, ^{old}\mathbf{r}}{\mathbf{n}^T \, \mathbb{C} \, \mathbf{M}} \tag{104.124}$$

and

$$\left\{ \begin{array}{c} \mathrm{d}\sigma_{mn} \\ \mathrm{d}q_B \end{array} \right\} = -\mathbb{C} \left(^{old}\mathbf{r} + \mathrm{d}(\Delta\lambda)\mathbf{m} \right) \tag{104.125}$$

104.4.2 Backward Euler Algorithms: Starting Points

Some remarks are necessary in order to clarify the Backward Euler Algorithm. It is a well known fact that the rate of convergence of the Newton - Raphson Method , or even obtaining convergence at all, is closely tied to the starting point for the iterative procedure. Bad initial or starting points might lead our algorithm to an oscillating solution, i.e. the algorithm does not converge. In the following, starting points for the Newton - Raphson iterative procedure will be established for one– and two–vector return algorithms.

104.4.2.1 Single Vector Return Algorithm Starting Point.

One of the proposed starting points (Crisfield, 1991) uses the normal at the elastic trial point[44] ${}^{pred}\sigma_{ij}$. A first order Taylor expansion about point ${}^{pred}\sigma_{ij}$ yields:

$$\begin{aligned} {}^{pred}F^{new} &= {}^{pred}F^{old} + \left.\frac{\partial F}{\partial \sigma_{mn}}\right|_{pred} d\left({}^{pred}\sigma_{mn}\right) + \left.\frac{\partial F}{\partial q_A}\right|_{pred} dq_A = \\ &= {}^{pred}F^{old} + {}^{pred}n_{mn}\, d\sigma_{mn} + \xi_A h_A d\lambda = 0 \end{aligned} \tag{104.126}$$

It is assumed that the total incremental strain ϵ_{kl} is applied in order to reach the point ${}^{pred}\sigma_{ij}$, i.e. ${}^{pred}\sigma_{ij} = E_{ijkl}\,\epsilon_{kl}$ so that any further stress "relaxation" toward the yield surface takes place under zero total strain condition $\epsilon_{kl} = \emptyset$. From the differential form of equation (104.16) it follows:

$$\begin{aligned} d\left({}^{pred}\sigma_{mn}\right) &= E_{mnpq}\left(d\left({}^{pred}\epsilon_{pq}\right) - d\left({}^{pred}\epsilon^{p}_{pq}\right)\right) = \\ &= -E_{mnpq}\, d\left({}^{pred}\epsilon^{p}_{pq}\right) = -E_{mnpq}\, d\lambda\left({}^{pred}m_{pq}\right) \end{aligned}$$

and equation (104.126) becomes:

$${}^{pred}F^{old} - {}^{pred}n_{mn}\, E_{mnpq}\, d\lambda {}^{pred}m_{pq} + \xi_A h_A d\lambda = 0$$

and it follows:

$$d\lambda = \frac{{}^{pred}F^{old}}{{}^{pred}n_{mn}\, E_{mnpq}\, {}^{pred}m_{pq} - \xi_A h_A}$$

With this solution for $d\lambda$ we can obtain the starting point for the Newton-Raphson iterative procedure

$${}^{start}\sigma_{mn} = E_{mnpq}\, {}^{pred}\epsilon_{pq} - E_{mnpq}\, \frac{{}^{pred}F^{old}}{{}^{pred}n_{mn}\, E_{mnpq}\, {}^{pred}m_{pq} - \xi_A h_A}\, {}^{pred}m_{pq} \tag{104.127}$$

This starting point in six dimensional stress space will in general not satisfy the yield condition $F = 0$, but it will provide a good initial guess for the upcoming Newton-Raphson iterative procedure.

It should be mentioned, however, that this scheme for returning to the yield surface is the well known Radial Return Algorithm , if the yield criterion under consideration is of the von Mises type. In the special case the normal at the elastic trial point ${}^{pred}\sigma_{ij}$ coincides with the normal at the final stress state ${}^{n+1}\sigma_{ij}$, the return is exact, i.e. the yield condition is satisfied in one step.

Another possible and readily available starting point can be obtained by applying one Forward Euler step[45]. To be able to use the Forward Euler integration scheme, an intersection point has to be found. The procedure for calculating intersection points is given in section (104.2.4).

[44] I have named this scheme as semi Backward Euler scheme.

[45] or more steps for really large strain increments, for example over 10% in deviatoric direction. What has actually been done is to divide the θ region into several parts and depending on the curvature of the yield surface in deviatoric plane, use different schemes and different number of subincrements (the more curved, the more subincrements) to get the first, good initial guess. In the region around $\theta = 0$, one step of the semi Backward Euler scheme is appropriate, but close to $\theta = \pi/3$ the Forward Euler subincrementation works better.

A first order Taylor expansion about intersection point ${}^{cross}\sigma_{ij}$ yields:

$$\begin{aligned} F^{new} &= F^{old} + \left.\frac{\partial F}{\partial \sigma_{mn}}\right|_{cross} d\left({}^{cross}\sigma_{mn}\right) + \left.\frac{\partial F}{\partial q_A}\right|_{cross} dq_A = \\ &= {}^{cross}n_{mn}\, d\sigma_{mn} + \xi_A h_A d\lambda = 0 \end{aligned} \tag{104.128}$$

From the differential form of equation (104.16) it follows:

$$d\left({}^{fE}\sigma_{mn}\right) = E_{mnpq}\left(d\left(\epsilon_{pq}\right) - d\left(\epsilon^{p}_{pq}\right)\right) =$$
$$= E_{mnpq} d\left(\epsilon_{pq}\right) - E_{mnpq}\, d\left(\epsilon^{p}_{pq}\right) = E_{mnpq} d\left(\epsilon_{pq}\right) - E_{mnpq}\, d\lambda\left({}^{cross}m_{pq}\right)$$

and equation (104.128) becomes:

$$-{}^{cross}n_{mn}\, E_{mnpq}\, d\epsilon_{pq} - {}^{cross}n_{mn}\, E_{mnpq}\, d\lambda\, {}^{cross}m_{pq} + \xi_A h_A d\lambda = 0$$

and it follows

$$d\lambda = \frac{{}^{cross}n_{mn}\, E_{mnpq}\, d\epsilon_{pq}}{{}^{cros}n_{mn}\, E_{mnpq}\, {}^{cros}m_{pq} - \xi_A h_A}$$

With this solution for $d\lambda$ we can obtain the starting point for the Newton-Raphson iterative procedure

$${}^{start}\sigma_{mn} = E_{mnpq}\, d\epsilon_{pq} - E_{mnpq}\, \frac{{}^{cross}n_{rs}\, E_{rstu}\, d\epsilon_{tu}}{{}^{cross}n_{ab}\, E_{abcd}\, {}^{cross}m_{cd} - \xi_A h_A}\, {}^{cross}m_{pq} \tag{104.129}$$

This starting point in six–dimensional stress space will again not satisfy the yield condition[46] $F = 0$, but will provide a good initial estimate for the upcoming Newton-Raphson iterative procedure.

104.4.3 Consistent Tangent Stiffness Tensor

The final goal in deriving the Backward Euler scheme for integration of elasto–plastic constitutive equations is to use that scheme in finite element computations. If the Newton – Raphson iterative scheme is used at the global equilibrium level then the use of the so called traditional tangent stiffness tensor[47] E^{ep}_{ijkl} destroys the quadratic rate of asymptotic convergence of the iterative scheme. In order to preserve such a quadratic rate, a consistent, also called algorithmic, tangent stiffness tensor is derived. The consistent tangent stiffness tensor make use of derivatives of direction[48] normal to the potential function, and they are derived at the final, final at each iteration, that converges to the final stress point on the yield surface, stress point. The traditional forward scheme has a constant derivative, m_{ij} that is evaluated at the intersection point.

[46] except for the yield criteria that have flat yield surfaces (in the stress invariant space) so that the first order Taylor linear expansion, is exact.

[47] the one obtained with the Forward Euler method, i.e. where parameter $\alpha = 0$.

[48] $m_{ij} = \partial Q/\partial\sigma_{ij}$, i.e. $\partial m_{ij}/\partial\sigma_{kl} = \partial^2 Q/\partial\sigma_{ij}\partial\sigma_{kl}$.

It appears that Simo and Taylor (1985) and Runesson and Samuelsson (1985) have first derived the consistent tangent stiffness tensor. Other interesting articles on the subject can be found in Simo and Taylor (1986), Simo and Govindjee (1988), Jetteur (1986), Braudel et al. (1986), Crisfield (1987), Ramm and Matzenmiller (1988) and Mitchell and Owen (1988). As a consequence of consistency, the use of the consistent tangent stiffness tensor significantly improves the convergence characteristics of the overall equilibrium iterations, if a Newton - Raphson scheme is used for the latter. Use of the consistent tangent stiffness tensor yields a quadratic convergence rate of Newton - Raphson equilibrium iterations. In what follows, two derivations are given, namely the consistent tangent stiffness tensor for single– and two–vector return algorithms.

The concept of consistent linearization was introduced by Hughes and Pister (1978), while detailed explanation is given by Simo and Hughes (1998). The consistent tangent stiffness leads to quadratic convergence rates at global level.

It should be mentioned that there are various 'equivalent' forms of consistent tangent stiffness depending on the specific implicit algorithm equations. For instance, Simo and Hughes (1998), and Belytschko et al. (2001) derived the consistent tangent stiffness by taking current plastic strain as unknown and seeking its derivatives in the stress space; Pérez-Foguet and Huerta (1997) and Pérez-Foguet et al. (2000) used the numerical differentiation to calculate the consistent tangent stiffness in a compact matrix-vector form; Choi (2004) adopted the compact matrix-vector form by Pérez-Foguet and Huerta (1997) and Pérez-Foguet et al. (2000) but taking current plastic strain as unknown and seeking its derivatives in the elastic strain space. Slightly different from the above strategies, in this work the implicit algorithm is adopting the traditional form but taking current stress as unknown and seeking its derivatives in the stress space. Provided these differences, the consistent tangent stiffness in this work is slightly different from those in the above work.

104.4.3.1 Single Vector Return Algorithm.

In implicit algorithm, a very important advantage is that it may lead to consistent (algorithmic) tangent stiffness (Equation 104.137). The concept of consistent linearization was introduced in Hughes and Pister (1978), more details on consistent tangent stiffness were explained in Simo and Hughes (1998). The consistent tangent stiffness leads to quadratic convergence rates at global level.

It should be mentioned that there are various 'equivalent' forms of consistent tangent stiffness depending on the specific implicit algorithm equations. For instance, Simo and Hughes (1998), and Belytschko et al. (2001) derived the consistent tangent stiffness by taking current plastic strain as unknown and seeking its derivatives in the stress space; Pérez-Foguet and Huerta (1997) and Pérez-Foguet et al. (2000) used the numerical differentiation to calculate the consistent tangent stiffness in a

compact matrix-vector form; Choi (2004) adopted the compact matrix-vector form by Pérez-Foguet and Huerta (1997) and Pérez-Foguet et al. (2000) but taking current plastic strain as unknown and seeking its derivatives in the elastic strain space. Slightly different from the above strategies, in this work (section 104.4) the implicit algorithm is adopting the traditional form but taking current stress as unknown and seeking its derivatives in the stress space. Provided these differences, the consistent tangent stiffness in this work is slightly different from those in the above work. The detail derivation will be followed.

When seeking the algorithmic tangent stiffness, we look into the explicit expression of $\mathrm{d}\sigma_{ij}/\mathrm{d}\epsilon^{pred}_{mn}$. At the same time, the internal variables are initialized the values at the previous time step, in other words, they are fixed within the time step when seeking the algorithmic tangent stiffness.

Linearize Equation 104.103, one obtains

$$\mathrm{d}\sigma_{ij} = E_{ijkl}\ \mathrm{d}\epsilon^{pred}_{kl} - \mathrm{d}(\Delta\lambda)\ E_{ijkl}\ m_{kl} - \Delta\lambda\ E_{ijkl}\ \left(\frac{\partial m_{kl}}{\partial \sigma_{mn}}\mathrm{d}\sigma_{mn} + \frac{\partial m_{kl}}{\partial q_A}\mathrm{d}q_A\right) \tag{104.130}$$

Similarly, linearize Equation 104.108, one obtains

$$\mathrm{d}q_A = \mathrm{d}(\Delta\lambda)\ h_A + \Delta\lambda\ \left(\frac{\partial h_A}{\partial \sigma_{ij}}\mathrm{d}\sigma_{ij} + \frac{\partial h_A}{\partial q_B}\mathrm{d}q_B\right) \tag{104.131}$$

From equation 104.130 and 104.131, one obtains

$$\begin{bmatrix} I^s_{ijmn} + \Delta\lambda E_{ijkl}\frac{\partial m_{kl}}{\partial \sigma_{mn}} & \Delta\lambda E_{ijkl}\frac{\partial m_{kl}}{\partial q_A} \\ -\Delta\lambda\frac{\partial h_A}{\partial \sigma_{ij}} & \delta_{AB} - \Delta\lambda\frac{\partial h_A}{\partial q_B} \end{bmatrix} \begin{Bmatrix} \mathrm{d}\sigma_{mn} \\ \mathrm{d}q_B \end{Bmatrix} + \mathrm{d}(\Delta\lambda) \begin{Bmatrix} E_{ijkl}m_{kl} \\ -h_A \end{Bmatrix} = \begin{Bmatrix} E_{ijkl}\ \mathrm{d}\epsilon^{pred}_{kl} \\ 0 \end{Bmatrix} \tag{104.132}$$

If one use the definitions of 104.115, 104.122 and 104.121, Equation 104.132 can be simplified to

$$\mathbb{C}^{-1} \begin{Bmatrix} \mathrm{d}\sigma_{mn} \\ \mathrm{d}q_B \end{Bmatrix} + \mathrm{d}(\Delta\lambda)\mathbf{m} = \begin{Bmatrix} E_{ijkl}\ \mathrm{d}\epsilon^{pred}_{kl} \\ 0 \end{Bmatrix} \tag{104.133}$$

Linearize the yield function $f(\sigma_{ij}, q_A) = 0$, one obtains

$$n_{mn}\mathrm{d}\sigma_{mn} + \xi_B \mathrm{d}q_B = 0 \tag{104.134}$$

or in a simplified form

$$\mathbf{n}^{\mathbf{T}} \begin{Bmatrix} \mathrm{d}\sigma_{mn} \\ \mathrm{d}q_B \end{Bmatrix} = \mathbf{0} \tag{104.135}$$

From Equations 104.133 and 104.135, one obtain

$$\mathrm{d}(\Delta\lambda) = \frac{\mathbf{n}^{\mathbf{T}}\mathbb{C}}{\mathbf{n}^{\mathbf{T}}\mathbb{C}\mathbf{m}} \begin{Bmatrix} E_{ijmn}\ \mathrm{d}\epsilon^{pred}_{mn} \\ 0 \end{Bmatrix} \tag{104.136}$$

Substitute expression 104.136 into 104.133, one obtains

$$\begin{Bmatrix} \mathrm{d}\sigma_{ij} \\ \mathrm{d}q_A \end{Bmatrix} = \left\{ \mathbb{C} - \frac{\mathbb{C}\mathbf{m}\mathbf{n}^T\mathbb{C}}{\mathbf{n}^T\,\mathbb{C}\,\mathbf{m}} \right\} \begin{Bmatrix} E_{ijmn}\,\mathrm{d}\epsilon^{pred}_{mn} \\ 0 \end{Bmatrix} \tag{104.137}$$

This equation gives the explicit expression of the consistent tangent stiffness $\mathrm{d}\sigma_{ij}/\mathrm{d}\epsilon^{pred}_{mn}$ for the implicit algorithm.

From section 104.4, if there are interactions between internal variables, the implicit algorithm will become very complicated. Simple models (e.g. von Mises model, or sometimes termed as J_2 model) have been proved efficient and good performance by the implicit algorithm (Simo and Hughes, 1998). Evidently, the implicit algorithm is mathematically based on the Newton-Raphson nonlinear equation solving method as well as the Eulerian backward integration method. Theoretically, the Newton-Raphson method may have quadratic convergence rate. However, Newton-Raphson method is not unconditional stable, and sometimes the iteration will diverge (Press et al., 1988a). Any bad starting point, non-continuous derivatives around solution, high nonlinearity, and interactions between internal variables, will deteriorate the implicit algorithm performance. A complicated model cannot guarantee good performance or quadratic convergence by the implicit algorithm Crisfield (1997a). The task to obtain the analytical expressions (Equations 104.116 to 104.120) may prove exceeding laborious for complicated plasticity models Simo and Hughes (1998).

104.4.4 Gradients to the Potential Function

In the derivation of the Backward Euler algorithm and the Consistent Tangent Matrix it is necessary to derive the first and the second derivatives of the potential function. The function Q is the function of the stress tensor σ_{ij} and the plastic variable tensor q_A. Derivatives with respect to the stress tensor σ_{ij} and plastic variable tensor q_A are given here. It is assumed that any stress state can be represented with the three stress invariants p, q and θ given in the following form:

$$p = -\frac{1}{3}I_1 \quad q = \sqrt{3J_{2D}} \quad \cos 3\theta = \frac{3\sqrt{3}}{2}\frac{J_{3D}}{\sqrt{(J_{2D})^3}} \tag{104.138}$$

$$I_1 = \sigma_{kk} \quad J_{2D} = \frac{1}{2}s_{ij}s_{ij} \quad J_{3D} = \frac{1}{3}s_{ij}s_{jk}s_{ki} \quad s_{ij} = \sigma_{ij} - \frac{1}{3}\sigma_{kk}\delta_{ij} \tag{104.139}$$

Stresses are here chosen as positive in tension. The definition of Lode's angle θ in equation (104.138) implies that $\theta = 0$ defines the meridian of conventional triaxial extension (CTE), while $\theta = \pi/3$ denotes the meridian of conventional triaxial compression (CTC).

The Potential Function is given in the following form:

$$Q = Q(p, q, \theta) \tag{104.140}$$

The complete derivation of the closed form gradients is given in Appendix 703.

104.4.4.1 Analytical Gradients

The first derivative of the function Q in stress space is:

$$\frac{\partial Q}{\partial \sigma_{ij}} = \frac{\partial Q}{\partial p}\frac{\partial p}{\partial \sigma_{ij}} + \frac{\partial Q}{\partial q}\frac{\partial q}{\partial \sigma_{ij}} + \frac{\partial Q}{\partial \theta}\frac{\partial \theta}{\partial \sigma_{ij}} \tag{104.141}$$

and subsequently the first derivatives of the chosen stress invariants are

$$\frac{\partial p}{\partial \sigma_{ij}} = -\frac{1}{3}\,\delta_{ij} \tag{104.142}$$

$$\frac{\partial q}{\partial \sigma_{ij}} = \frac{3}{2}\,\frac{1}{q}s_{ij} \tag{104.143}$$

$$\frac{\partial \theta}{\partial \sigma_{ij}} = \frac{3}{2}\,\frac{\cos(3\theta)}{q^2\sin(3\theta)}s_{ij} - \frac{9}{2}\,\frac{1}{q^3\sin(3\theta)}t_{ij} \tag{104.144}$$

where:

$$t_{ij} = \frac{\partial J_{3D}}{\partial \sigma_{ij}}$$

The second derivative of the function Q in stress space is

$$\begin{aligned}
\frac{\partial^2 Q}{\partial \sigma_{pq}\partial \sigma_{mn}} &= \\
&\left(\frac{\partial^2 Q}{\partial p^2}\frac{\partial p}{\partial \sigma_{mn}} + \frac{\partial^2 Q}{\partial p \partial q}\frac{\partial q}{\partial \sigma_{mn}} + \frac{\partial^2 Q}{\partial p \partial \theta}\frac{\partial \theta}{\partial \sigma_{mn}}\right)\frac{\partial p}{\partial \sigma_{pq}} + \frac{\partial Q}{\partial p}\frac{\partial^2 p}{\partial \sigma_{pq}\partial \sigma_{mn}} \quad + \\
&+\left(\frac{\partial^2 Q}{\partial q \partial p}\frac{\partial p}{\partial \sigma_{mn}} + \frac{\partial^2 Q}{\partial q^2}\frac{\partial q}{\partial \sigma_{mn}} + \frac{\partial^2 Q}{\partial q \partial \theta}\frac{\partial \theta}{\partial \sigma_{mn}}\right)\frac{\partial q}{\partial \sigma_{pq}} + \frac{\partial Q}{\partial q}\frac{\partial^2 q}{\partial \sigma_{pq}\partial \sigma_{mn}} \quad + \\
&+\left(\frac{\partial^2 Q}{\partial \theta \partial p}\frac{\partial p}{\partial \sigma_{mn}} + \frac{\partial^2 Q}{\partial \theta \partial q}\frac{\partial q}{\partial \sigma_{mn}} + \frac{\partial^2 Q}{\partial \theta^2}\frac{\partial \theta}{\partial \sigma_{mn}}\right)\frac{\partial \theta}{\partial \sigma_{pq}} + \frac{\partial Q}{\partial \theta}\frac{\partial^2 \theta}{\partial \sigma_{pq}\partial \sigma_{mn}}
\end{aligned} \tag{104.145}$$

and the second derivatives of the stress invariants are

$$\frac{\partial^2 p}{\partial\sigma_{pq}\partial\sigma_{mn}} = \emptyset \tag{104.146}$$

$$\frac{\partial^2 q}{\partial\sigma_{pq}\partial\sigma_{mn}} = \frac{3}{2}\frac{1}{q}\left(\delta_{pm}\delta_{nq} - \frac{1}{3}\delta_{pq}\delta_{nm}\right) - \frac{9}{4}\frac{1}{q^3}\, s_{mn}s_{pq} \tag{104.147}$$

$$\begin{aligned}\frac{\partial^2\theta}{\partial\sigma_{pq}\partial\sigma_{mn}} = \\ -\left(\frac{9}{2}\frac{\cos 3\theta}{q^4\sin(3\theta)} + \frac{27}{4}\frac{\cos 3\theta}{q^4\sin^3 3\theta}\right)\, s_{pq}\, s_{mn} + \frac{81}{4}\frac{1}{q^5\sin^3 3\theta}\, s_{pq}\, t_{mn} + \\ +\left(\frac{81}{4}\frac{1}{q^5\sin 3\theta} + \frac{81}{4}\frac{\cos^2 3\theta}{q^5\sin^3 3\theta}\right)\, t_{pq}\, s_{mn} - \frac{243}{4}\frac{\cos 3\theta}{q^6\sin^3 3\theta}\, t_{pq}\, t_{mn} + \\ +\frac{3}{2}\frac{\cos(3\theta)}{q^2\sin(3\theta)}\, p_{pqmn} - \frac{9}{2}\frac{1}{q^3\sin(3\theta)}\, w_{pqmn}\end{aligned} \tag{104.148}$$

where:

$$w_{pqmn} = \frac{\partial t_{pq}}{\partial\sigma_{mn}} = s_{np}\delta_{qm} + s_{qm}\delta_{np} - \frac{2}{3}s_{qp}\delta_{nm} - \frac{2}{3}\delta_{pq}s_{mn}$$

and:

$$p_{pqmn} = \frac{\partial s_{pq}}{\partial\sigma_{mn}} = \left(\delta_{mp}\delta_{nq} - \frac{1}{3}\delta_{pq}\delta_{mn}\right)$$

Another important gradient is:

$$\begin{aligned}\frac{\partial^2 Q}{\partial\sigma_{ij}\partial q_A} = \frac{\partial m_{ij}}{\partial q_A} = \\ = \frac{\partial\frac{\partial Q}{\partial p}}{\partial q_A}\frac{\partial p}{\partial\sigma_{ij}} + \frac{\partial\frac{\partial Q}{\partial q}}{\partial q_A}\frac{\partial q}{\partial\sigma_{ij}} + \frac{\partial\frac{\partial Q}{\partial\theta}}{\partial q_A}\frac{\partial\theta}{\partial\sigma_{ij}} = \\ = \frac{\partial^2 Q}{\partial p\partial q_A}\frac{\partial p}{\partial\sigma_{ij}} + \frac{\partial^2 Q}{\partial q\partial q_A}\frac{\partial q}{\partial\sigma_{ij}} + \frac{\partial^2 Q}{\partial\theta\partial q_A}\frac{\partial\theta}{\partial\sigma_{ij}}\end{aligned} \tag{104.149}$$

104.4.4.2 Finite Difference Gradients

After having developed the closed form, analytical derivatives[49] the author of this thesis asked himself: "is there a simpler way of finding these derivatives?" One of the proposed ways to check the analytical solution is found in Dennis and Schnabel (1983). Dennis and Schnabel proposes the finite difference method for approximating derivatives if these derivatives are not analytically available and as a tool to check your analytical derivatives if they are derived.

Another good reason for developing alternative gradients is that for $\theta = 0, \pi/3$ gradients are not defined, i.e. indefinite terms as $0/0$ are appearing. One possible solution is the use of l'Hospital's rule. This has been done in Perić (1991). The solution to the problem in this work went in a different direction, i.e. instead of aiming for the analytical form, numerical derivatives are derived.

We should recall that for a function f of a single variable, the finite difference approximation to $f'(x)$, by using forward finite difference approach, is given by:

$$a = \frac{f(x+h) - f(x)}{h} \tag{104.150}$$

where h is a vanishingly small quantity. The same definition was used in deriving the finite difference approximation for the first derivative of the yield function F and potential function Q. The first derivative of F (or Q) with respect to the stress tensor σ_{ij} for diagonal elements is[50] :

$$^{approx.}F_{,ii} = \frac{F(\sigma_{ii} + h_{ii}) - F(\sigma_{ii})}{h_{ii}} \tag{104.151}$$

and for non-diagonal elements[51]:

$$^{approx.}F_{,ij} = \frac{F(\sigma_{ij} + h_{ij} + h_{ji}) - F(\sigma_{ij})}{2h_{ij}} \tag{104.152}$$

where h_{ij} is the step size which, because of finite precision arithmetic, is a variable[52].

The accuracy of the finite difference approximation to the analytical derivatives is closely bound to the step size h_{ij}. It is suggested in Dennis and Schnabel (1983)[section 5.4.] that for functions given by the simple formula, the number h should be $h = \sqrt{macheps}$, while for more complicated functions

[49] see Appendix (703).

[50] no sum convention implied, just the position of the element.

[51] since the stress tensor σ_{ij} is symmetric, change in one non-diagonal element triggers the other to be changed as well.

[52] it is actually one small number, h, that is multiplied with the current stress value so that the relative order of magnitude is retained.

that number should be larger. Here *macheps* is the so called machine epsilon. It is defined as the smallest distinguishable positive number[53], such that $1.0 + macheps > 1.0$ on the given platform. For example[54], on the Intel x86 platform[55] $macheps = 1.08E-19$ while on the SUNSparc and DEC platforms $macheps = 2.22E-16$. It has been found that in the case of yield or potential functions the best approximation of analytical gradients is obtained by using $h = \sqrt{macheps}\ 10^3$. The three order of magnitude increase in the finite difference step is due to a rather complicated[56] formula for yield and potential functions. The error in the approximation, ${}^{approx.}F_{,ij}$ is found to be after the N^{th} decimal place, where N is the order of *macheps*, i.e. $macheps = O(N)$.

Second derivative approximations for one variable function are given in the form:

$$a = \frac{\big(f(x + h_i e_i + h_j e_j) - f(x + h_i e_i)\big) - \big(f(x + h_j e_j) - f(x)\big)}{h_i h_j} \tag{104.153}$$

If the first derivatives are available in closed form, one could use equations (104.151) and (104.152) just by replacing the function values with tensor values for analytical derivatives[57].

However, if the analytic derivatives are not available, one has to devise a formula that will create a fourth order tensor from the changes in two dimensional stress tensors, σ_{ij} and σ_{kl}. Using the scheme employed in equation (104.153) the following scheme has been devised:

$$ {}^{approx.}Q_{,ijkl} = \frac{\big(Q(\sigma_{mn} + h_{ij} + h_{kl}) - Q(\sigma_{mn} + h_{ij})\big) - \big(Q(\sigma_{mn} + h_{kl}) - Q(\sigma_{mn})\big)}{h_{ij} h_{kl}} \tag{104.154}$$

Special considerations are necessary in order to retain symmetry of the fourth order tensor. At the moment it has not been possible to figure out how to build the finite difference approximation to the second derivatives of yield/potential functions for a general stress state. The only finite difference approximation of the second derivatives that appears to have worked was the one devised in principal stress space. Namely, diagonal elements of the analytical and the approximate gradients matched exactly, but development of non-diagonal elements, and the whole scheme of symmetrizing the fourth order approximation, still remain a mystery. However, some pattern was observed in non–diagonal elements, and the work on symmetrizing it is in progress.

[53] in a given precision, i.e. float (real*4), double (real*8) or long double (real*10).

[54] the precision sought was double (real*8).

[55] PC computers.

[56] One should not forget that we work with six dimensional tensor formulae directly.

[57] see Dennis and Schnabel (1983), section 5.6.

For many different potential functions (or yield functions) the only task left would be the derivation of the first derivatives of F and Q and the second derivatives of Q with respect to p, q and θ, namely the first derivatives $\frac{\partial Q}{\partial p}$, $\frac{\partial Q}{\partial q}$ and $\frac{\partial Q}{\partial \theta}$ and $\frac{\partial Q}{\partial p}$, $\frac{\partial Q}{\partial q}$ and $\frac{\partial Q}{\partial \theta}$ and the second derivatives $\frac{\partial^2 Q}{\partial p^2}$, $\frac{\partial^2 Q}{\partial p \partial q}$, $\frac{\partial^2 Q}{\partial p \partial \theta}$, $\frac{\partial^2 Q}{\partial q \partial p}$, $\frac{\partial^2 Q}{\partial q^2}$, $\frac{\partial^2 Q}{\partial q \partial \theta}$, $\frac{\partial^2 Q}{\partial \theta \partial p}$, $\frac{\partial^2 Q}{\partial \theta \partial q}$ and $\frac{\partial^2 Q}{\partial \theta^2}$. If the potential function is twice differentiable with respect to the stress tensor σ_{ij}, and if it is continuous then the Hessian matrix is symmetric.

104.5 Line Search Technique for Constitutive Elastic-Plastic Integration

This section is entirely based on Jeremić (2001). There exist a repetition of some previously defined equations...

104.6 Elastic and Elastic–Plastic Material Models for Solids

In this section we present elements of general elastic and elastic–plastic material models for engineering materials. We describe various forms of the yield functions, plastic flow directions and hardening and softening laws.

104.6.1 Elasticity

DSL COMMANDS for the elastic material models are given in section 205.3 on page 827.

In linear elasticity the relationship between the stress tensor σ_{ij} and the strain tensor ϵ_{kl} can be represented in the following form:

$$\sigma_{ij} = \sigma\left(\epsilon_{ij}\right) \tag{104.155}$$

If we assume the existence of a strain energy function[58] $W\left(\epsilon_{ij}\right)$ then the stress strain relation is:

$$\sigma_{ij} = \frac{\partial W\left(\epsilon_{ij}\right)}{\partial \epsilon_{ij}} \tag{104.156}$$

The introduction of the strain energy density function into elasticity is due to Green, and elastic solids for which such a function is assumed to exist are called Green elastic or hyperelastic solids.

[58] per unit volume.

Linearization of an elastic continuum is carried out with respect to a reference configuration which is stress free at temperature T_0, so that ${}^0\sigma_{ij} = 0$. If we denote as E_{ijkl} an isothermal modulus tensor, then under isothermal conditions, we obtain the generalized Hooke's law:

$$\sigma_{ij} = E_{ijkl}\epsilon_{kl} \tag{104.157}$$

where E_{ijkl} is the fourth order elastic stiffness tensor with 81 independent components in total. The elastic stiffness tensor features both minor symmetry $E_{ijkl} = E_{jikl} = E_{ijlk}$ and major symmetry $E_{ijkl} = E_{klij}$ (Jeremić and Sture, 1997). The number of independent components for such elastic stiffness tensor is 21 (Spencer, 1980).

$$E_{ijkl} = \left| \frac{\partial^2 W}{\partial\epsilon_{ij}\,\partial\epsilon_{kl}} \right|_{\epsilon=0} = \left| \frac{\partial^2 W}{\partial\epsilon_{kl}\,\partial\epsilon_{ij}} \right|_{\epsilon=0} \tag{104.158}$$

We will restrain our considerations to the isotropic case. The most general form of the isotropic tensor of rank 4 has the following representation:

$$I_4 = \lambda\delta_{ij}\delta_{kl} + \mu\delta_{ik}\delta_{jl} + \nu\delta_{il}\delta_{jk} \tag{104.159}$$

If E_{ijkl} has this form then in order to satisfy the symmetry condition[59] $E_{ijkl} = E_{jikl}$ we must have $\nu = \mu$. The symmetry condition[60] $E_{ijkl} = E_{klji}$ is then automatically satisfied. The elastic constant tensor has the following form:

$$E_{ijkl} = \lambda\delta_{ij}\delta_{kl} + \mu\left(\delta_{ik}\delta_{jl} + \delta_{il}\delta_{jk}\right) \tag{104.160}$$

where λ and μ are the Lamé coefficients:

$$\lambda = \frac{\nu E}{(1+\nu)(1-2\nu)} \quad ; \quad \mu = \frac{E}{2(1+\nu)} \tag{104.161}$$

and E and ν are Young's Modulus and Poisson's ratio respectively. The symmetric part of the fourth order unit tensor is :

$$I^{sym}_{ijkl} = \frac{1}{2}\left(\delta_{ik}\delta_{jl} + \delta_{il}\delta_{jl}\right) \tag{104.162}$$

and can be found as multiplier of μ in equation (104.160). Equation (104.160) can be written in terms of E and ν as:

$$E_{ijkl} = \frac{E}{2(1+\nu)}\left(\frac{2\nu}{1-2\nu}\,\delta_{ij}\delta_{kl} + \delta_{ik}\delta_{jl} + \delta_{il}\delta_{jk}\right) \tag{104.163}$$

The same relation in terms of bulk modulus K and shear modulus G is:

[59] symmetry in stress tensor.

[60] existence of strain energy function.

$$E_{ijkl} = K\delta_{ij}\delta_{kl} + G\left(-\frac{2}{3}\delta_{ij}\delta_{kl} + \delta_{ik}\delta_{jl} + \delta_{il}\delta_{jk}\right) \tag{104.164}$$

where K and G are given as:

$$K = \lambda + \frac{2}{3}\mu \quad ; \quad G = \mu \tag{104.165}$$

The relation between the strain tensor, ϵ_{kl} and the stress tensor, σ_{ij} is:

$$\epsilon_{kl} = D_{klpq}\sigma_{pq} \tag{104.166}$$

where D_{klpq} is the elastic compliance fourth order tensor, defined as:

$$D_{klpq} = \frac{-\lambda}{2\mu\,(3\lambda + 2\mu)}\,\delta_{kl}\delta_{pq} + \frac{1}{4\mu}\left(\delta_{kp}\delta_{lq} + \delta_{kq}\delta_{lp}\right) \tag{104.167}$$

or in terms of E and ν:

$$D_{klpq} = \frac{1+\nu}{2E}\left(\frac{-2\nu}{1+\nu}\,\delta_{kl}\delta_{pq} + \delta_{kp}\delta_{lq} + \delta_{kq}\delta_{lp}\right) \tag{104.168}$$

of in terms of K and G:

$$D_{klpq} = \frac{1}{9K}\,\left(\delta_{kl}\delta_{pq}\right) + \frac{1}{2G}\left(-\frac{1}{3}\delta_{kl}\delta_{pq} + \frac{1}{2}\left(\delta_{kp}\delta_{lq} + \delta_{kq}\delta_{lp}\right)\right) \tag{104.169}$$

It is worthwhile noting that the part adjacent to the inverse of the bulk modulus K:

$$\left(\delta_{kl}\delta_{pq}\right)$$

controls the volumetric response and that the part adjacent to the inverse of the shear modulus G:

$$\left(-\frac{1}{3}\delta_{kl}\delta_{pq} + \frac{1}{2}\left(\delta_{kp}\delta_{lq} + \delta_{kq}\delta_{lp}\right)\right)$$

controls the shear response! This note will prove useful later on. Linear transformation of the stress tensor σ_{pq} into itself, i.e. σ_{ij} is defined as:

$$\sigma_{ij} = E_{ijkl}\epsilon_{kl} = E_{ijkl}D_{klpq}\sigma_{pq} \tag{104.170}$$

where

$$E_{ijkl}D_{klpq} = \frac{1}{2}\left(\delta_{ip}\delta_{jq} + \delta_{iq}\delta_{jp}\right) = I^{sym}_{ijpq} \tag{104.171}$$

104.6.1.1 Elastic Model

Linear elastic law is the simplest one and assumes constant Young's modulus E and constant Poisson's Ration ν.

104.6.1.2 Non–linear Elastic Model #1

This nonlinear model (Janbu, 1963), (Duncan and Chang, 1970) assumes dependence of the Young's modulus on the minor principal stress $\sigma_3 = \sigma_{min}$ in the form

$$E = K p_a \left(\frac{\sigma_3}{p_a}\right)^n \tag{104.172}$$

Here, p_a is the atmospheric pressure in the same units as E and stress. The two material constants K and n are constant for a given void ratio.

104.6.1.3 Non–linear Elastic Model #2

If Young's modulus and Poisson's ratio are replaced by the shear modulus G and bulk modulus K the non–linear elastic relationship can be expressed in terms of the normal effective mean stress p as

$$G \quad \text{and/or} \quad K = AF(e, OCR)p^n \tag{104.173}$$

where e is the void ratio, OCR is the overconsolidation ratio and $p = \sigma_{ii}/3$ is the mean effective stress (Hardin, 1978).

104.6.1.4 Lade's Non–linear Elastic Model

Lade and Nelson (1987) and Lade (1988a) proposed a nonlinear elastic model based on Hooke's law in which Poisson ratio ν is kept constant. According to this model, Young's modulus can be expressed in terms of a power law as:

$$E = M\ p_a \left(\left(\frac{I_1}{p_a}\right)^2 + \left(6\frac{1+\nu}{1-2\nu}\right)\frac{J_{2D}}{p_a^2}\right)^{\lambda} \tag{104.174}$$

where $I_1 = \sigma_{ii}$ is the first invariant of the stress tensor and $J_{2D} = (s_{ij}s_{ij})/2$ is the second invariant of the deviatoric stress tensor $s_{ij} = \sigma_{ij} - \sigma_{kk}\delta_{ij}/3$. The parameter p_a is atmospheric pressure expressed in the same unit as E, I_1 and $\sqrt{J_{2D}}$ and the modulus number M and the exponent λ are constant, dimensionless numbers.

104.6.1.5 Cross Anisotropic Linear Elastic Model

104.6.2 Yield Functions

The typical plastic behavior of frictional materials is influenced by both normal and shear stresses. It is usually assumed that there exists a yield surface F in the stress space that encompasses the elastic region. States of stress inside the yield surface are assumed to be elastic (linear or non–linear). Stress

states on the surface are assumed to produce plastic deformations. Yield surfaces for geomaterials are usually shaped as asymmetric tar drops with smoothly rounded triangular cross sections. In addition to that, simpler yield surfaces, based on the Drucker–Prager cone or Mohr–Coulomb hexagon can also be successfully used if matched with appropriate hardening laws. Yield surface shown in Figure 104.6 Lade (1988b) represent typical meridian plane trace for an isotropic granular material. Line BC represents stress path for conventional triaxial compression test. Figure 104.7 represents the view of the yield

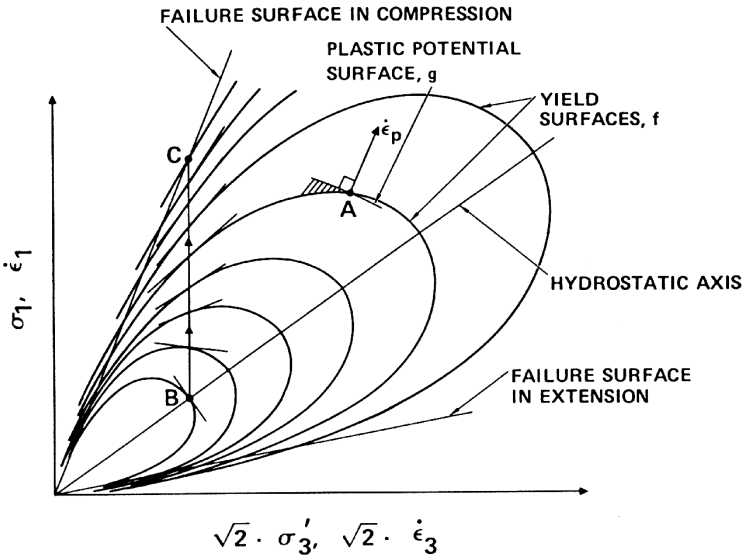

Figure 104.6: Yield surface patterns in the meridian plane for isotropic granular materials (from Lade (1988b))

surface traces in the deviatoric plane.

104.6.3 Plastic Flow Directions

Plastic flow directions are traditionally derived from a potential surface which to some extent reassembles the yield surface. Potential surfaces for metals are the same as their yield surfaces but experimental evidence suggests that it is not the case for geomaterials. The non–associated flow rules, used in geomechanics, rely on the potential surface, which is different from the yield surface, to provide the plastic flow directions. It should be noted that the potential surface is used for convenience and there is no physical reason to assume that the plastic strain rates are related to a potential surface Q (Vardoulakis and Sulem, 1995). Instead of defining a plastic potential, one may assume that the plastic flow direction is derived from an tensor function which does not have to possess a potential function.

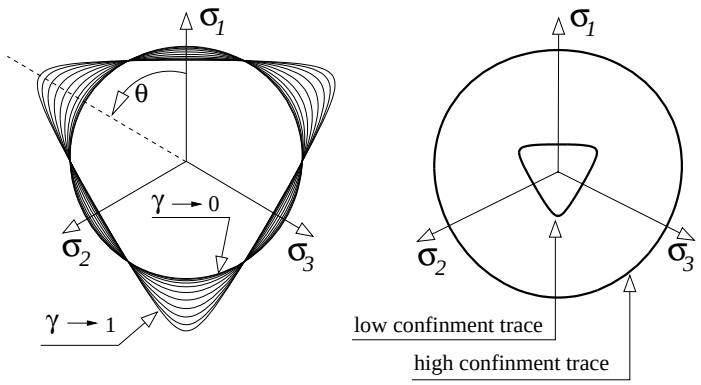

Figure 104.7: Deviatoric trace of typical yield surface for pressure sensitive materials.

104.6.4 Hardening–Softening Evolution Laws

The change in size and/or shape of the yield and potential surfaces is controlled by the hardening–softening evolution laws. Physically, these laws control the hardening and/or softening process during loading. Depending on the evolution type they control, these laws can be in general separated into isotropic and kinematic (also called anisotropic). The isotropic evolution laws control the size of the yield surface through a single scalar variable. This is usually related to the Coulomb friction or to the mean stress values at isotropic yielding. The non–isotropic evolution laws can be further specialized to rotational, translational kinematic and distortional. It should be noted that all of the kinematic evolution laws can be treated as special case of the general, distortional laws (Baltov and Sawczuk, 1965). Figure 104.8 depicts various types of evolution laws (for the control of hardening–softening) in the meridian

plane[61].

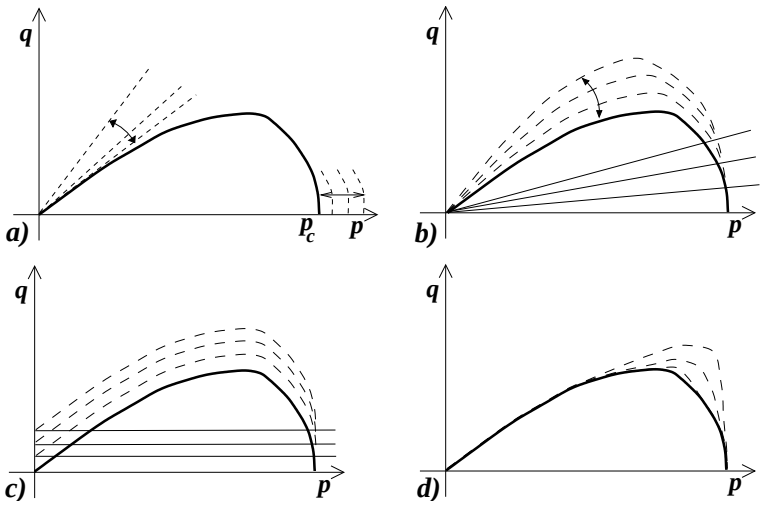

Figure 104.8: Various types of evolution laws that control hardening and/or softening of elastic–plastic material models: (a) Isotropic (scalar) controlling equivalent friction angle and isotropic yield stress. (b) Rotational kinematic hardening (second order tensor) controlling pivoting around fixed point (usually stress origin) of the yield surface. (c) Translational kinematic hardening (second order tensor) controlling translation of the yield surface. (d) Distortional (fourth order tensor) controlling the shape of the yield surface.

104.6.5 Tresca Model

The first yield criteria in the metal plasticity is Tresca yield criteria. Tresca yield criteria states that when the maximum shear stress or, the half difference of the maximum and minimum principal stresses, reaches the shear strength, τ_s, the material will begin yielding. It is can be expressed by the yield function

$$f = |\tau_{max}| - \tau_s = \frac{1}{2}|\sigma_1 - \sigma_3| - \tau_s = 0 \tag{104.175}$$

Tresca yield surface in the principal stress space is a regular hexagonal cylinder. It is implied that the intermediate principal stress plays no role in the yielding for Tresca yield criteria.

104.6.6 von Mises Model

DSL COMMANDS for the von Mises material models are given in section 205.3 on page 827.

[61] The meridian plane is chosen just for illustration purposes, similar sketch can be produced in deviatoric plane as well.

Experimental data showed that for most metals, von Mises yield criteria is more accurate than Tresca criteria. von Mises yield function can be expressed by

$$f = 3J_2 - k^2 = 0 \tag{104.176}$$

or if extended to include the kinematic hardening,

$$f = \frac{3}{2}(s_{ij} - \alpha_{ij})(s_{ij} - \alpha_{ij}) - k^2 = 0 \tag{104.177}$$

where k is the scalar internal variable; its initial value is the uniaxial tension strength. α_{ij} is the tensor internal variable called the back stress. Similar to s_{ij}, α_{ij} is also a deviatoric symmetric tensor.

Although von Mises model is mainly for the metal plasticity analysis, for undrained analysis in geomechanics, von Mises model can be approximately used to simulate the undrained behaviors, (Yang and Jeremić, 2002), (Yang and Jeremić, 2003).

The stress derivative of the yield function is

$$\frac{\partial f}{\partial \sigma_{ij}} = 3(s_{ij} - \alpha_{ij}) \tag{104.178}$$

From Equation 104.178, it is easily to derive that

$$\frac{\partial f}{\partial \alpha_{ij}} = -3(s_{ij} - \alpha_{ij}) \tag{104.179}$$

and

$$\frac{\partial f}{\partial k} = -2k \tag{104.180}$$

If the associated plastic flow rule $g = f$ is assumed, then

$$m_{ij} = \frac{\partial g}{\partial \sigma_{ij}} = 3(s_{ij} - \alpha_{ij}) \tag{104.181}$$

$$\frac{\partial m_{ij}}{\partial \sigma_{mn}} = 3I^s_{ijmn} - \delta_{ij}\delta_{mn} \tag{104.182}$$

$$\frac{\partial m_{ij}}{\partial \alpha_{mn}} = -3I^s_{ijmn} \tag{104.183}$$

where I^s_{ijmn} is the symmetric unit rank-4 tensor.

It is interesting that from the Equation 104.181, von Mises model gives

$$\dot{\epsilon}^p_v = \dot{\epsilon}^p_{ii} = \dot{\lambda} m_{ii} = 3\dot{\lambda}(s_{ii} - \alpha_{ii}) = 0 \tag{104.184}$$

which accords with the phenomena that no plastic volumetric strain occurs for metals. It is implied that the isotropic stress (hydrostatic pressure) can never make the metal yield for this yield criteria. von Mises model is therefore pressure-independent.

If k is assumed a linear relation to the equivalent plastic strain ϵ^p_q, or by the equation

$$\dot{k} = H_s \dot{\epsilon}^p_{eq} = \dot{\lambda} H_s \left(\frac{2}{3} m^{dev}_{ij} m^{dev}_{ij} \right)^{0.5} \tag{104.185}$$

where H_s is the linear hardening/softening modulus to the equivalent plastic strain, the corresponding h_A is then

$$h = H_s \left(\frac{2}{3} m^{dev}_{ij} m^{dev}_{ij} \right)^{0.5} \tag{104.186}$$

where m^{dev}_{ij} is the 'deviatoric' plastic flow, and if it is associated plasticity,

$$h = 2 H_s k \tag{104.187}$$

If α_{ij} is assumed a linear relation to the plastic strain tensor ϵ^p_{ij}, or by the equation

$$\dot{\alpha}_{ij} = H_t \dot{\epsilon}^p_{ij} = \dot{\lambda} H_t m_{ij} \tag{104.188}$$

if it is associated plasticity,

$$\dot{\alpha}_{ij} = 3 \dot{\lambda} H_t (s_{ij} - \alpha_{ij}) \tag{104.189}$$

where H_t is the linear hardening/softening modulus to plastic strain tensor, the corresponding h_A is then

$$h_{ij} = H_t m_{ij} \tag{104.190}$$

if it is associated plasticity,

$$h_{ij} = 3 H_t (s_{ij} - \alpha_{ij}) \tag{104.191}$$

A saturation-type kinematic hardening rule is the Armstrong-Frederick hardening (Armstrong and Frederick, 1966),

$$\dot{\alpha}_{ij} = \frac{2}{3} h_a \dot{\epsilon}^p_{ij} - c_r \dot{\epsilon}^p_{eq} \alpha_{ij} \tag{104.192}$$

if it is associated plasticity,

$$\dot{\alpha}_{ij} = \dot{\lambda} [h_a (s_{ij} - \alpha_{ij}) - 2 c_r k \alpha_{ij}] \tag{104.193}$$

where h_a and c_r are material constants. The corresponding h_A is then

$$h_{ij} = \frac{2}{3} h_a m_{ij} - c_r m_{eq} \alpha_{ij} \tag{104.194}$$

where m_{eq} is the 'equivalent' plastic flow, and if it is associated plasticity,

$$h_{ij} = 2 h_a s_{ij} - 2 (h_a + c_r k) \alpha_{ij} \tag{104.195}$$

104.6.6.1 Yield and Plastic Potential Functions: von Mises Model (form I)

Yield function and related derivatives

$$f = \frac{3}{2}\left[\left(s_{ij} - \alpha_{ij}\right)\left(s_{ij} - \alpha_{ij}\right)\right] - k^2 = 0 \tag{104.196}$$

$$\begin{aligned}\frac{\partial f}{\partial \sigma_{ij}} &= 3\frac{\partial s_{kl}}{\partial \sigma_{ij}}\left(s_{kl} - \alpha_{kl}\right) \\ &= 3\left(\delta_{ki}\delta_{lj} - \frac{1}{3}\delta_{kl}\delta_{ij}\right)\left(s_{kl} - \alpha_{kl}\right) \\ &= 3\left(s_{ij} - \alpha_{ij}\right)\end{aligned} \tag{104.197}$$

$$\begin{aligned}\frac{\partial f}{\partial \alpha_{ij}} &= -3\frac{\partial \alpha_{kl}}{\partial \alpha_{ij}}\left(s_{kl} - \alpha_{kl}\right) \\ &= -3\delta_{ki}\delta_{lj}\left(s_{kl} - \alpha_{kl}\right) \\ &= -3\left(s_{ij} - \alpha_{ij}\right)\end{aligned} \tag{104.198}$$

$$\frac{\partial f}{\partial k} = -2k \tag{104.199}$$

Plastic flow (associated plasticity) and related derivatives

$$m_{ij} = \frac{\partial f}{\partial \sigma_{ij}} = 3\left(s_{ij} - \alpha_{ij}\right) \tag{104.200}$$

$$\frac{\partial m_{ij}}{\partial \sigma_{mn}} = 3\delta_{im}\delta_{jn} - \delta_{ij}\delta_{mn} \tag{104.201}$$

$$\frac{\partial m_{ij}}{\partial k} = 0 \tag{104.202}$$

$$\frac{\partial m_{ij}}{\partial \alpha_{mn}} = -3\delta_{im}\delta_{jn} \tag{104.203}$$

104.6.6.2 Yield and Plastic Potential Functions: von Mises Model (form II)

Yield function and related derivatives

$$f = \left[\left(s_{ij} - \alpha_{ij}\right)\left(s_{ij} - \alpha_{ij}\right)\right]^{0.5} - \sqrt{\frac{2}{3}}k = 0 \tag{104.204}$$

$$\begin{aligned}\frac{\partial f}{\partial \sigma_{ij}} &= \frac{\partial s_{kl}}{\partial \sigma_{ij}}\left(s_{kl} - \alpha_{kl}\right)\left[\left(s_{mn} - \alpha_{mn}\right)\left(s_{mn} - \alpha_{mn}\right)\right]^{-0.5} \\ &= \left(\delta_{ki}\delta_{lj} - \frac{1}{3}\delta_{kl}\delta_{ij}\right)\left(s_{kl} - \alpha_{kl}\right)\left[\left(s_{mn} - \alpha_{mn}\right)\left(s_{mn} - \alpha_{mn}\right)\right]^{-0.5} \\ &= \left(s_{ij} - \alpha_{ij}\right)\left[\left(s_{mn} - \alpha_{mn}\right)\left(s_{mn} - \alpha_{mn}\right)\right]^{-0.5}\end{aligned} \tag{104.205}$$

$$\frac{\partial f}{\partial \alpha_{ij}} = -\left(s_{ij} - \alpha_{ij}\right)\left[\left(s_{mn} - \alpha_{mn}\right)\left(s_{mn} - \alpha_{mn}\right)\right]^{-0.5} \tag{104.206}$$

$$\frac{\partial f}{\partial k} = -\sqrt{\frac{2}{3}} \tag{104.207}$$

Plastic flow (associated plasticity) and related derivatives

$$m_{ij} = \frac{\partial f}{\partial \sigma_{ij}} = \left(s_{ij} - \alpha_{ij}\right)\left[\left(s_{mn} - \alpha_{mn}\right)\left(s_{mn} - \alpha_{mn}\right)\right]^{-0.5} \tag{104.208}$$

$$\frac{\partial m_{ij}}{\partial \sigma_{mn}} = \left(\delta_{im}\delta_{jn} - \frac{1}{3}\delta_{ij}\delta_{mn}\right)\left[\left(s_{rs} - \alpha_{rs}\right)\left(s_{rs} - \alpha_{rs}\right)\right]^{-0.5} - \left(s_{ij} - \alpha_{ij}\right)\left(s_{mn} - \alpha_{mn}\right)\left[\left(s_{rs} - \alpha_{rs}\right)\left(s_{rs} - \alpha_{rs}\right)\right]^{-1.5} \tag{104.209}$$

$$\frac{\partial m_{ij}}{\partial k} = 0 \tag{104.210}$$

$$\frac{\partial m_{ij}}{\partial \alpha_{mn}} = -\delta_{im}\delta_{jn}\left[\left(s_{rs} - \alpha_{rs}\right)\left(s_{rs} - \alpha_{rs}\right)\right]^{-0.5} + \left(s_{ij} - \alpha_{ij}\right)\left(s_{mn} - \alpha_{mn}\right)\left[\left(s_{rs} - \alpha_{rs}\right)\left(s_{rs} - \alpha_{rs}\right)\right]^{-1.5} \tag{104.211}$$

104.6.6.3 Hardening and Softening Functions: von Mises Model

Linear isotropic hardening and related derivatives

$$\bar{k} = Hm^{equivalent} = H\left(\frac{2}{3}m_{ij}m_{ij}\right)^{0.5} \tag{104.212}$$

$$\frac{\partial \bar{k}}{\partial \sigma_{ij}} = \frac{2}{3}Hm_{pq}\frac{\partial m_{pq}}{\partial \sigma_{ij}}\left(\frac{2}{3}m_{mn}m_{mn}\right)^{-0.5} \tag{104.213}$$

$$\frac{\partial \bar{k}}{\partial k} = \frac{2}{3}Hm_{pq}\frac{\partial m_{pq}}{\partial k}\left(\frac{2}{3}m_{mn}m_{mn}\right)^{-0.5} \tag{104.214}$$

$$\frac{\partial \bar{k}}{\partial \alpha_{ij}} = \frac{2}{3}Hm_{pq}\frac{\partial m_{pq}}{\partial \alpha_{ij}}\left(\frac{2}{3}m_{mn}m_{mn}\right)^{-0.5} \tag{104.215}$$

Linear kinematic hardening and related derivatives

$$\bar{\alpha}_{ij} = Hm_{ij}^{dev} = H\left(m_{ij} - \frac{1}{3}m_{kl}\delta_{kl}\delta_{ij}\right) \tag{104.216}$$

$$\frac{\partial \bar{\alpha}_{ij}}{\partial \sigma_{mn}} = H\left(\frac{\partial m_{ij}}{\partial \sigma_{mn}} - \frac{1}{3}\frac{\partial m_{kl}}{\partial \sigma_{mn}}\delta_{kl}\delta_{ij}\right) \tag{104.217}$$

$$\frac{\partial \bar{\alpha}_{ij}}{\partial k} = H\left(\frac{\partial m_{ij}}{\partial k} - \frac{1}{3}\frac{\partial m_{kl}}{\partial k}\delta_{kl}\delta_{ij}\right) \tag{104.218}$$

$$\frac{\partial \bar{\alpha}_{ij}}{\partial \alpha_{mn}} = H\left(\frac{\partial m_{ij}}{\partial \alpha_{mn}} - \frac{1}{3}\frac{\partial m_{kl}}{\partial \alpha_{mn}}\delta_{kl}\delta_{ij}\right) \tag{104.219}$$

Armstrong-Frederick kinematic hardening for von Mises

$$\bar{\alpha}_{ij} = \frac{2}{3}h_a m_{ij}^{dev} - c_r\left(\frac{2}{3}m_{rs}^{dev}m_{rs}^{dev}\right)^{0.5}\alpha_{ij} \tag{104.220}$$

The unit of parameter h_a is Pascal. The parameter c_r is unitless. The unit of α_{ij} is Pascal.

The deviatoric component of m is employed because the backstress α_{ij} is the center of yield surface in the deviatoric stress space.

When the derivative of backstress $\bar{\alpha}_{ij} = 0$, the tensor α_{ij} reaches the tensor limit.

$$\alpha_{ij}^{lim} = \sqrt{\frac{2}{3}}\frac{h_a}{c_r}\frac{m_{ij}^{dev}}{\sqrt{m_{rs}^{dev}m_{rs}^{dev}}} \tag{104.221}$$

Some useful tensor derivatives for von Mises $\bar{\alpha}$.

$$m_{ij}^{dev} = m_{ij} - \frac{1}{3}m_{kl}\delta_{kl}\delta_{ij} \tag{104.222}$$

- Useful tensor derivatives for von Mises $\bar{\alpha}$ with respect to σ.

$$\frac{\partial\bar{\alpha}_{ij}}{\partial\sigma_{mn}} = \frac{2}{3}h_a\frac{\partial m_{ij}^{dev}}{\partial\sigma_{mn}} - \frac{2}{3}c_r m_{rs}^{dev}\frac{\partial m_{rs}^{dev}}{\partial\sigma_{mn}}\left(\frac{2}{3}m_{kl}^{dev}m_{kl}^{dev}\right)^{-0.5}\alpha_{ij} \tag{104.223}$$

where

$$\frac{\partial m_{ij}^{dev}}{\partial\sigma_{mn}} = \frac{\partial m_{ij}}{\partial\sigma_{mn}} - \frac{1}{3}\frac{\partial m_{ot}}{\partial\sigma_{mn}}\delta_{ot}\delta_{ij} \tag{104.224}$$

- Useful tensor derivatives for von Mises $\bar{\alpha}$ with respect to α.

$$\frac{\partial\bar{\alpha}_{ij}}{\partial\alpha_{mn}} = \frac{2}{3}h_a\frac{\partial m_{ij}^{dev}}{\partial\alpha_{mn}} - \frac{2}{3}c_r m_{rs}^{dev}\frac{\partial m_{rs}^{dev}}{\partial\alpha_{mn}}\left(\frac{2}{3}m_{kl}^{dev}m_{kl}^{dev}\right)^{-0.5}\alpha_{ij} - c_r\left(\frac{2}{3}m_{pq}^{dev}m_{pq}^{dev}\right)^{0.5}\delta_{im}\delta_{jn} \tag{104.225}$$

where

$$\frac{\partial m_{ij}^{dev}}{\partial\alpha_{mn}} = \frac{\partial m_{ij}}{\partial\alpha_{mn}} - \frac{1}{3}\frac{\partial m_{ot}}{\partial\alpha_{mn}}\delta_{ot}\delta_{ij} \tag{104.226}$$

- Useful tensor derivatives for von Mises $\bar{\alpha}$ with respect to k.

$$\frac{\partial\bar{\alpha}_{ij}}{\partial k} = \frac{2}{3}h_a\frac{\partial m_{ij}^{dev}}{\partial k} - \sqrt{\frac{2}{3}}c_r\alpha_{ij}(m_{rs}^{dev}m_{rs}^{dev})^{-0.5}\frac{\partial m_{pq}^{dev}}{\partial k}m_{pq}^{dev} \tag{104.227}$$

where

$$\frac{\partial m_{ij}^{dev}}{\partial k} = \frac{\partial m_{ij}}{\partial k} - \frac{1}{3}\frac{\partial m_{ot}}{\partial k}\delta_{ot}\delta_{ij} \tag{104.228}$$

104.6.7 Drucker-Prager Model

DSL COMMANDS for the Drucker Prager material models are given in section 205.3 on page 827.

Drucker and Prager (1952) proposed a right circle cone to match with the Mohr-Coulomb irregular hexagonal pyramid, which can be expressed by

$$f = \alpha I_1 + \sqrt{J_2} - \beta = 0 \tag{104.229}$$

or if considering the kinematic hardening,

$$f = \alpha I_1 + [\frac{1}{2}(s_{ij} - p\alpha_{ij})(s_{ij} - p\alpha_{ij})]^{\frac{1}{2}} - \beta = 0 \tag{104.230}$$

where α and β are material constants.

By coinciding Drucker-Prager cone with the outer apexes of the Mohr-Coulomb hexagon locus, we get the compressive cone of Drucker-Prager model, with the constants as

$$\alpha = \frac{2\sin\phi}{\sqrt{3}(3-\sin\phi)}, \quad \beta = \frac{6\cos\phi}{\sqrt{3}(3-\sin\phi)}c \tag{104.231}$$

By coinciding Drucker-Prager cone with the inner apexes of the Mohr-Coulomb hexagon locus, we get the tensile cone of Drucker-Prager model, with the constants as

$$\alpha = \frac{2\sin\phi}{\sqrt{3}(3+\sin\phi)}, \quad \beta = \frac{6\cos\phi}{\sqrt{3}(3+\sin\phi)}c \tag{104.232}$$

We can also get the mean cone of the compressive and tensile cone, with the constants as

$$\alpha = \frac{\sqrt{3}\sin\phi}{9-\sin^2\phi}, \quad \beta = \frac{2\sqrt{3}\cos\phi}{9-\sin^2\phi}c \tag{104.233}$$

Another inner-tangent cone to the the Mohr-Coulomb pyramid, with the constants as

$$\alpha = \frac{\tan\phi}{\sqrt{9+12\tan^2\phi}}, \quad \beta = \frac{3c}{\sqrt{9+12\tan^2\phi}} \tag{104.234}$$

Obviously, in practice α and β are not directly obtained from experiments. They are functions of Mohr-Coulomb parameters, the cohesion c and the friction angle ϕ, which can be determined by experiments. The shape of Drucker-Prager yield surface has different types. They only partially satisfy the above requirements for locus in the π plane: they do not coincide with both compressive and tensile experimental points.

A useful formulation on Equation 104.229 is

$$\frac{\partial f}{\partial \sigma_{ij}} = \alpha\delta_{ij} + \frac{s_{ij}}{2\sqrt{J_2}} \tag{104.235}$$

For cohesionless sands, $k = 0$, Drucker-Prager yield function can thus be simplified as

$$f = \alpha I_1 + \sqrt{J_2} = 0 \tag{104.236}$$

or in terms of p and q,

$$f = q - Mp = 0 \tag{104.237}$$

If Equation 104.231 is adopted, then M can be easily derived as

$$M = \frac{6\sin\phi}{3-\sin\phi} \tag{104.238}$$

If the kinematic hardening is taken account, Equation 104.237 can be extended into

$$f = \frac{3}{2}[(s_{ij}-p\alpha_{ij})(s_{ij}-p\alpha_{ij})] - M^2p^2 = 0 \tag{104.239}$$

Useful formulations for this yield function are

$$\frac{\partial f}{\partial \sigma_{ij}} = 3\bar{s}_{ij} + \left(\bar{s}_{mn}\alpha_{mn} + \frac{2}{3}M^2 p\right)\delta_{ij} \tag{104.240}$$

$$\frac{\partial f}{\partial \alpha_{ij}} = -3p\bar{s}_{ij} \tag{104.241}$$

where $\bar{s}_{ij} = s_{ij} - p\alpha_{ij}$.

If the plastic flow is assumed associated, $g = f$, then

$$m_{ij} = \frac{\partial g}{\partial \sigma_{ij}} = 3\bar{s}_{ij} + \left(\bar{s}_{mn}\alpha_{mn} + \frac{2}{3}M^2 p\right)\delta_{ij} \tag{104.242}$$

the 'deviatoric' plastic flow is therefore

$$m_{eq} = 2Mp \tag{104.243}$$

104.6.7.1 Yield and Plastic Potential Functions: Drucker-Prager Model (form I)

Yield function and related derivatives

$$f = \frac{3}{2}\left[\left(s_{ij} - p\alpha_{ij}\right)\left(s_{ij} - p\alpha_{ij}\right)\right] - k^2p^2 = 0 \tag{104.244}$$

$$\begin{aligned}\frac{\partial f}{\partial \sigma_{ij}} &= \frac{3}{2}\left[2\frac{\partial s_{mn}}{\partial \sigma_{ij}}\left(s_{mn} - p\alpha_{mn}\right)\right] + \frac{3}{2}\left[-2\alpha_{mn}\frac{\partial p}{\partial \sigma_{ij}}\left(s_{mn} - p\alpha_{mn}\right)\right] - 2k^2p\frac{\partial p}{\partial \sigma_{ij}} \\ &= 3\left(\delta_{mi}\delta_{nj} - \frac{1}{3}\delta_{mn}\delta_{ij}\right)\left(s_{mn} - p\alpha_{mn}\right) + 3\left[\alpha_{mn}\frac{1}{3}\delta_{ij}\left(s_{mn} - p\alpha_{mn}\right)\right] + \frac{2}{3}k^2p\delta_{ij} \\ &= 3\left(s_{ij} - p\alpha_{ij}\right) + \alpha_{mn}\left(s_{mn} - p\alpha_{mn}\right)\delta_{ij} + \frac{2}{3}k^2p\delta_{ij}\end{aligned} \tag{104.245}$$

$$\frac{\partial f}{\partial \alpha_{ij}} = -3p\left(s_{ij} - p\alpha_{ij}\right) \tag{104.246}$$

$$\frac{\partial f}{\partial k} = -2kp^2 \tag{104.247}$$

Plastic flow (associated plasticity) and related derivatives

$$m_{ij} = \frac{\partial f}{\partial \sigma_{ij}} = 3\left(s_{ij} - p\alpha_{ij}\right) + \alpha_{rs}\left(s_{rs} - p\alpha_{rs}\right)\delta_{ij} + \frac{2}{3}k^2 p\delta_{ij} \tag{104.248}$$

$$\begin{aligned}\frac{\partial m_{ij}}{\partial \sigma_{mn}} &= 3\left(\left(\delta_{im}\delta_{jn} - \frac{1}{3}\delta_{ij}\delta_{mn}\right) - \frac{1}{3}\delta_{mn}\alpha_{ij}\right) + \alpha_{rs}\frac{\partial\left(s_{rs} - p\alpha_{rs}\right)}{\partial \sigma_{mn}}\delta_{ij} + \frac{2}{3}k^2\frac{\partial p}{\partial \sigma_{mn}}\delta_{ij} \\ &= 3\delta_{im}\delta_{jn} - \delta_{ij}\delta_{mn} - \delta_{mn}\alpha_{ij} + \alpha_{rs}\left(\delta_{rm}\delta_{sn} - \frac{1}{3}\delta_{rs}\delta_{mn} + \frac{1}{3}\delta_{mn}\alpha_{rs}\right)\delta_{ij} + \frac{2}{3}k^2\frac{\partial p}{\partial \sigma_{mn}}\delta_{ij} \\ &= 3\delta_{im}\delta_{jn} - \delta_{ij}\delta_{mn} - \delta_{mn}\alpha_{ij} + \alpha_{mn}\delta_{ij} + \frac{1}{3}\delta_{mn}\alpha_{rs}\alpha_{rs}\delta_{ij} - \frac{2}{9}k^2\delta_{mn}\delta_{ij} \\ &= 3\delta_{im}\delta_{jn} + \left(-1 + \frac{1}{3}\alpha_{rs}\alpha_{rs} - \frac{2}{9}k^2\right)\delta_{ij}\delta_{mn} - \delta_{mn}\alpha_{ij} + \alpha_{mn}\delta_{ij}\end{aligned} \tag{104.249}$$

$$\frac{\partial m_{ij}}{\partial k} = \frac{4}{3}kp\delta_{ij} \tag{104.250}$$

$$\begin{aligned}\frac{\partial m_{ij}}{\partial \alpha_{mn}} &= -3p\delta_{im}\delta_{jn} + \delta_{rm}\delta_{sn}\left(s_{rs} - p\alpha_{rs}\right)\delta_{ij} - \alpha_{rs}p\delta_{rm}\delta_{sn}\delta_{ij} \\ &= -3p\delta_{im}\delta_{jn} + \left(s_{mn} - p\alpha_{mn}\right)\delta_{ij} - \alpha_{mn}p\delta_{ij} \\ &= -3p\delta_{im}\delta_{jn} + s_{mn}\delta_{ij} - 2p\alpha_{mn}\delta_{ij}\end{aligned} \tag{104.251}$$

104.6.7.2 Yield and Plastic Potential Functions: Drucker-Prager Model (form II)

Yield function and related derivatives

$$f = \left[\left(s_{ij} - p\alpha_{ij}\right)\left(s_{ij} - p\alpha_{ij}\right)\right]^{0.5} - \sqrt{\frac{2}{3}}kp = 0 \tag{104.252}$$

$$\begin{aligned}\frac{\partial f}{\partial \sigma_{ij}} &= \left(\frac{\partial s_{mn}}{\partial \sigma_{ij}} - \alpha_{mn}\frac{\partial p}{\partial \sigma_{ij}}\right)\left(s_{mn} - p\alpha_{mn}\right)\left[\left(s_{rs} - p\alpha_{rs}\right)\left(s_{rs} - p\alpha_{rs}\right)\right]^{-0.5} - \sqrt{\frac{2}{3}}k\frac{\partial p}{\partial \sigma_{ij}} \\ &= \left(\delta_{mi}\delta_{nj} - \frac{1}{3}\delta_{mn}\delta_{ij} + \frac{1}{3}\alpha_{mn}\delta_{ij}\right)\left(s_{mn} - p\alpha_{mn}\right)\left[\left(s_{rs} - p\alpha_{rs}\right)\left(s_{rs} - p\alpha_{rs}\right)\right]^{-0.5} + \sqrt{\frac{2}{27}}k\delta_{ij} \\ &= \left[\left(s_{ij} - p\alpha_{ij}\right) + \frac{1}{3}\alpha_{mn}\delta_{ij}\left(s_{mn} - p\alpha_{mn}\right)\right]\left[\left(s_{rs} - p\alpha_{rs}\right)\left(s_{rs} - p\alpha_{rs}\right)\right]^{-0.5} + \sqrt{\frac{2}{27}}k\delta_{ij}\end{aligned} \tag{104.253}$$

$$\begin{aligned}\frac{\partial f}{\partial \alpha_{ij}} &= -p\delta_{mi}\delta_{nj}\left(s_{mn} - p\alpha_{mn}\right)\left[\left(s_{rs} - p\alpha_{rs}\right)\left(s_{rs} - p\alpha_{rs}\right)\right]^{-0.5} \\ &= -p\left(s_{ij} - p\alpha_{ij}\right)\left[\left(s_{rs} - p\alpha_{rs}\right)\left(s_{rs} - p\alpha_{rs}\right)\right]^{-0.5}\end{aligned} \tag{104.254}$$

$$\frac{\partial f}{\partial k} = -\sqrt{\frac{2}{3}}p \tag{104.255}$$

Plastic flow (associated plasticity) and related derivatives

$$m_{ij} = \frac{\partial f}{\partial \sigma_{ij}} = \left[\left(s_{ij} - p\alpha_{ij}\right) + \frac{1}{3}\alpha_{pq}\delta_{ij}\left(s_{pq} - p\alpha_{pq}\right) \right] \left[\left(s_{rs} - p\alpha_{rs}\right)\left(s_{rs} - p\alpha_{rs}\right) \right]^{-0.5} + \sqrt{\frac{2}{27}} k \delta_{ij} \quad (104.256)$$

$$\begin{aligned} \frac{\partial m_{ij}}{\partial \sigma_{mn}} = & \left[\left(\delta_{mi}\delta_{nj} - \frac{1}{3}\delta_{mn}\delta_{ij} + \frac{1}{3}\delta_{mn}\alpha_{ij} \right) + \frac{1}{3}\alpha_{pq}\delta_{ij}\left(\delta_{mp}\delta_{nq} - \frac{1}{3}\delta_{mn}\delta_{pq} + \frac{1}{3}\delta_{mn}\alpha_{pq} \right) \right] \\ & \left[\left(s_{rs} - p\alpha_{rs}\right)\left(s_{rs} - p\alpha_{rs}\right) \right]^{-0.5} \\ - & \left[\left(s_{ij} - p\alpha_{ij}\right) + \frac{1}{3}\alpha_{pq}\delta_{ij}\left(s_{pq} - p\alpha_{pq}\right) \right] \left(\delta_{mr}\delta_{ns} - \frac{1}{3}\delta_{mn}\delta_{rs} + \frac{1}{3}\delta_{mn}\alpha_{rs} \right) \\ & \left(s_{rs} - p\alpha_{rs}\right) \left[\left(s_{tu} - p\alpha_{tu}\right)\left(s_{tu} - p\alpha_{tu}\right) \right]^{-1.5} \end{aligned} \quad (104.257)$$

$$\frac{\partial m_{ij}}{\partial k} = \sqrt{\frac{2}{27}}\delta_{ij} \quad (104.258)$$

$$\begin{aligned} \frac{\partial m_{ij}}{\partial \alpha_{mn}} = & \left[-p\delta_{mi}\delta_{nj} + \frac{1}{3}\delta_{mp}\delta_{nq}\delta_{ij}\left(s_{pq} - p\alpha_{pq}\right) - \frac{1}{3}p\alpha_{pq}\delta_{ij}\delta_{mp}\delta_{nq} \right] \left[\left(s_{rs} - p\alpha_{rs}\right)\left(s_{rs} - p\alpha_{rs}\right) \right]^{-0.5} \\ & - \left[\left(s_{ij} - p\alpha_{ij}\right) + \frac{1}{3}\alpha_{pq}\delta_{ij}\left(s_{pq} - p\alpha_{pq}\right) \right] \left[-p\delta_{rm}\delta_{sn}\left(s_{rs} - p\alpha_{rs}\right) \right] \left[\left(s_{tu} - p\alpha_{tu}\right)\left(s_{tu} - p\alpha_{tu}\right) \right]^{-1.5} \end{aligned} \quad (104.259)$$

Plastic flow (non-associated plasticity) and related derivatives

$$m_{ij} = \left(\frac{\partial f}{\partial \sigma_{ij}} \right)^{dev} - \frac{1}{3}D\delta_{ij} = \left(s_{ij} - p\alpha_{ij}\right) \left[\left(s_{rs} - p\alpha_{rs}\right)\left(s_{rs} - p\alpha_{rs}\right) \right]^{-0.5} - \frac{1}{3}D\delta_{ij} \quad (104.260)$$

where

$$D = \xi \left(\sqrt{\frac{2}{3}} k_d - \frac{\sqrt{s_{mn}s_{mn}}}{p} \right) \quad (104.261)$$

$$\frac{\partial D}{\partial \sigma_{mn}} = -p^{-1}s_{mn}(s_{kl}s_{kl})^{-0.5} - \frac{1}{3}p^{-2}\delta_{mn}(s_{ot}s_{ot})^{0.5} \quad (104.262)$$

Therefore,

$$\begin{aligned} \frac{\partial m_{ij}}{\partial \sigma_{mn}} = & \left(\delta_{mi}\delta_{nj} - \frac{1}{3}\delta_{mn}\delta_{ij} + \frac{1}{3}\delta_{mn}\alpha_{ij} \right) \left[\left(s_{rs} - p\alpha_{rs}\right)\left(s_{rs} - p\alpha_{rs}\right) \right]^{-0.5} \\ & - \left(s_{ij} - p\alpha_{ij}\right) \left(\delta_{mr}\delta_{ns} - \frac{1}{3}\delta_{mn}\delta_{rs} + \frac{1}{3}\delta_{mn}\alpha_{rs} \right) \\ & \left(s_{rs} - p\alpha_{rs}\right) \left[\left(s_{tu} - p\alpha_{tu}\right)\left(s_{tu} - p\alpha_{tu}\right) \right]^{-1.5} \\ & + \frac{1}{3}\delta_{ij}s_{mn}p^{-1}(s_{kl}s_{kl})^{-0.5} + \frac{1}{9}\delta_{ij}\delta_{mn}p^{-2}(s_{ot}s_{ot})^{0.5} \end{aligned} \quad (104.263)$$

$$\frac{\partial m_{ij}}{\partial k} = 0 \tag{104.264}$$

$$\begin{aligned}\frac{\partial m_{ij}}{\partial \alpha_{mn}} &= -p\delta_{mi}\delta_{nj}\left[(s_{rs}-p\alpha_{rs})\,(s_{rs}-p\alpha_{rs})\right]^{-0.5} \\ &\quad -\left(s_{ij}-p\alpha_{ij}\right)\left[-p\delta_{rm}\delta_{sn}\,(s_{rs}-p\alpha_{rs})\right]\left[(s_{tu}-p\alpha_{tu})\,(s_{tu}-p\alpha_{tu})\right]^{-1.5}\end{aligned} \tag{104.265}$$

104.6.7.3 Hardening and Softening Functions: Drucker-Prager Model

Note that the linear isotropic and linear kinematic hardening equations for Drucker-Prager model are the same as the ones for von Mises model. Here they are shown again for completeness.

Linear isotropic hardening and related derivatives

$$\bar{k} = Hm^{equivalent} = H\left(\frac{2}{3}m_{ij}m_{ij}\right)^{0.5} \tag{104.266}$$

$$\frac{\partial \bar{k}}{\partial \sigma_{ij}} = \frac{2}{3}Hm_{pq}\frac{\partial m_{pq}}{\partial \sigma_{ij}}\left(\frac{2}{3}m_{mn}m_{mn}\right)^{-0.5} \tag{104.267}$$

$$\frac{\partial \bar{k}}{\partial k} = \frac{2}{3}Hm_{pq}\frac{\partial m_{pq}}{\partial k}\left(\frac{2}{3}m_{mn}m_{mn}\right)^{-0.5} \tag{104.268}$$

$$\frac{\partial \bar{k}}{\partial \alpha_{ij}} = \frac{2}{3}Hm_{pq}\frac{\partial m_{pq}}{\partial \alpha_{ij}}\left(\frac{2}{3}m_{mn}m_{mn}\right)^{-0.5} \tag{104.269}$$

Linear kinematic hardening and related derivatives

$$\bar{\alpha}_{ij} = Hm_{ij}^{dev} = H\left(m_{ij} - \frac{1}{3}m_{kl}\delta_{kl}\delta_{ij}\right) \tag{104.270}$$

$$\frac{\partial \bar{\alpha}_{ij}}{\partial \sigma_{mn}} = H\left(\frac{\partial m_{ij}}{\partial \sigma_{mn}} - \frac{1}{3}\frac{\partial m_{kl}}{\partial \sigma_{mn}}\delta_{kl}\delta_{ij}\right) \tag{104.271}$$

$$\frac{\partial \bar{\alpha}_{ij}}{\partial k} = H\left(\frac{\partial m_{ij}}{\partial k} - \frac{1}{3}\frac{\partial m_{kl}}{\partial k}\delta_{kl}\delta_{ij}\right) \tag{104.272}$$

$$\frac{\partial \bar{\alpha}_{ij}}{\partial \alpha_{mn}} = H\left(\frac{\partial m_{ij}}{\partial \alpha_{mn}} - \frac{1}{3}\frac{\partial m_{kl}}{\partial \alpha_{mn}}\delta_{kl}\delta_{ij}\right) \tag{104.273}$$

Armstrong-Frederick Kinematic Hardening for Drucker-Prager

$$\bar{\alpha}_{ij} = \frac{2}{3}\frac{h_a}{p} m_{ij}^{dev} - c_r \left(\frac{2}{3} m_{rs}^{dev} m_{rs}^{dev}\right)^{0.5} \alpha_{ij} \tag{104.274}$$

where p is pressure of the current stress state. The unit of parameter h_a is Pascal. The parameter c_r is unitless. The α_{ij} in Drucker-Prager is unitless.

The pressure p is introduced for two reasons.

- The center of the yield surface is $p\alpha_{ij}$, not α_{ij}. The kinematic hardening rule is to control the center of the yield surface.
- The unit in equation (104.303) matches after the pressure p is introduced.

When the derivative of backstress $\bar{\alpha}_{ij} = 0$, the tensor α_{ij} reaches the tensor limit.

$$\alpha_{ij}^{lim} = \sqrt{\frac{2}{3}}\frac{h_a}{pc_r}\frac{m_{ij}^{dev}}{\sqrt{m_{rs}^{dev} m_{rs}^{dev}}} \tag{104.275}$$

Some useful tensor derivatives for Drucker-Prager $\bar{\alpha}$.

$$m_{ij}^{dev} = m_{ij} - \frac{1}{3} m_{kl}\delta_{kl}\delta_{ij} \tag{104.276}$$

- Useful tensor derivatives for Drucker-Prager $\bar{\alpha}$ with respect to σ.

$$\frac{\partial \bar{\alpha}_{ij}}{\partial \sigma_{mn}} = \frac{2}{3}\frac{h_a}{p}\frac{\partial m_{ij}^{dev}}{\partial \sigma_{mn}} + \frac{2}{9p^2} h_a m_{ij}^{dev}\delta_{mn} - \frac{2}{3} c_r m_{rs}^{dev}\frac{\partial m_{rs}^{dev}}{\partial \sigma_{mn}}\left(\frac{2}{3} m_{kl}^{dev} m_{kl}^{dev}\right)^{-0.5}\alpha_{ij} \tag{104.277}$$

where

$$\frac{\partial m_{ij}^{dev}}{\partial \sigma_{mn}} = \frac{\partial m_{ij}}{\partial \sigma_{mn}} - \frac{1}{3}\frac{\partial m_{ot}}{\partial \sigma_{mn}}\delta_{ot}\delta_{ij} \tag{104.278}$$

- Useful tensor derivatives for Drucker-Prager $\bar{\alpha}$ with respect to α.

$$\frac{\partial \bar{\alpha}_{ij}}{\partial \alpha_{mn}} = \frac{2}{3}\frac{h_a}{p}\frac{\partial m_{ij}^{dev}}{\partial \alpha_{mn}} - \frac{2}{3} c_r m_{rs}^{dev}\frac{\partial m_{rs}^{dev}}{\partial \alpha_{mn}}\left(\frac{2}{3} m_{kl}^{dev} m_{kl}^{dev}\right)^{-0.5}\alpha_{ij} - c_r\left(\frac{2}{3} m_{pq}^{dev} m_{pq}^{dev}\right)^{0.5}\delta_{im}\delta_{jn} \tag{104.279}$$

where

$$\frac{\partial m_{ij}^{dev}}{\partial \alpha_{mn}} = \frac{\partial m_{ij}}{\partial \alpha_{mn}} - \frac{1}{3}\frac{\partial m_{ot}}{\partial \alpha_{mn}}\delta_{ot}\delta_{ij} \tag{104.280}$$

- Useful tensor derivatives for Drucker-Prager $\bar{\alpha}$ with respect to k.

$$\frac{\partial \bar{\alpha}_{ij}}{\partial k} = \frac{2}{3}\frac{h_a}{p}\frac{\partial m_{ij}^{dev}}{\partial k} - \sqrt{\frac{2}{3}} c_r \alpha_{ij}(m_{rs}^{dev} m_{rs}^{dev})^{-0.5}\frac{\partial m_{pq}^{dev}}{\partial k} m_{pq}^{dev} \tag{104.281}$$

where

$$\frac{\partial m_{ij}^{dev}}{\partial k} = \frac{\partial m_{ij}}{\partial k} - \frac{1}{3}\frac{\partial m_{ot}}{\partial k}\delta_{ot}\delta_{ij} \tag{104.282}$$

104.6.7.4 Federico's Description of a Drucker–Prager Kinematic Hardenig Model

Presented is a concise description of nonlinear rotational kinematic hardening (Armstrong-Frederick) Drucker-Prager model (Lemaitre and Chaboche, 1990).

Elastic behavior The standard Hooke's law has been assumed for the sake of simplicity.

Yield function The yield locus is of the same kind described by Prevost (1985a) and Manzari and Dafalias (1997), i.e. conical and allowed to rotate around its apex (the centre of rotation coincides – for cohesionless materials – with the origin of the principal stress space):

$$f = \sqrt{\left(s_{ij} - p\alpha_{ij}\right)\left(s_{ij} - p\alpha_{ij}\right)} - \sqrt{\frac{2}{3}}kp = 0 \tag{104.283}$$

in which p is the isotropic mean pressure, α_{ij} the back–stress ratio tensor and k a constitutive surface parameter[62]. While this latter governs the opening angle of the cone, α_{ij} is a second–rank deviatoric tensor determining the yield locus rotation.

Plastic flow rule As usual, the incremental plastic strain tensor can be expressed as:

$$\epsilon^p_{ij} = \dot{\lambda} m_{ij} \tag{104.284}$$

where $\dot{\lambda}$ is a scalar plastic multiplier and m_{ij} assigning the direction of the plastic flow. While in the associated version of the model m_{ij} would coincide with the stress gradient of the yield function (104.283), here the following non–associated flow rule has been adopted (Prevost, 1985a; Manzari and Dafalias, 1997):

$$m_{ij} = \left(\frac{\partial f}{\partial \sigma_{ij}}\right)^{dev} - \frac{1}{3} D \delta_{ij} \tag{104.285}$$

where the superscript $^{\text{dev}}$ and δ_{ij} denote the "deviatoric" tensor operator and the Kronecker hydrostatic tensor, respectively, and D is a dilatancy coefficient defined as:

$$D = \xi \left(\sqrt{\frac{2}{3}} k_d - \sqrt{r_{mn} r_{mn}}\right) \tag{104.286}$$

Here, we defined normalized deviatoric stress tensor $r_{ij} = s_{ij}/p$.

[62] stresses are meant here to be effective

Apparently, the flow rule (104.285) implies the deviatoric plastic strain increment to be associated, while non-associativeness holds for the volumetric component. The definition (104.286) requires two consitutive parameters to be identified, namely k_d and ξ: the former represents the stress obliquity for the transition from contractive to dilative response; the latter quantitatively governs the volumetric plastic strain rate. Specifically, k_d denotes the existence of a "dilatancy surface", the soil response being contractive for inner stress states and dilative otherwise; this surface – characterized by no volumetric plastic strain – is still a Drucker–Prager conical locus, fixed in the principal stress space and with an opening angle given by k_d.

Armstrong–Frederick kinematic hardening rule The last ingredient in the model formulation is represented by the hardening rule for the internal variable α_{ij}. Here, an Armstrong–Frederick hardening (Armstrong and Frederick, 1966; Lemaitre and Chaboche, 1990) has been introduced:

$$\dot{\alpha}_{ij} = \frac{2}{3} h_a \left(\epsilon^p_{ij}\right)^{dev} - c_r \alpha_{ij} \sqrt{\frac{2}{3} \left(\epsilon^p_{rs}\right)^{dev} \left(\epsilon^p_{rs}\right)^{dev}} \tag{104.287}$$

where h_a and c_r are two hardening constitutive parameters. Equation (104.287) yields a saturation–type evolution under deviatoric plastic straining, up to the achievement of a limit back–stress ratio α^{lim}_{ij}. Starting from (104.287), it could be easily proven that:

$$\left\| \alpha^{lim}_{ij} \right\| = \sqrt{\frac{2}{3}} \frac{h_a}{c_r} \tag{104.288}$$

i.e. the norm of the limit tensor α^{lim}_{ij} exclusively depends on the h_a/c_r ratio for any value of the Lode angle. The existence of an outer bound for α_{ij} implies all feasible stress states to lie within a so–called bounding surface, determined both by α^{lim}_{ij} and the opening of the yield locus $f = 0$ (104.283). The bounding surface, governing the shear strength of the material, is in this case a Lode–angle insensitive Drucker–Prager cone: in the simplest case of triaxial loading, the limit stress obliquity M can be shown to equal:

$$M = \left(\frac{q}{p'}\right)_{failure} = k + \frac{h_a}{c_r} \tag{104.289}$$

both in compression and extension. From the above analytical relationships it can be inferred that the material shear strength is ruled by the ratio h_a/c_r, whereas c_r determines the evolution rate of the back–stress tensor α_{ij}.

104.6.7.5 Han's Description of Drucker–Prager Model with Armstrong–Frederick Kinematic Hardening

Presented is a new description of non-associated Drucker-Prager model with nonlinear Armstrong-Frederick kinematic hardening. Compared with the traditional description shown in earlier sections, the main difference in this description is taking into consideration of the symmetry nature of stress and strain tensors. As a result, some of the derivatives of plastic flow and internal variable are different. More importantly, this change leads to a consistent stiffness tensor that has minor symmetry.

Elastic Behavior The elastic behavior is modeled as linear elastic, following classic generalized Hook's law. The elastic stiffness tensor is that for isotropic, linear elastic material (Equation 104.163).

$$E_{ijkl} = \frac{E}{2\,(1+\nu)}\left(\frac{2\nu}{1-2\nu}\,\delta_{ij}\delta_{kl} + \delta_{ik}\delta_{jl} + \delta_{il}\delta_{jk}\right) \tag{104.290}$$

Yield Function The yield function and its derivatives remain unchanged.

$$f = \left[\left(s_{ij} - p\alpha_{ij}\right)\left(s_{ij} - p\alpha_{ij}\right)\right]^{0.5} - \sqrt{\frac{2}{3}}kp = 0 \tag{104.291}$$

$$\frac{\partial f}{\partial \sigma_{ij}} = \left[\left(s_{ij} - p\alpha_{ij}\right) + \frac{1}{3}\alpha_{mn}\delta_{ij}\left(s_{mn} - p\alpha_{mn}\right)\right]\left[\left(s_{rs} - p\alpha_{rs}\right)\left(s_{rs} - p\alpha_{rs}\right)\right]^{-0.5} + \sqrt{\frac{2}{27}}k\delta_{ij} \tag{104.292}$$

$$\frac{\partial f}{\partial \alpha_{ij}} = -p\left(s_{ij} - p\alpha_{ij}\right)\left[\left(s_{rs} - p\alpha_{rs}\right)\left(s_{rs} - p\alpha_{rs}\right)\right]^{-0.5} \tag{104.293}$$

$$\frac{\partial f}{\partial k} = -\sqrt{\frac{2}{3}}p \tag{104.294}$$

Plastic Flow The changes in derivatives of plastic flow, and later in hardening, comes from the clarification of derivative of the stress tensor with respect to itself. According to Park (2018), since the stress tensor is intrinsically symmetric, its derivative with respect to itself should be:

$$\frac{\partial \sigma_{ij}}{\partial \sigma_{mn}} = \frac{1}{2}\left(\delta_{im}\delta_{jn} + \delta_{in}\delta_{jm}\right) \tag{104.295}$$

Then, the derivative of deviatoric stress with respect to stress becomes:

$$\frac{\partial s_{ij}}{\partial \sigma_{mn}} = \frac{1}{2}\delta_{im}\delta_{jn} + \frac{1}{2}\delta_{in}\delta_{jm} - \frac{1}{3}\delta_{mn}\delta_{ij} \tag{104.296}$$

The non-associated plastic flow still has the same form:

$$m_{ij} = \left(\frac{\partial f}{\partial \sigma_{ij}}\right)^{dev} - \frac{1}{3}D\delta_{ij} = \left(s_{ij} - p\alpha_{ij}\right)\left[\left(s_{rs} - p\alpha_{rs}\right)\left(s_{rs} - p\alpha_{rs}\right)\right]^{-0.5} - \frac{1}{3}D\delta_{ij} \tag{104.297}$$

where

$$D = \xi \left(\sqrt{\frac{2}{3}} k_d - \frac{\sqrt{s_{mn} s_{mn}}}{p} \right) \tag{104.298}$$

and

$$\frac{\partial D}{\partial \sigma_{mn}} = -\xi \left[p^{-1} s_{mn} (s_{kl} s_{kl})^{-0.5} + \frac{1}{3} p^{-2} \delta_{mn} (s_{ot} s_{ot})^{0.5} \right] \tag{104.299}$$

Therefore,

$$\begin{aligned} \frac{\partial m_{ij}}{\partial \sigma_{mn}} = & \left(\frac{1}{2}\delta_{im}\delta_{jn} + \frac{1}{2}\delta_{in}\delta_{jm} - \frac{1}{3}\delta_{mn}\delta_{ij} + \frac{1}{3}\delta_{mn}\alpha_{ij} \right) \left[(s_{rs} - p\alpha_{rs})(s_{rs} - p\alpha_{rs}) \right]^{-0.5} \\ & - \left(s_{ij} - p\alpha_{ij} \right) \left[(s_{mn} - p\alpha_{mn}) + \frac{1}{3}\alpha_{rs} (s_{rs} - p\alpha_{rs}) \delta_{mn} \right] \left[(s_{tu} - p\alpha_{tu})(s_{tu} - p\alpha_{tu}) \right]^{-1.5} \\ & + \frac{1}{3}\xi \left[s_{mn} p^{-1} (s_{kl} s_{kl})^{-0.5} + \frac{1}{3}\delta_{mn} p^{-2} (s_{ot} s_{ot})^{0.5} \right] \delta_{ij} \end{aligned} \tag{104.300}$$

$$\frac{\partial m_{ij}}{\partial k} = 0 \tag{104.301}$$

$$\begin{aligned} \frac{\partial m_{ij}}{\partial \alpha_{mn}} = & -p \left(\frac{1}{2}\delta_{mi}\delta_{nj} + \frac{1}{2}\delta_{mj}\delta_{ni} \right) \left[(s_{rs} - p\alpha_{rs})(s_{rs} - p\alpha_{rs}) \right]^{-0.5} \\ & + p \left(s_{ij} - p\alpha_{ij} \right) (s_{mn} - p\alpha_{mn}) \left[(s_{tu} - p\alpha_{tu})(s_{tu} - p\alpha_{tu}) \right]^{-1.5} \end{aligned} \tag{104.302}$$

Armstrong-Frederick kinematic hardening for Drucker-Prager

$$\bar{\alpha}_{ij} = \frac{2}{3} \frac{h_a}{p_{atm}} m_{ij}^{dev} - c_r \left(\frac{2}{3} m_{rs}^{dev} m_{rs}^{dev} \right)^{0.5} \alpha_{ij} \tag{104.303}$$

where p_{atm} is the atmospheric pressure of 101.325 kPa. The unit of parameter h_a is Pascal. The parameter c_r is unitless. The α_{ij} in Drucker-Prager is unitless. The atmospheric pressure p_{atm} is introduced so that the unit in equation (104.303) matches.

Notice that

$$m_{rs}^{dev} m_{rs}^{dev} = (s_{rs} - p\alpha_{rs})(s_{rs} - p\alpha_{rs}) \left[(s_{tu} - p\alpha_{tu})(s_{tu} - p\alpha_{tu}) \right]^{-1} = 1 \tag{104.304}$$

This means the hardening equation and related derivatives can be simplified:

$$\bar{\alpha}_{ij} = \frac{2}{3} \frac{h_a}{p_{atm}} m_{ij}^{dev} - \sqrt{\frac{2}{3}} c_r \alpha_{ij} \tag{104.305}$$

When the derivative of backstress $\bar{\alpha}_{ij} = 0$, the tensor α_{ij} reaches the tensor limit:

$$\alpha_{ij}^{lim} = \sqrt{\frac{2}{3}} \frac{h_a}{p_{atm} c_r} m_{ij}^{dev} \tag{104.306}$$

Some useful tensor derivatives for Drucker-Prager $\bar{\alpha}$.

$$m_{ij}^{dev} = \left(s_{ij} - p\alpha_{ij}\right) \left[\left(s_{rs} - p\alpha_{rs}\right)\left(s_{rs} - p\alpha_{rs}\right)\right]^{-0.5} \tag{104.307}$$

$$\begin{aligned} \frac{\partial m_{ij}^{dev}}{\partial \sigma_{mn}} = & \left(\frac{1}{2}\delta_{im}\delta_{jn} + \frac{1}{2}\delta_{in}\delta_{jm} - \frac{1}{3}\delta_{mn}\delta_{ij} + \frac{1}{3}\delta_{mn}\alpha_{ij}\right) \left[\left(s_{rs} - p\alpha_{rs}\right)\left(s_{rs} - p\alpha_{rs}\right)\right]^{-0.5} \\ & - \left(s_{ij} - p\alpha_{ij}\right) \left[\left(s_{mn} - p\alpha_{mn}\right) + \frac{1}{3}\alpha_{rs}\left(s_{rs} - p\alpha_{rs}\right)\delta_{mn}\right] \left[\left(s_{tu} - p\alpha_{tu}\right)\left(s_{tu} - p\alpha_{tu}\right)\right]^{-1.5} \end{aligned} \tag{104.308}$$

$$\frac{\partial m_{ij}^{dev}}{\partial k} = 0 \tag{104.309}$$

$$\begin{aligned} \frac{\partial m_{ij}^{dev}}{\partial \alpha_{mn}} = & -p \left(\frac{1}{2}\delta_{im}\delta_{jn} + \frac{1}{2}\delta_{in}\delta_{jm}\right) \left[\left(s_{rs} - p\alpha_{rs}\right)\left(s_{rs} - p\alpha_{rs}\right)\right]^{-0.5} \\ & - p\left(s_{ij} - p\alpha_{ij}\right)\left(s_{mn} - p\alpha_{mn}\right) \left[\left(s_{tu} - p\alpha_{tu}\right)\left(s_{tu} - p\alpha_{tu}\right)\right]^{-1.5} \end{aligned} \tag{104.310}$$

- Tensor derivative of Drucker-Prager $\bar{\alpha}_{ij}$ with respect to σ_{ij}.

$$\frac{\partial \bar{\alpha}_{ij}}{\partial \sigma_{mn}} = \frac{2h_a}{3p_{atm}} \frac{\partial m_{ij}^{dev}}{\partial \sigma_{mn}} \tag{104.311}$$

- Tensor derivative of Drucker-Prager $\bar{\alpha}_{ij}$ with respect to k.

$$\frac{\partial \bar{\alpha}_{ij}}{\partial k} = 0 \tag{104.312}$$

- Tensor derivative of Drucker-Prager $\bar{\alpha}_{ij}$ with respect to α_{ij}.

$$\frac{\partial \bar{\alpha}_{ij}}{\partial \alpha_{mn}} = \frac{2h_a}{3p_{atm}} \frac{\partial m_{ij}^{dev}}{\partial \alpha_{mn}} - \sqrt{\frac{2}{3}} c_r \left(\frac{1}{2}\delta_{im}\delta_{jn} + \frac{1}{2}\delta_{in}\delta_{jm}\right) \tag{104.313}$$

104.6.8 Hyperbolic Drucker Prager Model

104.6.8.1 Original Yield Function and Hyperbolic Function

The original Drucker-Prager yield function is

$$\Phi(\sigma) = \sqrt{J_2} - \eta p - \xi \tag{104.314}$$

where

$$\eta = \frac{3tan\phi}{\sqrt{9 + 12tan^2\phi}} \tag{104.315}$$

$$\xi = \frac{3c}{\sqrt{9 + 12tan^2\phi}} \tag{104.316}$$

where ϕ is the friction ratio, and c is the cohesion. Besides, the constant η is unitless. The unit of constant ξ is *Pascal*. In addition, here we define that p is compression-positive. Namely, $p = -\frac{\sigma_{ii}}{3}$.

Rewrite the yield function (104.314) with p, q such that

$$\Phi(\sigma) = \frac{q}{\sqrt{3}} - \eta p - \xi \tag{104.317}$$

The slope of the yield surface is $\sqrt{3}\eta$, and the hydrostatic cutoff point is at $(-\frac{\xi}{\eta}, 0)$.

104.6.8.2 Hyperbolic Drucker Prager Model

Assume a standard hyperbolic function is

$$\left(\frac{x-d}{a}\right)^2 - \left(\frac{y}{b}\right)^2 = 1 \tag{104.318}$$

In the hyperbolic function, as showed in the Figure 104.9, the distance between the original apex to the rounded hydrostatic cut-off is a, and the corresponding y value is b. The hydrostatic cut off of the asymptotic line is d.

104.6.8.3 Modified Hyperbolic Drucker Prager

Mapping the Hyperbolic Equation. In the modified hyperbolic Drucker Prager yield surface, the asymptotic line is the original yield surface.

The slope of the asymptotic line is

$$\frac{b}{a} = \sqrt{3}\eta \tag{104.319}$$

The hydrostatic cut-off of the asymptotic line is

$$d = \frac{\xi}{\eta} \tag{104.320}$$

The rounded distance a of the hyperbolic line is a new parameter.

The hyperbolic function is

$$\left(\frac{p + \frac{\xi}{\eta}}{a}\right)^2 - \left(\frac{q}{\sqrt{3}\ a\ \eta}\right)^2 = 1 \tag{104.321}$$

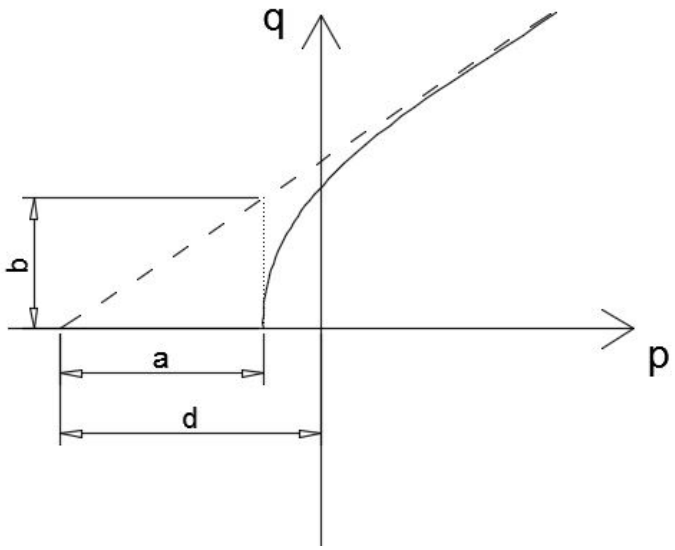

Figure 104.9: The standard hyperbolic function parameters.

Removing the Negative Branch. To remove the negative branch, we need the pressure $(p + \frac{\xi}{\eta})$ always be positive. Therefore,

$$\left(\frac{p+\frac{\xi}{\eta}}{a}\right)^2 = \left(\frac{q}{\sqrt{3}\,a\,\eta}\right)^2 + 1 \tag{104.322}$$

Take the root on both sides,

$$\frac{p+\frac{\xi}{\eta}}{a} = \sqrt{\left(\frac{q}{\sqrt{3}\,a\,\eta}\right)^2 + 1} \tag{104.323}$$

Inside the hyperbolic To make the yield surface value smaller than zero when the stress state is inside the modified cone, the yield surface is

$$0 = \sqrt{\left(\frac{q}{\sqrt{3}\,a\,\eta}\right)^2 + 1} - \frac{p+\frac{\xi}{\eta}}{a} \tag{104.324}$$

Avoiding Zero Denominator. To avoid the zero denominator situation, multiply the equation on both sides by η and a.

$$0 = \sqrt{\left(\frac{q}{\sqrt{3}}\right)^2 + a^2\eta^2} - \eta p - \xi \tag{104.325}$$

The basic yield function The yield function now has one internal variable η for isotropic hardening.

$$\Phi(\sigma,\eta) = \sqrt{\left(\frac{q}{\sqrt{3}}\right)^2 + a^2\eta^2} - \eta p - \xi \tag{104.326}$$

Simplify the yield function and substitute $q = \sqrt{\frac{3}{2}s_{ij}s_{ij}}$, we have

$$\Phi(\sigma,\eta) = \sqrt{\frac{1}{2}s_{ij}s_{ij} + a^2\eta^2} - \eta p - \xi \tag{104.327}$$

Introduce the capability of rotational kinematic hardening by α.

$$\Phi(\sigma,\eta,\alpha) = \sqrt{\frac{1}{2}(s_{ij} - p\alpha_{ij})(s_{ij} - p\alpha_{ij}) + a^2\eta^2} - \eta p - \xi \tag{104.328}$$

104.6.8.4 The Non-Associative Plastic Potential Function.

The non-associative plastic flow direction is

$$m_{ij} = \left(\frac{\partial f}{\partial \sigma_{ij}}\right)^{dev} + \frac{1}{3}\bar{\eta}\delta_{ij} \tag{104.329}$$

where $\bar{\eta}$ controls the plastic flow direction. When $\bar{\eta} = 0$, the material has the deviatoric plastic flow only.

The relation between the dilatancy angle and $\bar{\eta}$ is similar to the relation between the friction angle and η.

$$\bar{\eta} = \frac{3tan\psi}{\sqrt{9 + 12tan^2\psi}} \tag{104.330}$$

where ψ is the dilatancy angle.

Numerical Issues in the Non-Associative Plastic Potential Function. The non-associative plastic flow rule will have asymmetric stiffness matrix, which requires a asymmetric solver. The non-associative requires smaller subincrements for convergence. One important non-associative plastic potential is the purely deviatoric plastic flow.

The purely deviatoric plastic flow may have the numerical issues for the convergence. For example, in Fig 104.10, the purely deviatoric plastic flow direction can never return back to the yield surface. Subincrements can solve this problem.

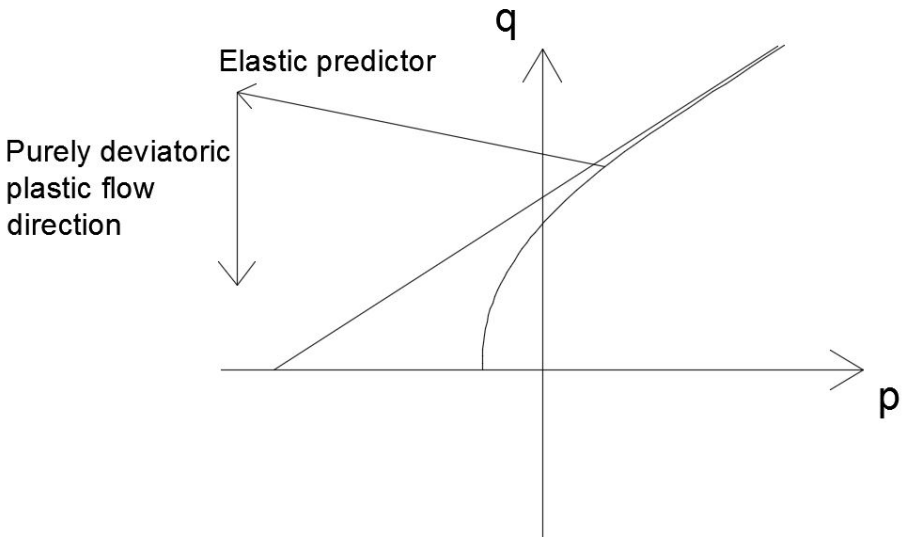

Figure 104.10: The inconvergence situation for purely deviatoric plastic flow.

104.6.8.5 Han's Description of Hyperbolic Drucker–Prager Model with Armstrong–Frederick Kinematic Hardening

Presented is a new description of non-associated hyperbolic Drucker-Prager model with nonlinear Armstrong-Frederick kinematic hardening. It's intended to keep the same theoretical framework and the same set of material parameters as the Drucker-Prager material model shown in section 104.6.7.5.

Classic Drucker–Prager Yield Function with Cohesion This is the yield function shown in Equation 104.237, extended to considering cohesion

$$f = q - Mp - \sqrt{3}\beta \tag{104.331}$$

where

$$M = \frac{6\sin\phi}{3-\sin\phi} \quad \text{and} \quad \beta = \frac{6\cos\phi_0}{\sqrt{3}\,(3-\sin\phi_0)}c \tag{104.332}$$

Note that ϕ is the friction angle, which can evolve if hardening is present in the model, and ϕ_0 is the initial friction angle.

Rewrite Equation 104.333 using the parameters in Real-ESSI implementation

$$f = \sqrt{\left(s_{ij}-p\alpha_{ij}\right)\left(s_{ij}-p\alpha_{ij}\right)} - \sqrt{\frac{2}{3}}kp - \sqrt{2}\beta \tag{104.333}$$

Hyperbolic Drucker–Prager Yield Function Assume the same generic hyperbolic function shown in Equation 104.318, the hyperbolic Drucker-Prager yield function considering isotropic and kinematic

hardening is given as

$$f = \sqrt{\left(s_{ij} - p\alpha_{ij}\right)\left(s_{ij} - p\alpha_{ij}\right) + \frac{2}{3}k^2a^2} - \sqrt{\frac{2}{3}}kp - \sqrt{2}\beta \tag{104.334}$$

where a is the rounded distance shown in Figure 104.9.

Derivatives of the yield function Equation 104.334 are shown below.

$$\frac{\partial f}{\partial \sigma_{ij}} = \left[\left(s_{ij} - p\alpha_{ij}\right) + \frac{1}{3}\alpha_{kl}\left(s_{kl} - p\alpha_{kl}\right)\delta_{ij}\right]\left[\left(s_{mn} - p\alpha_{mn}\right)\left(s_{mn} - p\alpha_{mn}\right) + \frac{2}{3}k^2a^2\right]^{-0.5} + \sqrt{\frac{2}{27}}k\delta_{ij} \tag{104.335}$$

$$\frac{\partial f}{\partial \alpha_{ij}} = -p\left(s_{ij} - p\alpha_{ij}\right)\left[\left(s_{mn} - p\alpha_{mn}\right)\left(s_{mn} - p\alpha_{mn}\right) + \frac{2}{3}k^2a^2\right]^{-0.5} \tag{104.336}$$

$$\frac{\partial f}{\partial k} = \frac{2}{3}ka^2\left[\left(s_{mn} - p\alpha_{mn}\right)\left(s_{mn} - p\alpha_{mn}\right) + \frac{2}{3}k^2a^2\right]^{-0.5} - \sqrt{\frac{2}{3}}p \tag{104.337}$$

Plastic Flow The non-associated plastic flow is defined as

$$m_{ij} = \left(\frac{\partial f}{\partial \sigma_{ij}}\right)^{dev} - \frac{1}{3}D\delta_{ij} = \left(s_{ij} - p\alpha_{ij}\right)\left[\left(s_{rs} - p\alpha_{rs}\right)\left(s_{rs} - p\alpha_{rs}\right) + \frac{2}{3}k^2a^2\right]^{-0.5} - \frac{1}{3}D\delta_{ij} \tag{104.338}$$

where

$$D = \xi\left(\sqrt{\frac{2}{3}}k_d - \frac{\sqrt{s_{mn}s_{mn}}}{p}\right) \tag{104.339}$$

The derivatives of the plastic flow are shown below.

$$\begin{aligned}\frac{\partial m_{ij}}{\partial \sigma_{mn}} = {} & \left(\frac{1}{2}\delta_{im}\delta_{jn} + \frac{1}{2}\delta_{in}\delta_{jm} - \frac{1}{3}\delta_{mn}\delta_{ij} + \frac{1}{3}\delta_{mn}\alpha_{ij}\right)\left[\left(s_{rs} - p\alpha_{rs}\right)\left(s_{rs} - p\alpha_{rs}\right) + \frac{2}{3}k^2a^2\right]^{-0.5} \\ & - \left(s_{ij} - p\alpha_{ij}\right)\left[\left(s_{mn} - p\alpha_{mn}\right) + \frac{1}{3}\alpha_{rs}\left(s_{rs} - p\alpha_{rs}\right)\delta_{mn}\right]\left[\left(s_{tu} - p\alpha_{tu}\right)\left(s_{tu} - p\alpha_{tu}\right) + \frac{2}{3}k^2a^2\right]^{-1.5} \\ & + \frac{1}{3}\xi\left[s_{mn}p^{-1}(s_{kl}s_{kl})^{-0.5} + \frac{1}{3}\delta_{mn}p^{-2}(s_{ot}s_{ot})^{0.5}\right]\delta_{ij}\end{aligned} \tag{104.340}$$

$$\begin{aligned}\frac{\partial m_{ij}}{\partial \alpha_{mn}} = {} & -p\left(\frac{1}{2}\delta_{mi}\delta_{nj} + \frac{1}{2}\delta_{mj}\delta_{ni}\right)\left[\left(s_{rs} - p\alpha_{rs}\right)\left(s_{rs} - p\alpha_{rs}\right) + \frac{2}{3}k^2a^2\right]^{-0.5} \\ & + p\left(s_{ij} - p\alpha_{ij}\right)\left(s_{mn} - p\alpha_{mn}\right)\left[\left(s_{tu} - p\alpha_{tu}\right)\left(s_{tu} - p\alpha_{tu}\right) + \frac{2}{3}k^2a^2\right]^{-1.5}\end{aligned} \tag{104.341}$$

$$\frac{\partial m_{ij}}{\partial k} = -\frac{2}{3}ka^2\left(s_{ij} - p\alpha_{ij}\right)\left(s_{mn} - p\alpha_{mn}\right)\left[\left(s_{tu} - p\alpha_{tu}\right)\left(s_{tu} - p\alpha_{tu}\right) + \frac{2}{3}k^2a^2\right]^{-1.5} \tag{104.342}$$

Linear Isotropic Hardening Linear isotropic hardening is used for this material model. The evolution of the internal variable k is defined as

$$\bar{k} = Hm^{equi} \quad , \quad m^{equi} = \left(\frac{2}{3}m_{ij}m_{ij}\right)^{0.5} \tag{104.343}$$

where H is a material constant.

The derivatives of the internal variable k are shown below.

$$\frac{\partial \bar{k}}{\partial \sigma_{ij}} = \frac{2H}{3}m_{kl}\frac{\partial m_{kl}}{\partial \sigma_{ij}}\left(m^{equi}\right)^{-1} \tag{104.344}$$

$$\frac{\partial \bar{k}}{\partial \alpha_{ij}} = \frac{2H}{3}m_{kl}\frac{\partial m_{kl}}{\partial \alpha_{ij}}\left(m^{equi}\right)^{-1} \tag{104.345}$$

$$\frac{\partial \bar{k}}{\partial k} = \frac{2H}{3}m_{kl}\frac{\partial m_{kl}}{\partial k}\left(m^{equi}\right)^{-1} \tag{104.346}$$

Armstrong-Frederick kinematic hardening for Hyperbolic Drucker-Prager

$$\bar{\alpha}_{ij} = \frac{2}{3}\frac{h_a}{p_{atm}}m_{ij}^{dev} - c_r\left(\frac{2}{3}m_{rs}^{dev}m_{rs}^{dev}\right)^{0.5}\alpha_{ij} \tag{104.347}$$

where p_{atm} is the atmospheric pressure of 101.325 kPa. The unit of parameter h_a is Pascal. The parameter c_r is unitless. The α_{ij} in Drucker-Prager is unitless.

Some useful tensor derivatives for Drucker-Prager $\bar{\alpha}$.

$$m_{ij}^{dev} = \left(s_{ij} - p\alpha_{ij}\right)\left[\left(s_{rs} - p\alpha_{rs}\right)\left(s_{rs} - p\alpha_{rs}\right) + \frac{2}{3}k^2a^2\right]^{-0.5} \tag{104.348}$$

$$\begin{aligned}\frac{\partial m_{ij}^{dev}}{\partial \sigma_{mn}} = {} & \left(\frac{1}{2}\delta_{im}\delta_{jn} + \frac{1}{2}\delta_{in}\delta_{jm} - \frac{1}{3}\delta_{mn}\delta_{ij} + \frac{1}{3}\delta_{mn}\alpha_{ij}\right)\left[\left(s_{rs} - p\alpha_{rs}\right)\left(s_{rs} - p\alpha_{rs}\right) + \frac{2}{3}k^2a^2\right]^{-0.5} \\ & - \left(s_{ij} - p\alpha_{ij}\right)\left[\left(s_{mn} - p\alpha_{mn}\right) + \frac{1}{3}\alpha_{rs}\left(s_{rs} - p\alpha_{rs}\right)\delta_{mn}\right]\left[\left(s_{tu} - p\alpha_{tu}\right)\left(s_{tu} - p\alpha_{tu}\right) + \frac{2}{3}k^2a^2\right]^{-1.5}\end{aligned} \tag{104.349}$$

$$\begin{aligned}\frac{\partial m_{ij}^{dev}}{\partial \alpha_{mn}} = {} & -p\left(\frac{1}{2}\delta_{im}\delta_{jn} + \frac{1}{2}\delta_{in}\delta_{jm}\right)\left[\left(s_{rs} - p\alpha_{rs}\right)\left(s_{rs} - p\alpha_{rs}\right) + \frac{2}{3}k^2a^2\right]^{-0.5} \\ & - p\left(s_{ij} - p\alpha_{ij}\right)\left(s_{mn} - p\alpha_{mn}\right)\left[\left(s_{tu} - p\alpha_{tu}\right)\left(s_{tu} - p\alpha_{tu}\right) + \frac{2}{3}k^2a^2\right]^{-1.5}\end{aligned} \tag{104.350}$$

$$\frac{\partial m_{ij}^{dev}}{\partial k} = -\frac{2}{3}ka^2\left(s_{ij}-p\alpha_{ij}\right)\left(s_{mn}-p\alpha_{mn}\right)\left[\left(s_{tu}-p\alpha_{tu}\right)\left(s_{tu}-p\alpha_{tu}\right)+\frac{2}{3}k^2a^2\right]^{-1.5} \tag{104.351}$$

Tensor derivative of Drucker-Prager $\bar{\alpha}_{ij}$ with respect to σ_{ij}.

$$\frac{\partial \bar{\alpha}_{ij}}{\partial \sigma_{mn}} = \frac{2h_a}{3p_{atm}}\frac{\partial m_{ij}^{dev}}{\partial \sigma_{mn}} - \frac{2}{3}c_r m_{kl}^{dev}\frac{\partial m_{kl}^{dev}}{\partial \sigma_{mn}}\left(\frac{2}{3}m_{rs}^{dev}m_{rs}^{dev}\right)^{-0.5}\alpha_{ij} \tag{104.352}$$

Tensor derivative of Drucker-Prager $\bar{\alpha}_{ij}$ with respect to α_{ij}.

$$\begin{aligned}\frac{\partial \bar{\alpha}_{ij}}{\partial \alpha_{mn}} = {} & \frac{2h_a}{3p_{atm}}\frac{\partial m_{ij}^{dev}}{\partial \alpha_{mn}} - \frac{2}{3}c_r m_{kl}^{dev}\frac{\partial m_{kl}^{dev}}{\partial \alpha_{mn}}\left(\frac{2}{3}m_{rs}^{dev}m_{rs}^{dev}\right)^{-0.5}\alpha_{ij} \\ & - c_r\left(\frac{2}{3}m_{rs}^{dev}m_{rs}^{dev}\right)^{0.5}\left(\frac{1}{2}\delta_{mi}\delta_{nj}+\frac{1}{2}\delta_{mj}\delta_{ni}\right)\end{aligned} \tag{104.353}$$

Tensor derivative of Drucker-Prager $\bar{\alpha}_{ij}$ with respect to k.

$$\frac{\partial \bar{\alpha}_{ij}}{\partial k} = \frac{2h_a}{3p_{atm}}\frac{\partial m_{ij}^{dev}}{\partial k} - \frac{2}{3}c_r m_{kl}^{dev}\frac{\partial m_{kl}^{dev}}{\partial k}\left(\frac{2}{3}m_{rs}^{dev}m_{rs}^{dev}\right)^{-0.5}\alpha_{ij} \tag{104.354}$$

104.6.9 Rounded Mohr-Coulomb Model

DSL COMMANDS for the rounded Mohr-Coulomb material models are given in section 205.3 on page 827.

The model consists of a smooth conical yield surface. This conical yield surface has an apex that is located at the zero of stress coordinate system or to the extension side, depending on the cohesion characteristic of material in question. The yield surface is defined by:

$$F\left(p,q,\theta,\kappa_{cone}\right) = q\left(1+\frac{q}{q_a}\right)^m g\left(\theta\right) - \eta_{cone}\left(\kappa_{cone}\right)\left(p-p_c\right) \tag{104.355}$$

where q_a is a (positive) reference deviator stress, m is a material constant such that $0 \leq m \leq 1$, controlling the curvature of the cone in the meridian $(p,\ q)$ planes, η_{cone} represents the angle of internal friction, and p_c represents the cohesion. η_{cone} is a function of the hardening variable κ_{cone} which, in turn, is a function of the plastic work. Moreover, an asymmetric trace of the yield surface in the deviatoric plane is generated through the introduction of $g(\theta)$ according to the expression by Willam and Warnke (1974):

$$g\left(\theta\right) = \frac{4\left(1-e^2\right)\cos^2\theta + (2e-1)^2}{2\left(1-e^2\right)\cos\theta + (2e-1)\sqrt{4\left(1-e^2\right)\cos^2\theta + 5e^2 - 4e}} \tag{104.356}$$

and e is an eccentricity parameter that satisfies the condition $1/2 < e \leq 1$. From eqn. (104.356) we conclude that $g\left(0\right) = 1/e$ and $g\left(\pi/3\right) = 1$. For $e = 1 \quad \Rightarrow \quad g\left(\theta\right) = 1$, so the influence of the third stress

invariant via θ is dropped and the conical surface represents a curved cone[63]. For $e \to 1/2$ the triangular cone[64] is obtained. A nice pictorial representation of function $1/g(\theta)$ is presented in the Figure (104.6.9), showing material model traces in the deviatoric plane.

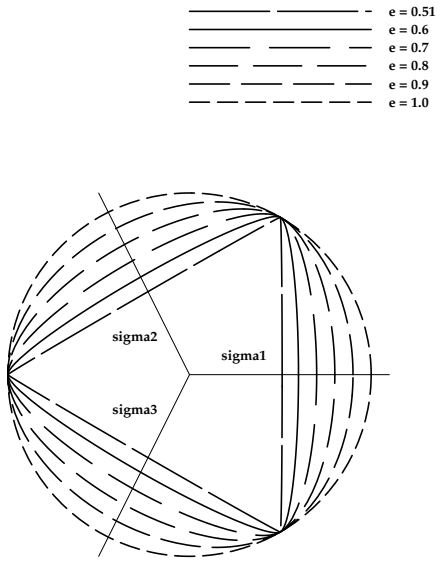

Figure 104.11: Willam Warnke function 1/g for different values of e (e = 0.51, 0.6, 0.7, 0.8, 0.9, 1.0) representing traces of rounded Mohr-Coulomb model in deviatoric space.

104.6.10 Modified Cam-Clay Model

DSL COMMANDS for the Modified Cam Clay material models are given in section 205.3 on page 827.

The pioneering research work on the critical state soil mechanics by the researchers at Cambridge University (Roscoe et al., 1958), (Roscoe and Burland, 1968), (Muir Wood, 1990)) has made great contribution on the modern soil elastoplastic models. The original Cam Clay model (Roscoe et al., 1963), and later the modified Cam Clay model (Schofield and Wroth, 1968) were within the critical state soil mechanics framework. We focus on only the modified Cam Clay model and herein the word 'modified' is omitted to shorten writing.

[63] extended Drucker Prager cone.
[64] extended Rankine yield criteria.

104.6.10.1 Critical State

The critical state line (CSL) takes the form

$$e_c = e_{c,r} - \lambda_c \ln p_c \tag{104.357}$$

where e_c is the critical void ratio at the critical mean effective stress p_c [65], $e_{c,r}$ is the reference critical void ratio, λ_c is the normal consolidation slope.

The critical state soil mechanics assumes that the normal consolidation line (NRL) is parallel to the CSL, which is expressed by

$$e = e_\lambda - \lambda \ln p \tag{104.358}$$

where e_λ is the intercept on the NRL at $p = 1$. λ is the normal consolidation slope or the elastoplastic slope of $e - \ln p$ relation, and $\lambda_c = \lambda$.

The unloading-reloading line (URL) take the similar form but with different slope by

$$e = e_\kappa - \kappa \ln p \tag{104.359}$$

where e_κ is the intercept on the URL at $p = 1$. λ_c is the normal consolidation slope or the elastoplastic slope of $e - \ln p$ relation.

104.6.10.2 Elasticity

The elastic bulk modulus K can be directly derived from the Equation 104.359 and takes the form

$$K = \frac{(1+e)\,p}{\kappa} \tag{104.360}$$

If a constant Poisson's ratio ν is assumed, since the isotropic elasticity needs only two material constants, the shear elastic modulus can be obtained in terms of K and ν by

$$G = \frac{3\,(1-2\nu)}{2\,(1+\nu)} K = \frac{3\,(1-2\nu)\,(1+e)}{2\,(1+\nu)\,\kappa} p \tag{104.361}$$

Alternatively, a constant shear elastic modulus G can be assumed and then the Poisson's ratio ν is expressed in terms of K and G as

$$\nu = \frac{3K - 2G}{2\,(G+3K)} \tag{104.362}$$

[65] In this chapter, only single-phase (dry phase) is studied, the total and effective stresses are thus identical, e.g. $p'_c = p_c$.

104.6.10.3 Yield Function

The yield function of the Cam Clay model is defined by

$$f = q^2 - M_c^2[p\,(p_0 - p)] = 0 \tag{104.363}$$

where M_c is the critical state stress ration in the $q-p$ plane, and the p_0 is the initial internal scalar variable, which is controlled by the change of the plastic volumetric strain.

The gradient of the yield surface to the stress can be obtained as

$$\frac{\partial f}{\partial \sigma_{ij}} = 2q\frac{\partial q}{\partial \sigma_{ij}} - M_c^2\,(2p - p_0)\,\frac{\partial p}{\partial \sigma_{ij}} = 3s_{ij} + \frac{1}{3}M_c^2\,(p_0 - 2p)\,\delta_{ij} \tag{104.364}$$

where $\partial q/\partial \sigma_{ij}$ and $\partial p/\partial \sigma_{ij}$ are independent of the yield function.

The gradient of the yield surface to p_0 will be used in the integration algorithm, and can be expressed by

$$\frac{\partial f}{\partial p_0} = M_c^2 p \tag{104.365}$$

104.6.10.4 Plastic Flow

The plastic flow of the Cam Clay model is associated with its yield function, in other words, the plastic flow is defined by the potential function, g, which is assumed the same as the yield function, f.

$$g = f = q^2 - M_c^2[p\,(p_0 - p)] = 0 \tag{104.366}$$

The stress gradient to the yield surface can be obtained as

$$m_{ij} = \frac{\partial g}{\partial \sigma_{ij}} = 2q\frac{\partial q}{\partial \sigma_{ij}} + M_c^2\,(2p - p_0)\,\frac{\partial p}{\partial \sigma_{ij}} = 3s_{ij} + \frac{1}{3}M_c^2\,(p_0 - 2p)\,\delta_{ij} \tag{104.367}$$

It can define the plastic dilation angle β, which is related to the ratio of plastic volumetric and deviatoric strain (Muir Wood, 1990), by

$$\tan\beta = -\frac{\Delta\epsilon_v^p}{\Delta\epsilon_q^p} = \frac{M_c^2\,(p_0 - 2p)}{2q} \tag{104.368}$$

It is interesting to find that from Equation 104.368, when $p < p_0/2$, the plastic dilation angle is positive; when $p > p_0/2$, the plastic dilation angle is negative. If $p = p_0/2$, the plastic dilation angle is zero, which is corresponding to the critical state. This is evidently more realistic than Drucker-Prager model, whose associated plastic flow always gives positive plastic dilation angle.

104.6.10.5 Evolution Law

The evolution law of the Cam Clay model is a scalar one, which can be expressed by

$$\dot{p}_0 = \frac{(1+e)\,p_0}{\lambda-\kappa}\dot{\epsilon}_v^p \tag{104.369}$$

With this scalar evolution law, the change of p_0 is decided by the change of plastic volumetric strain. When it reaches the critical state, or when there is no plastic volumetric strain, the evolution of p_0 will cease. From Equation 104.369, one gets

$$\dot{p}_0 = \dot{\lambda}\frac{(1+e)\,p_0}{\lambda-\kappa}m_{ii} \tag{104.370}$$

so if using Equation 104.367 further, one obtains

$$h = \frac{(1+e)\,p_0}{\lambda-\kappa}M_c^2\,(2p-p_0) \tag{104.371}$$

or using dilation angle,

$$h = \frac{2\,(1+e)\,p_0 q}{\lambda-\kappa}\tan\beta \tag{104.372}$$

104.6.10.6 Yield and Plastic Potential Functions: Cam-Clay Model

Yield function and related derivatives

$$f = q^2 - M_c^2[p\,(p_0-p)] = 0 \tag{104.373}$$

$$\begin{aligned}\frac{\partial f}{\partial\sigma_{ij}} &= 2q\frac{\partial q}{\partial\sigma_{ij}} - M_c^2\,(2p-p_0)\,\frac{\partial p}{\partial\sigma_{ij}}\\ &= 3s_{ij}+\frac{1}{3}M_c^2\,(p_0-2p)\,\delta_{ij}\end{aligned} \tag{104.374}$$

$$\frac{\partial f}{\partial p_0} = -M_c^2 p \tag{104.375}$$

Plastic flow (associated plasticity) and related derivatives

$$m_{ij} = \frac{\partial f}{\partial\sigma_{ij}} = 3s_{ij} + \frac{1}{3}M_c^2\,(p_0-2p)\,\delta_{ij} \tag{104.376}$$

$$\begin{aligned}\frac{\partial m_{ij}}{\partial\sigma_{mn}} &= 3\frac{\partial s_{ij}}{\partial\sigma_{mn}} - \frac{2}{3}M_c^2\delta_{ij}\frac{\partial p}{\partial\sigma_{mn}}\\ &= 3\delta_{im}\delta_{jn} - \delta_{ij}\delta_{mn} + \frac{2}{9}M_c^2\delta_{ij}\delta_{mn}\\ &= 3\delta_{im}\delta_{jn} + \left(\frac{2}{9}M_c^2 - 1\right)\delta_{ij}\delta_{mn}\end{aligned} \tag{104.377}$$

$$\frac{\partial m_{ij}}{\partial p_0} = \frac{1}{3} M_c^2 \delta_{ij} \tag{104.378}$$

Isotropic Hardening and related derivatives (CC_Ev) Note the due to the current definition of p (i.e. $p = -\frac{1}{3}\sigma_{ii}$), a minus sign appears in from of the evolution of p_0 as follows:

$$\bar{p}_0 = -\frac{(1+e)\, p_0}{\lambda - \kappa} m_{ii} \tag{104.379}$$

$$= \frac{(1+e)\, p_0}{\lambda - \kappa} M_c^2 \, (2p - p_0) \tag{104.380}$$

$$\frac{\partial \bar{p}_0}{\partial \sigma_{ij}} = \frac{(1+e)\, p_0}{\lambda - \kappa} M_c^2 \left(-\frac{2}{3} \delta_{ij} \right) \tag{104.381}$$

$$\frac{\partial \bar{p}_0}{\partial p_0} = \frac{2\,(1+e)}{\lambda - \kappa} M_c^2 \, (p - p_0) \tag{104.382}$$

104.6.11 SaniSand2004 (aka Dafalias-Manzari) Model

DSL COMMANDS for the Dafalias-Manzari material models are given in section 205.3 on page 827.

Within the critical state soil mechanics framework, Manzari and Dafalias (1997) proposed a two-surface sand model. This model considered the effects of the state parameter on the behaviors of the dense or loose sands. The features of this model include successfully predicting the softening at the dense state in drained loading, and also softening at the loose state but in the undrained loading. Dafalias and Manzari (2004a) later presented an improved version. This version introduced the fabric dilatancy tensor which has a significant effect on the contraction unloading response. It is also considered the Lode's angle effect on the bounding surface, which produces more realistic responses in non-triaxial conditions. Here only the new version is summarized. The compression stress is assumed negative here, which is different from the original reference by Dafalias and Manzari (2004a).

104.6.11.1 Critical State

Instead of using the most common linear line of critical void ration vs. logarithmic critical mean effective stress, the power relation recently suggested by Li and Wang (1998) was used:

$$e_c = e_{c,r} - \lambda_c \left(\frac{p_c}{P_{at}} \right)^{\xi} \tag{104.383}$$

where e_c is the critical void ratio at the critical man effective stress p'_c, $e_{c,r}$ is the reference critical void ratio, λ_c and ξ (for most sands, $\xi = 0.7$) are material constants, and P_{at} is the atmospheric pressure for normalization.

104.6.11.2 Elasticity

The elastic incremental moduli of shear and bulk, are following Richart et al. (1970):

$$G = G_0 \frac{(2.97-e)^2}{(1+e)} \left(\frac{p}{P_{at}}\right)^{0.5} P_{at} \;\; ; \;\; K = \frac{2(1+\nu)}{3(1-2\nu)} G \tag{104.384}$$

where G_0 is a material constant, e is the void ratio, and ν is the Poisson's ratio.

The isotropic hypoelasticity is then defined by

$$\dot{e}^e_{ij} = \frac{\dot{s}_{ij}}{2G}, \;\; \dot{\epsilon}^e_v = \frac{\dot{p}}{K} \tag{104.385}$$

104.6.11.3 Yield Function

The yield function is defined by

$$f = |\Lambda| - \sqrt{\frac{2}{3}} mp = 0 \tag{104.386}$$

where s_{ij} is the deviatoric stress tensor, α_{ij} is the deviatoric back stress-ratio tensor, m is a material constant, and

$$|\Lambda| = \left\| s_{ij} - p\alpha_{ij} \right\| = [(s_{ij} - p\alpha_{ij})(s_{ij} - p\alpha_{ij})]^{0.5} \tag{104.387}$$

The gradient of the yield surface to the stress can be obtained as

$$\frac{\partial f}{\partial \sigma_{ij}} = n_{ij} + \frac{1}{3}(\alpha_{pq} n_{pq} + \sqrt{\frac{2}{3}} m)\delta_{ij} \tag{104.388}$$

where $r_{ij} = s_{ij}/p$ is the normalized deviatoric stress tensor, and n_{ij} is the unit gradient tensor to the yield surface defined by

$$n_{ij} = \frac{s_{ij} - p\alpha_{ij}}{|\Lambda|} \tag{104.389}$$

It is evident that $n_{ii} \equiv 0$ and $n_{ij} n_{ij} \equiv 1$.

The gradient of the yield surface to α_{ij} can be easily obtained as

$$\frac{\partial f}{\partial \alpha_{ij}} = -p n_{ij} \tag{104.390}$$

The tensor of n_{ij} is to defined θ_n, the Lode's angle of the yield gradient, by the equation

$$\cos 3\theta_n = -\sqrt{6} n_{ij} n_{jk} n_{ki} \tag{104.391}$$

where $0 \leq \theta_n \leq \pi/6$ and $\theta_n = 0$ at triaxial compression and $\theta_n = \pi/6$ at triaxial extension.

The critical stress ratio M at any stress state can be interpolated between M_c, the triaxial compression critical stress ratio, and M_e, the triaxial extension critical stress ratio.

$$M = M_c g(\theta_n, c), \quad g(\theta_n, c) = \frac{2c}{(1+c) - (1-c)\cos 3\theta_n}, \quad c = \frac{M_e}{M_c} \tag{104.392}$$

The line from the origin of the π plane parallel to n_{ij} will intersect the bounding, critical and dilation surfaces at three 'image' back-stress ratio tensor α^b_{ij}, α^c_{ij}, and α^d_{ij} respectively (Figure 104.12), which are expressed as

$$\alpha^b_{ij} = \sqrt{\frac{2}{3}}[M \exp(-n^b \psi) - m] n_{ij} = \left(\sqrt{\frac{2}{3}}\alpha^b_\theta\right) n_{ij} \tag{104.393}$$

$$\alpha^c_{ij} = \sqrt{\frac{2}{3}}[M - m] n_{ij} = \left(\sqrt{\frac{2}{3}}\alpha^c_\theta\right) n_{ij} \tag{104.394}$$

$$\alpha^d_{ij} = \sqrt{\frac{2}{3}}[M \exp(n^d \psi) - m] n_{ij} = \left(\sqrt{\frac{2}{3}}\alpha^d_\theta\right) n_{ij} \tag{104.395}$$

where $\psi = e - e_c$ is the state parameter; n^b and n^d are material constants.

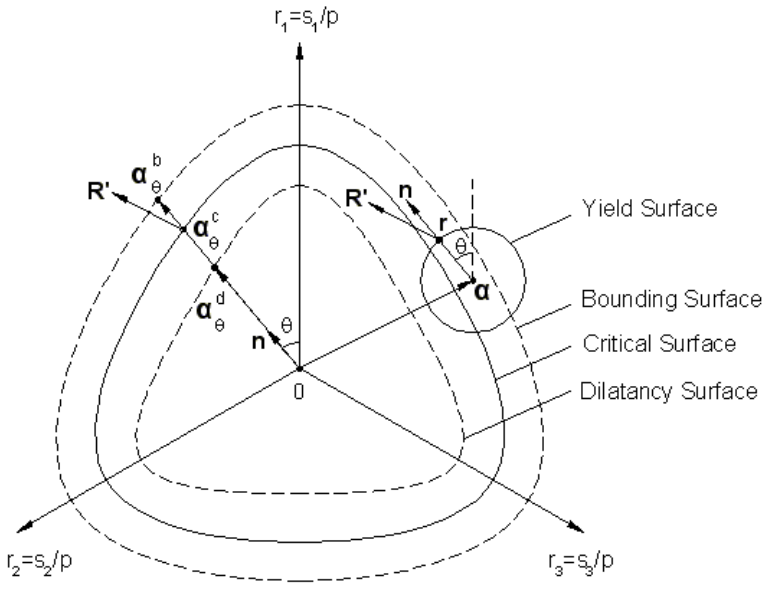

Figure 104.12: Schematic illustration of the yield, critical, dilatancy, and bounding surfaces in the π-plane of deviatoric stress ratio space (after Dafalias and Manzari 2004).

104.6.11.4 Plastic Flow

The plastic strain is given by

$$\dot{\epsilon}^p_{ij} = \dot{\lambda} R_{ij} = \dot{\lambda}(R'_{ij} + \frac{1}{3} D \delta_{ij}) \tag{104.396}$$

The deviatoric plastic flow tensor is

$$R'_{ij} = B n_{ij} + C(n_{ik} n_{kj} - \frac{1}{3}\delta_{ij}) \tag{104.397}$$

where

$$B = 1 + \frac{3}{2}\frac{1-c}{c} g \cos 3\theta_n, \quad C = 3\sqrt{\frac{3}{2}}\frac{1-c}{c} g \tag{104.398}$$

The volumetric plastic flow part is

$$D = -A_d(\alpha^d_{ij} - \alpha_{ij}) n_{ij} = -A_d \left(\sqrt{\frac{2}{3}} \alpha^d_\theta - \alpha_{ij} n_{ij} \right) \tag{104.399}$$

where

$$A_d = A_0(1 + \langle z_{ij} n_{ij} \rangle) \tag{104.400}$$

A_0 is a material constant, and z_{ij} is the fabric dilation tensor. The Macauley brackets $\langle\rangle$ is defined that $\langle x \rangle = x$, if $x > 0$ and $\langle x \rangle = 0$, if $x \leq 0$.

104.6.11.5 Evolution Laws

This model has two tensorial evolution internal variable, namely, the back stress-ratio tensor α_{ij} and the fabric dilation tensor z_{ij}.

The evolution law for the back stress-ratio tensor α_{ij} is

$$\dot{\alpha}_{ij} = \dot{\lambda}[\frac{2}{3} h(\alpha^b_{ij} - \alpha_{ij})] \tag{104.401}$$

with

$$h = \frac{b_0}{(\alpha_{ij} - \tilde{\alpha}_{ij}) n_{ij}} \tag{104.402}$$

where $\tilde{\alpha}_{ij}$ is the initial value of α_{ij} at initiation of a new loading process and is updated to the new value when the denominator of Equation 104.402 becomes negative. b_0 is expressed by

$$b_0 = G_0 h_0 (1 - c_h e) \left(\frac{p}{P_{at}} \right)^{-0.5} \tag{104.403}$$

where h_0 and c_h are material constants.

The evolution law for the fabric dilation tensor z_{ij} is

$$\dot{z}_{ij} = -c_z \langle \dot{D} \rangle (z_{max} n_{ij} + z_{ij}) \tag{104.404}$$

where c_z and z_{max} are material constants.

104.6.11.6 Analytical Derivatives for the Implicit Algorithm

When implemented into an implicit algorithm for the Dafalias-Manzari model, some complicated additional analytical derivatives are needed. This section gives the analytical derivatives expressions based on the tensor calculus.

Analytical expression of $\frac{\partial m_{ij}}{\partial \sigma_{kl}}$:

$$\begin{aligned}\frac{\partial m_{ij}}{\partial \sigma_{mn}} &= B\frac{\partial n_{ij}}{\partial \sigma_{mn}} + n_{ij}\frac{\partial B}{\partial \sigma_{mn}} + C\frac{\partial n_{ik}}{\partial \sigma_{mn}}n_{kj} + (n_{ik}n_{kj} - \frac{1}{3}\delta_{ij})\frac{\partial C}{\partial \sigma_{mn}} \\ &\quad + \frac{1}{3}\delta_{ij}\frac{\partial D}{\partial \sigma_{mn}}\end{aligned} \tag{104.405}$$

where

$$\frac{\partial n_{ij}}{\partial \sigma_{mn}} = \frac{1}{|\Lambda|}\left[I^s_{ijmn} - \frac{1}{3}\delta_{ij}\delta_{mn} + \frac{1}{3}\alpha_{ij}\delta_{mn} - n_{ij}n_{mn} - \frac{1}{3}(\alpha_{ab}n_{ab})n_{ij}\delta_{mn}\right] \tag{104.406}$$

$$\frac{\partial D}{\partial \sigma_{mn}} = -\frac{\partial A_d}{\partial \sigma_{mn}}\left(\sqrt{\frac{2}{3}}\alpha^d_\theta - \alpha_{ab}n_{ab}\right) - A_d\left(\sqrt{\frac{2}{3}}\frac{\partial \alpha^d_\theta}{\partial \sigma_{mn}} - \alpha_{ab}\frac{\partial n_{ab}}{\partial \sigma_{mn}}\right) \tag{104.407}$$

and

$$\frac{\partial B}{\partial \sigma_{mn}} = \frac{3}{2}\left(\frac{1-c}{c}\right)\left(\frac{\partial g}{\partial \sigma_{mn}}\cos 3\theta + g\frac{\partial \cos 3\theta}{\partial \sigma_{mn}}\right) \tag{104.408}$$

$$\frac{\partial C}{\partial \sigma_{mn}} = 3\sqrt{\frac{3}{2}}\left(\frac{1-c}{c}\right)\frac{\partial \alpha^d_\theta}{\partial \sigma_{mn}} \tag{104.409}$$

$$\frac{\partial \alpha^d_\theta}{\partial \sigma_{mn}} = M_c \exp(n^d\psi)\left(gn^d\frac{\partial \psi}{\partial \sigma_{mn}} + \frac{\partial g}{\partial \sigma_{mn}}\right) \tag{104.410}$$

$$\frac{\partial \psi}{\partial \sigma_{mn}} = -\frac{\xi\lambda_c}{3P_{at}}\left(\frac{p}{P_{at}}\right)^{(\xi-1)}\delta_{mn} \tag{104.411}$$

$$\frac{\partial g}{\partial \sigma_{mn}} = g^2\left(\frac{1-c}{2c}\right)\frac{\partial \cos 3\theta}{\partial \sigma_{mn}} \tag{104.412}$$

$$\frac{\partial \cos 3\theta}{\partial \sigma_{mn}} = -3\sqrt{6}\frac{\partial n_{ij}}{\partial \sigma_{mn}}(n_{jk}n_{ki}) \tag{104.413}$$

$$\frac{\partial A_d}{\partial \sigma_{mn}} = A_0 z_{ab}\frac{\partial n_{ab}}{\partial \sigma_{mn}}\{\overline{z_{ab}n_{ab}}\} \tag{104.414}$$

and define $\{\overline{X}\} = 1$ if $X > 0$, and $\{\overline{X}\} = 0$ if $X \leq 0$.

Analytical expression of $\frac{\partial m_{ij}}{\partial \alpha_{kl}}$:

$$\frac{\partial m_{ij}}{\partial \alpha_{mn}} = B\frac{\partial n_{ij}}{\partial \alpha_{mn}} + n_{ij}\frac{\partial B}{\partial \alpha_{mn}} + C\frac{\partial n_{ik}}{\partial \alpha_{mn}}n_{kj} + (n_{ik}n_{kj} - \frac{1}{3}\delta_{ij})\frac{\partial C}{\partial \alpha_{mn}} + \frac{1}{3}\delta_{ij}\frac{\partial D}{\partial \alpha_{mn}} \tag{104.415}$$

where

$$\frac{\partial n_{ij}}{\partial \alpha_{mn}} = \frac{p}{|\Lambda|}\left(n_{ij}n_{mn} - I^s_{ijmn}\right) \tag{104.416}$$

$$\frac{\partial D}{\partial \alpha_{mn}} = -\frac{\partial A_d}{\partial \alpha_{mn}}\left(\sqrt{\frac{2}{3}}\alpha^d_\theta - \alpha_{ab}n_{ab}\right) - A_d\left(\sqrt{\frac{2}{3}}\frac{\partial \alpha^d_\theta}{\partial \alpha_{mn}} - n_{mn} - \alpha_{ab}\frac{\partial n_{ab}}{\partial \alpha_{mn}}\right) \tag{104.417}$$

and

$$\frac{\partial B}{\partial \alpha_{mn}} = \frac{3}{2}\left(\frac{1-c}{c}\right)\left(\frac{\partial g}{\partial \alpha_{mn}}\cos 3\theta + g\frac{\partial \cos 3\theta}{\partial \alpha_{mn}}\right) \tag{104.418}$$

$$\frac{\partial C}{\partial \alpha_{mn}} = 3\sqrt{\frac{3}{2}}\left(\frac{1-c}{c}\right)\frac{\partial \alpha^d_\theta}{\partial \alpha_{mn}} \tag{104.419}$$

$$\frac{\partial \alpha^d_\theta}{\partial \alpha_{mn}} = M_c \exp(n^d\psi)\frac{\partial g}{\partial \alpha_{mn}} \tag{104.420}$$

$$\frac{\partial g}{\partial \alpha_{mn}} = g^2\left(\frac{1-c}{2c}\right)\frac{\partial \cos 3\theta}{\partial \alpha_{mn}} \tag{104.421}$$

$$\frac{\partial \cos 3\theta}{\partial \alpha_{mn}} = -3\sqrt{6}\frac{\partial n_{ij}}{\partial \alpha_{mn}}(n_{jk}n_{ki}) \tag{104.422}$$

$$\frac{\partial A_d}{\partial \alpha_{mn}} = A_0 z_{ab}\frac{\partial n_{ab}}{\partial \alpha_{mn}}\{\overline{z_{ab}n_{ab}}\} \tag{104.423}$$

Analytical expression of $\frac{\partial m_{ij}}{\partial z_{mn}}$:

$$\frac{\partial m_{ij}}{\partial z_{mn}} = \frac{1}{3}\delta_{ij}\frac{\partial D}{\partial z_{mn}} \tag{104.424}$$

where

$$\frac{\partial D}{\partial z_{mn}} = -\frac{\partial A_d}{\partial z_{mn}}\left(\sqrt{\frac{2}{3}}\alpha^d_\theta - \alpha_{ab}n_{ab}\right) \tag{104.425}$$

and

$$\frac{\partial A_d}{\partial z_{mn}} = A_0 n_{mn} \{\overline{z_{ab} n_{ab}}\} \tag{104.426}$$

Analytical expression of $\frac{\partial A_{ij}}{\partial \sigma_{mn}}$:

$$\frac{\partial A_{ij}}{\partial \sigma_{mn}} = \frac{2}{3}\left[\frac{\partial h}{\partial \sigma_{mn}}\left(\sqrt{\frac{2}{3}}\alpha_\theta^b n_{ij} - \alpha_{ij}\right) + \sqrt{\frac{2}{3}} h \left(n_{ij}\frac{\partial \alpha_\theta^b}{\partial \sigma_{mn}} + \alpha_\theta^b \frac{\partial n_{ij}}{\partial \sigma_{mn}}\right)\right] \tag{104.427}$$

where

$$\frac{\partial \alpha_\theta^b}{\partial \sigma_{mn}} = M_c \exp(-n^b \psi)\left(\frac{\partial g}{\partial \sigma_{mn}} - n^b g \frac{\partial \psi}{\partial \sigma_{mn}}\right) \tag{104.428}$$

$$\frac{\partial h}{\partial \sigma_{mn}} = \frac{1}{(\alpha_{ab} - \alpha_{ab}^{in}) n_{ab}}\left[\frac{\partial b_0}{\partial \sigma_{mn}} - h(\alpha_{pq} - \alpha_{pq}^{in})\frac{\partial n_{pq}}{\partial \sigma_{mn}}\right] \tag{104.429}$$

and

$$\frac{\partial b_0}{\partial \sigma_{mn}} = \frac{b_0}{6p}\delta_{mn} \tag{104.430}$$

Analytical expression of $\frac{\partial A_{ij}}{\partial \alpha_{mn}}$:

$$\begin{aligned}\frac{\partial A_{ij}}{\partial \alpha_{mn}} = \frac{2}{3}\Bigg[&\left(\sqrt{\frac{2}{3}}\alpha_\theta^b n_{ij} - \alpha_{ij}\right)\frac{\partial h}{\partial \alpha_{mn}} \\ &+ \sqrt{\frac{2}{3}} h \left(n_{ij}\frac{\partial \alpha_\theta^b}{\partial \alpha_{mn}} + \alpha_\theta^b \frac{\partial n_{ij}}{\partial \alpha_{mn}} - I^s_{ijmn}\right)\Bigg]\end{aligned} \tag{104.431}$$

where

$$\frac{\partial \alpha_\theta^b}{\partial \alpha_{mn}} = M_c \exp(-n^b \psi)\frac{\partial g}{\partial \alpha_{mn}} \tag{104.432}$$

$$\frac{\partial h}{\partial \alpha_{mn}} = -\frac{h}{(\alpha_{ab} - \alpha_{ab}^{in}) n_{ab}}\left[n_{mn} + (\alpha_{pq} - \alpha_{pq}^{in})\frac{\partial n_{pq}}{\partial \alpha_{mn}}\right] \tag{104.433}$$

Analytical expression of $\frac{\partial A_{ij}}{\partial z_{mn}}$:

$$\frac{\partial A_{ij}}{\partial z_{mn}} = \emptyset \tag{104.434}$$

Analytical expression of $\frac{\partial Z_{ij}}{\partial \sigma_{mn}}$:

$$\frac{\partial Z_{ij}}{\partial \sigma_{mn}} = -c_z \left[(z_{max} n_{ij} + z_{ij}) \frac{\partial D}{\partial \sigma_{mn}} + z_{max} D \frac{\partial n_{ij}}{\partial \sigma_{mn}} \right] \{\overline{D}\} \tag{104.435}$$

Analytical expression of $\frac{\partial Z_{ij}}{\partial \alpha_{mn}}$:

$$\frac{\partial Z_{ij}}{\partial \alpha_{mn}} = -c_z \left[(z_{max} n_{ij} + z_{ij}) \frac{\partial D}{\partial \alpha_{mn}} + z_{max} D \frac{\partial n_{ij}}{\partial \alpha_{mn}} \right] \{\overline{D}\} \tag{104.436}$$

Analytical expression of $\frac{\partial Z_{ij}}{\partial z_{mn}}$:

$$\frac{\partial Z_{ij}}{\partial z_{mn}} = -c_z \left(D I^s_{ijmn} + z_{max} n_{ij} \frac{\partial D}{\partial z_{mn}} \right) \{\overline{D}\} \tag{104.437}$$

104.6.12 SaniSand2008 (aka SANISAND) Model

Taiebat and Dafalias (2008)

104.6.13 SANICLAY Model

Dafalias et al. (2006)

104.6.14 G/G_{max} Modeling

Modeling of stiffness reduction using G/G_{max} curves is frequently used. It is important to note that such modeling is essentially using linear elastic stiffness, reduced stiffness, secant stiffness to model an inelastic, nonlinear process. As such, some important simplifying assumptions are made. As noted by Pecker et al. (2022), using G/G_{max} models is appropriate if certain conditions are met, as shown in Figure 104.13.

104.6.15 Pisanò Elastic-Plastic Model with Vanishing Elastic Region (for G/G_{max} Modeling)

A more recent description of this model is available by Pisanò and Jeremić (2014).

Modeling the mechanical behavior of soils under cyclic/dynamic loading is crucial in most Geotechnical Earthquake Engineering (GEE) applications, including site response analysis and soil structure interaction (SSI) problems. In the last decades, a number of experimental studies (Ishihara, 1996; di Prisco and Wood, 2012) pointed out the complexity of such behavior – especially in the presence of pore

CYCLIC SHEAR STRAIN AMPLITUDE γ		BEHAVIOUR	ELASTICITY and PLASTICIY	CYCLIC DEGRADATION in STAURATED SOILS	MODELLING
Very small	$0 \le \gamma \le \gamma_s$	Practically linear	Practically elastic	Non degradable	Linear elastic
Small	$\gamma_s \le \gamma \le \gamma_v$	Non-linear	Moderately elasto-plastic	Practically non-degradable	Viscoelastic Equivalent linear
Moderate to large	$\gamma_v \le \gamma$	Non-linear	Elasto-plastic	Degradable	Non-linear

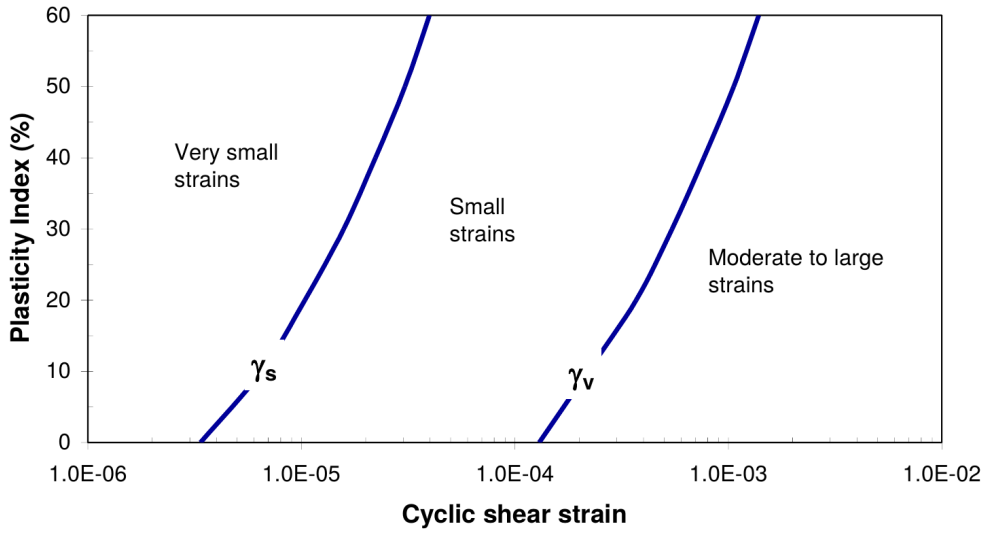

Figure 104.13: Pecker thresholds for G/G_{max} modeling.

fluid(s) – characterized by non-linearity, irreversibility, anisotropy, barotropy, picnotropy, rate-sensitivity, etc. In principle, a comprehensive soil model should be capable of reproducing all the aspects of the mechanical response for any loading condition, as well as predicting the occurrence of liquefaction and cyclic mobility, distinguishing the conditions for shakedown or ratcheting under repeated loads and so forth. However, such an ideal model would probably require too many data for calibration, along with a cumbersome numerical treatment.

Traditionally, many GEE problems are still tackled in the frequency domain through 1D (equivalent) linear models, mainly because of their computational convenience and straightforward calibration. In the light of a Kelvin-Voigt visco-elastic idealization, the dynamic soil behavior is fully described in terms of strain-dependent stiffness degradation (G/G_{max}) and damping (ζ) ratios (Kramer, 1996a). As it holds in

the linear regime, the shear and the volumetric responses are assumed to be decoupled, so that G/G_{max} and ζ curves are derived from the experimental cyclic shear tests (triaxial, simple shear or torsional) as a function of the cyclic shear strain amplitude.

Owing to the availability of computer programs for 1D site response analysis (SHAKE (Schnabel et al., 1972), EERA (Bardet et al., 2000), DEEPSOIL (Hashash and Park, 2001)) and SSI problems (SASSI (Lysmer, 1988)), the visco-elastic approach has become more and more popular among practitioners, regardless of drawbacks:

- despite a non-negligible rate-sensitiveness, most energy dissipation in soils derives from frictional inter-granular mechanisms rather than viscous flow (as it is implicitly assumed by using G/G^{max} and damping approaches);
- G/G_{max} and ζ curves do not allow to evaluate irreversible deformations, nor the influence of pore fluid(s);
- adopting 1D shear constitutive relationships has poor mechanical soundness, since soil behavior exhibits a pronounced deviatoric-volumetric multiaxial coupling;
- the meaning of cyclic shear strain amplitude for the choice of G/G_{max} and ζ values is not evident in the presence of irregular seismic loads.

The above observations justify the need for alternative approaches and more physically consistent soil models. From this standpoint, the incremental elastic-plastic theory represents the main modeling framework, within which significant efforts have been spent in the last decades to simulate the response of cyclically loaded soils. Several approaches have been explored and gradually refined, including e.g. "multi-surface plasticity", "bounding surface plasticity", "generalized plasticity" and "hypoplasticity". Comprehensive overviews on cyclic elasto-plasticity modeling can be found in Lemaitre and Chaboche (1990) and, with specific reference to soils, Prevost and Popescu (1996), Zienkiewicz et al. (1999b) and di Prisco and Wood (2012). In most cases, rotational kinematic hardening formulations have been adopted in conjunction with increasingly accurate flow rules and hardening laws; a number of valuable contributions are worth citing, such as – to mention only a few – Mróz et al. (1978); Prevost (1985a); Borja and Amies (1994); Manzari and Dafalias (1997); Papadimitriou and Bouckovalas (2002); Elgamal et al. (2002); Taiebat and Dafalias (2008); recently, it has been also shown how a good simulation of dynamic properties can be achieved by means of even elastic-perfectly plastic models, as long as formulated in a probabilistic elastic-plastic framework (Sett et al., 2011b). The major issues about the practical use of elastic-plastic models concern the complexity of the mathematical formulations, the computer implementation and the possible high number of material parameters. For a model to appeal

to practicing engineers, a tradeoff is needed between the overall accuracy and the number of parameters to be calibrated, particularly provided the frequent lack of detailed *in situ* or laboratory data.

Among the aforementioned models, the one by Borja and Amies (1994) is here taken into special consideration. These authors proposed a total-stress von Mises-type model in the framework of kinematic-hardening bounding surface plasticity, then successfully applied to the seismic simulation of fine-grained deposits at Lotung site in Taiwan (Borja et al., 1999, 2000). Based on work by Dafalias and Popov (1977) and Dafalias (1979), the multiaxial model is characterized by the assumption of vanishing elastic domain, thus implying soil plastification under any load level and a redefinition of the standard loading/unloading criterion. Apart from the mathematical aspects, the model possesses sufficient flexibility to reproduce the undrained dynamic properties of clayey/silty soils, while keeping a minimum number of physically-based parameters.

In this paper similar bounding surface approach with vanishing elastic region is adopted to derive a Drucker-Prager effective-stress model, incorporating pressure sensitivity and non-associativeness, essential ingredients for material modeling of granular materials. As a result, the following constitutive relationship is suitable for the effective-stress time-domain analysis of even liquefiable soils. In addition, the dissipative model performance is here explored in combination with a further viscous mechanism, which can be wisely exploited to improve the simulation of the experimental damping. Although numerical convenience often motivates the embedment of viscous dissipation into elastic-plastic computations, it has a *de facto* physical origin, coming from rate-dependent processes occurring at both inter-granular contacts and grain/pore fluid interfaces.

104.6.15.1 Frictional and viscous dissipative mechanisms

The time-domain finite element (FE) solution of dynamic problems is usually carried out by solving an incremental discrete system of the following form (Bathe, 1982; Zienkiewicz and Taylor, 1991a):

$$\mathbf{M}\Delta\ddot{\mathbf{U}} + \mathbf{C}\Delta\dot{\mathbf{U}} + \mathbf{K}^t\Delta\mathbf{U} = \Delta\mathbf{F}^{ext} \tag{104.438}$$

where Δ and dots stand respectively for step increment and time derivative, $\mathbf{U}$ is the generalized DOF vector (nodal displacement for example), $\mathbf{F}^{ext}$ the nodal external force vector and $\mathbf{M}$, $\mathbf{C}$, $\mathbf{K}^t$ are the mass, damping and (tangent) stiffness matrices, respectively.

In system (104.438) two dissipative sources are readily recognizable, namely the viscous (velocity-proportional) and the frictional (displacement-proportional) terms (Argyris and Mlejnek, 1991). While the latter is given by the variation of the elastic-plastic tangent stiffness $\mathbf{K}^t$, the viscous term related to the damping matrix $\mathbf{C}$ can represent interaction of solid skeleton and pore fluid, and constitutive time-sensitiveness of the soil skeleton. The above combination of frictional and viscous dissipation can

be interpreted in terms of two distinct effective stress components acting on the soil skeleton:

$$\sigma_{ij} = \sigma^{f}_{ij} + \sigma^{v}_{ij} \tag{104.439}$$

where the effective stress tensor σ_{ij} has been split into frictional (elastic-plastic) and viscous stresses[66]. From a rheological point of view, the resulting scheme can be defined as visco-elastic-plastic – not elastic-viscoplastic – as the elastic-plastic response is rate-independent and accompanied by a parallel viscous resisting mechanism. In what follows, the frictional component is first specified via the formulation of the bounding surface model with vanishing elastic domain; then, the role and the calibration of the linear viscous term is discussed.

Index tensor notation is used, along with the standard Einstein convention for repeated indices; the norm of any second-order tensor x_{ij} is defined as $\|x_{ij}\| = \sqrt{x_{ij}x_{ij}}$, whereas the deviatoric component can be extracted as $x^{dev}_{ij} = x_{ij} - x_{kk}\delta_{ij}/3$ (δ_{ij} is the Kronecker delta). In accordance with usual Solid Mechanics conventions, positive tensile stresses/strains are considered, whereas – as is done in Fluid Mechanics – only the isotropic mean pressure is positive if compressive.

104.6.15.2 Bounding surface frictional model with vanishing elastic domain

The formulated constitutive model represents the frictional effective-stress version of the previous work by Borja and Amies (1994); for the sake of clarity, the presentation sequence of the former publication is here maintained, highlighting both differences and similarities. As was expected, the introduction of pressure-dependence into the constitutive equations implies somewhat more involved derivations, so that the analytical details skipped in this section are reported toward the end in section 104.6.15.7; the superscript f referring to the frictional component of the global effective stress (Equation (104.439)) is avoided for the sake of brevity.

Elastic relationship Provided the usual additive (incremental) strain split into elastic and plastic components $d\epsilon_{ij} = d\epsilon^{e}_{ij} + d\epsilon^{p}_{ij}$, the incremental linear elastic Hooke's law is expressed as follows:

$$d\sigma_{ij} = D^{e}_{ijhk}\left(d\epsilon_{hk} - d\epsilon^{p}_{hk}\right) \tag{104.440}$$

where d stands for a differentially small increment of strain and D^{e}_{ijhk} is the fourth-order elastic stiffness tensor. Under the elastic deviatoric/volumetric decoupling, the deviatoric and volumetric counterparts of Equation (104.440) can be also given:

$$ds_{ij} = 2G_{max}\left(de_{hk} - de^{p}_{hk}\right) \tag{104.441}$$

[66] Henceforth, effective stresses are exclusively accounted for

$$dp = -K\left(d\epsilon_{vol} - d\epsilon^{p}_{vol}\right) \tag{104.442}$$

in which $p = -\sigma_{kk}/3$ is the mean stress, $\epsilon_{vol} = \epsilon_{kk}$ is the volumetric strain, $s_{ij} = \sigma^{dev}_{ij}$ is the stress deviator, and $e_{ij} = \epsilon^{dev}_{ij}$ is the strain deviator. The shear modulus $G_{max} = E/2\,(1+\nu)$ and the bulk modulus $K = E/3\,(1-2\nu)$ are derived from the Young modulus E and the Poisson's ratio ν. Henceforth, G_{max} will be always used for the elastic small-strain shear modulus, whereas the secant cyclic shear stiffness will be referred to as G.

Drucker-Prager yield and bounding loci A conical Drucker-Prager type yield locus is first introduced, similar to what is used by Prevost (1985a) and Manzari and Dafalias (1997):

$$f_y = \frac{3}{2}\left(s_{ij} - p\alpha_{ij}\right)\left(s_{ij} - p\alpha_{ij}\right) - k^2p^2 = 0 \tag{104.443}$$

where α_{ij} is the so called deviatoric back-stress ratio ($\alpha_{kk} = 0$) governing the kinematic hardening of the yield surface; k is a parameter determining the opening angle of the cone. It is also important to note that the variation of the back-stress ratio α_{ij} in (104.443) determines a rigid rotation of the yield locus and, therefore, a rotational kinematic hardening.

The stress derivative of the yield function is also reported for the following developments:

$$\frac{\partial f_y}{\partial \sigma_{ij}} = \left(\frac{\partial f_y}{\partial \sigma_{ij}}\right)^{dev} + \left(\frac{\partial f_y}{\partial \sigma_{ij}}\right)^{vol} = 3\left(s_{ij} - p\alpha_{ij}\right) + \left[\alpha_{hk}\left(s_{hk} - p\alpha_{hk}\right) + \frac{2}{3}k^2p\right]\delta_{ij} \tag{104.444}$$

The yield locus must always reside within the so called bounding surface, here assumed to be a further Drucker-Prager cone (non kinematically hardening, fixed in size):

$$f_B = \frac{3}{2}s_{ij}s_{ij} - M^2p^2 = 0 \tag{104.445}$$

where M provides the bounding cone opening and, as a consequence, the material shear strength (as a function of the mean effective pressure p).

Plastic flow and translation rule When dealing with granular materials, a non-associated plastic flow rule is needed (Nova and Wood, 1979), allowing for plastic contractancy or dilatancy depending on whether loose or dense materials are analyzed. Here, the plastic flow rule is borrowed from Manzari and Dafalias (1997):

$$d\epsilon^{p}_{hk} = d\lambda \left(n^{dev}_{ij} - \frac{1}{3} D \delta_{ij} \right) \tag{104.446}$$

where $d\lambda$ is the plastic multiplier, n^{dev}_{ij} is a deviatoric unit tensor ($\|n^{dev}_{ij}\| = 1$) and D is a dilatancy coefficient defined as (Manzari and Dafalias, 1997):

$$D = \xi \left(\alpha^{d}_{ij} - \alpha_{ij} \right) n^{dev}_{ij} = \xi \left(\sqrt{\frac{2}{3}} k_d n^{dev}_{ij} - \alpha_{ij} \right) n^{dev}_{ij} \tag{104.447}$$

in which ξ and k_d are two positive constitutive parameters. While the former controls the amount of volumetric plastic strain, the latter determines the position of the so called "dilatancy surface" and rules the transition from contractive ($D > 0$) to dilative ($D < 0$) behavior.

The kinematic hardening evolution of the yield locus is imposed via the standard Prager translation rule for the (deviatoric) back-stress ratio (Borja and Amies, 1994):

$$d\alpha_{ij} = \|d\alpha_{ij}\| n^{dev}_{ij} \tag{104.448}$$

with both n^{dev}_{ij} and the norm $\|d\alpha_{ij}\|$ to be determined.

Vanishing elastic region and consistency condition As previously mentioned, the most notable feature of the present model concerns the vanishing elastic domain, corresponding with the limit $k \to 0$ in Equation (104.443). Accordingly, the Drucker-Prager cone reduces to its symmetry axis, so that:

$$\lim_{k \to 0} f_y = 0 \Rightarrow \lim_{k \to 0} s_{ij} = p\alpha_{ij} \Rightarrow ds_{ij} = d\alpha_{ij} p + \alpha_{ij} dp \tag{104.449}$$

and, after substituting the Prager rule (104.448) (for more detailed derivation, see section 104.6.15.7):

$$n^{dev}_{ij} = \frac{ds_{ij} - \alpha_{ij} dp}{\|ds_{ij} - \alpha_{ij} dp\|} \tag{104.450}$$

The direction of the deviatoric plastic strain increment n^{dev}_{ij} depends on the variation of both the stress deviator and the mean pressure, which differs from the cohesive version by Borja and Amies (1994). It is also worth noting that purely hydrostatic stress increments ($ds_{ij} = 0$) from initial hydrostatic states ($\alpha_{ij} = 0$) yield $n^{dev}_{ij} = 0$ and thus generates no deviatoric plastic strains.

From a theoretical standpoint, since the direction of the deviatoric plastic strain increment n^{dev}_{ij} depends on $d\sigma_{ij}$, the resulting constitutive formulation can be properly defined as "hypoplastic", this being a spontaneous outcome of the limit operation applied on the elastic region (Dafalias, 1986).

The norm of the back-stress increment in Equation (104.448) is obtained by imposing the standard consistency condition, that is the fulfillment of $df_y = 0$ during plastic loading (section 104.6.15.7):

$$df_y = 0 \Leftrightarrow \frac{\partial f}{\partial \sigma_{ij}} d\sigma_{ij} + \frac{\partial f}{\partial \alpha_{ij}} d\alpha_{ij} = 0 \tag{104.451}$$

whence:

$$\|d\alpha_{ij}\| = \frac{1}{pN^{dev}} \frac{\partial f}{\partial \sigma_{ij}} d\sigma_{ij} \tag{104.452}$$

and $N^{dev} = \| \left(\partial f_y / \partial \sigma_{ij}\right)^{dev} \| = 3\|s_{ij} - p\alpha_{ij}\|$. From Equation (104.452), the norm of $d\alpha_{ij}$ can be further specified for the case of radial loading paths in the deviatoric plane, characterized by the nullity of dp and the coaxiality of s_{ij}, α_{ij} and their increments. After simple manipulations (see section 104.6.15.7) this results in:

$$\|d\alpha_{ij}\| = \sqrt{\frac{2}{3}} \frac{dq}{p} \tag{104.453}$$

where $q = \sqrt{3/2}\|s_{ij}\|$ stands for the usual deviatoric stress invariant.

Hardening relationship and plastic multiplier An incremental hardening relationship is directly established (Borja and Amies, 1994):

$$dq = \sqrt{\frac{2}{3}} H \|de^p_{ij}\| \tag{104.454}$$

where H is the hardening modulus. Then, the substitution of both the flow rule (104.446) and the hardening relationship (104.454) into (104.453) leads to:

$$\|d\alpha_{ij}\| = \frac{2}{3} \frac{Hd\lambda}{p} \tag{104.455}$$

By equaling the right–hand sides of Equations (104.441) and (104.449) the following relationship is obtained:

$$2G_{max} \left(de_{ij} - d\lambda n^{dev}_{ij}\right) = \|d\alpha_{ij}\| n^{dev}_{ij} p + \alpha_{ij} dp = \frac{2}{3} \frac{Hd\lambda}{p} n^{dev}_{ij} p - \alpha_{ij} K \left(d\epsilon_{vol} + d\lambda D\right) \tag{104.456}$$

whence:

$$d\lambda = \frac{2G_{max}\|de_{ij}\| + Kd\epsilon_{vol}\alpha_{ij}n_{ij}^{dev}}{2G + \frac{2}{3}H - KD\alpha_{ij}n_{ij}^{dev}} \tag{104.457}$$

Equation (104.457) represents the consistent "frictional" generalization of Equation (18) in Borja and Amies (1994), as well as the limit of Equation (12) in Manzari and Dafalias (1997)[67] for a vanishing yield locus size.

Stress projection, hardening modulus and unloading criterion The bounding surface plasticity theory relies on the basic concept that the plastic modulus explicitly depends on the distance between the current stress state and an *ad hoc* stress projection onto the bounding surface. While Borja and Amies (1994) defined a purely deviatoric projection operator, here the whole stress state is involved:

$$\bar{\sigma}_{ij} = \sigma_{ij} + \beta\left(\sigma_{ij} - \sigma_{ij}^{0}\right) \tag{104.458}$$

where β is a scalar distance coefficient and σ_{ij}^{0} embodies the stress state at the last stress reversal (Figure 104.14). The coefficient β must be such that the projected stress $\bar{\sigma}_{ij}$ lies on the bounding surface (Equation (104.445)):

$$\frac{3}{2}\bar{s}_{ij}\bar{s}_{ij} = M^2\bar{p}^2 \tag{104.459}$$

whence, after substituting (104.458) into (104.459), β can be obtained as the positive root of the following second-order algebraic equation:

$$\begin{aligned}\left[\left\|s_{ij} - s_{ij}^{0}\right\|^2 - \frac{2}{3}M^2\left(p - p_0\right)^2\right]\beta^2 + \\ 2\left[\left(s_{ij} - s_{ij}^{0}\right)s_{ij} - \frac{2}{3}M^2 p\left(p - p_0\right)\right]\beta + \\ \left[\|s_{ij}\|^2 - \frac{2}{3}M^2p^2\right] = 0\end{aligned} \tag{104.460}$$

Apparently, the limit situations $\beta = 0$ and $\beta \to \infty$ correspond with the current stress state being right on the bounding locus or at instantaneous unloading (stress reversal).

In principle, any analytical relationship can be adopted to relate H and β, as long as two fundamental requirements are satisfied, i.e. $H(\beta = 0) = 0$ and $H(\beta \to \infty) \to \infty$: the former ensures the material shear strength to be fully mobilized when the bounding surface is attained; the latter guarantees an

[67] Different signs result because of the opposite sign conventions adopted by these authors

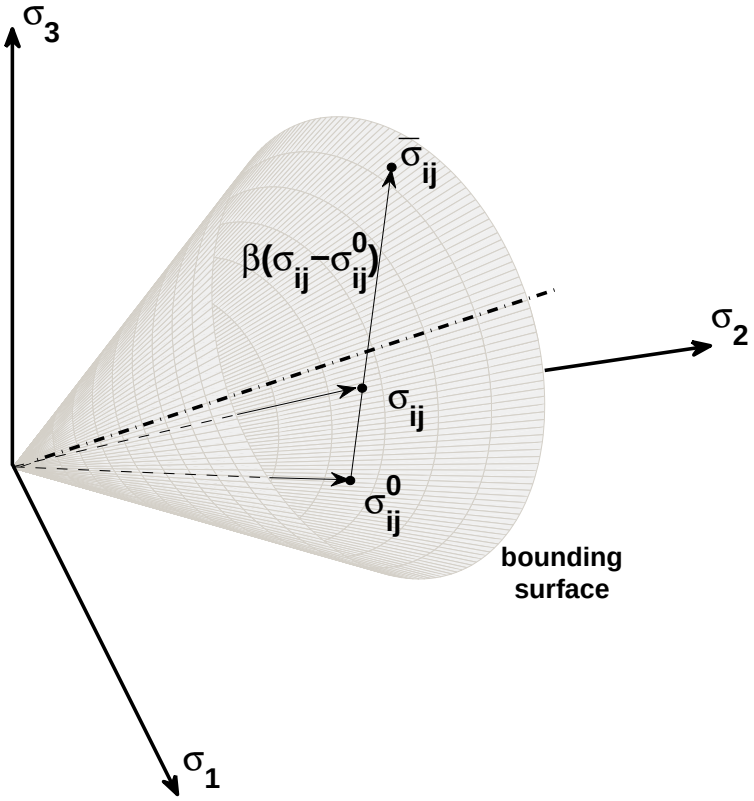

Figure 104.14: Representation of the stress projection onto the bounding surface.

instantaneous elastic stiffness upon any stress reversal, as is explained next. In this case, the expression by Borja and Amies (1994) has been extended to frictional media by accounting for the influence of the mean pressure:

$$H = ph\beta^m \tag{104.461}$$

in which h and m are two additional constitutive parameters.

The last element of the model formulation is the unloading criterion, which in this case is ill-defined due to the lack of the elastic region and the yield surface. The same multiaxial unloading criterion suggested by Borja and Amies (1994) is employed, based on the observation that the hardening modulus H increases at the onset of unloading. Accordingly, as long as $H(\beta)$ is a monotonically increasing function, instantaneous unloading is assumed to occur whenever $dH > 0$, i.e. $d\beta > 0$. The variation of β (and thus its sign) can be readily derived by substituting (104.458) into (104.459), and then

differentiating the latter with respect to β:

$$d\beta = -(1+\beta)\frac{\bar{s}_{ij}ds_{ij} - \frac{2}{3}M^2\bar{p}dp}{\bar{s}_{ij}\left(s_{ij}-s^0_{ij}\right) - \frac{2}{3}M^2\bar{p}\left(p-p^0\right)} > 0 \tag{104.462}$$

It is worth noting that the variation of β, $d\beta$, plays here the same role of the scalar product $\left(\partial f/\sigma_{ij}\right)d\sigma_{ij}$ in standard elastic-plastic models, i.e. it defines the alternatives of elastic-plastic loading ($d\beta < 0$), neutral loading ($d\beta = 0$) or elastic unloading ($d\beta > 0$). The last key point concerns the update of the stress σ^0_{ij} in Equation (104.458), which must be set equal to the current stress state when $d\beta > 0$ is instantaneously found.

Possible refinements The frictional model has been developed trying to keep the number of material parameters as low as possible, even with a non-associated flow rule. However, it is worth mentioning which kind of improvements might be introduced if required by the problem under examination.

It should be first noted that, as a Drucker-Prager type bounding surface has been adopted, the material shear strength is unaffected by the Lode angle, so that for instance the same failure obliquity is predicted for triaxial compression and extension. This drawback could be easily remedied by modifying the deviatoric cross-section of the bounding surface itself, e.g. by adopting the well known Mohr-Coulomb deviatoric locus or other smooth loci (Matsuoka and Nakai, 1974; Willam and Warnke, 1974; Lade, 1977). A change in the deviatoric cross-section would negligibly influence the overall formulation, as just the evaluation of the projection distance β and of its increment should be modified (Equations (104.459)-(104.460) and (104.462)).

Secondly, the present version of the model cannot predict a possible brittle behavior of the soil, usually taking place in the case of dense materials. Constitutive brittleness could be accounted for by incorporating a further isotropic hardening mechanism at the bounding surface level, allowing for a gradual shrinkage of the outer surface during plastifications.

Another relevant point is about the fact that different parameters must be calibrated for different relative densities of the same granular material, as if distinct materials were indeed considered. As a matter of fact, continuous transitions from loose to dense states (and vice versa) spontaneously take place during straining: this aspect has been successfully addressed and reproduced via the concept of "state parameter" (Been and Jefferies, 1985; Wood et al., 1994; Manzari and Dafalias, 1997), which could be also introduced into a critical-state version of the proposed model.

The above and further refinements – related for instance to non-linear elastic behavior, anisotropy, fabric effects, delayed plastic response, etc. – might result in a more accurate soil model, implying though higher difficulties in terms of calibration, implementation and, as a consequence, practical employment.

104.6.15.3 The role of linear viscous damping

An additional viscous mechanism (Equation (104.439)) can be usually exploited in finite element (FE) analysis, even though it is not directly included in the constitutive model. Indeed, many numerical codes solve discrete systems with a viscous damping term (Equation (104.438)), usually assembled as a linear combination of the mass and the (elastic) stiffness matrices (Rayleigh formulation (Argyris and Mlejnek, 1991; Chopra, 2000)):

$$\mathbf{C} = a_0\mathbf{M} + a_1\mathbf{K}^e \tag{104.463}$$

where a_0 and a_1 are two constant parameters, related to the n^{th} modal damping ratio ζ_n of the discrete structural system.

It could be easily shown that a constitutive viscosity of the form:

$$\sigma^v_{ij} = D^v_{ijhk}\dot{\epsilon}_{hk} \tag{104.464}$$

gives rise to a stiffness-proportional damping matrix, which can be equivalently reproduced through the following calibration of the Rayleigh damping parameters (Borja et al., 2000; Hashash and Park, 2002):

$$a_0 = 0 \qquad a_1 = \frac{2\zeta_0}{\omega} \tag{104.465}$$

The calibration (104.465) establishes the same ratio between tangential/bulk elastic and the viscous moduli, that is $G^e_{max}/G^v_{max} = K^e/K^v$. More importantly, a damping ratio ζ_0 is ensured for a given circular frequency ω, as long as the parallel resisting mechanism (σ^f_{ij}) is purely elastic; as a consequence, provided the a_1 value at the beginning of the analysis, modal frequencies and the corresponding damping ratios are linearly related.

It is also worth remarking some further points about the implications of linear viscous damping in conjunction with non-linear soil models. If a soil element undergoes an imposed shear strain history, the overall shear stress/strain cycles $\tau - \gamma$ differ from the purely frictional component $\tau^f - \gamma$, this difference being due to the viscous shear stress τ^v. As will be shown in next section, the viscous component implies smoother cycles and avoid the sharp transitions at stress reversal usually exhibited by purely elastic-plastic responses (Borja et al., 2000). However, the overall G/G_{max} ratio between the average cyclic stiffness and the elastic shear modulus is unaffected by viscosity.

As far as the damping ratio is concerned, its standard definition (Kramer, 1996a) can be easily adapted to point out the frictional/viscous splitting of the energy ΔW dissipated in a loading cycle:

$$\zeta = \frac{\Delta W}{2\pi G \gamma_{max}^2} = \frac{\Delta W^f + \Delta W^v}{2\pi G \gamma_{max}^2} = \zeta^f + \zeta^v \tag{104.466}$$

where γ_{max} is the imposed cyclic shear strain amplitude and G the corresponding (secant) cyclic shear stiffness. As γ_{max} approaches zero, the plastic dissipation tends to zero as well, so that $\zeta = \zeta^v$; therefore, the Rayleigh parameter a_1 can be calibrated to obtain $\zeta(\gamma_{max} \to 0) = \zeta_0$ for a given circular frequency ω (see Equation (104.465)). This is a desirable feature of the model, as natural soils are well known to dissipate energy at even very small strain amplitudes.

At progressively larger strains, both the frictional and viscous components contribute to the global damping, although the relative quantitative significance is hard to assess *a priori*. In addition, the viscous component of the ζ–γ_{max} curve is not constant, since ζ^v depends on the strain-dependent secant modulus $G(\gamma_{max})$ and, implicitly, on the strain rate. This is different to what has been argued by Borja et al. (2000).

As an example, consider the response of an elastic-perfectly plastic model with additional viscosity under a sinusoidal shear excitation $\gamma(t) = \gamma_{max} \sin(\omega t)$. The simplicity of the elastic-perfectly plastic response allows derivation of instructive analytical formulas for the G/G_{max} and the damping ratios, even in the presence of viscous dissipation. While $\gamma_{max} < \gamma_y$ (yielding shear strain), the material behavior is linear elastic, so that $G/G_{max} = 1$ and ζ equals the purely viscous contribution at $\gamma_{max} = 0$, i.e. $\zeta = \zeta_0$; γ_y depends on the elastic stiffness and the shear strength of the material, $\gamma_y = \tau_{lim}/G_{max}$, where τ_{lim} is the limit (frictional) shear stress for a given confining pressure. For $\gamma_{max} > \gamma_y$ plastifications take place with a flat elastic-perfectly plastic $\tau^f - \gamma$ branch, and the following expressions can be easily derived:

$$\frac{G}{G_{max}} = \frac{\tau_{lim}}{G_{max}\gamma_{max}} \tag{104.467}$$

$$\zeta = \frac{\Delta W^f + \Delta W^v}{2\pi G \gamma_{max}^2} = \underbrace{\frac{2}{\pi}\left(1 - \frac{\tau_{lim}}{G_{max}\gamma_{max}}\right)}_{\zeta^f} + \underbrace{\zeta_0 \frac{G_{max}\gamma_{max}}{\tau_{lim}}}_{\zeta^v} \tag{104.468}$$

In Figure 104.15 the G/G_{max} and ζ ratios are plotted for increasing ζ_0 values. As γ_{max} increases, the frictional damping tends to $2/\pi \approx 0.63$, while the viscous one keeps increasing because of the reduction in the secant stiffness and the increase in the shear strain rate (depending on the strain amplitude). Hence, the value of ζ_0 is to be carefully chosen, in order to avoid excessive dissipation when medium/large strains are induced by the loading process.

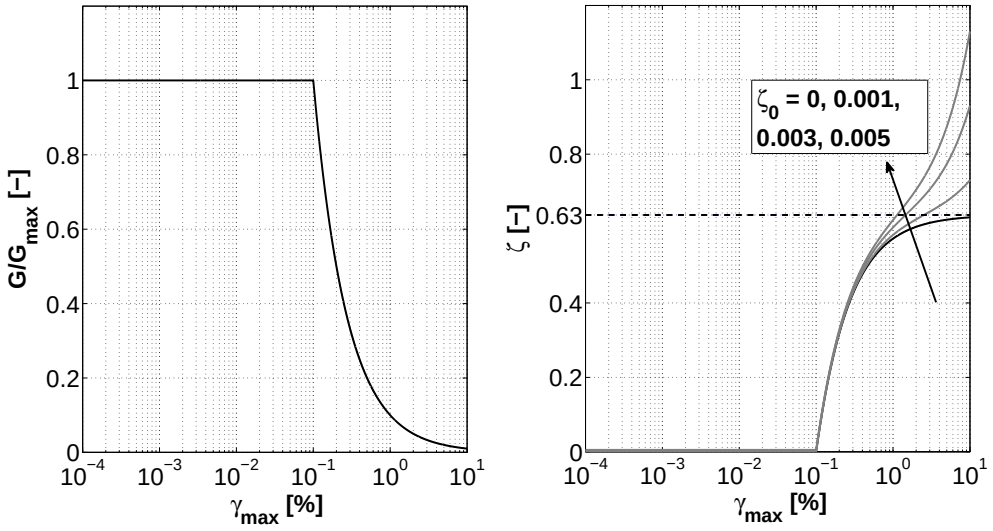

Figure 104.15: G/G_{max} and damping curves for a elastic-perfectly plastic model with linear viscous damping at varying ζ_0 (τ_{lim}=100 kPa, G_{max}=100 MPa)

The fact that the viscous mechanism can modify the purely frictional $\zeta - \gamma_{max}$ curve without altering the cyclic stiffness degradation can be fruitfully exploited to remedy the (frequent) cases in which the experimental-numerical agreement is not satisfactory in terms of energy dissipation properties.

104.6.15.4 Model performance and calibration

The frictional mechanism of the above model is characterized by a rather low number of material parameters, namely the following seven:

- two elastic parameters, the Young modulus E (or the shear modulus G_{max}) and the Poisson's ratio ν;
- the shear strength parameter M for the definition of the bounding surface (Equation (104.445));
- the flow rule parameters, ξ and k_d, governing the increment of the volumetric plastic strain under shearing and the size of the dilatancy surface, respectively (Equation (104.446));
- the hardening parameters h and m for the dependence of the hardening modulus on the distance coefficient β (Equation (104.461)), affecting the pre-failure deformational behavior and, in overall, the resulting dynamic properties (G/G_{max} and damping curves).

Provided a reasonable value for the Poisson's ratio (usually in the range $0.25 - 0.3$), the small-strain elastic stiffness can be evaluated from dynamic laboratory (RC tests) or *in situ* (seismic geophysical

surveys) tests. As far as the shear strength is concerned, the parameter M can be related to the friction angle ϕ as follows:

$$M = \frac{6 \sin \phi}{3 \pm \sin \phi} \tag{104.469}$$

depending on whether triaxial compression (sign – in (104.469)) or extension (sign + in (104.469)) failure conditions are to be reproduced (a change in the deviatoric section of the bounding surface would allow to capture both compressive and extensive limits).

The calibration of the flow rule parameters, ξ and k_d, requires at least a triaxial test to be performed, in order to obtain some information about the volumetric behavior. Figure 104.16 shows the predicted triaxial response for three different values of k_d (and fixed ξ), that is by varying the opening angle of the dilatancy surface (the employed parameters are reported in the figure caption, where p_0 stands for the initial mean pressure).

While the limit stress deviator q is exclusively given by M, the pre-failure behavior is influenced by the plastic deformability and therefore by k_d. The model possesses sufficient flexibility to reproduce contractive, dilative or contractive/dilative behavior; also, such a feature is necessary to reproduce undrained conditions (liquefying and non-liquefying responses), this being a further motivation for non-associativeness when dealing with sandy materials.

Figure 104.17 exemplifies the response predicted under pure shear (PS) cyclic loading, applied as a sinusoidal shear strain history ($\gamma_{max} = 0.2\%, 20\%$, period $T{=}2\pi$ s) at constant normal stresses (and thus constant mean pressure p_0 as well. This corresponds with a radial loading path on the deviatoric plane); for the sake of clarity, the volumetric plastic response has been inhibited ($\xi{=}0$), in order to evaluate the deviatoric mechanism exclusively. Both purely frictional (solid line) and frictional/viscous (dashed line) responses are plotted.

Owing to the kinematic hardening of the vanished yield locus, the model is capable of reproducing both the Bauschinger and the Masing effects, the latter implying the stabilization of the cyclic response to take place after more than one loading cycle. As expected, the additional viscous damping increases the area of the cyclic loop and therefore the overall dissipated energy; however, the effect of the viscous dissipation becomes significant only at medium-high shear strains, corresponding – for a given loading frequency – with higher strain rates. Further, viscosity causes the aforementioned "smoothing" of stress reversals, as it can be readily noticed in Figure 104.18 by comparing the purely frictional and the frictional/viscous responses.

Given the elastic stiffness and the strength of the soil, the shape of the resulting loading cycles is totally governed by the hardening properties, by h and m in Equation (104.461): this directly affects the simulation of experimental G/G_{max} and damping curves, which can be therefore exploited for the

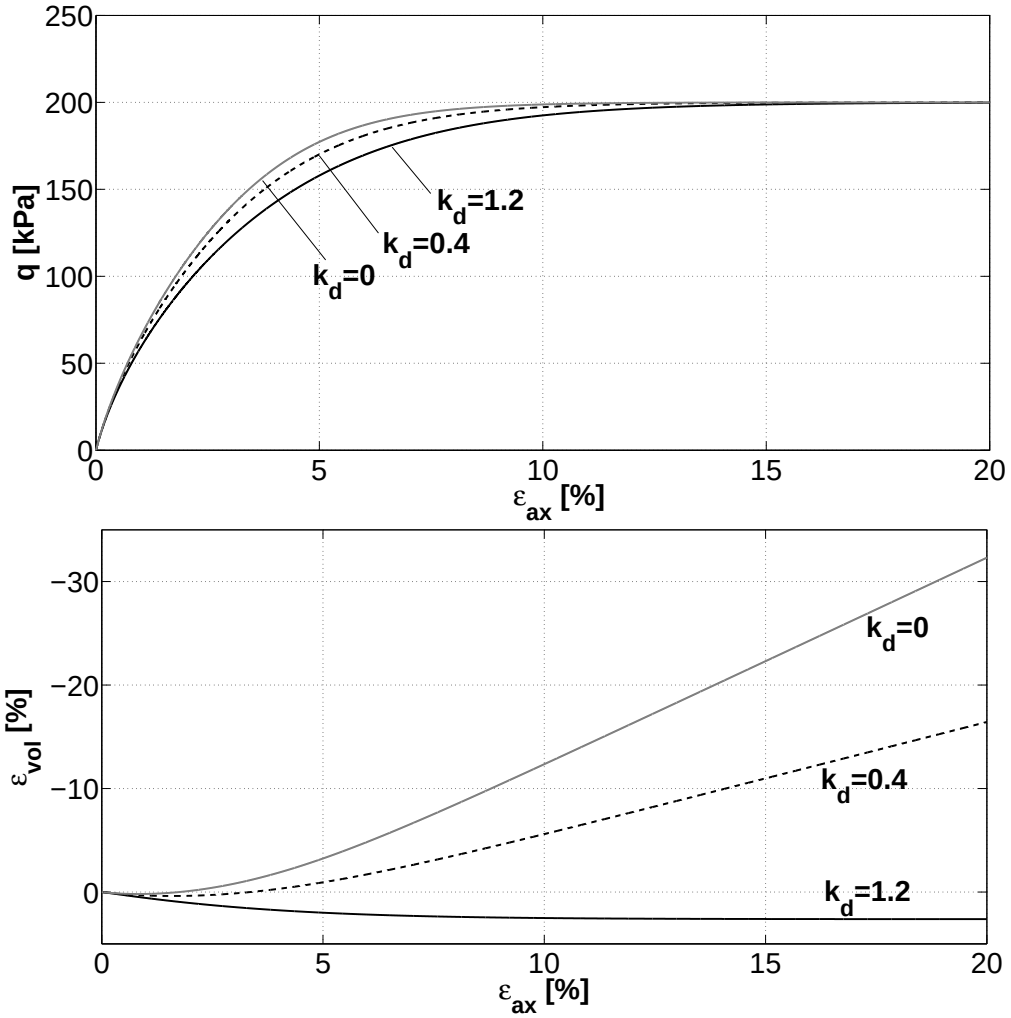

Figure 104.16: Predicted triaxial responses for different dilatancy surfaces (p_0=100 kPa, G_{max} = 4 MPa, ν=0.25, M=1.2, ξ=1, h=$G/(1.5p_0)$, m=1)

calibration of both h and m. As can be easily demonstrated (the proof is given in section 104.6.15.7), the following equality holds under PS loading conditions, i.e. under constant pressure shearing:

$$1 = \frac{G}{G_{max}} \left[1 + \frac{6G_{max}}{hp_0\gamma_{max}} \int_0^{\gamma_{max}} \left(\frac{\gamma}{\tau_{lim}/G - 2\gamma + \gamma_{max}} \right)^m d\gamma \right] \tag{104.470}$$

where $\tau_{lim} = Mp_0/\sqrt{3}$. Relationship (104.470) has been obtained by integrating the constitutive equations over the first loading cycle, and represents the frictional counterpart of Equation (6) in Borja et al. (2000) – as is testified by the explicit influence of the confining pressure p_0. The proper use of Equation (104.470) requires first the choice of two meaningful points on the G/G_{max} experimental curve, i.e. two $(\gamma_{max}, G/G_{max})$ couples; then, the unknowns h and m are obtained by solving the integral system arising

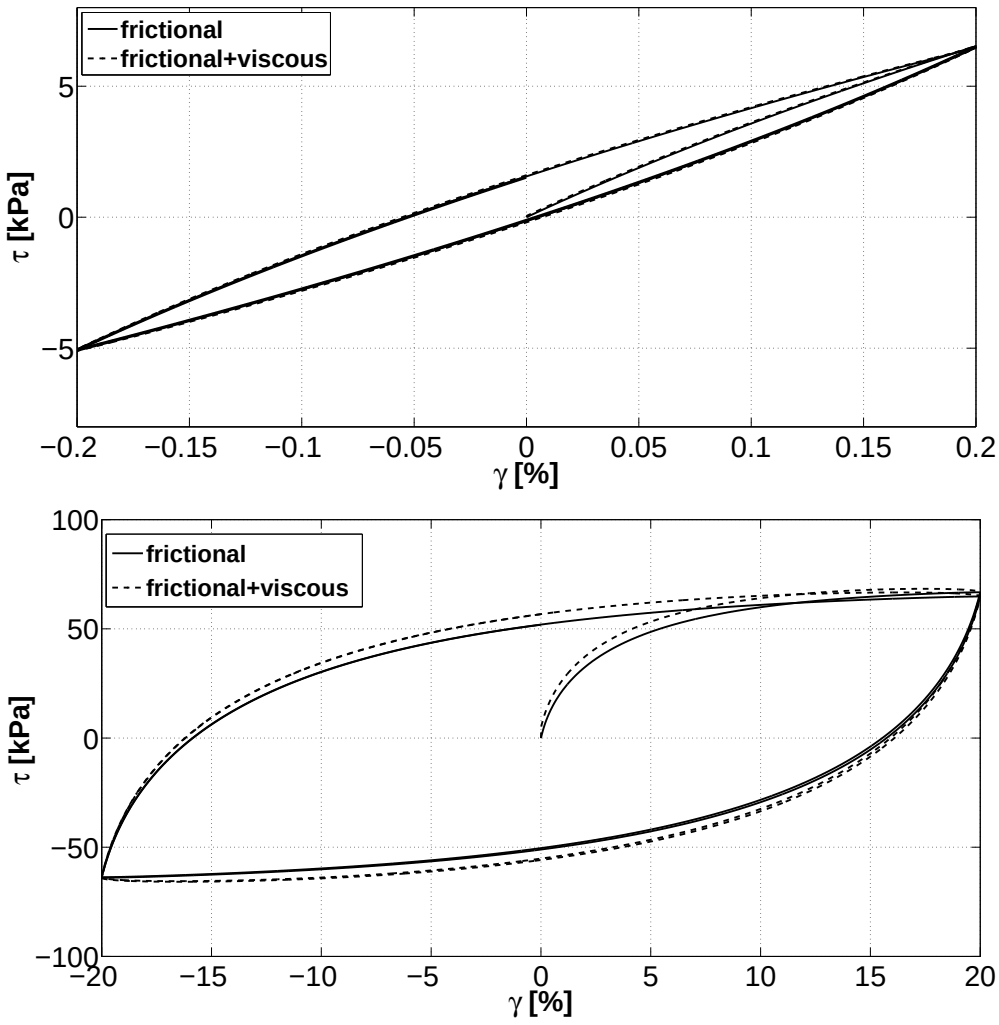

Figure 104.17: Predicted pure shear response at two different shear strain amplitudes (p_0=100 kPa, T=2π s, ζ_0 = 0.003, G_{max}= 4 MPa, ν=0.25, M=1.2, k_d=ξ=0, h=$G/(1.5p_0)$, m=1)

from the specification of Equation (104.470) for both selected $(\gamma_{max}, G/G_{max})$ couples.

Figure 104.19 illustrates the result of the above calibration procedure, applied on the G/G_{max} and ζ curves for sands implemented into the code EERA (Bardet et al., 2000) and formerly obtained by Seed and Idriss (1970b).

Since Equation (104.470) exclusively accounts for the G/G_{max} curve, the very satisfactory agreement in terms of stiffness degradation (viscosity has no effect on it) should not surprise. On the other hand, once h and m are set, the predicted damping curve may or may not match the experimental outcome irrespective of the calibration procedure. In this respect, Figure 104.19 also presents the comparison between the damping curve by Seed and Idriss and the model prediction. The frictional ζ curve lies in the same experimental range, even though the accuracy at γ_{max} = 0.03 – 1% is not as good as for the

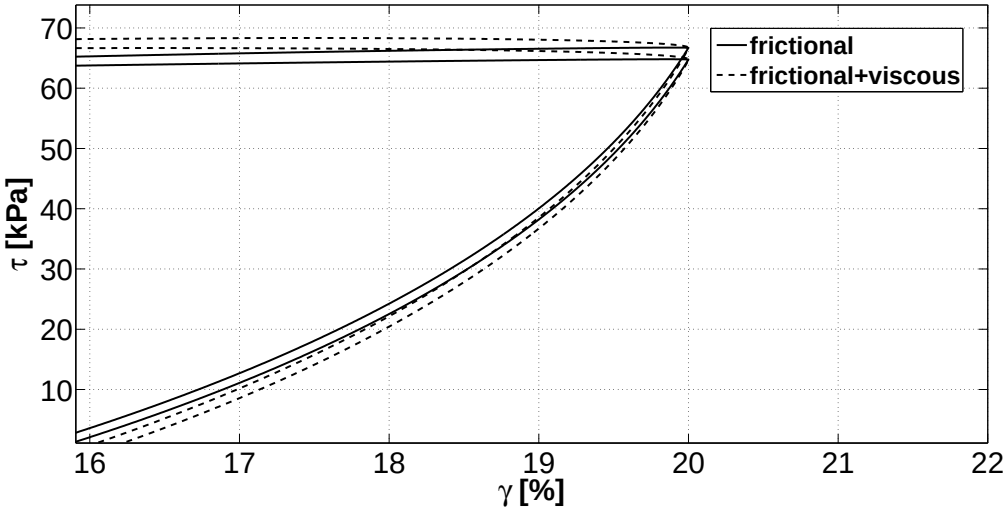

Figure 104.18: Detail of stress reversals for the pure shear response in Figure 104.17 (γ_{max} = 20%)

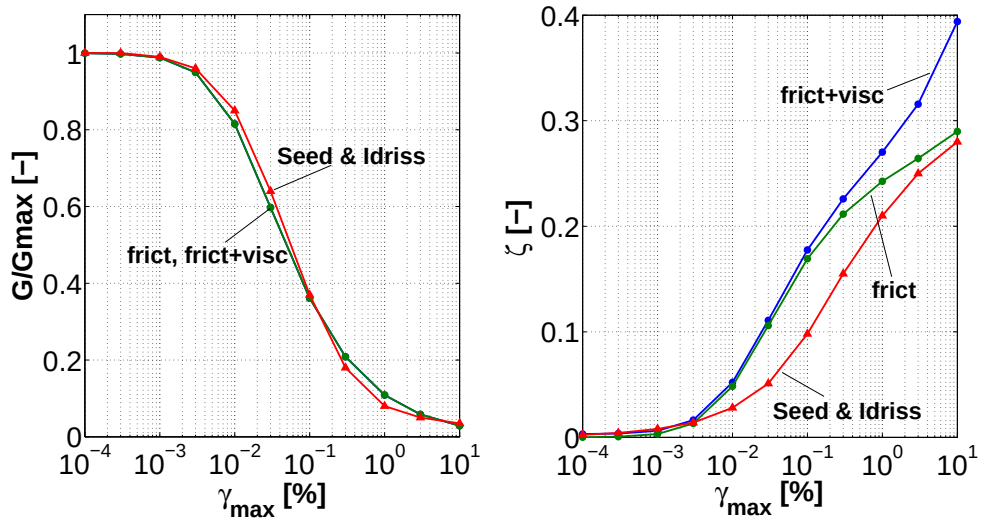

Figure 104.19: Comparison between experimental and simulated G/G_{max} and damping curves (p_0=100 kPa, T=2π s, ζ = 0.003, G_{max} = 4 MPa, ν=0.25, M=1.2, k_d=ξ=0, h=$G/(112p_0)$, m=1.38)

G/G_{max} ratio. In this case, the contribution of the viscous mechanism is practically non-existent, as it only increases the total ζ ratio for $\gamma_{max} > 0.1\%$.

Depending on the specific application, a "trial and error" calibration might be preferable, sacrificing some of the accuracy in terms of G/G_{max} ratio to improve the damping performance. A possible outcome of a manual calibration is plotted in Figure 104.20: apparently, while the simulation of the stiffness curve is still acceptable, the damping curve appears to be much better than the previous one. The use of the viscous mechanism seems to be highly beneficial, since it remedies the lack of accuracy in the frictional

curve at medium/large cyclic strains.

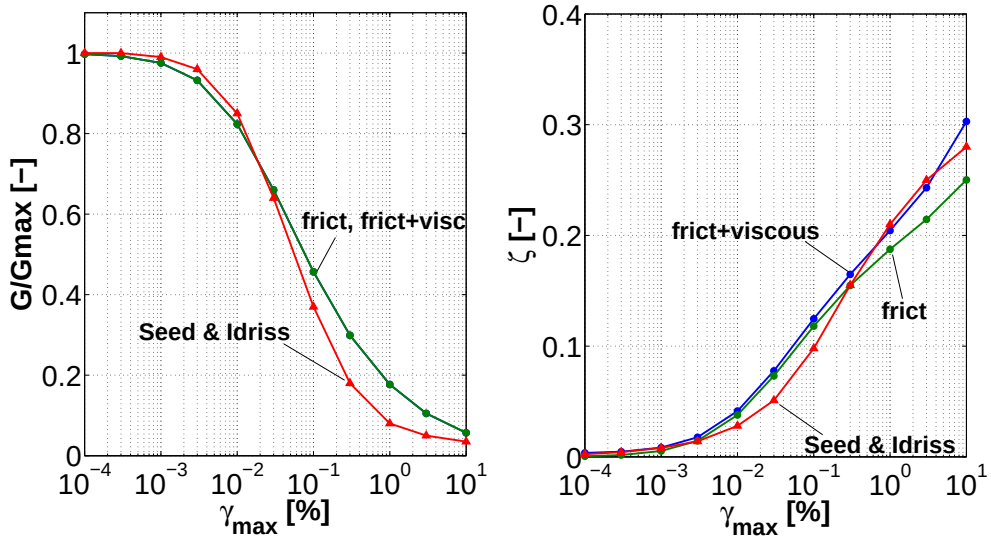

Figure 104.20: Comparison between experimental and simulated G/G_{max} and damping curves (p_0=100 kPa, T=2π s, $\zeta = 0.003$, $G_{max} = 4$ MPa, ν=0.25, M=1.2, k_d=ξ=0, h=$G_{max}/(15p_0)$, m=1)

It is also worth noting that the experimental/numerical agreement is good up to γ_{max} = 10%, this being a rather high cyclic strain level, for equivalent elastic modeling of soil. In fact, even though the interpretation of experimental cyclic tests is questionable when substantial plasticity occurs, the proposed model produces, within a different framework, the same mechanical response incorporated into traditional equivalent-linear approaches. Besides, if the experimental data under examination are unsatisfactorily reproduced for any h and m combination, the user still has the chance of substituting the interpolation function (104.461) with no further changes in the model formulation.

104.6.15.5 Parametric analysis

In this section the sensitivity of the model predictions to some relevant input parameters is parametrically investigated.

Influence of the confining pressure Figure 104.21 illustrates the sensitivity, under PS loading, of both G/G_{max} and damping frictional curves to the initial confining pressure. As can be noticed, increasing p_0 does enlarge the "pseudo-elastic" range, that is the strain interval within which the deviation by the elastic behavior is negligible even with a vanishing yield locus. It is also noted that the variations in the confining pressure do not imply appreciable changes in the shape of the curves.

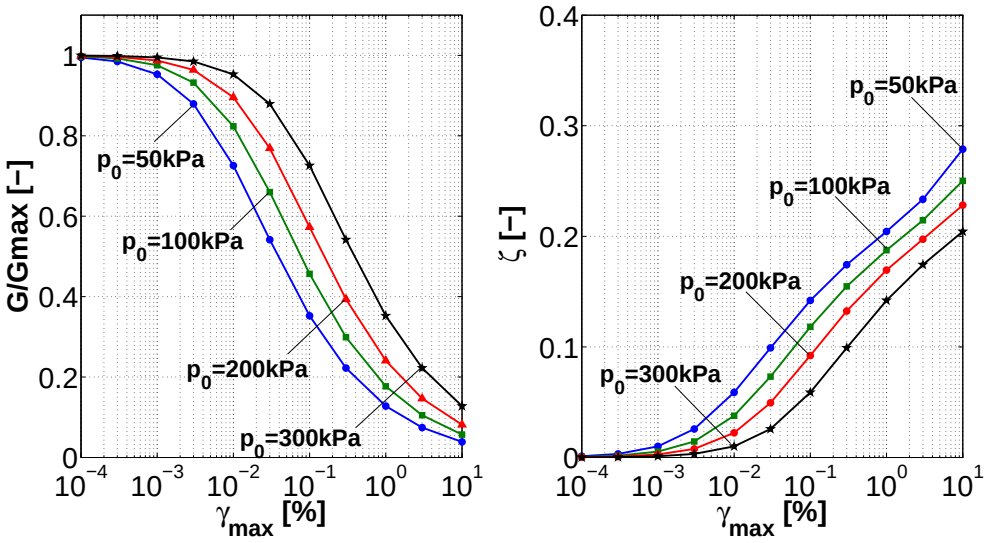

Figure 104.21: Simulated G/G_{max} and damping curves at varying confining pressure (T=2π s, G_{max} = 4 MPa, ν=0.25, M=1.2, k_d=ξ=0, h=$G/(15p_0)$, m=1)

Influence of the hardening parameters Figures 104.22 and 104.23 show the influence of the hardening parameters h and m on the predicted cyclic properties. As the material strain-hardening is accelerated by decreasing either h or m, the pseudo-elastic range tends to disappear, so that $G/G_{max} < 1$ and $\zeta > 0$ at even γ_{max} = 10^{-4}%; conversely, an extended pseudo-elastic behavior can be obtained over a large strain range by increasing the hardening parameters. Apparently, the model ensures high flexibility in terms of cyclic curve shapes, so that the response of standard elastic-plastic models (i.e. with non-vanishing elastic region) can be smoothly approximated (compare for instance the m = 3 curves in Figure 104.23 and the analytical elastic-perfectly plastic frictional curves in Figure 104.15).

Influence of the viscous mechanism The influence of the viscous parameter ζ_0 on the resulting frictional/viscous damping curve is illustrated in Figure 104.24 (the G/G_{max} is not affected by the parallel viscous mechanism). As was expected, an increase in ζ_0 induce larger values of $\zeta\,(\gamma_{max} \to 0)$, as well as a faster increase of the ζ curve at medium/high cyclic strains. Figure 104.24 confirms the suitability of the viscous mechanism, as an additional degree of freedom for reproducing the cyclic dissipative soil behavior.

Influence of the volumetric behavior in constrained problems So far, all the simulations have been performed by inhibiting the elastic-plastic soil dilatancy (ξ = 0), which in most cases cannot be done to represent real soil behavior. As previously shown for triaxial loading conditions (Figure 104.16), in the absence of kinematic boundary constraints, a variation in the volumetric behavior slightly affects only the

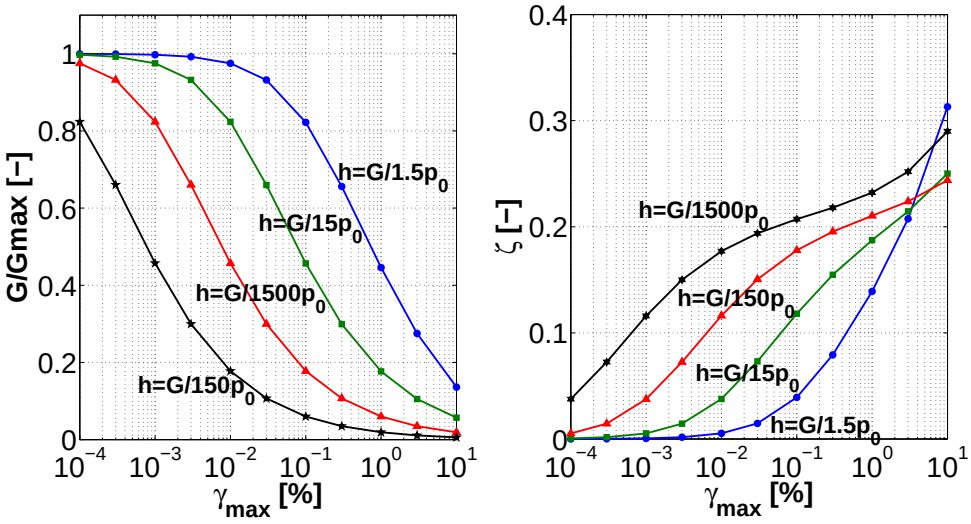

Figure 104.22: Simulated G/G_{max} and damping curves at varying h (p_0=100 kPa, T=2π s, G_{max} = 4 MPa, ν=0.25, M=1.2, k_d=ξ=0, m=1)

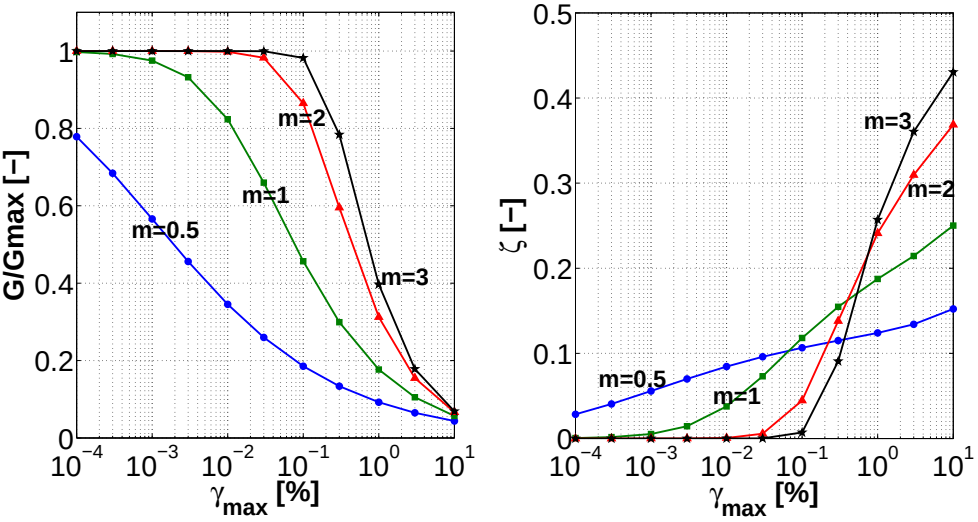

Figure 104.23: Simulated G/G_{max} and damping curves at varying m (p_0=100 kPa, T=2π s, G_{max} = 4 MPa, ν=0.25, M=1.2, k_d=ξ=0, h=$G_{max}/(15p_0)$)

hardening evolution of the stress-strain response toward the limit shear strength; a similar consideration applies to PS loading conditions, since even in this case the normal confinement is statically determined.

However, computational (FE) models contain kinematic constraints arising from certain symmetries (consider plane strain or one-dimensional schemes) (Prevost, 1989; Borja et al., 1999; di Prisco et al., 2012). In addition, for SSI problems, where soil interacts with a (stiff) structural foundations and wall, the soil volume change plays an important role. The presence of kinematic constraints implies that some

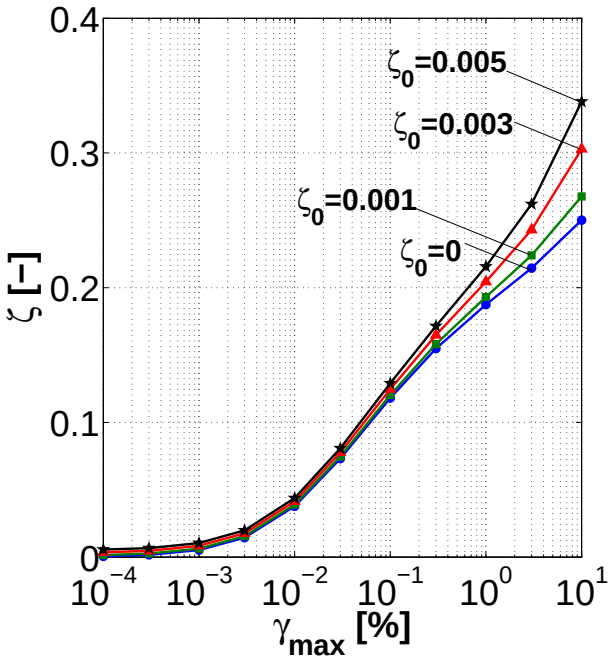

Figure 104.24: Damping curves simulated at varying ζ_0 (p_0=100 kPa, T=2π s, G_{max} = 4 MPa, ν=0.25, M=1.2, k_d=ξ=0, h=$G_{max}/(15p_0)$, m=1)

stress components are to be derived through compatibility conditions (e.g. prevented lateral expansion). That means that the local mean confinement is directly affected by the tendency of the material to dilate or contract. In particular, dilative frictional materials will increase the limit shear stress (with respect to unconfined conditions), while compactive frictional materials will decrease the limit shear stress. Further, not only the limit shear stress, but also the whole pre-failure response depends on the plastic flow rule whenever kinematic constraints are imposed (di Prisco and Pisanò, 2011; di Prisco et al., 2012).

The above considerations suggest that both experimental and numerical results are certainly affected by the kinematics of the system, even though this effect is not easy to be *a priori* quantified in terms of, for instance, G/G_{max} and damping curves. The kinematic conditions of an infinite soil layer during 1D shear wave propagation are experimentally approximated through the well known "simple shear (SS) apparatus" (Wood, 2004), in which the soil specimen is cyclically sheared with no lateral expansion allowed. In order to assess how the kinematic confinement influences the cyclic response, stiffness degradation and damping curves are hereafter simulated under SS conditions by varying the volumetric response of the soil; in particular, three different calibrations of the plastic flow rule (104.446) are considered, namely (i) isochoric ($k_d = \xi = 0$), (ii) compactive ($k_d = M$, $\xi = 1$) and (iii) dilative ($k_d = 0.4$, $\xi = 1$)

The results reported in Figure 104.25 provide an insight into the possible effect of the volumetric

response in combination with constrained loading conditions. In the isochoric case, the PS and the SS curves perfectly match (compare e.g. with the p_0 =100 kPa curves in Figure 104.21), as, with no plastic expansion (or contraction), the lateral constraints do not affect the mean pressure during the shear loading; conversely, non-negligible SS-PS differences arise when dilative or contractive materials are considered. As is evident in Figure 104.25, the discrepancy between isochoric and non-isochoric curves becomes evident at medium/high cyclic strains, i.e. at the onset of significant plastifications. Indeed, while the mechanical response is barely inelastic, the deviatoric and the volumetric responses are practically decoupled, so that no variation of the normal confinement takes place.

Apparently, the quantitative significance of the above effects is strictly related to the actual dilational properties and confinement conditions. It can be in general concluded that the cyclic properties are expected to vary depending on specific loading conditions (triaxial, biaxial, simple shear, torsional shear, etc), so that, when numerical models are calibrated, this aspect should be always explicitly considered.

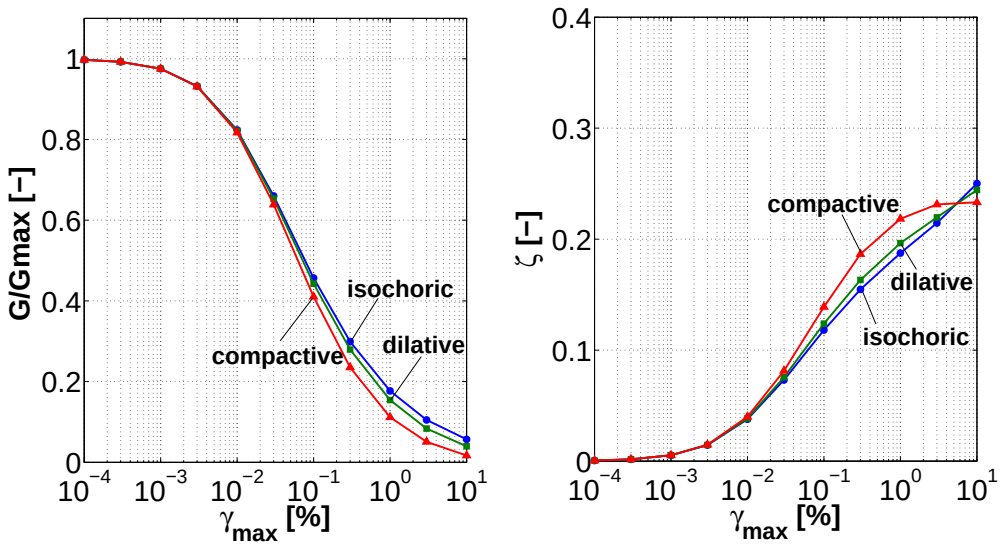

Figure 104.25: G/G_{max} and damping curves simulated under SS conditions and different volumetric responses (p_0=100 kPa, T=2π s, G_{max} = 4 MPa, ν=0.25, M=1.2, k_d=[1.2, 0.4], ξ=[0,1], h=$G_{max}/(15p_0)$, m=1)

104.6.15.6 Concluding remarks

An incremental 3D elastic-plastic constitutive model was developed to reproduce the mechanical response of soils under cyclic/dynamic loading. The model is based on an effective-stress formulation with two parallel dissipative mechanisms, purely frictional (elastic-plastic) and viscous.

As far as the frictional mechanism is concerned, a bounding surface formulation with vanishing elastic

region was adopted, extending to the case of pressure-sensitive non-associative soils the previous cohesive model by Borja and Amies (1994) for total-stress analysis. Notable features of the frictional model are: (i) the vanishing yield locus implies an elastic-plastic response at any load levels, as is observed in real experiments; (ii) a minimum number of physically meaningful parameters, which can be easily calibrated on the basis of a few experimental data; (iii) excellent performance and flexibility in reproducing in the elasto-plastic framework the standard stiffness degradation and damping curves. With reference to these latter, the parallel viscous mechanism – easy to be introduced in FE computations – was shown to provide an additional degree of freedom to improve the simulation of the cyclic energy dissipation, as long as the viscous parameter is properly calibrated. As a matter of fact, the viscous mechanism, used here, does physically exist in the form of viscous interaction between the soil solid skeleton and the pore fluid(s), and needs to be taken into account (as for example done here).

Future work will concern the investigation of the model performance in dynamic problems with pronounced hydro-mechanical coupling (cyclic mobility and liquefaction), as well as the comparison of the present model and traditional equivalent-linear approaches in seismic site response and SSI analysis. Further research is also needed to evaluate the accuracy of the model under non-symmetric loading conditions, these being particularly important in seismic slope stability applications.

104.6.15.7 Derivations of Various Equations

Derivation for Equation (104.449) The vanishing size of the yield locus implies:

$$\lim_{k\to 0} s_{ij} = p\alpha_{ij} \Rightarrow ds_{ij} = d\alpha_{ij}p + \alpha_{ij}dp = \|d\alpha_{ij}\| n_{ij}^{dev} p + \alpha_{ij}dp \tag{104.471}$$

and, after substituting the Prager translation rule (104.448):

$$n_{ij}^{dev} = \frac{ds_{ij} - \alpha_{ij}dp}{\|d\alpha_{ij}\|p} = \frac{ds_{ij} - \alpha_{ij}dp}{\|ds_{ij} - \alpha_{ij}dp\|} \tag{104.472}$$

In this last equality the property $\|n_{ij}^{dev}\| = 1$ has been exploited.

Derivations for Equations (104.452) – (104.453) The consistency condition:

$$df_y = 0 \Leftrightarrow \frac{\partial f}{\partial \sigma_{ij}} d\sigma_{ij} + \frac{\partial f}{\partial \alpha_{ij}} d\alpha_{ij} = 0 \tag{104.473}$$

results in the following equality chain

$$\frac{\partial f}{\partial \sigma_{ij}} d\sigma_{ij} = 3p\left(s_{ij} - p\alpha_{ij}\right) \|d\alpha_{ij}\| n_{ij}^{dev} = 3p\left(s_{ij} - p\alpha_{ij}\right) \|d\alpha_{ij}\| \frac{3\left(s_{ij} - p\alpha_{ij}\right)}{N^{dev}} = 0 \tag{104.474}$$

leading to:

$$\|d\alpha_{ij}\| = \frac{\frac{\partial f}{\partial \sigma_{ij}} d\sigma_{ij}}{pN^{dev}} \tag{104.475}$$

where $N^{dev} = \| \left(\partial f_y/\partial \sigma_{ij}\right)^{dev} \| = 3\|s_{ij} - p\alpha_{ij}\|$. The above equation can be further simplified for the case of radial loading paths in the deviatoric plane, characterized by $d\sigma_{ij} = ds_{ij}$ and coaxiality between the current stress state and its increment:

$$\|d\alpha_{ij}\| = \frac{\frac{\partial f}{\partial \sigma_{ij}} d\sigma_{ij}}{pN^{dev}} = \frac{\frac{\partial f}{\partial \sigma_{ij}} ds_{ij}}{pN^{dev}} = \frac{\frac{\partial f}{\partial \sigma_{ij}}^{dev} ds_{ij}}{pN^{dev}} = \frac{n_{ij}^{dev} ds_{ij}}{p} = \frac{s_{ij} ds_{ij}}{p\|s_{ij}\|} \tag{104.476}$$

The final relationship can be re-expressed in terms of standards invariants $q = \sqrt{3/2}\|s_{ij}\|$ and p:

$$\|d\alpha_{ij}\| = \sqrt{\frac{2}{3}} \frac{dq}{p} \tag{104.477}$$

Derivation for Equation (104.470) Under PS loading conditions (constant mean pressure), Equation (104.458) can be reduced to a simpler scalar form:

$$\beta = \frac{\tau_{lim} - \tau}{\tau - \tau_0} \tag{104.478}$$

where $\tau_{lim} = Mp_0/\sqrt{3}$. By exploiting the previous definitions of deviatoric stress and strain invariants, the elastic-plastic response can be expressed as:

$$d\epsilon_d = \frac{dq}{3G_{max}} + \left(\frac{\tau - \tau_0}{\tau_{lim} - \tau}\right)^m \frac{dq}{hp_0} \tag{104.479}$$

and specialized to the case of PS loading:

$$\frac{d\gamma}{\sqrt{3}} = \frac{\sqrt{3}d\tau}{3G_{max}} + \left(\frac{\tau - \tau_0}{\tau_{lim} - \tau}\right)^m \frac{\sqrt{3}d\tau}{hp_0} \tag{104.480}$$

Integration over a strain interval between two stress reversals ($\gamma \in [-\gamma_{max}; \gamma_{max}]$) yields:

$$2\gamma_{max} = \frac{2\tau}{G_{max}} + \frac{3}{hp_0} \int_{-\tau}^{\tau} \left(\frac{\tau' + \tau}{\tau_{lim} - \tau'}\right)^m d\tau' \tag{104.481}$$

where $\tau_0 = -\tau$ has been set. Straightforward variable changes lead to:

$$1 = \frac{G}{G_{max}} + \frac{3}{2hp_0\gamma_{max}} \int_0^{2G\gamma_{max}} \left(\frac{\tau''}{\tau_{lim} - \tau'' + G\gamma_{max}}\right)^m d\tau'' \tag{104.482}$$

$$1 = \frac{G}{G_{max}} \left[1 + \frac{6G_{max}}{hp_0\gamma_{max}} \int_0^{\gamma_{max}} \left(\frac{\gamma}{\tau_{lim}/G - 2\gamma + \gamma_{max}} \right)^m d\gamma \right] \tag{104.483}$$

It is worth highlighting that two approximations are implicitly contained in Equation (104.483): (i) the integration over the first loading cycle does not exactly reproduce the stabilized cyclic response (because of the aforementioned Masing effect); (ii) a symmetric loading cycle in terms of shear strain does not in general ensure the symmetry of the corresponding shear stress range (as it is assumed in Equation (104.481)). However, such approximations do not prevent reasonable values for the hardening parameters h and m to be obtained.

104.6.16 Cosserat Elastoplasticity

Four components of the classical elastoplasticity.

- Elasticity law, E_{ijkl} and C_{ijkl}.
- Yield surface, $f(\sigma, t, \kappa)$
- Plastic flow direction, $m_{ij}^{force} = \frac{\partial Q(\sigma,t,\kappa)}{\partial \sigma_{ij}}$ and $m_{ij}^{curvature} = \frac{\partial Q(\sigma,t,\kappa)}{\partial t}$.
- Hardening law for internal variables, $\kappa = d\lambda h(\sigma, t)$.

where σ is the stress, and t is the couple-stress.

104.6.16.1 Elasticity Law

$$\begin{aligned} E_{ijkl} &= \lambda\delta_{ij}\delta_{kl} + \mu\delta_{ik}\delta_{jl} + (\mu + \chi)\delta_{jk}\delta_{il} \\ C_{ijkl} &= \pi_1\delta_{ij}\delta_{kl} + \pi_2\delta_{ik}\delta_{jl} + \pi_3\delta_{jk}\delta_{il} \end{aligned} \tag{104.484}$$

104.6.16.2 Yield Criterion

Hencky (1924) provided a physical interpretation of von Mises criterion suggesting that yielding begins when the elastic energy of distortion reaches a critical value.[4] So von Mises is called maximum distortion strain energy yield criterion.

In the von-Mises plasticity for the classical elasticity, the distortion extent is measured by

$$J_2 = \frac{1}{2} s_{ij} s_{ij} \tag{104.485}$$

where,

$$s_{ij} = \sigma_{ij} + p\delta_{ij} \tag{104.486}$$

In the von-Mises plasticity for the Cosserat elasticity, the distortion extent de Borst (1993) can be measured by

$$J_2 = \frac{1}{2}(h_1 s_{ij}s_{ij} + h_2 s_{ij}s_{ji} + h_3 t_{kl}t_{kl}/l^2) \tag{104.487}$$

where, $h_1 = 3/4$, $h_2 = -1/4$, and $h_3 = 1/8$. The length l is the characteristic length. The yield strength is

$$\sigma_y = \sqrt{3J_2} \tag{104.488}$$

such that the yield criterion is

$$f(\sigma, t) = \sqrt{3J_2} - k = \sqrt{\frac{3}{2}(h_1 s_{ij}s_{ij} + h_2 s_{ij}s_{ji} + h_3 t_{kl}t_{kl}/l^2)} - k \tag{104.489}$$

where k is a constant for perfectly plasticity, and k is a function of stress and couple-stress for hardening materials.

104.6.16.3 Plastic Flow

The plastic flow direction is

$$\begin{aligned} m_{ij}^{force} &= \frac{\partial Q(\sigma, t, \kappa)}{\partial \sigma_{ij}} \quad , \quad d\sigma_{ij} = d\lambda m_{ij}^{force} \\ m_{ij}^{curvature} &= \frac{\partial Q(\sigma, t, \kappa)}{\partial t} \quad , \quad dt_{ij} = d\lambda m_{ij}^{curvature} \end{aligned} \tag{104.490}$$

In the conventional elastoplasticity, the plastic potential function Q is a function of stress σ and the internal variables κ.

In the Cosserat elastoplasticity, the plastic potential function Q is a function of stress σ, couple-stress t, and the internal variables κ.

104.6.16.4 Hardening Rule

The hardening rule describes how to update the internal variables with the plastic multiplier.

$$dq = d\lambda h(\sigma, t, \kappa) \tag{104.491}$$

In the conventional elastoplasticity, the hardening rule is a function of stress σ and the internal variables κ.

In the Cosserat elastoplasticity, the hardening rule is a function for stress σ, couple-stress t, and the internal variables κ.

104.6.16.5 Forward Euler Algorithm

Forward Euler Algorithm uses the cross point on the yield surface as the starting point to calculate the plastic flow direction and the normal to the yield surface.

104.6.16.6 Explicit Formulation

The governing equation of the forward Euler, explicit algorithm is

$$\begin{aligned} {}^{n+1}\boldsymbol{\sigma} + \lambda \boldsymbol{C}^{force} \boldsymbol{m}({}^{cross}\boldsymbol{\sigma}, {}^{cross}\boldsymbol{t}, {}^{cross}\boldsymbol{\kappa}) &= {}^{n}\boldsymbol{\sigma} + \boldsymbol{C}^{force} \triangle \boldsymbol{\epsilon} \\ {}^{n+1}\boldsymbol{t} + \lambda \boldsymbol{C}^{curvature} \boldsymbol{m}({}^{cross}\boldsymbol{\sigma}, {}^{cross}\boldsymbol{t}, {}^{cross}\boldsymbol{\kappa}) &= {}^{n}\boldsymbol{t} + \boldsymbol{C}^{curvature} \triangle \boldsymbol{\omega} \\ {}^{n+1}\boldsymbol{\kappa} - \lambda \boldsymbol{h}({}^{cross}\boldsymbol{\sigma}, {}^{cross}\boldsymbol{t}, {}^{cross}\boldsymbol{\kappa}) &= {}^{n}\boldsymbol{\kappa} \\ F({}^{cross}\boldsymbol{\sigma}, {}^{cross}\boldsymbol{t}, {}^{cross}\boldsymbol{\kappa}) &= 0 \end{aligned} \tag{104.492}$$

where ${}^{n}\boldsymbol{\sigma}$, ${}^{n}\boldsymbol{t}$, $\triangle\boldsymbol{\epsilon}$, $\triangle\boldsymbol{\omega}$, and ${}^{n}\boldsymbol{\kappa}$ are known, which represents the stress state, couple-stress state, total strain increment, and internal variables state in the previous step. The four unknowns are ${}^{n+1}\boldsymbol{\sigma}$, ${}^{n+1}\boldsymbol{t}$, ${}^{n+1}\boldsymbol{\kappa}$ and λ, which represents the stress state, internal variables state, and plastic multiplier in the current step.

Continuum Stiffness Tensor The explicit algorithm is derived by starting from the first order Taylor expansion about the starting point $(\sigma_{ij},\ t,\ \kappa)$.

$$f^{new} = f^{old} + \frac{\partial f}{\partial \sigma_{ij}} d\sigma_{ij} + \frac{\partial f}{\partial t_{kl}} dt_{kl} + \frac{\partial f}{\partial \kappa} d\kappa \tag{104.493}$$

Since both yield surface values should be zeroes, the Taylor expansion is simplified to

$$\begin{aligned} &\frac{\partial f}{\partial \sigma_{ij}} d\sigma_{ij} + \frac{\partial f}{\partial t_{kl}} dt_{kl} + \frac{\partial f}{\partial \kappa} d\kappa = 0 \\ &\frac{\partial f}{\partial \sigma_{ij}} (E_{ijkl} d\epsilon - E_{ijkl} d\lambda m^{s}_{kl}) + \frac{\partial f}{\partial t_{kl}} (C_{ijkl} d\omega - C_{ijkl} d\lambda m^{c}_{kl}) + \xi_* h_* d\lambda = 0 \\ &d\lambda = \frac{\frac{\partial f}{\partial \sigma_{ij}} E_{ijkl} d\epsilon + \frac{\partial f}{\partial t_{kl}} C_{ijkl} d\omega}{\frac{\partial f}{\partial \sigma_{ij}} E_{ijkl} m^{s}_{kl} + \frac{\partial f}{\partial t_{kl}} C_{ijkl} m^{c}_{kl} - \xi_* h_*} \end{aligned} \tag{104.494}$$

Simplify the $d\lambda$ expression by $n^{s}_{ij} = \frac{\partial f}{\partial \sigma_{ij}}$ and $n^{c}_{ij} = \frac{\partial f}{\partial t_{ij}}$. So we have

$$d\lambda = \frac{n^{s}_{ij} E_{ijkl} d\epsilon + n^{c}_{ij} C_{ijkl} d\omega}{n^{s}_{ij} E_{ijkl} m^{s}_{kl} + n^{c}_{ij} C_{ijkl} m^{c}_{kl} - \xi_* h_*} \tag{104.495}$$

104.6.16.7 Backward Euler, Implicit Algorithm

Forward Euler Algorithm uses the final stress state to calculate the plastic flow direction and the normal to the yield surface.

Iterations are required to find the final stress state.

Implicit Formulation The governing equations of the backward Euler, implicit algorithm

$$\begin{aligned} {}^{n+1}\boldsymbol{\sigma} + \lambda \boldsymbol{E}\boldsymbol{m}^s({}^{n+1}\boldsymbol{\sigma}, {}^{n+1}\boldsymbol{t}, {}^{n+1}\boldsymbol{\kappa}) &= {}^{n}\boldsymbol{\sigma} + \boldsymbol{E}\triangle\boldsymbol{\epsilon} \\ {}^{n+1}\boldsymbol{t} + \lambda \boldsymbol{C}\boldsymbol{m}^c({}^{n+1}\boldsymbol{\sigma}, {}^{n+1}\boldsymbol{t}, {}^{n+1}\boldsymbol{\kappa}) &= {}^{n}\boldsymbol{t} + \boldsymbol{C}\triangle\boldsymbol{\omega} \\ {}^{n+1}\boldsymbol{\kappa} - \lambda \boldsymbol{h}({}^{n+1}\boldsymbol{\sigma}, {}^{n+1}\boldsymbol{t}, {}^{n+1}\boldsymbol{\kappa}) &= {}^{n}\boldsymbol{\kappa} \\ F({}^{n+1}\boldsymbol{\sigma}, {}^{n+1}\boldsymbol{t}, {}^{n+1}\boldsymbol{\kappa}) &= 0 \end{aligned} \tag{104.496}$$

where ${}^{n}\boldsymbol{\sigma}$, ${}^{n}\boldsymbol{t}$, $\triangle\boldsymbol{\epsilon}$, $\triangle\boldsymbol{\omega}$, and ${}^{n}\boldsymbol{\kappa}$ are known, which represents the stress state, couple-stress state, total strain increment, and internal variables state in the previous step. The four unknowns are ${}^{n+1}\boldsymbol{\sigma}$, ${}^{n+1}\boldsymbol{t}$, ${}^{n+1}\boldsymbol{\kappa}$ and λ, which represents the stress state, internal variables state, and plastic multiplier in the current step.

Consistent Stiffness Tensor The consistent stiffness tensor for a Cosserat elastoplastic algorithm is extended from the classic elastoplastic algorithmPérez-Foguet et al. (2001). The Jacobian of the backward algorithm can be written as

$${}^{n+1}\boldsymbol{J} = \begin{pmatrix} (\boldsymbol{I} + \lambda \boldsymbol{E}\frac{\partial \boldsymbol{m}^s}{\partial \boldsymbol{\sigma}}) & (\frac{\partial \boldsymbol{\sigma}}{\partial t} + \lambda \boldsymbol{E}\frac{\partial \boldsymbol{m}^s}{\partial t}) & \lambda \boldsymbol{E}\frac{\partial \boldsymbol{m}^s}{\partial \boldsymbol{\kappa}} & \boldsymbol{E}\boldsymbol{m}^s \\ (\frac{\partial \boldsymbol{t}}{\partial \boldsymbol{\sigma}} + \lambda \boldsymbol{C}\frac{\partial \boldsymbol{m}^c}{\partial \boldsymbol{\sigma}}) & (\boldsymbol{I} + \lambda \boldsymbol{C}\frac{\partial \boldsymbol{m}^c}{\partial t}) & \lambda \boldsymbol{C}\frac{\partial \boldsymbol{m}^c}{\partial \boldsymbol{\kappa}} & \boldsymbol{C}\boldsymbol{m}^c \\ -\lambda \frac{\partial \boldsymbol{h}}{\partial \boldsymbol{\sigma}} & -\lambda \frac{\partial \boldsymbol{h}}{\partial t} & (\boldsymbol{I} - \lambda \frac{\partial \boldsymbol{h}}{\partial \boldsymbol{\kappa}}) & -\boldsymbol{h} \\ \boldsymbol{n}_s^T & \boldsymbol{n}_c^T & \boldsymbol{\xi}^T & 0 \end{pmatrix} \tag{104.497}$$

104.6.17 Cosserat von-Mises Elastoplastic Model

Following the fundamental Cosserat elastoplastic material model defined above, an full Cosserat von-Mises plastic model is defined below.

104.6.17.1 Cosserat Plastic Model

Cosserat von-Mises Yield Surface :

$$f(\sigma,t) = \left(\frac{1}{2}s_{ij}s_{ij} + \frac{1}{2}s_{ij}s_{ji} + \frac{1}{2l_p^2}(t_{ij}t_{ij} + t_{ij}t_{ji})\right)^{1/2} - \sqrt{\frac{2}{3}}k \tag{104.498}$$

The normal to the yield surface with respect to the force

$$\begin{aligned} n^f &= \frac{\partial f}{\partial \sigma} \\ &= \frac{1}{2}(s_{ij} + s_{ji})\left(\frac{1}{2}s_{ij}s_{ij} + \frac{1}{2}s_{ij}s_{ji} + \frac{1}{2l_p^2}(t_{ij}t_{ij} + t_{ij}t_{ji})\right)^{-1/2} \end{aligned} \tag{104.499}$$

The normal to the yield surface with respect to the curvature

$$\begin{aligned} n^c =& \frac{\partial f}{\partial t} \\ =& \frac{1}{2l_p^2}(t_{ij} + t_{ji})\left(\frac{1}{2}s_{ij}s_{ij} + \frac{1}{2}s_{ij}s_{ji} + \frac{1}{2l_p^2}(t_{ij}t_{ij} + t_{ij}t_{ji})\right)^{-1/2} \end{aligned} \tag{104.500}$$

Plastic Flow :

$$\begin{aligned} m^f &= n^f \\ m^c &= n^c \end{aligned} \tag{104.501}$$

Hardening Law:

$$\bar{k} = Hm_{equiv} = H\left(\frac{1}{3}m_{ij}^f m_{ij}^f + \frac{1}{3}m_{ij}^f m_{ji}^f + \frac{1}{3}l_p^2(m_{ij}^c m_{ij}^c + m_{ij}^c m_{ji}^c)\right)^{0.5} \tag{104.502}$$

Calculation of dλ : The algorithm is derived by starting from the first order Taylor expansion about the starting point (σ_{ij}, t, κ).

$$f^{new} = f^{old} + \frac{\partial f}{\partial \sigma_{ij}}d\sigma_{ij} + \frac{\partial f}{\partial t_{kl}}dt_{kl} + \frac{\partial f}{\partial \kappa}d\kappa \tag{104.503}$$

Since both yield surface values should be zeros, the Taylor expansion is simplified to

$$\begin{aligned} &\frac{\partial f}{\partial \sigma_{ij}}d\sigma_{ij} + \frac{\partial f}{\partial t_{kl}}dt_{kl} + \frac{\partial f}{\partial \kappa}d\kappa = 0 \\ &\frac{\partial f}{\partial \sigma_{ij}}(E_{ijkl}d\epsilon - E_{ijkl}d\lambda m_{kl}^s) + \frac{\partial f}{\partial t_{kl}}(C_{ijkl}d\omega - C_{ijkl}d\lambda m_{kl}^c) + \xi_* h_* d\lambda = 0 \\ &d\lambda = \frac{\frac{\partial f}{\partial \sigma_{ij}}E_{ijkl}d\epsilon + \frac{\partial f}{\partial t_{kl}}C_{ijkl}d\omega}{\frac{\partial f}{\partial \sigma_{ij}}E_{ijkl}m_{kl}^s + \frac{\partial f}{\partial t_{kl}}C_{ijkl}m_{kl}^c - \xi_* h_*} \end{aligned} \tag{104.504}$$

Simplify the $d\lambda$ expression by $n^s_{ij} = \frac{\partial f}{\partial \sigma_{ij}}$ and $n^c_{ij} = \frac{\partial f}{\partial t_{ij}}$. So we have

$$d\lambda = \frac{n^s_{ij} E_{ijkl} d\epsilon + n^c_{ij} C_{ijkl} d\omega}{n^s_{ij} E_{ijkl} m^s_{kl} + n^c_{ij} C_{ijkl} m^c_{kl} - \xi_* h_*} \tag{104.505}$$

For this Cosserat von-Mises isotropic hardening case,

$$\xi_* = \frac{\partial f}{\partial k} = -\sqrt{\frac{2}{3}} \tag{104.506}$$

$$h_* = \bar{k} = H m_{equiv} \tag{104.507}$$

104.6.17.2 Analysis of Cosserat Elastoplastic Solids

For the elastoplastic analysis, a rectangular plate of 10 m width and 20 m height is horizontally fixed at one end while the other end is subjected to a given horizontal displacement. The geometry and boundary conditions used for the plate are shown in Fig.104.26. In addition, the upper left corner of the plate is vertically fixed. The elastic material constants are $\lambda = 20MPa$, $\mu = 10MPa$, $\chi = 0$, $\pi_1 = 10MN$, $\pi_2 = 0$, $\pi_3 = 1kN$, and the plastic constants are internal length $l_p = 1E-6m$, von-Mises radius $k = 50kPa$, and hardening (softening) rate $H = -500kPa$. For the sake of comparison, the geometry, material properties and loadings used in this problem are the same as the ones used where classical elasticity is employed.

Fig.104.27 illustrates the plastic zone obtained for the problem when the classical and Cosserat theories with different discretization are used. As it is expected, the plastic zone obtained for the classical theory becomes narrowed as the discretization refines. In fact, the plastic zone is two elements wide for all discretization which shows the mesh-dependency of the results based on the classical theory. One the other hand, the plastic zone obtained for the Cosserat theory approximately remains the unchanged when discretization refines.

104.6.18 Accelerated Constitutive Models

One of the concerns of elastic-plastic analysis is the computational effort. In this section developed are closed form elastic-plastic stress increments and elastic-plastic tangent stiffness matrices for commonly used elastic-plastic models. This is achieved by multiplying, in closed form, explicit, forward Euler elastic-plastic stress incremental solution and explicit, tangent elastic-plastic stiffness tensor, as developed in section 104.3 on page 206.

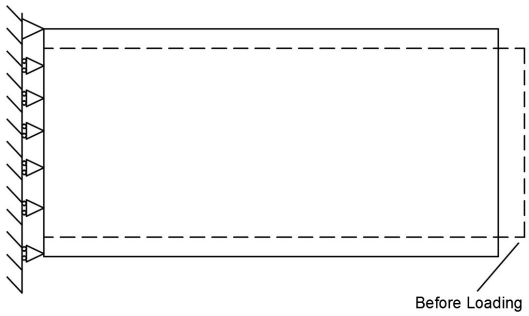

Figure 104.26: Loading Condition and Boundary Conditions of the Cosserat Elastoplastic Model.

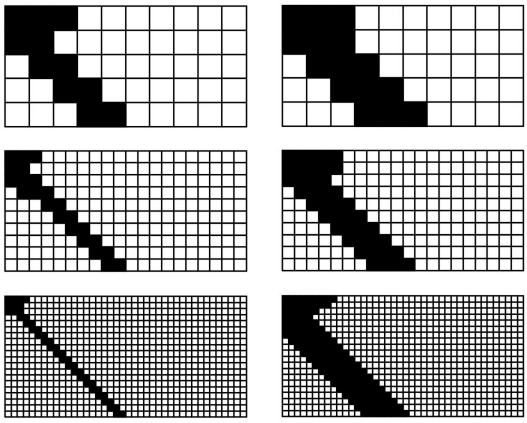

Figure 104.27: Comparison of the Plastic Zone of the Cosserat Elastoplastic Model. Left side is the classical elastoplastic material model, where the mesh refinement leads to localization of the plastic zone. Right side is the Cosserat elastoplastic material model, where the plastic zone is independent of the mesh sizes.

Relation between stress increment $d\sigma_{ij}$ and strain increments $d\epsilon_{kl}$ can be written for linear isotropic elasticity as:

$$d\sigma_{ij} = E_{ijkl} d\epsilon_{kl} \tag{104.508}$$

where E_{ijkl} is the fourth order elastic stiffness tensor. The elastic stiffness tensor features both minor symmetry $E_{ijkl} = E_{jikl} = E_{ijlk}$ and major symmetry $E_{ijkl} = E_{klij}$ (Jeremić and Sture (1997)). The elastic stiffness tensor for isotropic material can be written as:

$$E_{ijkl} = \lambda \delta_{ij} \delta_{kl} + \mu \left(\delta_{ik} \delta_{jl} + \delta_{il} \delta_{jk} \right) \tag{104.509}$$

where λ and μ are the Lamé constants and E and ν are Young's Modulus and Poisson's ratio, respectively:

$$\lambda = \frac{\nu E}{(1+\nu)(1-2\nu)} \quad ; \quad \mu = \frac{E}{2(1+\nu)} \tag{104.510}$$

The relation between the stress tensor increment $d\sigma_{ij}$ and strain tensor increment $d\epsilon_{kl}$ is:

$$d\epsilon_{kl} = D_{klpq} d\sigma_{pq} \tag{104.511}$$

where D_{klpq} is the elastic compliance fourth order tensor, defined as:

$$D_{klpq} = \frac{-\lambda}{2\mu\,(3\lambda + 2\mu)}\,\delta_{kl}\delta_{pq} + \frac{1}{4\mu}\left(\delta_{kp}\delta_{lq} + \delta_{kq}\delta_{lp}\right) \tag{104.512}$$

104.6.18.1 Elasto-plasticity

Using developments from section 104.3 on page 206, one can write

$$d\sigma_{ij} = E_{ijkl} d\epsilon^{e}_{kl} \tag{104.513}$$

$$d\epsilon^{p}_{ij} = d\lambda\,\frac{\partial Q}{\partial \sigma_{ij}} = d\lambda\, m_{ij}(\sigma_{ij}, q) \tag{104.514}$$

$$d\epsilon_{ij} = d\epsilon^{e}_{ij} + d\epsilon^{p}_{ij} \tag{104.515}$$

$$dq_{*} = d\lambda\, h(\tau_{ij}, q) \tag{104.516}$$

where, ϵ_{ij}, ϵ^{e}_{ij}, and ϵ^{p}_{ij} are total, elastic, and plastic strain tensors respectively, σ_{ij} is stress tensor, and q_{*} represents internal variables. Moreover, m_{ij} is the plastic flow direction, h is the plastic moduli, and $d\lambda$ is a plastic constistency parameter that is to be determined. Equation (104.513) is the Hooke's law that relates stress to elastic strain using the stiffness tensor E_{ijkl}. Equation(104.514) shows relations of plastic strains to the associated or non-associated plastic flow rule. Equation (104.515) represents the additive decomposition of strain increment into elastic strain increment and plastic strain increments, that is applicable for small deformation analysis. Equation (104.516) represents evolution law for internal variables.

104.6.18.2 Elastic-Plastic Constitutive Models

For each elastic-plastic constitutive model, there are four components to be specified. Those components are (a) elasticity relation, (b) yield function, (c) plastic flow function, and (d) hardening and/or softening laws.

Once those four components are chosen, specified, elastic-plastic stiffness tensor, developed earlier in section 104.3 on page 206, can be developed for each model, by analytically multiplying functions and tensor equations for each component. In following sections this is done for von Mises, Drucker-Prager, and Cam-Clay material models.

The tanget elastic-plastic tensor is written as

$$E^{el-pl}_{pqmn} = E_{pqmn} - \frac{E_{pqkl}\,{}^{n}m_{kl}\,{}^{n}n_{ij}E_{ijmn}}{{}^{n}n_{ot}E_{otrs}\,{}^{n}m_{rs} - \xi_*\,h_*} \tag{104.517}$$

For perfectly plastic materials ξ_* and h_* would be zero while for the cases with evolution laws, the appropriate evolution laws should be used in derivation of tangent stiffness E^{el-pl}_{pqmn}. Elastic modulus tensor is written as:

$$E_{ijkl} = \lambda\delta_{ij}\delta_{kl} + \mu(\delta_{ik}\delta_{jl} + \delta_{il}\delta_{jk}) \tag{104.518}$$

where $\lambda = \nu E/(1+\nu)(1-2\nu)$, $\mu = E/2(1+\nu)$.

104.6.18.3 von Mises Model

von Mises yield criteria can be written as

$$f = \left[\left(s_{ij} - \alpha_{ij}\right)\left(s_{ij} - \alpha_{ij}\right)\right]^{0.5} - \sqrt{\frac{3}{2}}k = 0 \tag{104.519}$$

where k is the scalar internal variable where initial value is related to the uniaxial tension strength, α_{ij} is the tensorial internal variable, the so called back stress that controls translational kinematic hardening.

The stress derivative of the yield function is

$$n_{ij} = \frac{\partial f}{\partial \sigma_{ij}} = \frac{1}{\sqrt{(s_{ij} - \alpha_{ij})(s_{ij} - \alpha_{ij})}}(s_{ij} - \alpha_{ij}) \tag{104.520}$$

In case of associated plastic flow rule where the plastic potential function is considered to be the same of yield function, stress derivative of plastic flow function is:

$$m_{ij} = \frac{\partial g}{\partial \sigma_{ij}} = \frac{1}{\sqrt{(s_{ij} - \alpha_{ij})(s_{ij} - \alpha_{ij})}}(s_{ij} - \alpha_{ij}) \tag{104.521}$$

In order to find the closed form equation for elastic-plastic modulus for case of perfectly-plastic, Equation (104.519) is used for both yield surface and plastic potential and no evolution law is considered. Relevant stress derivatives are:

$$n_{ij} = \frac{1}{\sqrt{s_{ij}s_{ij}}}s_{ij} \quad ; \quad m_{ij} = \frac{1}{\sqrt{s_{ij}s_{ij}}}s_{ij} \tag{104.522}$$

Base on obtained stress derivatives, plastic consistency parameter is derived as

$$d\lambda = \frac{n_{ij}E_{ijpq}d\epsilon_{pq}}{n_{ij}E_{ijkl}m_{kl}} = \frac{n_{ij}d\sigma_{ij}}{2\mu} \tag{104.523}$$

The elastic-plastic tangent tensor is then

$$\begin{aligned} E^{pl}_{pqmn} &= \frac{E_{pqkl}n_{kl}m_{ij}E_{ijmn}}{n_{ab}E_{abcd}m_{cd}} = 2\mu n_{pq}n_{mn} \\ &= 2\mu\frac{1}{\sqrt{s_{kl}s_{kl}}}s_{pq}\frac{1}{\sqrt{s_{ij}s_{ij}}}s_{mn} = 2\mu\frac{1}{s_{kl}s_{kl}}s_{pq}s_{mn} \end{aligned} \tag{104.524}$$

In case isotropic hardening, ξ and h are not zero anymore, since k is scalar internal variable that is updated in each increment. Harderning/softenig functions, scalar functions in this case. ξ and h can be calculated as

$$\xi = -\sqrt{\frac{2}{3}} \tag{104.525}$$

$$h = \sqrt{\frac{2}{3}m_{ij}m_{ij}}k = \sqrt{\frac{2}{3}}k \tag{104.526}$$

Therefore, plastic parameter ($d\lambda$) and tangnet elastic-plastic tensor (E^{pl}_{pqmn}) can be written as:

$$d\lambda = \frac{n_{ij}E_{ijpq}d\epsilon_{pq}}{n_{ij}E_{ijkl}m_{kl} - \xi\, h} = \frac{n_{ij}d\sigma_{ij}}{2\mu + \frac{2}{3}k} \tag{104.527}$$

$$\begin{aligned} E^{pl}_{pqmn} &= \frac{E_{pqkl}n_{kl}m_{ij}E_{ijmn}}{n_{ab}E_{abcd}m_{cd} - \xi\, h} = \frac{4\mu^2 n_{pq}n_{mn}}{2\mu + \frac{2}{3}k} \\ &= \frac{4\mu^2\frac{1}{\sqrt{s_{kl}s_{kl}}}s_{pq}\frac{1}{\sqrt{s_{ij}s_{ij}}}s_{mn}}{2\mu - \frac{2}{3}k} = \frac{4\mu^2\frac{1}{s_{kl}s_{kl}}s_{pq}s_{mn}}{2\mu + \frac{2}{3}k} \end{aligned} \tag{104.528}$$

The value of k should be updated at each step using the following equation:

$$k^{updated} = k + dk = k + hd\lambda = k + \sqrt{\frac{2}{3}}kd\lambda = k(1 + \sqrt{\frac{2}{3}}d\lambda) \tag{104.529}$$

For case the of von Mises with kinematic hardening, α_{ij} is the tensorial internal variable to be updated at each step of analysis, while tensor functions ξ_{ab} and h_{ab} can be calculated from the following equations using Armstrong-Frederick saturation-type kinematic hardening rule (Armstrong and Frederick (1966); Lemaitre and Chaboche (1990)) :

$$\xi_{ab} = \frac{\partial F}{\partial \alpha_{ab}} = -\frac{1}{\sqrt{(s_{ab} - \alpha_{ab})(s_{ab} - \alpha_{ab})}}(s_{ab} - \alpha_{ab}) \tag{104.530}$$

Recall that $dq_{ij} = d\alpha_{ij} = d\lambda h_{ij}$, and $d\epsilon^{pl}_{ij} = d\lambda m_{ij}$ and that the Armstrong-Frederic kinematic hardening rule for the internal variable α_{ij} is given as:

$$d\alpha_{ij} = \frac{2}{3}h_a \left(d\epsilon^p_{ij}\right)^{dev} - c_r \alpha_{ij}\sqrt{\frac{2}{3}\left(d\epsilon^p_{st}\right)^{dev}\left(d\epsilon^p_{st}\right)^{dev}} \tag{104.531}$$

so that

$$h_{st} = \frac{2}{3}h_a m_{st} - \alpha_{st} c_r \sqrt{\frac{2}{3}} \tag{104.532}$$

since $\sqrt{m_{ij}m_{ij}} = 1$.

Plastic consistency parameter ($d\lambda$) and tanget elastic-plastic tensor (E^{pl}_{pqmn}) can be expressed as:

$$d\lambda = \frac{n_{ij}E_{ijpq}d\epsilon_{pq}}{n_{ij}E_{ijkl}m_{kl} - \xi\, h} = \frac{n_{ij}d\sigma_{ij}}{2\mu - \xi_{ab}\, h_{ab}} \tag{104.533}$$

$$E^{pl}_{pqmn} = \frac{E_{pqkl}n_{kl}m_{ij}E_{ijmn}}{n_{ab}E_{abcd}m_{cd} - \xi\, h} = \frac{4\mu^2 n_{pq}n_{mn}}{2\mu - \xi_{ij}\, h_{ij}} \tag{104.534}$$

Full, developed form of tangent elastic-plastic stiffness can be written as

$$E^{pl}_{pqmn} = \frac{E_{pqkl}\left(\frac{1}{\sqrt{(s_{ab}-\alpha_{ab})(s_{ab}-\alpha_{ab})}}(s_{kl}-\alpha_{kl})\right)\left(\frac{1}{\sqrt{(s_{ab}-\alpha_{ab})(s_{ab}-\alpha_{ab})}}(s_{ij}-\alpha_{ij})\right)E_{ijmn}}{\left(\frac{1}{\sqrt{(s_{mn}-\alpha_{mn})(s_{mn}-\alpha_{mn})}}(s_{ab}-\alpha_{ab})\right)E_{abcd}\left(\frac{1}{\sqrt{(s_{mn}-\alpha_{mn})(s_{mn}-\alpha_{mn})}}(s_{cd}-\alpha_{cd})\right)-\left(-\frac{1}{\sqrt{(s_{ab}-\alpha_{ab})(s_{ab}-\alpha_{ab})}}(s_{rs}-\alpha_{rs})\right)\left(\frac{2}{3}h_a m_{ab}-\frac{2}{3}\alpha_{rs}c_r\right)} \tag{104.535}$$

Above equation can be simplified, written in a shorter form by using a substitution

$$\mathbb{A} = \frac{1}{\sqrt{(s_{ab} - \alpha_{ab})(s_{ab} - \alpha_{ab})}} \tag{104.536}$$

it can be written as:

$$E^{pl}_{pqmn} = \frac{E_{pqkl}\left(\mathbb{A}\left(s_{kl} - \alpha_{kl}\right)\right)\left(\mathbb{A}\left(s_{ij} - \alpha_{ij}\right)\right)E_{ijmn}}{\left(\mathbb{A}\left(s_{ab} - \alpha_{ab}\right)\right)E_{abcd}\left(\mathbb{A}\left(s_{ab} - \alpha_{ab}\right)\right) - (-\mathbb{A})\left(\frac{2}{3}h_a\left(\mathbb{A}\left(s_{cd} - \alpha_{cd}\right)\right) - \sqrt{\frac{2}{3}}\alpha_{cd}c_r\right)\left(s_{cd} - \alpha_{cd}\right)} \tag{104.537}$$

Finally the full elastic-plastic tangent stiffness tensor can be written as:

$$\begin{aligned} &E^{el-pl}_{pqmn} = \\ &E^{el}_{pqmn} - E^{pl}_{pqmn} = \\ &E^{el}_{pqmn} - \frac{E_{pqkl}\left(\mathbb{A}\left(s_{kl} - \alpha_{kl}\right)\right)\left(\mathbb{A}\left(s_{ij} - \alpha_{ij}\right)\right)E_{ijmn}}{\left(\mathbb{A}\left(s_{ab} - \alpha_{ab}\right)\right)E_{abcd}\left(\mathbb{A}\left(s_{cd} - \alpha_{cd}\right)\right) - (-\mathbb{A})\left(\frac{2}{3}h_a\ \left(\mathbb{A}\left(s_{cd} - \alpha_{cd}\right)\right) - \sqrt{\frac{2}{3}}\alpha_{cd}c_r\right)\left(s_{cd} - \alpha_{cd}\right)} \end{aligned} \tag{104.538}$$

104.6.18.4 Nonlinear Elastic Model in 1D based on Armstrong Frederick Equation

$$d\sigma_{ij} = d\alpha_{ij} = \frac{2}{3}h_a\left(d\epsilon^p_{ij}\right)^{dev} - c_r\sigma_{ij}\sqrt{\frac{2}{3}\left(d\epsilon^p_{st}\right)^{dev}\left(d\epsilon^p_{st}\right)^{dev}} \tag{104.539}$$

104.6.18.5 Drucker-Prager Model

Drucker-Prager model yield surface, including rotational kinematic hardening can be written as

$$f = \alpha I_1 + [\frac{1}{2}(s_{ij} - p\alpha_{ij})(s_{ij} - p\alpha_{ij})]^{\frac{1}{2}} - \beta = 0 \tag{104.540}$$

where α and β are material constants.

By coinciding Drucker-Prager cone with the outer apexes of the Mohr-Coulomb hexagon locus, the constants for compressive cone of Drucker-Prager can be evaluated as shown in Equation (104.541) by knowing the soil strength parameters of cohesion (c) and friction angle (ϕ):

$$\alpha = \frac{2\sin\phi}{\sqrt{3}(3 - \sin\phi)}, \quad \beta = \frac{6\cos\phi}{\sqrt{3}(3 - \sin\phi)}c \tag{104.541}$$

Drucker-Prager yield function for cohesionless sands ($k = 0$) can be obtained as:

$$f = \alpha I_1 + \sqrt{J_2} = 0 \tag{104.542}$$

or in $p-q$ space:

$$f = q - Mp = 0 \tag{104.543}$$

which then M can be obtained as:

$$M = \frac{6\sin\phi}{3-\sin\phi} \tag{104.544}$$

By considering kinematic hardening, Equation (104.543) can be expressed as:

$$f = \left[\left(s_{ij} - p\alpha_{ij}\right)\left(s_{ij} - p\alpha_{ij}\right)\right]^{0.5} - \sqrt{\frac{2}{3}}kp = 0 \tag{104.545}$$

which then stress derivative of yield function and plastic potential function in case of associated plasticity can be defined as:

$$\begin{aligned} n_{ij} &= m_{ij} = \frac{\partial f}{\partial \sigma_{ij}} = \frac{\partial g}{\partial \sigma_{ij}} \\ &= \left[\left(s_{ij} - p\alpha_{ij}\right) + \frac{1}{3}\alpha_{pq}\delta_{ij}\left(s_{pq} - p\alpha_{pq}\right)\right]\left[\left(s_{rs} - p\alpha_{rs}\right)\left(s_{rs} - p\alpha_{rs}\right)\right]^{-0.5} \\ &+ \sqrt{\frac{2}{27}}k\delta_{ij} \end{aligned} \tag{104.546}$$

To find the closed form equation of elastic-plastic modulus for case of perfectly-plastic, Equation (104.545) is used for associated plasticity rule with no hardening. By these assumptions stress derivative is calculated as:

$$n_{ij} = m_{ij} = \frac{1}{\sqrt{s_{ij}s_{ij}}}s_{ij} + \sqrt{\frac{2}{27}}k\delta_{ij} \tag{104.547}$$

Splitting plastic modulus to different parts:

$$\begin{aligned} Hq_{ij} &= E_{ijkl}m_{kl} = \{\lambda\delta_{ij}\delta_{kkl} + \mu(\delta_{ik}\delta_{jl} + \delta_{il}\delta_{jk})\}\{\frac{1}{\sqrt{s_{mn}s_{mn}}}s_{kl} + \sqrt{\frac{2}{27}}k\delta_{kl}\} \\ &= 2\mu\frac{1}{\sqrt{s_{mn}s_{mn}}}s_{ij} + \delta_{ij}\{\frac{1}{\sqrt{s_{mn}s_{mn}}}\lambda(s_{pq}\delta_{pq}) + \sqrt{\frac{2}{27}}k(3\lambda+2\mu)\} \\ &= 2\mu\frac{1}{\sqrt{s_{mn}s_{mn}}}s_{ij} + B\delta_{ij} \end{aligned} \tag{104.548}$$